BULLETIN NO
STOCKHOLM 2000
ISRN KTH-BYT/R—2000/180-SE
ISSN 0346-5918

180

Division of
BUILDING TECHNOLOGY

Department of Building Sciences
Kungl Tekniska Högskolan

The ORC Method – Effective Modelling of Thermal Performance of Multilayer Building Components.

Jan Akander

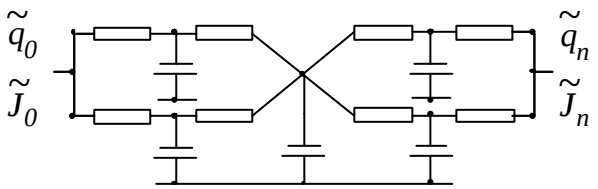

Doctoral Dissertation
Stockholm 2000

KUNGL TEKNISKA HÖGSKOLAN
Dept. of Building Sciences
Div. of Building Technology

The ORC Method – Effective Modelling of Thermal Performance of Multilayer Building Components

Jan Akander

Akademisk avhandling

Som med tillstånd av Kungliga Tekniska Högskolan i Stockholm framlägges till offentlig granskning för avläggande av teknologie doktorsexamen den 8:mars 2000 kl 14:00 i sal L1, Drottning Kristinas väg 30, Stockholm. Avhandlingen försvaras på engelska.

Fakultetsopponent: Professor Joe A. Clarke, University of Strathclyde
Huvudhandledare: Professor Guðni Jóhannesson, KTH

ISSN 0346-5918, ISRN KTH-BYT/--00/180-SE

Stockholm 2000

The ORC Method – Effective Modelling of Thermal Performance of Multilayer Building Components

Jan Akander
Div. of Building Technology
Dept. of Building Sciences
Kungliga Tekniska Högskolan
SE – 100 44 Stockholm

Abstract

The ORC Method (Optimised RC-networks) provides a means of modelling one- or multidimensional heat transfer in building components, in this context within building simulation environments. The methodology is shown, primarily applied to heat transfer in multilayer building components. For multilayer building components, the analytical thermal performance is known, given layer thickness and material properties. The aim of the ORC Method is to optimise the values of the thermal resistances and heat capacities of an RC-model such as to give model performance a good agreement with the analytical performance, for a wide range of frequencies. The optimisation procedure is made in the frequency domain, where the over-all deviation between model and analytical frequency response, in terms of admittance and dynamic transmittance, is minimised. It is shown that ORC's are effective in terms of accuracy and computational time in comparison to finite difference models when used in building simulations, in this case with IDA/ICE. An ORC configuration of five mass nodes has been found to model building components in Nordic countries well, within the application of thermal comfort and energy requirement simulations.

Simple RC-networks, such as the surface heat capacity and the simple R-C-configuration are not appropriate for detailed building simulation. However, these can be used as basis for defining the effective heat capacity of a building component. An approximate method is suggested on how to determine the effective heat capacity without the use of complex numbers. This entity can be calculated on basis of layer thickness and material properties with the help of two time constants. The approximate method can give inaccuracies corresponding to 20%.

In-situ measurements have been carried out in an experimental building with the purpose of establishing the effective heat capacity of external building components that are subjected to normal thermal conditions. The auxiliary wall method was practised and the building was subjected to excitation with radiators. In a comparison, there were discrepancies between analytical and measured effective heat capacities. It was found that high-frequency discrepancies were to a large extent caused by the heat flux sensors. Low-frequency discrepancies are explained by the fact that the exterior climate contained other frequencies than those assumed in the interior climate.

Key words : Building component, building simulation, heat transfer, thermal performance, frequency response, RC-network, finite difference model.

KUNGL TEKNISKA HÖGSKOLAN
Dept. of Building Sciences
Div. of Building Technology

The ORC Method – Effective Modelling of Thermal Performance of Multilayer Building Components

Doctoral Dissertation
Jan Akander
Stockholm 2000-02-06

ISRN KTH-BYT/R-2000/180-SE
ISSN 0346-5918

Doctoral Dissertation
ISRN KTH-BYT/R-2000/180-SE
ISSN 0346-5918
Printed by TS-Tryck & Kopiering, KTH, Stockholm, Feb 2000

PREFACE

I would like to thank Professor Guðni Jóhannesson for initiation of the projects, for constructive guidance through these projects and for the trust he has given me on coming forth with results within the projects. I am him indebt for introducing me to the fascinating field of frequency response with application to building physics. Also, the help and fruitful discussions with my colleagues at the Department of Building Sciences are warmly appreciated. A special gratitude is directed to PhD. Guofeng Mao, for assisting within the field of dynamic multi-dimensional heat transfer calculations and heat transfer in general, and to Christer Hägglund for practical advice on experimental matters. A thanks is also put forth to my co-authors Dr Asima Norén, Associate Prof. Engelbrekt Isfält and Prof. Ove Söderström. I happened to stumble into that project during a coffee break - is this when business actually is done...? A blessing is extended to Ms. Ninni Bodin, who kept track of all my paperwork.

A sincere gratitude is directed to Hans Persson, Maj Persson and Bill Hermansson at AB Svensk Leca for their co-operation within the Röskär project. Their curiosity, wise ideas and patient understanding is acknowledged.

The fellows at Brisdata AB are not forgotten. The useful ideas, positive criticism and software related issues from Axel Bring and Per Sahlin are well appreciated. I wish Mika Voulle at HUT, Finland, continued success in component library modelling. Keep up the good work!

I wish Håkan Rodin at Flooré AB all future success on electrical and water borne floor heating systems. It started with a project on measurements of a radiant floor in 1992...

Last but not least, I would like to thank the support and understanding that my wife Ulrika and energy bundles (my children) Sara and Sebastian have shown during the darkest and sunnier moments in times of research.

The grants from the Swedish Council for Building Research (BFR) and AB Svensk Leca are gratefully acknowledged.

Jan Akander
Stockholm, Feb 2000

TABLE OF CONTENTS

1 SCOPE 7

2 A BRIEF OVERVIEW OF THIS THESIS 9

3 BACKGROUND 12

4 THERMAL FREQUENCY RESPONSE 13

4.1 The thermal performance of multilayer building components 13
4.1.1 The frequency domain solution of the heat conduction equation 13
4.1.2 Admittance and dynamic transmittance 15
4.1.3 Informative asymptotes of admittance 15
4.1.4 The Bode Diagram 16
4.1.5 Switching frequencies 18

5 EFFECTIVE HEAT CAPACITY 19

5.1 Measurement of the effective heat capacity 20
5.1.1 The measurement method 22
5.1.2 The boundary conditions 22
5.1.3 Measured results in comparison with analytical results 23
5.1.4 Reasons for deviation in analytical and experimental results 25

5.2 The approximate method 26

5.3 EN832 - A calculation method that makes use of the effective heat capacity 28

6 THERMAL MODELS 30

6.1 The heat transfer matrix of serially connected thermal resistances and heat capacities 30

6.2 Finite difference method 30
6.2.1 Modelling the response of the semi-infinite solid 31

6.3 The ORC Method 33
6.3.1 Model deviation procedure 33
6.3.2 Optimisation of RC-networks 34
6.3.3 Fields of application: State-of-the-art and future perspectives 38

7 REFERENCE LIST 41

1 Scope

This thesis focuses to a large extent on thermal frequency response of multilayer building components. The work is therefore relevant to thermal performance of building components; how thermal performance can be characterised, how thermal performance can be modelled and experimentally be validated. The target reader group is therefore scientists within the research field of heat transfer in buildings.

Within the scope of this thesis, the thermal performance of multilayer components is characterised with applications in the Bode diagram, which is a well-know way of putting forth transfer functions. In this application, the Bode diagram is used to analyse the thermal performance of multilayer building components, in terms of what type of response is obtained for various frequencies of thermal processes. The frequency response can be that of a semi-infinite solid, or that of a simple mass or it can be purely resistive. The admittance procedure and dynamic transmittance (Danter 1973, Milbank and Harrington-Lynn 1974) are key issues within this context. Attention is focused at which frequencies a change in these types of responses occur on basis of material layer properties and layer order within building components. These frequencies are here called switching frequencies.

An informative quantification of frequency response is the entity called effective heat capacity. Actually, this term is widely accepted and used, though the definition is not clearly defined. A discussion is put forth on the use of two models that serve as a basis for the definition, on the choice of boundary conditions, and within what context this term will or may be used. Pros and cons for the use of one of the two models are stated from a physical point of view and also from a more practical sense. In-situ measurements have been performed on various building components as to experimentally validate this entity, where measurement methodology and data treatment are important factors that influence the final results.

Moreover, the frequency domain analysis can be used to study the performance of thermal models that are composed of chains of thermal resistances and heat capacities, such as those of finite difference methods and RC-networks. For a given building component, the analytical thermal performance can be calculated with frequency domain solution of the heat conduction equation. The thermal performance of the model can be evaluated against the analytical performance within the frequency domain. An implication of this is therefore to optimise the thermal model with respect to model inaccuracy, boundary conditions and thermal processes within the simulated system. This is conveniently done by means of optimised RC-networks (ORC's) that represent multilayer building components. The ORC method is used for optimising the parameters of an RC-network within the frequency domain. When the agreement between analytical and model performance can be considered to be adequate, the ORC can be used in time domain simulations, such as building simulation programs. Modelling and results from the building simulation program IDA/ICE are shown, where a comparison is made when building components are modelled with finite differences or with ORC's. ORC's are convenient for modelling multidimensional heat transfer, such as dynamic heat flow through thermal bridges and ground heat loss (Mao 1997).

Special attention has been given to a set of proposed drafts and accepted standards within building physics. Since the results of calculation procedures of these standards are dependent on building component types - much due to climatic circumstances and national building traditions - it is necessary to test and validate these codes with application on national factors. Also, it is necessary to review the background theory and definitions within the standards, as to check that these conform to the state-of-the-art of the field of application. Parts of three standards are frequently referred to in one way or another within this thesis. These are:

- prEN ISO 13786: 1998 E. *Thermal Performance of Building Components - Dynamic thermal characteristics - Calculation methods.* CEN/TC 89/WG 4/N176, Brussels.
- EN 832 (1998). *Thermal performance of buildings - Calculation of energy use for heating - Residential buildings.* European Committee for Standardisation (CEN), Brussels.
- EN ISO 13370 (1998). *Thermal performance of buildings – Heat transfer via the ground – Calculation methods.* European Committee for Standardisation (CEN), Brussels

It should be noted that the aim of this thesis is not to validate these standards. Comparisons are made since this work and these standards have common fields of application, unless the standards have directly been used to provide numerical results.

The thesis summarises the six papers that are included as appendices. Consequently, the aim of this first part is to highlight important issues presented in these six papers, to underline conclusions and to tie up ”loose ends” between the papers. To a minor extent, some issues may be re-discussed as to give another viewpoint.

2 A brief overview of this thesis

This thesis is a summary of six papers that are enclosed. These papers primarily evolve the applications of one of the most fundamental equations within building physics, namely Fourier's equation for heat conduction in solids. The work made here is to a large degree based on the application of the frequency domain solution on multilayer building components, especially on the characterisation and the modelling of building component thermal performance. This field is by no means new, but it is indeed significant and necessary as reflected in a proposal to European (EN) and international (ISO) standard with the title "Thermal Performance of Building Components". For this reason, a series of articles have been produced with the title "Thermal Performance of Multilayer Building Components". This series is composed of totally four papers and are inserted in the end of this thesis under the chapters called Paper 1 to 4. Yet, each paper has been written so that it can be read as a stand-alone paper. Two additional papers with applications on heat transfer are included.

The title of this thesis, "The ORC Method – Effective Modelling of Thermal Performance of Multilayer Building Components", has the intention of summing up the contents of this thesis with respect to the methodology used for determining one (or multidimensional) heat transfer in building components. The analytical frequency domain solution of the heat conduction equation provides the "true" thermal performance of the building component. This thermal performance can be modelled, in the frequency and in the time domain, by means of RC-networks. When the parameters of an RC-network are determined as to give the model a thermal performance that agrees well with the analytical performance, for a wide range of frequencies, the outcome is an optimised RC-network (ORC). RC-networks are chains of thermal resistances and heat capacities (i.e. lumped parameter models) that can comprise a single heat capacity, for example an effective heat capacity, to more complex configurations, such the 5-node ORC configuration as illustrated on the cover.

The first paper (Paper 1) within the series, "The Thermal Performance of Multilayer Components - Applications of the Bode Diagram" contains fundamentals on the methodology used and serves as a platform for the other papers within the series. More specifically, the entities thermal admittance and dynamic transmittance are stated. These heat transfer functions, which are thermal performance characteristics of a building component, are conveniently displayed in the Bode diagram. The Bode diagram is widely used for example within automation and control theory. Within the current application, it serves as a visual aid as it reveals if the response of a building component is that of a simple mass, a pure thermal resistance or the semi-infinite solid. Switch frequencies quantify when there is a change in thermal performance. The Bode diagram also visualises asymptotes of admittance. This is penetrated to a greater extent in the second paper, but within the scope of the first paper, asymptotes and switching frequencies can be used for discretisation of cell size of a finite difference model applied to a building component. Model and analytical performance can be plotted in the Bode diagram, to be directly compared. This provides background theory to the fourth paper, where the optimised RC-network method (ORC) is introduced.

The second paper within the series (Paper 2) deals with the effective heat capacity of multilayer building components and is closely related to the proposed EN ISO standard on dynamic thermal performance of building components, prEN ISO 13786 (1998). In this paper, a discussion is put forth on what and how the effective heat capacity of a building component can be defined and determined. The main content of the paper is a proposal of a new method on determining the effective heat capacity by means of real numbers only: the material layer thermal properties and thickness. The "correct" (analytical) value involves calculations using real and imaginary numbers. The new method can be used as a complement to the present normative method of Annex A of prEN ISO 13786, since the method gives more reliable results than the proposed standard. The method gives an inaccuracy that in general is less than 20%.

The aim of the third paper is to validate effective heat capacity procedures experimentally (Paper 3 with the sub-title "Experimental Assessment of the Effective Heat Capacity"). Measurements were performed with the auxiliary wall method. The heating system of an experimental building was subjected to a Pseudo Random Binary Sequence (PRBS) to excite building components. The thermal response of various building components was recorded. Monitored data was transformed into the frequency domain

with Fast Fourier Transform (FFT), for calculation of the measured effective heat capacity. A comparison between theoretical and measured results shows adequate agreement. The paper also focuses on sources of experimental errors and shows that the choice of boundary conditions in the definition of effective heat capacity has a large influence on the result.

The fourth and last paper within the series concerns the optimisation of RC-networks as to give equivalent thermal performance as multilayer components. Having been stated in the first paper, the method for comparing model and analytical performance is essential in the optimisation procedure. The optimisation procedure involves minimising model performance deviation for a wide range of frequencies. Various RC-network configurations are shown, as well as their fields of application. Again, the definition of the effective heat capacity is discussed, since this entity is based on the configuration of a simple RC- (or C-) network. This paper also shows differences in ORC performance as opposed to the performance of a conventional finite difference model within the building simulation program IDA/ICE. Results of an ORC with five mass nodes give good agreement with results from a detailed finite difference model, but the ORC requires less computational time. A discussion is also put forth on the subject of modelling multidimensional heat transfer with ORCs. These are very efficient for this purpose and the method has been practised (Akander et al 1996, Mao 1997), but this application is beyond the scope of this thesis.

Papers 5 and 6 are beyond the scope of the series entitled ”The Thermal Performance of Multilayer Building Components”. However, Paper 5, with the title ”The Effect of Thermal Inertia on Energy Requirement in a Swedish Building – Results Obtained with Three Calculation Models”, is closely related to this series. This paper shows by means of simulations that the thermal inertia of a building has an influence on energy requirement of a multifamily building situated in a northern climate. Whereas two co-authors of the paper used detailed building simulation programs (TSBI3 and BRIS), the author of this thesis utilised the calculation procedure of European Standard EN832 (at the time it was a proposed standard). The simplified calculation procedures of prEN832, that makes use of the effective heat capacity of a building, gave results that agreed well with results of far more detailed simulation program TSBI3. A special note should be made at this stage: the proposed effective heat capacity procedure, that was a part of prEN832, that was at the time of working defined differently than at present.

Paper 6 is more or less miscellaneous within the frame of this dissertation. Having the title ”Reducing Ground Loss from a Heated Underfloor Space – A Numerical Steady-state Case Study”, this work is limited to steady-state calculations, focusing on heat loss from a heated underfloor space. The aim of that work was to reduce heat loss and system temperatures without affecting heat delivered to the living space, nor the building method for erecting the house. A comparison was made between results from models in two- and three dimensional heat transfer as well as calculated U-values from applications in EN ISO 13370 (1998). The agreement between 2-D and 3-D numerical models was very good. The U-value for a slab-on-ground according to the EN-ISO calculation procedure was considerably lower than for the numerical models. An EN-ISO equation was modified as to give the U-value of the heat transmittance from a heated underfloor space. The modified equation gave reliable results. As measurements and calculations on air infiltration in the underfloor space were conducted, the paper concluded that infiltrating air should be included in the heat balance of the underfloor space.

At the time that this doctoral dissertation was sent for publication, the status of the papers were:

PAPER 1: Submitted to Nordic Journal of Building Physics.

Akander J. and Jóhanneson G. The Thermal Performance of Multi-Layer Components - Applications of the Bode Diagram.

PAPER 2: Submitted to Nordic Journal of Building Physics.

Akander J. The Thermal Performance of Multilayer Building Components - A Method for Approximating the Effective Heat Capacity.

PAPER 3: Submitted to Nordic Journal of Building Physics.

Akander J. The Thermal Performance of Building Components – Experimental Assessment of the Effective Heat Capacity.

PAPER 4: Submitted to Nordic Journal of Building Physics and revised

Akander J. The Thermal Performance of Building Components – The Methodology of ORC and Applications.

PAPER 5: Published in International Journal of Low Energy and Sustainable Buildings.

Norén A., Akander J., Isfält E. and Söderström O. (1999). The Effect of Thermal Inertia on Energy Requirement in a Swedish Building – Results Obtained with Three Calculation Models. *International Journal of Low Energy and Sustainable Buildings, Vol 1*. Available at http://www.bim.kth.se/leas

3 Background

This thesis is a documentation of some of the results obtained from primarily two major projects. The first is ”Energiflöden i byggnadskomponenter - beräkningsmetoder - simuleringar”, which resulted in the licentiate thesis ”*Efficient Modelling of Energy Flow in Building Components - Parts 1 and 2*” (Akander 1995). To a large extent, the work focused on the modelling of multilayer building components by means of optimised RC-networks (ORC’s). The outcome was implemented within the building simulation program IDA/ICE. This did not mean that the development of optimisation procedures ended at the time when the project was officially terminated. Further development is summarised within this thesis.

The second project bears the name ”Två småhus på Röskär” (in English: ”Two residential houses at Röskär”). The so-called Röskär project was to allow the erection of experimental buildings by industrial companies and thereby to have special technical building solutions theoretically and experimentally analysed. This was the role of the Division of Building Technology within the Department of Building Sciences at KTH. Despite the depression within the Swedish national economy during the early and mid-nineties, which hit hard on the building sector, two experimental buildings were erected. One was the IEA house, which was built by the division and financed by the Swedish Council of Building Research. AB Svensk Leca built the other house. The main objective of the first stage of the project was to study the influence of heat capacity on energy requirement. For this reason and also due to that the division under the leadership of Professor Gudni Jóhannesson has a tradition of using frequency response analysis as method to tackle heat transfer problems, the effective heat capacity played an important role within the project. At the same time, Sweden is subject to a set of new European standards, whereof two as a matter of fact involve the so-called effective heat capacity. In one of these, which currently is a draft, the effective heat capacity is defined (prEN ISO 13786:1998 E. *Thermal Performance of Building Components - Dynamic thermal characteristics - Calculation methods.*). The other is a calculation method for determining the energy requirement of a residential building, EN 832 (1998), that makes use of the effective heat capacity when the thermal inertia of the building is taken into account. The Röskär project was therefore a golden opportunity for investigating the role of heat capacity on energy requirement, to review what the term effective heat capacity means and how it may be defined and measured, what results can be expected and how these are to be interpreted and used. The project has also lead to a communication and information exchange between the university and industrial parties, with industrial application of results. More general information on the Röskär project can be found in (Johannesson 1994) and (Akander and Jóhannesson 1997).

4 Thermal frequency response

Thermal frequency response is a central issue within this thesis. Reasons for analysing thermal behaviour in terms of frequency response are the following.

- There is a frequency domain solution to the Fourier's heat conduction equation if the considered system is linear. This means that analytical analysis can be made on thermal performance.
- Thermal performance can be characterised by using the definition of admittance and dynamic thermal transmittance, which are frequency dependent transfer functions.
- The effective heat capacity can be defined and calculated on basis of admittance.
- Thermal models composed of chains of thermal resistances and heat capacities, such as finite difference and RC-network models, can be optimised within the frequency domain as to give desired model accuracy. Model performance deviation can be determined since the analytical performance is known. By means of the ω-RC transform, these models can be used in time domain simulation programs.
- Multidimensional heat transfer in building components can be modelled with simple one- or multidimensional RC-networks. The multidimensional heat transfer of the building component can be modelled by means of finite difference programs that determine admittance and dynamic transmittance of various surfaces. This thermal performance can be modelled with simplified equivalent RC-networks. This point is beyond the scope of this paper, but is nevertheless a strong reason.
- Theory can experimentally be validated, even though a mathematical transformation of time domain data into the frequency domain (or vice-versa) is necessary.

A mandatory criterion that has to be fulfilled in frequency domain calculations is that the system is linear. In this thesis, it is mainly multilayer plane building components that are studied. If the building component is to be linear, all material properties and layer thickness have to be constant. For a linear system, each frequency component of a variable can be superposed. If the thermal entities in question are density of heat flow (heat flux) q and temperature $\boldsymbol{q}$ at the two surfaces, these can be represented as the sum of the steady state component and the sum of each frequency component, or mathematically formulated such that

$$q = \overline{q} + \sum_{j=1}^{\infty} \tilde{q}_j \tag{1a}$$

and

$$\boldsymbol{q} = \overline{\boldsymbol{q}} + \sum_{j=1}^{\infty} \tilde{\boldsymbol{q}}_j \tag{1b}$$

Here, $\overline{q}$ and $\overline{\boldsymbol{q}}$ depict the steady state component (i.e. the mean value of a long time series). The terms $\tilde{q}_j$ and $\tilde{\boldsymbol{q}}_j$ represent heat flux and temperature oscillation for *one* frequency. If the considered series is time limited, ∞ is substituted by an integer.

4.1 The thermal performance of multilayer building components

4.1.1 The frequency domain solution of the heat conduction equation

This thesis evolves around the solution of one equation. This equation is the heat conduction equation that was originally stated by Fourier. The equation, without a heat source term, is for heat transfer in one dimension expressed as

$$a\frac{\partial^2 \boldsymbol{q}}{\partial x^2} = \frac{\partial \boldsymbol{q}}{\partial t} \tag{2}$$

Here, a is thermal diffusivity of the material, x space co-ordinate and t time.

Various scientists have derived a frequency domain solution to the heat conduction equation. Some use the penetration depth of a heat wave, such as Claesson et al (1984) and also prEN ISO 13786 (1998). The set of equations used here were as formulated by Carslaw and Jaeger (1959). A heat transfer matrix of a sinusoidally excited slab was defined such that

$$\begin{bmatrix} \tilde{\boldsymbol{q}}_n \\ \tilde{q}_n \end{bmatrix} = \begin{bmatrix} A_1 & B_1 \\ C_1 & D_1 \end{bmatrix} \begin{bmatrix} \tilde{\boldsymbol{q}}_0 \\ \tilde{q}_0 \end{bmatrix} \tag{3}$$

Sinusoidal surface heat flux (density of heat flow rate) and surface temperature oscillations are denoted by $\tilde{q}$ and $\tilde{\boldsymbol{q}}$. These are functions of *one* angular frequency $\boldsymbol{w}$, here depicted by the superscript "~". Surface *0* is the excited surface, whereas surface *n* is the obverse surface that is subject to different boundary conditions discussed later. The heat transfer matrix contains complex elements, here

$$A_1 = \cosh(k \cdot l(1+i)) \tag{4a}$$

$$B_1 = -\frac{\sinh(k \cdot l(1+i))}{\boldsymbol{l} \cdot k(1+i)} \tag{4b}$$

$$C_1 = -\boldsymbol{l} \cdot k(1+i) \cdot \sinh(k \cdot l(1+i)) \tag{4c}$$

$$D_1 = \cosh(k \cdot l(1+i)) \tag{4d}$$

with

$$k = \sqrt{\frac{\boldsymbol{w}}{2 \cdot a}} \qquad \text{and} \qquad a = \frac{\boldsymbol{l}}{\boldsymbol{r} \cdot c} \tag{4e}$$

The determinant of the heat transfer matrix of a plane component is always unity.

For a multilayer component, the heat transfer matrix of the component is the product of the heat transfer matrix of each material layer. The matrix multiplication result in a 2x2 heat transfer matrix

$$\begin{bmatrix} \tilde{\boldsymbol{q}}_n \\ \tilde{q}_n \end{bmatrix} = \begin{bmatrix} A_3 & B_3 \\ C_3 & D_3 \end{bmatrix} \begin{bmatrix} A_2 & B_2 \\ C_2 & D_2 \end{bmatrix} \begin{bmatrix} A_1 & B_1 \\ C_1 & D_1 \end{bmatrix} \begin{bmatrix} \tilde{\boldsymbol{q}}_0 \\ \tilde{q}_0 \end{bmatrix} = \begin{bmatrix} A & B \\ C & D \end{bmatrix} \begin{bmatrix} \tilde{\boldsymbol{q}}_0 \\ \tilde{q}_0 \end{bmatrix} \tag{5}$$

The theory assumes that the system is linear. Each frequency component can be treated separately. Input values give oscillations of heat flux or temperature with the same frequency.

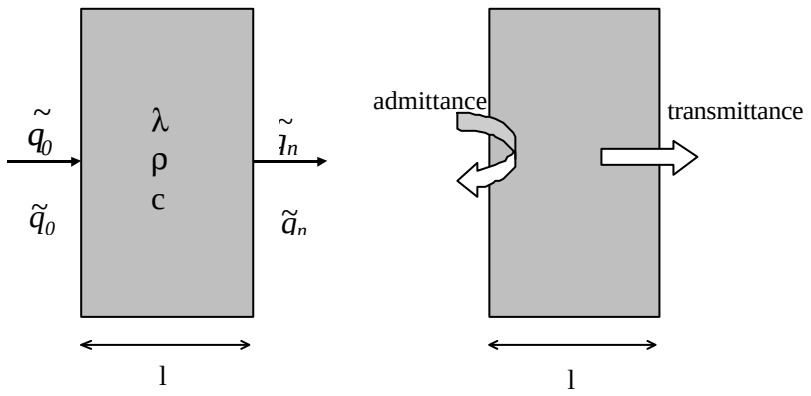

Figure 1: To the left: Material parameters, temperature oscillation and heat flux direction for a homogeneous slab. To the right: Illustration of admittance and transmittance (see section 4.1.2).

4.1.2 Admittance and dynamic transmittance

The admittance procedure, introduced by Danter (1973) and Milbank and Harrington-Lynn (1974), is a way of defining frequency response of a building component. Admittance is the quotient of heat flux and temperature oscillation at one surface of the component, thus having the unit W/(m^2·K). Admittance has direction, and is defined positive on leaving the component via the surface, see figure 1.

$$Y_0 = -\frac{\tilde{q}_0}{\tilde{\theta}_0} \tag{6}$$

Admittance is influenced by the boundary condition at the other surfaces. Here, applied to a multilayer building component, the admittance of surface 0 is such that

$$Y_0 = \frac{A}{B} \quad \left(\tilde{q}_n = 0\right) \tag{7a}$$

$$Y_0 = \frac{C}{D} \quad \left(\tilde{q}_n = 0\right) \tag{7b}$$

$$Y_0 = \frac{A-1}{B} \quad \left(\tilde{q}_n = \tilde{q}_0\right) \tag{7c}$$

Dynamic transmittance depicts heat flow at surface *n* due to a temperature oscillation at surface 0. Dynamic transmittance is the same in both directions, differing only by a minus sign.

$$T_D = \frac{\tilde{q}_n}{\tilde{\theta}_0} \tag{8}$$

The definition gives that

$$T_D = \frac{1}{B} \quad \left(\tilde{q}_n = 0\right) \tag{9}$$

This section is in more detailed described in Paper 1, including references to related work by other authors.

4.1.3 Informative asymptotes of admittance

When the value of angular frequency ω can be considered to be high or low, admittance converges to a certain value, see the appendix of Paper 2. For a *high frequency* thermal process, the value of admittance approaches

$$Y_0 = -\sqrt{\frac{\lambda_1 \cdot \rho_1 \cdot c_1 \cdot \omega}{2}}\left(1 + i\right) \tag{10}$$

This is the response of the semi-infinite solid, where the magnitude is $\sqrt{\lambda_1 \cdot \rho_1 \cdot c_1 \cdot \omega}$ W/(m^2·K) and phase shift -135°. The value is independent of the boundary condition at surface *n*.

If the considered thermal process takes place at a node that is coupled to the surface of a building component by means of a thermal surface resistance, R_{si} for example, admittance converges to the value

$$Y_i = -\frac{1}{R_{si}} \tag{11}$$

Here, the index i represents an internal node, such as a representative indoor air node.

If the thermal process is of a *low frequency* nature, the response will be boundary condition dependent, and in the case of multilayer components also influenced by material layer order. The asymptotic values for a homogeneous slab are such that

$$Y_0 \approx -\frac{1}{R} \quad \left(\tilde{q}_n = 0\right) \tag{12a}$$

$$Y_0 \approx -i\omega \cdot \rho \cdot c \cdot l \quad \left(\tilde{q}_n = 0\right) \tag{12b}$$

$$Y_0 \approx -i\omega \frac{\rho \cdot c \cdot l}{2} \quad \left(\tilde{q}_n = \tilde{q}_0\right) \tag{12c}$$

4.1.4 The Bode Diagram

The Bode diagram is commonly used within the field of automation and control systems for illustration of transfer functions in general (Åström 1968). Since admittance and dynamic transmittance are frequency-dependent transfer functions, the Bode diagram is suitable within this application as originally used by Jóhannesson (1981).

The Bode diagram plots magnitude and phase shift as function of frequency, though frequency has been converted to time period as this eases legibility. A general layout of the diagram is shown in figure 2. The upper diagram shows magnitude and the lower phase shift. Attention should be given to the upper diagram, where the lines with constant values are displayed. These ”constant” values can be compared with the asymptotic values of admittance (equations 10, 11 and 12a-c). On starting with the y-axis, thermal performance of resistive nature are plotted as horizontal lines, drawn in relation to the inverse of the thermal resistance of the building component, R_t.

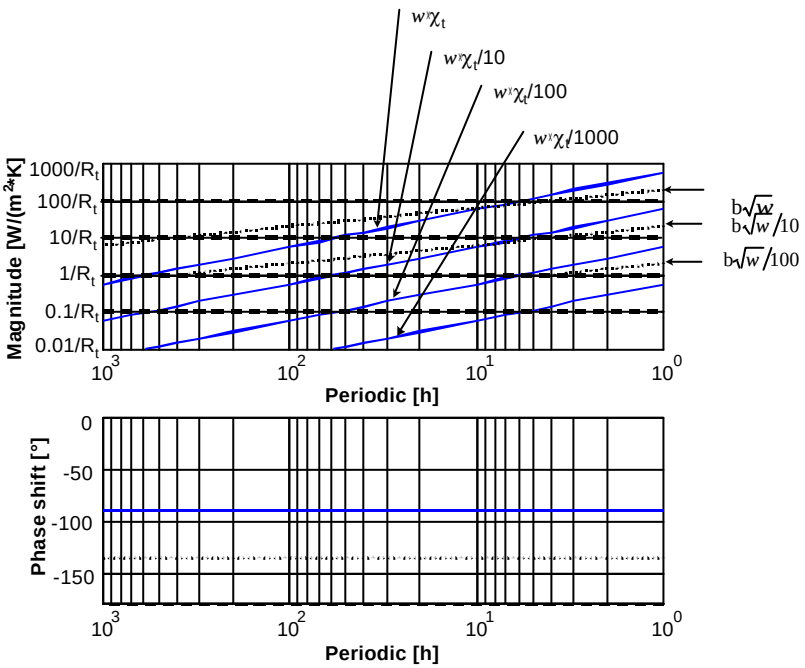

Figure 2: The upper diagram illustrates magnitude as function of periodicity. The y-axis, thus the horizontal lines, shows the response of a thermal resistance, with R_t being the total thermal resistance of the building component. The filled slanted lines show the response of a simple mass

($w \cdot c_t$), whereas the dotted lines represent the thermal response of the semi-infinite solid ($b\sqrt{w}$). The lower diagram shows phase shift for the three types of response as stated above.

Next, there are four lines with the slope 1:1, which depict the thermal performance of a simple mass, or as formulated in the figure, a function of angular frequency times a value corresponding to a heat capacity, here denoted by C_t. Three lines that do not go below the $1/R_t$ -level show the thermal response of the semi-infinite solid. These are parallel with the line $b\sqrt{w}$, where b is the thermal effusivity of a material and is defined as

$$b = \sqrt{l \cdot r \cdot c} \tag{13}$$

Phase shift is more easily interpreted. The phase shift of the semi-infinite solid is –135°, it is –90° for the simple mass and –180° for a pure thermal resistance.
An example from Appendix 1 is shown below, more can be found in Appendix 1, 3 and 4. The thermal performance of the exemplified wall of table 1 is plotted in figure 3. Here, the thermal performance is based on the assumed boundary condition $\tilde{q}_n = 0$.

Table 1: Material data for a roof. The innermost layer is listed first.

Material	d [m]	λ [W/(m·K)]	ρ [kg/m³]	c [J/(kg·K)]	R [(m²·K)/W]	χ [J/(m²·K)]
Concrete	0.040	1.2	2400	880	0.0333	84480
Mineral wool	0.120	0.04	200	750	3.0000	18000
Roofing felt	0.004	0.26	1100	1500	0.0154	6600

Three distinct types of admittance performances (stages 1 to 3) can be seen. Stage 1 is the range of periodicity where the thermal performance can roughly be regarded to be resistive. The dashed line depicts the asymptotic performance of a pure thermal resistance. Stage two is when the thermal performance of the component is said to have the performance of a simple mass. The asymptote (the dashed line) has values from the equation $-iw \cdot c_{concrete}$, where $c_{concrete}$ is the heat capacity of the concrete layer. In this case, the agreement between analytical response and the asymptote is good, and as seen, this provides a basis for what is called the "effective heat capacity" of a building component (see the following sections). The last range, stage 3, is when the response is that of the semi-infinite solid. Here, the thermal effusivity is that of the concrete layer. The periodicity ranges of the three types of responses can be estimated by means of switching frequencies, which are described in the next section.

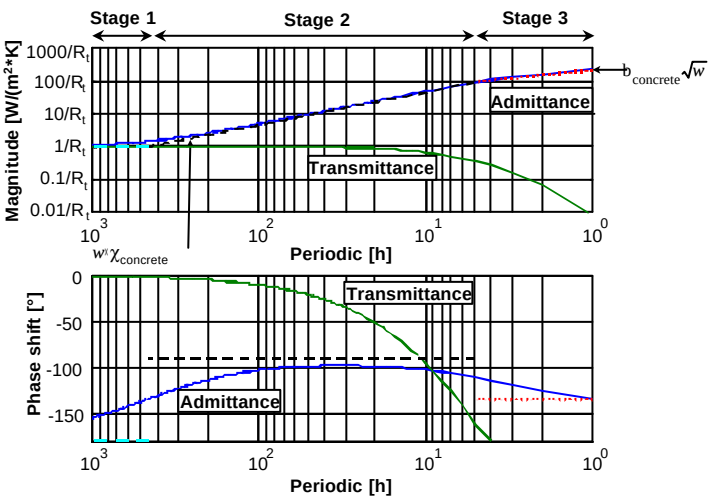

Figure 3: The Bode diagram of the building component as listed in table 1, with the boundary condition $\tilde{q}_n = 0$ *. Magnitude and phase shift is plotted (filled curves) for admittance and transmittance. Three ranges of periodicity are marked (stages 1 to 3) depending on response type, as well as admittance asymptotes (dashed lines) within each range.*

The response of a building component is dependent on the choice of boundary conditions. This will not explicitly be shown within this context as this issue is more thoroughly discussed in Paper 1.

4.1.5 Switching frequencies

Switching frequencies are useful for determining at what periodicity there is a change in response (thermal behaviour). In the current example, switching frequencies separate the three different stages.

Starting with stage 2, the response is virtually that of a simple mass, valid for a periodicity T between

$$2\pi \cdot R_1 \cdot c_1 / 3600 \leq T \leq 2\pi \cdot R_t \cdot c_1 / 3600 \tag{15}$$

In this example, c_1 was large, being 77% of the total heat capacity c_t. Therefore, a transient region is found at stage 3, where this region is approximately

$$2\pi \cdot R_t \cdot c_1 / 3600 \leq T \leq 2\pi \cdot R_t \cdot c_t / 3600 \tag{16}$$

The response of the building component is that of the semi-solid for periodicity that is faster than

$$T \leq 2\pi \cdot R_1 \cdot c_1 / 3600 \tag{17}$$

5 Effective heat capacity

The term effective heat capacity is actually a quantification that corresponds to the part of the total heat capacity of a building component that participates in dynamic heat exchange between the component and the environment. It is therefore natural to base the definition of effective heat capacity on admittance, as noted earlier in the applications of the Bode diagram. However, in order to complete the definition, a model has to be set up. Jóhannesson (1981) studied two models to determine what he called the ”active heat capacity”. The models are the surface heat capacity and the heat capacity of the RC-configuration (network) as displayed in figure 4. These two models have also appeared in various draft versions of prEN ISO 13786 with the title ”Thermal performance of building components- Dynamic thermal characteristics - Calculation methods”. The most recent versions use the latter model. Paper 2 deals to some extent on how the definition of effective heat capacity should be formulated. The following issues must be considered when the definition of the effective heat capacity is formulated.

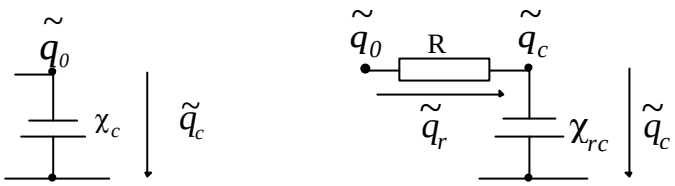

Figure 4: To the left*: The surface heat capacity model.* To the right*: The RC-configuration model.*

The surface heat capacity model has an admittance that mathematically is a pure imaginary number, whereas admittance is composed of a real and a complex number. However, on taking the absolute value of the analytical (Y_0) and model admittance, the magnitudes can be set equal such that

$$c_c = \frac{|Y_0|}{w} \tag{18}$$

The surface heat capacity can model magnitude of admittance for building components that have the response of a simple mass very well. It does not model phase shift well, since the value is constantly -90º. Building components that have the response of the semi-infinite solid can only be modelled at the frequency for which the effective heat capacity is calculated from. Examples are found in figures 2 and 4 of paper 4.

The RC-configuration model has an admittance that is composed of a real and an imaginary number. For a given frequency, the values of the thermal components within the model are determined such that

$$R = -\mathrm{Re}\left(\frac{1}{Y_0}\right) \; ; \qquad c_{rc} = \frac{1}{w \cdot \mathrm{Im}\left(\frac{1}{Y_0}\right)} \tag{19}$$

Analytical magnitude and phase shift is modelled exactly for the given frequency. Magnitude and phase shift is better modelled for a wider range of frequencies than the surface heat capacity model. However, the semi-infinite solid is again not well modelled, other than for the calculation frequency. This model consistently results in larger values than the surface heat capacity, as shown below in table 2.

A main issue is to determine what the results for such calculations are to be used for. In terms of product specifications, dynamic entities are welcome, such as the effective heat capacity and the decrement factor. The U-value is of course the most important entity that describes thermal performance. The effective heat capacity and the decrement factor are complements to the U-value, and the question is if these two values, that are based on the 24-hour periodic, are enough to give the entire thermal performance of a building component. For simulations, these entities are practically insufficient,

as pointed out by Kre (1993): these merely ”illuminate otherwise analysed principles”. The analytical equations 4 to 5 and the principle of superposition can be used for this purpose and give more reliable results. Therefore, the effective heat capacity is primarily an entity that describes how much heat can be stored within a building component, and secondarily an entity that describes when the storing takes place (this can only be done in combination with a thermal resistance). Hence, the RC-configuration gives the redundant value of the thermal resistance, and the value of the effective heat capacity will at the same time be meaningless if it does not interact with the resistance. These values are alone not comprehensive. Also, the modelled phase shift is redundant in practical calculations at this level of detail. For these purposes, the surface heat capacity is more comprehensive and practical to use.

So far, nothing has been mentioned about what boundary conditions should be assumed within the calculations. The three boundary conditions that may be used are that $\tilde{q}_n = 0$, $\tilde{q}_n = 0$ and $\tilde{q}_n = \tilde{q}_0$. On using asymptotic admittance values of equations 10 and 12a-c, the calculated heat capacities receive values as expressed in table 2. Note that the boundary condition $\tilde{q}_n = 0$ is inconvenient. The effective heat capacity interprets the setting of constant temperature at surface *n* as being done by an infinite mass when frequency approaches zero. The boundary condition $\tilde{q}_n = \tilde{q}_0$ is preferred among these options, as is the condition of the EN ISO standard proposal. However, the influence of the phase shift of $\tilde{q}_n / \tilde{q}_0$ has a large influence on the effective heat capacity, as will be shown in section 5.1.2 (from Paper 3). Table 2 also lists differences in results from the two models. The value of c_{RC} may exceed c_C by a factor ranging from 1 to $\sqrt{2}$.

Table 2: The values of effective heat capacities c_C and c_{RC} for a slab. These are boundary condition dependent. The values of c_{RC} may be larger values than c_C, as seen on the right hand side.

Heat capacity as $w \to 0$ s^{-1}	c_C	c_{RC}	Heat capacity as $w \to \infty$ s^{-1}	c_C	c_{RC}
$\tilde{q}_n = 0$	∞	∞	$\tilde{q}_n = 0$	$\sqrt{lrc/w}$	$\sqrt{2lrc/w}$
$\tilde{q}_n = 0$	c_t	c_t	$\tilde{q}_n = 0$	$\sqrt{lrc/w}$	$\sqrt{2lrc/w}$
$\tilde{q}_n = \tilde{q}_0$	$c_t/2$	$c_t/2$	$\tilde{q}_n = \tilde{q}_0$	$\sqrt{lrc/w}$	$\sqrt{2lrc/w}$

5.1 Measurement of the effective heat capacity

Theoretical work and analysis are a vital part in accumulating knowledge within any field of science. The empirical practice is equivalently important, and it is therefore necessary to have experimental validation of theoretical calculation procedures. Paper 3 deals with the in-situ measurement of the effective heat capacity of building components. The work is part of a joint research project with the company AB Svensk Leca. This company erected an experimental building in Röskär, whereas KTH conducted measurements and calculations. With the aim of determining the influence of heat capacity on energy requirement, and at the time the acceptance of EN 832 as European Norm, it became natural for KTH to experimentally investigate and validate theoretical calculation procedures of the effective heat capacity. Paper 3 focuses on the methodology of measuring the effective heat capacity of building components, a comparison between measured and calculated values, the influence of boundary conditions and on sources of measurement inaccuracy.

Results from one building component, the external wall facing North-Northeast, will be shown within this context. The wall is a massive type made of light expanded clay aggregates (LECA). Layer thickness and material properties are listed in table 3, and the thermal performance of the component is plotted in figure 5. The effective heat capacity was calculated for this component on basis of the surface heat capacity model, with results shown in figure 6.

Table 3: Layer thickness and material properties of a wall. The light expanded clay aggregate (LECA) material properties have been measured (SP 1996). The values of mortar are assumed.

Material layer	l [m]	λ [W/(m·K)]	ρ [kg/m³]	c [J/(kg·K)]
LECA high density	0.02	0.25	970	1040
LECA low density	0.30	0.16	540	1190
LECA high density	0.03	0.25	970	1040
Mortar	0.02	1.00	1800	950

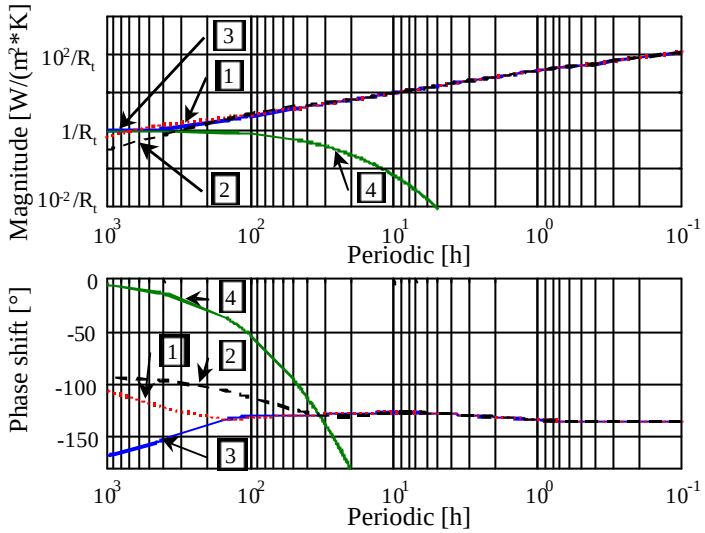

Figure 5: The Bode diagram for the building component. Curve [1](dotted) is admittance when the boundary condition $\tilde{q}_n = 0$ *is assumed, curve [2](dashed) when* $\tilde{q}_n = \tilde{q}_0$ *and curve [3](filled) when* $\tilde{q}_n = 0$*. Curve [4] represents dynamic transmittance. The calculated thermal resistance of the building component is* R_t *= 1.7938* $m^2 \cdot K/W$*.*

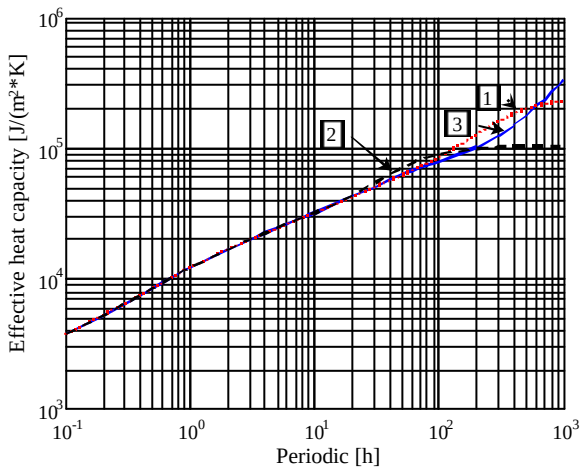

Figure 6: The analytical effective heat capacity (equation 18) of the wall as function of periodic. Curve [1](dotted) is derived when the boundary condition $\tilde{q}_n = 0$ *is assumed, curve [2](dashed) when* $\tilde{q}_n = \tilde{q}_0$ *and curve [3](filled) when* $\tilde{q}_n = 0$*.*

5.1.1 The measurement method

The measurements were made by means of the auxiliary wall method, commonly used to determine the thermal resistance of building components. In essence, a heat flux sensor is attached to a surface of the building component, usually on the internal surface. Next to this sensor, a thermocouple is placed on the internal and on the external surface. For measurement of the thermal resistance, data is collected during a number of weeks depending on the type of construction. Depending on how data is processed, the measurement time can be shortened by introducing statistical methods such as applied by Anderlind (1996).

Within this project, the dynamic performance was to be monitored. The thermal excitation was primarily made with electrical radiators by means of a Pseudo Random Binary Sequence (PRBS), see for example (Jensen 1979). This pulse train of pre-determined zeros and ones contains a specific frequency spectrum, such that the frequencies in the internal environment are known.

The acquired data of a measurement series is transformed with Fast Fourier Transform (FFT) into the frequency domain, preceded by a calculation for determining the effective heat capacity for each frequency present in the PRBS. This measured result can then be compared to results obtained from analytical equations, provided that boundary conditions are the same in both cases.

5.1.2 The boundary conditions

Thus far in the theoretical calculations, the boundary conditions of the external surface have been assumed to be constant ($\tilde{q}_n = 0$ or $\tilde{q}_n = 0$) or to have the same temperature oscillation as the internal surface ($\tilde{q}_n = \tilde{q}_0$). Now it may be expected that the measured temperature oscillation at the external surface does not fulfil these conditions. A calculation was made on the external wall (table 3) to study how the phase shift of $\tilde{q}_n / \tilde{q}_0$ influenced the effective heat capacity. The magnitude of $\tilde{q}_n / \tilde{q}_0$ was set to 1°C, while phase shift was varied in accordance to table 4. The influence was related to the effective heat capacity when the external surface temperature was assumed to be constant, such that

$$\boldsymbol{d} = \left(\left| \frac{\tilde{q}_0}{\tilde{q}_0} \right| - \left| Y_0 \right|_{\tilde{q}_n = 0} \right) \Big/ \left| Y_0 \right|_{\tilde{q}_n = 0} \tag{20}$$

From the results in figure 7, the conclusion is that phase shift in surface temperatures has a considerable influence on the effective heat capacity. An increase in amplitude of the external surface temperature oscillation will raise this effect, since the magnitude of the temperature ratio of this example is unity.

Table 4: Case number and boundary condition for calculation results shown in figure 7.

Case no.	1	2	3	4	5	6	7	8
$\tilde{q}_n / \tilde{q}_0$	1	$(1+i)/\sqrt{2}$	i	$(-1+i)/\sqrt{2}$	-1	$-(1+i)/\sqrt{2}$	$-i$	$(1-i)/\sqrt{2}$

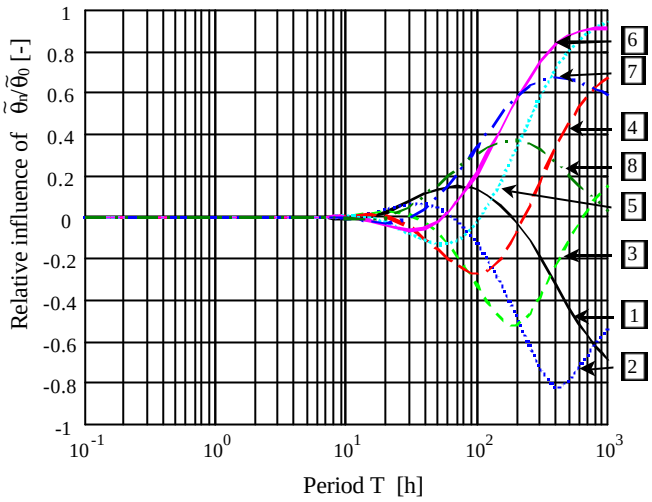

Figure 7: The relative influence $\boldsymbol{d}$*(equation 20) of* $\tilde{q}_n/\tilde{q}_0$ *on the effective heat capacity of the external wall as listed in table 3. Case number associated with each curve is defined in table 4. The amplitude of* $\tilde{q}_n/\tilde{q}_0$ *is here assumed to be unity.*

Within this experiment, it was wished to let temperatures and heat flows to be as ”natural” as possible. This means that the amplitude of the indoor temperature was not allowed to oscillate too much, as to measure the effective heat capacity in natural running conditions of a building, see for example the temperatures and heat flux measured at the surfaces of the external wall in figure 8. An amplification of the thermal loads in the internal environment may make thermal transmittance negligible.

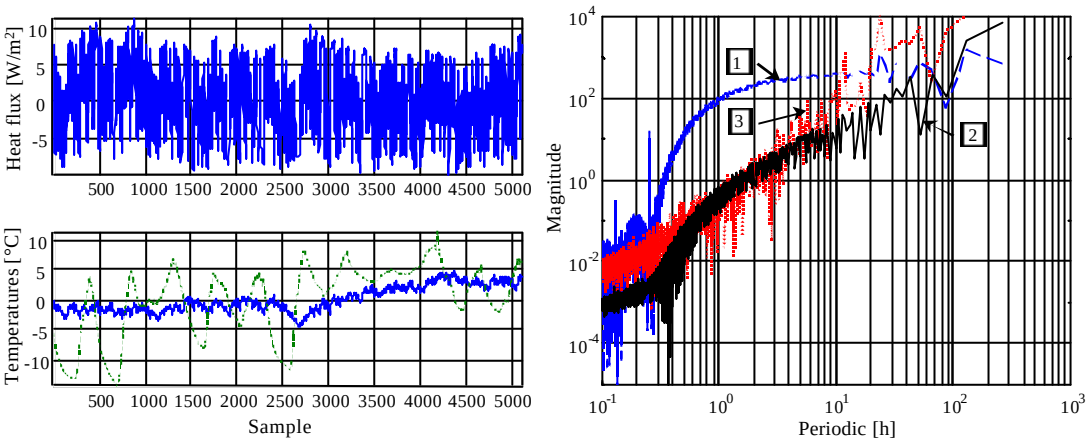

Figure 8: <u>To the left</u>: Measured heat flux and temperatures at the wall surfaces (external dashed, internal filled). The mean value of each series has been subtracted. <u>To the right</u>: Power spectrum of heat flux [1], internal surface temperature [2] and external surface temperature [3].

5.1.3 Measured results in comparison with analytical results

A couple of results are shown here, but there are more in the paper 3. First, some notations will be defined. The effective heat capacities that are calculated from measured data are denoted by c_0^* and $c_{A/B}^*$ as defined in equation 21.

$$c_0^* = \left| -\frac{\tilde{q}_0}{\tilde{q}_0} \right| \Big/ w; \qquad c_{A/B}^* = \left| -\frac{\tilde{q}_0}{\tilde{q}_0} + \frac{1}{B} \cdot \frac{\tilde{q}_n}{\tilde{q}_0} \right| \Big/ w; \tag{21a}$$

The first measured effective heat capacity, c_0^*, is the actual effective heat capacity of a building component in natural conditions, and is a direct application of the definition of admittance. The second type, $c_{A/B}^*$, has a compensation for dynamic transmittance as to make this measured entity directly comparable with the analytical entity $c_{A/B}$, which is calculated with the assumption that $\tilde{q}_n = 0$. The analytical value, $c_{(A-1)/B}$, calculated with the assumption that $\tilde{q}_n = \tilde{q}_0$ is also shown in figures. The analytical heat capacities are defined as

$$c_{A/B} = \left|\frac{A}{B}\right| \Big/ w; \qquad c_{(A-1)/B} = \left|\frac{A-1}{B}\right| \Big/ w \tag{21b}$$

The deviations of measured values are related to the analytical value, such that

$$d_0 = \left(c_0^* - c_{A/B}\right) \Big/ c_{A/B}\ ; \qquad d_{A/B} = \left(c_{A/B}^* - c_{A/B}\right) \Big/ c_{A/B} \tag{22}$$

Figure 9 shows the measured and analytical effective heat capacities. The results are quite typical for other measurement locations: a noisy measured curve is situated somewhat lower than the theoretical curves. The data has in this case been sampled in a rectangular window.

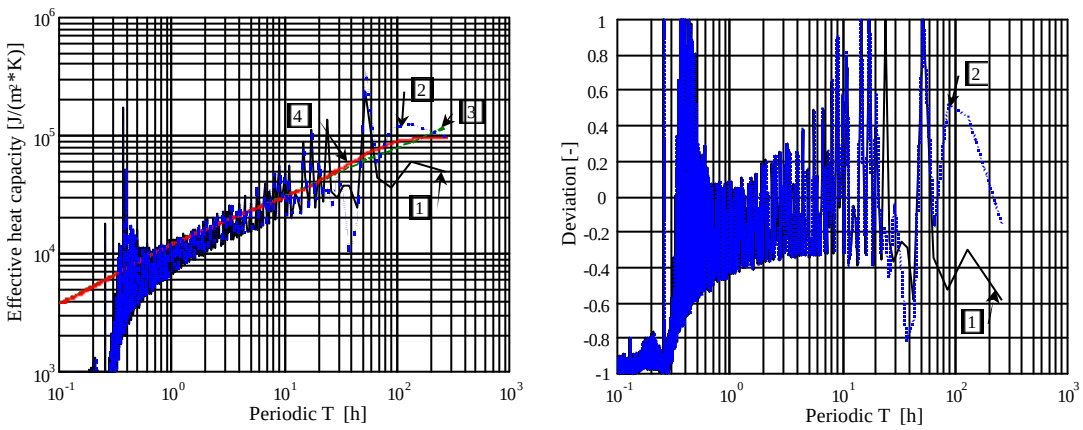

Figure 9: Results from the external wall based on data sampled from a rectangular window. <u>To the left:</u> Measured effective heat capacities c_0^* [1] and $c_{A/B}^*$ [2] (equation 21a), analytical effective heat capacities $c_{A/B}$ [3] and $c_{(A-1)/B}$ [4](equation 21b). <u>To the right</u>: Deviation between experimental and theoretical values, d_0 [1] and $d_{A/B}$ [2] (equation 22).

On sampling the data in a Hanning window (Ramirez 1985), the measured results change form since the Hanning window has the effect of ”smoothing” frequency data.

The curves of figure 10 are actually quite representative for results obtained for other components and measurement points. At high frequencies, it is typical for the deviation curves to be situated in the regions of -40%. As period increases, deviation steadily approaches zero at the periodicity of around 10 to 20 hours. For longer periods, the measurement values oscillate with large magnitudes in an irregular fashion around the zero deviation line.

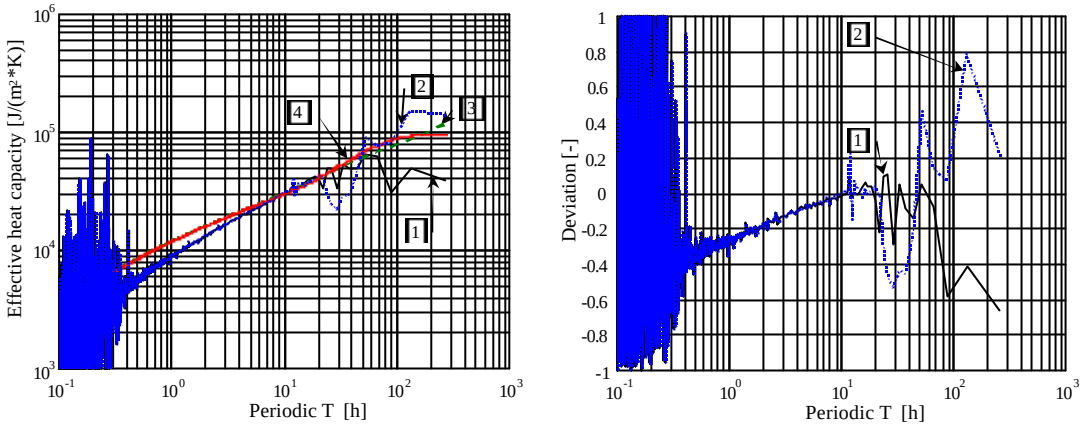

Figure 10: Results from the external wall based on data sampled from the Hanning window. <u>To the left</u>: Measured effective heat capacities c_0^* *[1] and* $c_{A/B}^*$ *[2](equation 21a) and analytical effective heat capacities* $c_{A/B}$ *[3] and* $c_{(A-1)/B}$ *[4] (equation 21b). <u>To the right</u>: Deviation between experimental and theoretical values,* d_0 *[1] and* $d_{A/B}$ *[2] (equation 22).*

5.1.4 Reasons for deviation in analytical and experimental results

These deviations can be explained. The systematic deviations at higher frequencies (below some 10 hour periodic) are mainly due to the heat flux sensor. Two finite difference programs calculating in the frequency domain were produced, using the calculation procedure as proposed by Andersson and Jóhannesson (1983). The first program models a homogeneous round slab placed on the surface of a cylindrical building component section. Calculations were performed as to determine how the circular sensor distorts heat flux at the wall surface. The second finite difference program, with Cartesian co-ordinates, models the central sensitive parts of a heat flux sensor composed of half-plated wound wire thermopiles. The temperature difference across the sensor is measured at the junction of the plated and non-plated part of the wire. Calibration is made at stead-state, and the heat flow through the sensor is directly proportional to the temperature difference. However, under the influence of dynamic processes, heat waves will be transmitted faster through the wire than through the plastic filling. The measured temperature difference will not conform to the heat flow through the sensor.

Some of the results from simulations are plotted in figure 11. The deviation is defined on basis of the "measured" heat flux in relation to the heat flux at an undisturbed section of the wall, such that

$$e = \frac{|\tilde{q}_{measured}| - |\tilde{q}_{wall}|}{|\tilde{q}_{wall}|} \tag{23}$$

Note that the design of the heat flux sensors that were used were not know; the results of figure 11 are based on a hypothetical design with exception to material properties, wire diameter and sensor thickness. However, the results indicate that the magnitude of effective heat capacity deviations in the previous section are of the order that may be expected for a heat flux sensor in dynamic conditions. Therefore, it is the influence of the measurement organ itself, the thermopile, that leads to the systematic deviations below frequencies corresponding to the 10 to 20 h periodic. Also note that other sources of inaccuracies, such as calibration inaccuracies (±5%), are not taken into consideration.

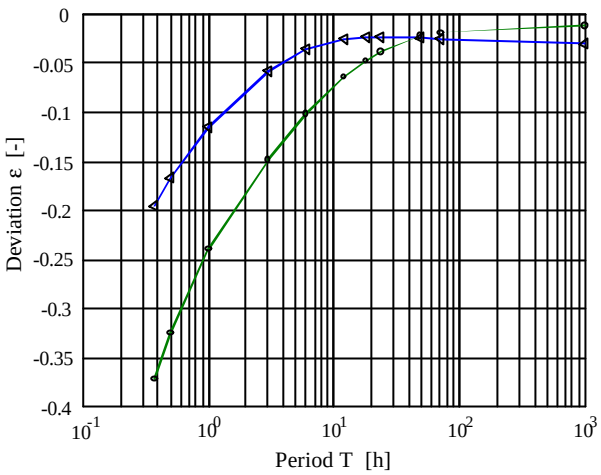

Figure 11: The two curves displays simulated deviation e *(equation 23) between "measured" heat flux and heat flux at an undisturbed wall surface. The curve with triangles displays results from a circular homogeneous slab composed of polyurethane, which is a common sensor filling material. The curve with rings shows results from a simulated central section of a heat flux sensor that contains constantan wire (the thermopile). Thus, the thermopile itself stands for a substantial part of deviations.*

The discrepancies at wave lengths larger than some 10 hours can be motivated by what is happening at the external surface. The phase shift in temperature oscillations (or thermal transmittance) has an impact on the effective heat capacity. However, this is not the whole truth, because a better agreement would be expected between compensated measured values and analytical values, as evaluated by $d_{A/B}$. The reason is the handling of measured data with FFT.

FFT assumes a periodicity in the sampled window: this window repeats itself in time. This means that the value at the start of the series should be the same as the last value of the series. For this to be possible, all frequencies within the window have to be integer multiples of the fundamental periodic, which is the length of the window. This is difficult to achieve in field measurements. If one or several frequency components are not integer multiples of the fundamental frequency, the use of FFT will lead to leakage (Ramirez 1985). Leakage occurs in the power spectrum, where the energy of one frequency component leaks to neighbouring frequencies. A problem is that the frequencies in the internal environment (the frequencies of the PRBS), which are used within the calculations, are not identical to frequencies present in the external environment. The energy of the frequencies present in the external environment will be distributed (leak) among the frequencies used in the calculations. In turn, the leakage at lower frequencies of the external environment may give rise to erroneous dynamic transmittance.

5.2 The approximate method

A new approximate method has been developed to determine the effective heat capacity of a multilayer building component, with definition based on the surface heat capacity model. In this method, only real numbers are used within the calculations, and these are founded on the thermal properties and thickness of the material layers. The new method gives more accurate results over a wider range of frequencies than the approximate methods of normative Annex A of prEN ISO 13786 (1998). A drawback is that the new method requires more work to produce the results than that of prEN ISO 13786. On the other hand, experience indicates that the inaccuracy seldom is larger than some 15 % and commonly less than 10 %. The approximate methods of prEN ISO 13786 give values that can have larger discrepancies than 50%, which makes any calculations with this method less worthwhile. Calculations with the new method require calculators, spreadsheet programs or mathematical programs that do not handle complex numbers.

The method is stated here, but the reader is advised to view Paper 2 for examples on application.

The new approximate method

The method consists of 5 calculation steps in junction with three tables. The first table lists the nomenclature of symbols used in the calculation procedure.

TAB. 1: Nomenclature and definitions.

Symbol	Unit	Comments
j	Index	Layer number. *1* is the internal surface material, *n* the external surface material.
d_j	m	Thickness of material layer *j*.
λ_j	W/(m·K)	Thermal conductivity of material layer *j*.
ρ_j	kg/m^3	Density of material layer *j*.
c_j	J/(kg·K)	Specific heat capacity of material layer *j*.
R_j	m^2·K/W	Thermal resistance of material layer *j*, $R_j = d_j / \lambda_j$
κ_j	J/(m^2·K)	Heat capacity of material layer *j*, $\kappa_j = d_j \cdot \rho_j \cdot c_j$
b_j	W·$\sqrt{s}$ /(m^2·K)	Thermal effusivity of material layer *j*, $b_j = \sqrt{\lambda_j \cdot \rho_j \cdot c_j}$

1. Acquire material data (λ_j , ρ_j and c_j) and geometry (d_j) of each material. Calculate R_j , κ_j and b_j for each layer *j*. Choose the time period T for which the areic heat capacity is to be calculated. The angular frequency ω (s^{-1}) is given by

$$\omega = 2\pi / T \tag{24}$$

2. Determine the maximum areic heat capacity κ_{c0} for the considered surface according to

$$\kappa_{c0} = \frac{1}{R_t} \cdot \left[\sum_{j=1}^{n} \kappa_j \left(\frac{R_j}{2} + \sum_{k=j+1}^{n+1} R_k \right) \right], \quad R_{n+1} = 0 ; \quad R_t = \sum_{j=1}^{n} R_j \tag{25}$$

3. Calculate the effective thickness d_{eff} by means of κ_{c0} . The number of layers x at the inner side of the adiabatic plane is established.

$$\kappa_{c0} = \sum_{j=1}^{x} \rho_j \cdot c_j \cdot d_j \text{ such that } \sum_{j=1}^{x} d_j = d_{eff} \tag{26}$$

The thickness of layer x can be adjusted to the length $d_{eff} - \sum_{j=1}^{x-1} d_j$.

4. Calculate time period values T_1 and T_2 (T_2 is omitted for slabs) according to

$$T_1 = 2\pi \cdot R_1 \cdot \kappa_1 \text{ and } \qquad T_2 = 4\pi \left[\frac{1}{b_2} \cdot \frac{(\kappa_1 + \kappa_2)^2 - \kappa_1^2}{\kappa_1 + \sqrt{2(\kappa_1 + \kappa_2)^2 - \kappa_1^2}} \right]^2 \tag{27}$$

Selection of formula for κ_c is based on fulfilment of criteria for the size of d_{eff} , T_1 and T_2 in TAB. 2.

5. Calculate κ_c . If κ_c is greater than κ_{c0} , then κ_c is set equal to κ_{c0} .

TAB. 2: Condition on the effective thickness and time period range of validity that gives the formula number for TAB. 3.

Condition nr	Condition on d_{eff}	Condition on T_1 and T_2	Select formula
1	$d_{eff} \le d_1$	$T < 2\pi \cdot \rho_1 \cdot c_1 \cdot d_{eff}^2 / \lambda_1$	Formula 1
2	$d_{eff} \le d_1$	$T \ge 2\pi \cdot \rho_1 \cdot c_1 \cdot d_{eff}^2 / \lambda_1$	Formula 4
3	$d_{eff} > d_1$	$T < T_1$ and $T_2 > T_1$	Formula 1
4	$d_{eff} > d_1$	$T_1 < T < T_2$	Formula 2
5	$d_{eff} > d_1$	$T_2 < T_1$ and $T < T_1$	Formula 1
6	$d_{eff} > d_1$	$T_2 < T_1$ and $T \ge T_1$	Formula 3
7	$d_{eff} > d_1$	$T_2 > T_1$ and $T > T_2$	Formula 3

TAB. 3: Table for determination of the effective heat capacity. Formula number is given by condition fulfilment in TAB. 2.

Formula nr	Effective heat capacity κ_c	Max value
1	$\kappa_c = b_1 / \sqrt{\omega}$	κ_{c0}
2	$\kappa_c = \sqrt{\dfrac{\omega \cdot \kappa_1^2 + \kappa_1 \cdot b_2 \sqrt{2\omega} + b_2^2}{\omega\left(1 + R_1 \cdot b_2 \sqrt{2\omega} + R_1^2 \cdot b_2^2 \cdot \omega\right)}}$	κ_{c0}
3	$\kappa_c = \sqrt{\dfrac{b_3^2\left(1 + (\omega \cdot R_2 \kappa_1)^2\right) + b_3 \sqrt{2\omega}(\kappa_1 + \kappa_2)(1 + \omega \cdot R_2 \kappa_1) + \omega(\kappa_1 + \kappa_2)^2}{\omega\left(1 + b_3^2 \cdot \omega(R_1 + R_2)^2 + b_3 \sqrt{2\omega}(R_1 + R_2)(1 + \omega \cdot R_1 \kappa_2) + (\omega \cdot R_1 \kappa_2)^2\right)}}$	κ_{c0}
4	$\kappa_c = \kappa_{c0}$	κ_{c0}

5.3 EN832 - A calculation method that makes use of the effective heat capacity

The European standard EN832 states a calculation procedure for determining the heating requirement of a residential building. The traditional steady-state heat balance of the building is used, but the standard introduces the so-called utilisation factor, which indicates the part of heat gains that are actually useful in terms of relieving the heating system from compensating for all heat loss. The utilisation factor is a function of the ratio between heat gains and heat loss, and the time constant of the building. Being the ratio between the total effective heat capacity and the heat loss factor of the building, the time constant is a quantification of thermal inertia. The calculation method of EN 832 is, in a sense, an application of the simplest of dynamic models: the effective heat capacity.

In paper 5, three building simulations programs were used to determine the influence of the thermal inertia on the heating requirement of a building situated in Stockholm. The detailed multi-zone building simulation programs TSBI3 (Johnsen and Grau 1994) and BRIS (Brown 1990) were used, and the far simpler calculation procedure of the proposed European standard prEN832 (at the time of paper review, the proposed standard was approved). The simulated object was a two-storey multi-family building, but several parameters were varied within the simulations. With the criterion that the heat loss factor was constant, the materials used in the building components were changed as to give the building different thermal inertia (see paper 5). Therefore, three building types were created, called the lightweight, the massive wood and the heavyweight building. In another simulation case, double-glazed windows substituted triple-glazed windows as to increase the heat loss factor and solar gains.

The results of the TSBI3 and EN832 runs are comparable since the simulated objects were the same (unlike the modelled object in BRIS). Results as shown in tables 5 and 6 indicate that heavyweight buildings require less bought heat than lightweight buildings.

Table 5: Results from TSBI3 and EN 832 calculations: bought energy per square meter floor (kWh/m^2) for the three building types as well as deviations of EN 832 results related to TSBI3 results.

Building type	Lightweight	Massive wood	Heavyweight
TSBI3 Triple-glazed	43.4 (100%)	39.5 (91%)	37.5 (86%)
EN 832 Triple-glazed	44.5 (100%)	39.1 (88%)	36.5 (82%)
Deviation Triple-glazed	2.5%	-1.0%	-2.7%
TSBI3 Double-glazed	46.5 (100%)	44.0 (95%)	42.8 (92%)
EN 832 Double-glazed	50.3 (100%)	44.6 (89%)	41.8 (83%)
Deviation Double-glazed	8.2%	1.4%	-2.3%

Table 6: The difference in specific bought energy (kWh/m^2) for a building type with triple-glazing and with double- glazing. The tendencies of EN 832 and TSBI3 are in conflict.

Building type	Lightweight	Massive wood	Heavyweight
TSBI3 – Difference	3.1	4.5	5.3
EN 832 – Difference	5.8	5.5	5.3

The results of this study show a good agreement between TSBI3 and EN832. A small issue of concern should however be directed to the tendencies that EN832 for the cases with double-glazed window, but nevertheless the results are in good agreement.

However, there is a matter that should be pointed out at this stage. The definition of effective heat capacity that was used in those calculations was as suggested in the draft version of prEN ISO 13786, in which the internal surface thermal resistance was included, with the effect that the value of effective heat capacity was reduced in comparison to later suggested definitions. Keeping in mind that the EN832 probably is ”calibrated” in accordance to this early definition; results with later definitions will give lower heating requirement.

Another aspect is how the time constants of the building vary with the later definitions. The Newtonian time constants calculated using BRIS differed radically from the periodic time constant, as pointed out in paper 5, much due to that these are differently defined, though the simulated objects were not identical. However, with the elimination of the surface thermal resistance from the definition of effective heat capacity, the periodic time constant increases dramatically for ”heavier” buildings.

In the opinion of this author, it was correct to eliminate the surface thermal resistance from the definition, primarily for two reasons. The first is a physical aspect. Solar irradiation stands for a substantial part of the heat gains in a building: this radiation does not pass through surface thermal resistances. The second reason is more a practical issue, and first a comparable example will be given. The U-value of a building component is calculated by inverting the sum of the thermal resistance of the building component and the internal and the external surface thermal resistance. The thermal resistance of the component can be calculated by inverting the U-value and subtracting the standard values of the surface thermal resistances. The thermal resistance is independent of material layer order. Now, the effective heat capacity is a real number, based on complex numbers, where “backward” calculations of the former type cannot be applied. If the surface thermal resistance is included in the definition, there is no means of solving what the effective heat capacity would have been without the surface thermal resistance.

6 Thermal models

A large number of building simulations exists, commercially available as well as research tools with limited availability. A list of some of these programs can be found in (Lomas et al 1997) and (Sahlin 1996). Building components within these programs are modelled in a number of different ways, where some of the most common ones are by means of response factor methods or finite difference methods. These methods can also be used as implementations of stand-alone programs.

The work that is currently presented is an application of the finite difference method and RC-networks, though there is no self-evident border that separates these methods apart. First, chains of thermal resistances and heat capacities in general will be treated, and how cell configuration influences the thermal performance of the model.

6.1 The heat transfer matrix of serially connected thermal resistances and heat capacities

The product of the heat transfer matrix of each model component can establish the thermal performance of chain, where each model component is modelled as a material layer. A purely resistive layer with the thermal resistance R has a heat transfer matrix expressed as

$$\begin{bmatrix} 1 & -R \\ 0 & 1 \end{bmatrix} \tag{28}$$

A purely capacitive layer with the heat capacity c has the following heat transfer matrix (Johannesson, 1981):

$$\begin{bmatrix} 1 & 0 \\ -iwc & 1 \end{bmatrix} \tag{29}$$

The sequential product of the chains' components determines the heat transfer matrix of the model as a whole. When the heat transfer matrix has been established, model admittance and dynamic transmittance can be calculated and compared with analytical admittance and dynamic transmittance. This procedure can be used to give a quality assurance as to how well a chain models the thermal behaviour of a building component. If the thermal performance of the model is poor, it may be wise to go farther with the discretisation and choose a finer mesh.

6.2 Finite difference method

Finite difference models (FDMs) are commonly based on a discretisation of material layers into cells. The cell can contain a mass node or two, at which the representative temperature of the cell or cell parts, are calculated. Mass nodes are coupled by means of thermal resistances (or conductances). The cell configuration can be formulated in two ways. One, the central capacity cell (CCC), is such that the thermal mass (heat capacity) of the cell is placed in the geometric centre of the cell, between two halves of the thermal resistance of the cell. The other, the edge capacity cell (ECC), has the thermal mass divided into two halves. Each half is placed at the cell boundary adjacent to the thermal resistance of the cell. The two cell types are illustrated in figure 12.

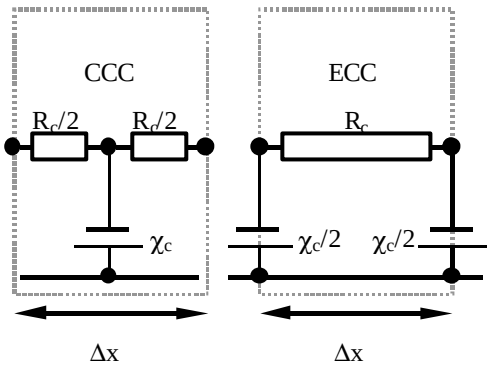

Figure 12: Two different types of cell configurations that model heat flow in one dimension. To the left: Central Capacity Cell (CCC). To the right: Edge Capacity Cell (ECC). R_c is the thermal resistance and c_c is the heat capacity of the cell.

The use of finite difference methods assumes that a building component is discretised into many cells. A model composed of many cells (mass nodes) give small model inaccuracy, but has the draw-back that the model requires more computational memory and that smaller simulation time steps have to be taken, certainly with the explicit forward finite difference method. The explicit forward method involves a heat balance at every node, where the new node temperature is solved after the time step Δt on basis of the temperatures prior to the time step. There is a mathematical limitation to how large the time step can be. This is the stability time step Δt_{stab} (Eftring 1990), which is dependent on mass node number *j* with heat capacity c_j and the adjacent thermal resistances R_j and R_{j+1} such that

$$\Delta t_{stab,\ j} = \frac{c_j}{\dfrac{1}{R_j} + \dfrac{1}{R_{j+1}}} \tag{30}$$

In a simulation, the shortest time step should be less than the smallest stability time step among the mass nodes.

6.2.1 Modelling the response of the semi-infinite solid

At higher frequencies, depending on the surface material thickness and thermal properties, the component will have the response of the semi-infinite solid. The response converges to the value

$$Y_0 = -\sqrt{\frac{l_1 \cdot r_1 \cdot c_1 \cdot w}{2}}(1+i) \tag{31}$$

Index *1* depicts the material layer at the interior surface of the building component. Independent of boundary conditions at the external surface, a rule of the thumb is that this type of response applies to time periods that are shorter than

$$T < 2p \cdot R_1 \cdot c_1 \tag{32}$$

The semi-infinite response cannot be modelled with a pure resistance or heat capacity as model surface component. Only a chain of at least two resistances and two heat capacities will model this response for a limited range of frequencies. With more mass nodes, discretised according to the traditional method, lower frequency response is well modelled. Therefore, it is actually the first two model surface components, the thermal resistance and the heat capacity, which can be used to determine at what frequency the model performance becomes inaccurate.

In order to set up a discretisation (cell size) based on inaccuracy rather than on simulation time steps, the admittance asymptote of the response of the semi-infinite solid is used along with the simple RC-configuration. Asymptotic admittance is set equal to the admittance of the simple RC-configuration.

$$\sqrt{\frac{\lambda_1 \cdot \rho_1 \cdot c_1 \cdot \omega}{2}}(1+i) = \frac{i\omega C}{1+R \cdot i\omega C} \tag{33}$$

On solving for R and C, these obtain the following values:

$$R = \frac{1}{\sqrt{2 \cdot \lambda_1 \cdot \rho_1 \cdot c_1 \cdot \omega}}; \qquad C = \sqrt{\frac{2 \cdot \lambda_1 \cdot \rho_1 \cdot c_1}{\omega}} \tag{34}$$

The effective penetration depth for R ($R = d_R / \lambda_1$) and C ($C = \rho_1 \cdot c_1 \cdot d_c$) are respectively

$$d_R = \sqrt{\frac{a_1}{2\omega}}; \qquad d_c = \sqrt{\frac{2a_1}{\omega}} \tag{35}$$

a_1 depicts thermal diffusivity. d_c is what is commonly known as the periodic penetration depth. Note that d_R is half the value of d_c. When using the central capacity cell, this is true since the length that each resistance is calculated from is in essence half the cell length, whereas the heat capacity is based on the whole cell length. Therefore, d_c is the largest cell size that can model this admittance at the periodicity T (corresponding to ω). Now, the periodicity T can be related to the stability time step. On assuming that the slab is equidistantly discretised, the smallest stability time step is found at the mass node at the surface, having the value corresponding to

$$\Delta t_{stab} = \frac{C_1}{\frac{1}{R_1} + \frac{1}{2R_1}} = \frac{d^2}{3 \cdot a_1} \tag{36}$$

By setting $d = d_c$, and inserting equation 35 above, the relationship between the stability time step and the periodicity is

$$T = 3\pi \cdot \Delta t_{stab} \tag{37}$$

In paper 1, a similar equation was obtained by using asymptotic values of admittance, and is more of an approximation. It differs from equation 37, as it is half of this value.

Another interesting aspect is the application of the Nyquist theorem (see for example Ramirez 1985), that states that the smallest period that contains information of a long-term process are twice the sampling period. In a simulation, the Nyquist period T_{Ny} is twice the simulation time step. If the simulation time step is almost equal to the stability time step, then

$$T_{Ny} \approx 2 \cdot \Delta t_{stab} \tag{38}$$

On inserting Δt_{stab} into equation 37, the outcome becomes

$$T = \frac{3\pi}{2} \cdot T_{Ny} \tag{39}$$

6.3 The ORC Method

Whereas the procedure on finite difference discretisation previously mentioned has a variable amount of nodes depending on material layer property and order, RC-networks allow a certain flexibility that has advantages over the traditional finite difference method. The finite difference method has the following advantages and disadvantages:

- The total thermal resistance and the total heat capacity of the building component are fully represented in the model. Therefore, model thermal performance gives good agreement with analytical performance at low frequencies.
- Thermal performance is commonly independent boundary conditions.
- The model is easy to implement.
- Cell size may be constricted by material layer thickness that may result in short simulation time steps, such as for steel sheets. However, the simulation time step depends on the method of solving the sets of algebraic- and differential equations.
- The model may result in many cells, thus occupying computational resources and run time. The number of nodes may be reduced with use of a performance deviation procedure (see below).

The RC-network is a type of finite difference method, but the determination of values of thermal resistances and heat capacities (i.e. cell size) are handled in a different manner. On the other hand, the very simplest models may be called RC-networks since these are more or less lumped parameter models.

The RC-network method has the following advantages and disadvantages:

- The parameters within the RC-network can be optimised for certain frequency ranges: in some cases giving the exact analytical solution.
- The total thermal resistance is fully represented in the model. However, the total heat capacity of the model does not need to be complete, as only ”effective” parts need to be modelled.
- The parameters are not material layer thickness dependent as cell size may be in the conventional finite difference technique.
- The optimisation procedures may be difficult to establish and to implement for RC-networks composed of may components. The reason is that there are very many degrees of freedom.
- Equivalent RC-networks can be made for modelling multi-dimensional heat transfer.

A major difference between RC-networks and the conventional finite difference model is that RC-networks are optimised given a fixed configuration (a constant number of nodes) whereas in the finite difference model, the number of nodes is variable. However, a calculation procedure can be done for an RC-network with a variable amount of nodes.

6.3.1 Model deviation procedure

The analytical solution of the heat conduction equation, equations 3-5, allows for the calculation of the analytical thermal performance of a building component, given material layer properties and thickness. These equations can be used for detailed and precise simulations by means of the super position principle see for example Anderlind (1997). At times, it is necessary to perform simulations in the time domain, for example if the thermal processes are non-linear, or if simulation time steps are variable. The use of finite difference models or RC-networks are a way of modelling building components. In the same manner as in experimental analysis, it is customary to study inaccuracies of results of thermal processes that are discrete in time and space, only that within simulations it is done on calculated results. The inaccuracy of the thermal performance of a model is valuable to know, prior to the simulation calculations in which the model is to participate. For this reason, an inaccuracy estimation procedure was developed (Akander 1995 and 1996) and applied by Mao (1997), see paper 1. The deviation of performance in terms of admittance, e_{Y0}, is defined as

$$e_{Y0}(w) = \left| \frac{Y_{0model} - Y_{0analyt}}{Y_{0analyt}} \right|_w \tag{40}$$

The nominator of the formula is the difference in analytical and model admittance. It is a sinusoidal entity. In words, this is the difference in heat flux in time given that the temperature oscillation is the same at the surface of the component and at the surface node of the model. Now, the nominator is divided by the analytical admittance and the absolute value is taken for the whole expression. This means that the magnitude of the difference is divided by the magnitude of the analytical admittance. It gives the maximal deviation that the model has for a given frequency. The same treatment can be applied to dynamic thermal transmittance by substituting the variable Y_0 with T_D.

This procedure can be used to evaluate the discretisation of a building component into a finite difference model prior to a simulation. If the inaccuracy of a model is too large in comparison to a desired value, the model can be re-discretised into more cells until the level of inaccuracy is acceptable. An application of this is made in paper 4, where several building components were subjected to a fine and a cruder discretisation.

Moreover, this procedure can be used to optimise the thermal performance of RC-networks. This subject is also treated in paper 4, where the thermal performance of a given RC-configuration is optimised for a range of frequencies, by finding suitable values for thermal resistances and heat capacities within the model.

6.3.2 Optimisation of RC-networks

The term ”optimisation” has within this context the meaning that the values of thermal resistances and heat capacities within the model are determined as to give a minimal deviation for a set of pre-chosen frequencies. Other authors have used this concept, for example Davies (1983). Davies used a least-squares method to minimise the deviation between transfer matrix elements of the model and the analytical solution as to determine the values of RC-networks.

The basis for the ORC method presented below is the T-chain, with the configuration as shown in figure 13. The T-chain allows admittance and transmittance to be approximated. In order to determine values, three equations have to be found. These are the real and the complex part of admittance for one frequency and the important steady state transmittance. The latter equation is that $R_{11} + R_{12} = R_t$. The heat transfer matrix, along with the boundary conditions, give the equations such that

$$\begin{bmatrix} 0 \\ \tilde{q}_1 \end{bmatrix} = \begin{bmatrix} 1 & -R_{12} \\ 0 & 1 \end{bmatrix} \begin{bmatrix} 1 & 0 \\ -i\omega c_1 & 1 \end{bmatrix} \begin{bmatrix} 1 & -R_{11} \\ 0 & 1 \end{bmatrix} \begin{bmatrix} \tilde{q}_0 \\ \tilde{q}_0 \end{bmatrix} \tag{41}$$

$$R_{12} = 1 \Big/ \mathrm{Re}\left(\frac{1}{R_t + 1/Y} \right); \qquad c_1 = 1 \Big/ R_{12}^2 \cdot \omega \cdot \mathrm{Im}\left(\frac{1}{R_t + 1/Y} \right) \tag{42}$$

The T-chain models admittance with the performance of a simple mass very well. Dynamic transmittance is poorly modelled.

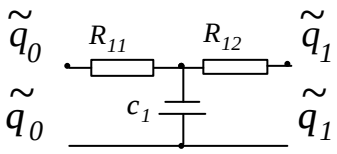

Figure 13: The T-chain is composed of two thermal resistances and one heat capacity.

The 5-node ORC is composed of two sets of parallel T-chains, which are connected by means of a central heat capacity. This heat capacity can be situated at the at the adiabatic plane of the building when the boundary conditions are assumed to be $\tilde{q}_n = \tilde{q}_1$, or in the middle as to give equal thermal

resistances on each side. Both assumptions work, but the first is preferred, since it gives possibility of modelling internal walls within the frame of building simulation programs.

Admittance is now optimised with respect to one side of the adiabatic plane, see figure 14. The heat transfer matrix for the parallel T-chains on one side of the component can be expressed as

$$\frac{B_1 \cdot B_2}{B_1 + B_2}\begin{bmatrix} \left(\frac{A_1}{B_1}+\frac{A_2}{B_2}\right) & 1 \\ \left(\frac{A_1}{B_1}+\frac{A_2}{B_2}\right)\left(\frac{D_1}{B_1}+\frac{D_2}{B_2}\right)-\left(\frac{B_1 \cdot B_2}{B_2+B_2}\right)^2 & \left(\frac{D_2}{B_2}+\frac{D_2}{B_2}\right) \end{bmatrix} \tag{43}$$

Index *1* represents parameters of the upper T-chain in the parallel circuit on the left-hand side of figure 6; index *2* is for the lower T-chain. On observing the first element of the matrix, A_1/B_1 is the admittance of the upper T-chain and the other term is admittance of the lower T-chain. In a computational iterative loop, the upper T-chain can be determined for a high frequency corresponding to ω_1, whereas the lower chain is calculated for a lower frequency, ω_2. For example, the admittance of the component $Y_0(\omega_1)$ is the sum of $Y_1(\omega_1)$ and $Y_2(\omega_1)$. Now, given the parameters of the lower circuit, $Y_2(\omega_1)$ is known and leaves the possibility of determining the admittance of the upper circuit, $Y_1(\omega_1)$. The equations for the two T-chains are therefore expressed as

$$Y_1(\omega_1) = Y_0(\omega_1) - \frac{1 + R_{22} \cdot i\omega_1 c_2}{-R_{t2} - R_{21} \cdot R_{22} \cdot i\omega_1 c_2}\ ; \tag{44a}$$

$$Y_2(\omega_2) = Y_0(\omega_2) - \frac{1 + R_{12} \cdot i\omega_2 c_1}{-R_{t1} - R_{11} \cdot R_{12} \cdot i\omega_2 c_1} \tag{44b}$$

These two equations have to be solved with iterations (normally 15 steps are enough), and suitable initial values are calculated from

$$Y_1(\omega_1) = Y_0(\omega_1); \qquad Y_2(\omega_2) = Y_0(\omega_2) \tag{45}$$

Admittances $Y_1(\omega_1)$ and $Y_2(\omega_2)$ are used for determining the values of the parameters within each T-chain, such as

$$R_{12} = 1\Big/ \mathrm{Re}\left(\frac{1}{R_{t1} + 1/Y_1(\omega_1)}\right); \quad R_{11} = R_{t1} - R_{12}\,;$$
$$c_1 = 1\Big/ R_{12}^2 \cdot \omega_1 \cdot \mathrm{Im}\left(\frac{1}{R_{t1} + 1/Y_1(\omega_1)}\right) \tag{46a}$$

$$R_{22} = 1\Big/ \mathrm{Re}\left(\frac{1}{R_{t2} + 1/Y_2(\omega_2)}\right); \quad R_{21} = R_{t2} - R_{22}\,;$$
$$c_1 = 1\Big/ R_{22}^2 \cdot \omega_2 \cdot \mathrm{Im}\left(\frac{1}{R_{t2} + 1/Y_2(\omega_2)}\right) \tag{46b}$$

The total thermal resistances of each T-chain are assumed to be equal, $R_{t2} = R_{t1}$. When the parameters of the T-chains on both sides of the adiabatic plane have been optimised and saved, the two model halves are linked together by the central capacity c_5, which has the value that gives the model the total heat capacity of the building component. The optimised parameters of each side are found when the set of parameters gives the smallest values for e_{Y0} and e_{Yn}, respectively. The time period vector for which the deviations are calculated from has integer values [1, 2, …, 9, 10, 20, …, 90, 100, 200, …, 900, 1000,

1100, …, 1600] hours, and the deviation for each period is summed. These periods can, of course, be alter as to weight periods that are reckoned to be important.

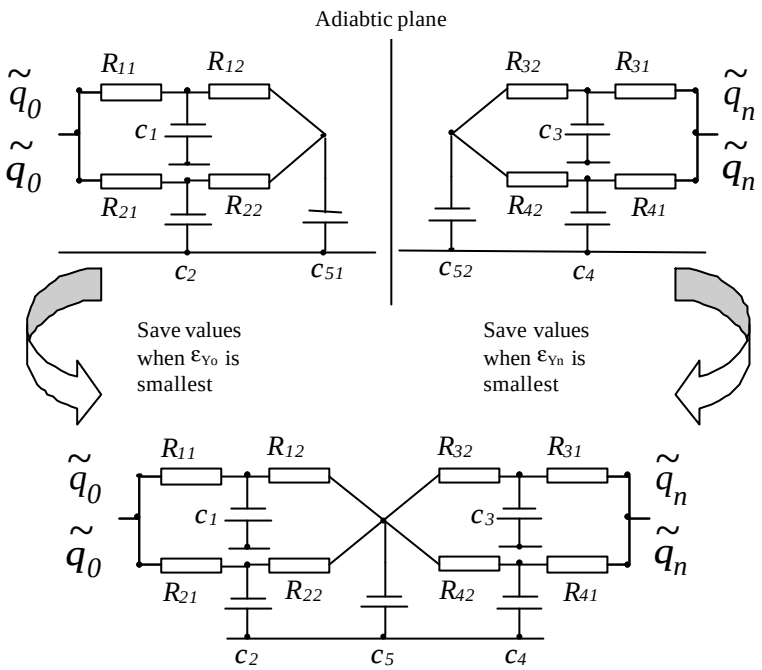

Figure 14: Schematic illustration of how a 5-node ORC is optimised.

To illustrate what type of results are obtained, an external wall with the layer properties as listed in table 7 is modelled (from paper 4). Tables 8 and 9 display the values of each model component after optimisation.

Table 7: Layer thickness and material properties of an external sandwich wall .The layers are of light expanded clay aggregates (LECA), expanded polystyrene (EPS) and mortar, giving the U-value 0.219 W/(m2·K).

Material layer	d [m]	λ [W/(m·K)]	ρ [kg/m^3]	c [J/(kg·K)]
Mortar	0.01	1.00	1800	950
LECA LK8	0.1	0.30	1050	1020
EPS	0.15	0.039	30	1300
LECA LK5	0.05	0.25	1000	1050
Mortar	0.02	1.00	1800	950

Table 8: Values for thermal resistances (m^2·K/W) of the ORC from modelling the component of table 7.

R_{11}	R_{12}	R_{21}	R_{22}	R_{31}	R_{32}	R_{41}	R_{42}
0.0096	0.7285	0.1267	0.6114	0.0094	8.0715	0.1002	7.9807

Table 9: Values for heat capacities (J/m^2·K) of the ORC from modelling the component of table 7.

χ_1	χ_2	χ_3	χ_4	χ_5
26017	48411	33476	53864	54528

The results on model thermal performance are plotted in the Bode diagram of figure 15, and deviations are shown in figure 16. As seen, the 5-node ORC is capable of modelling admittance well, whereas the agreement of dynamic transmittance is worse.

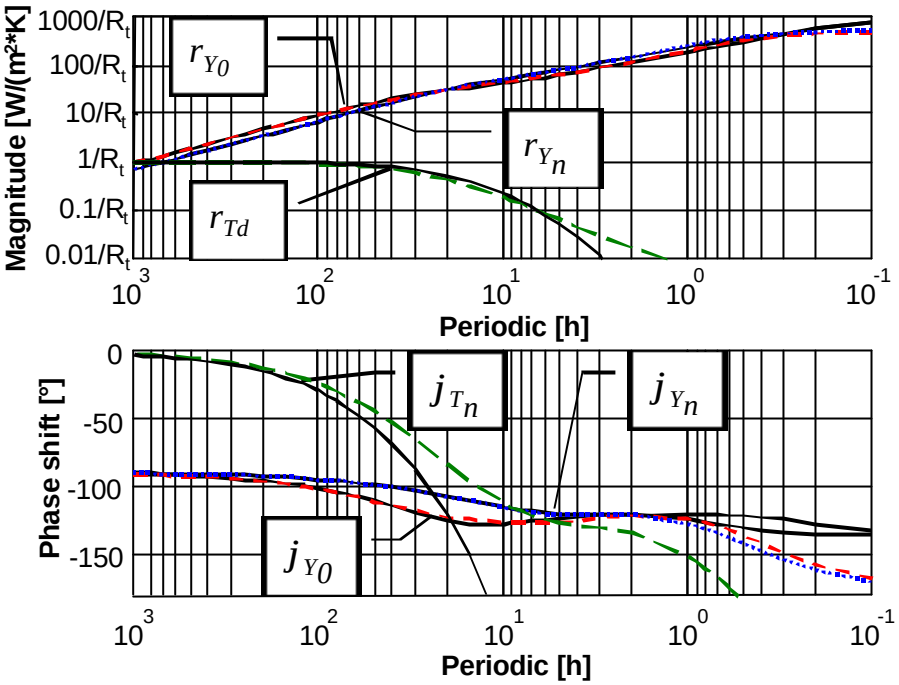

Figure 15: The Bode diagram of the external wall of table 7 as modelled by the 5-node ORC. Admittances are plotted for the boundary condition $\tilde{q}_n = \tilde{q}_0$. *The long dashed curves depict modelled dynamic transmittance, the short dashed curves represent admittance of the interior surface and the dotted curves admittance at the exterior surface.*

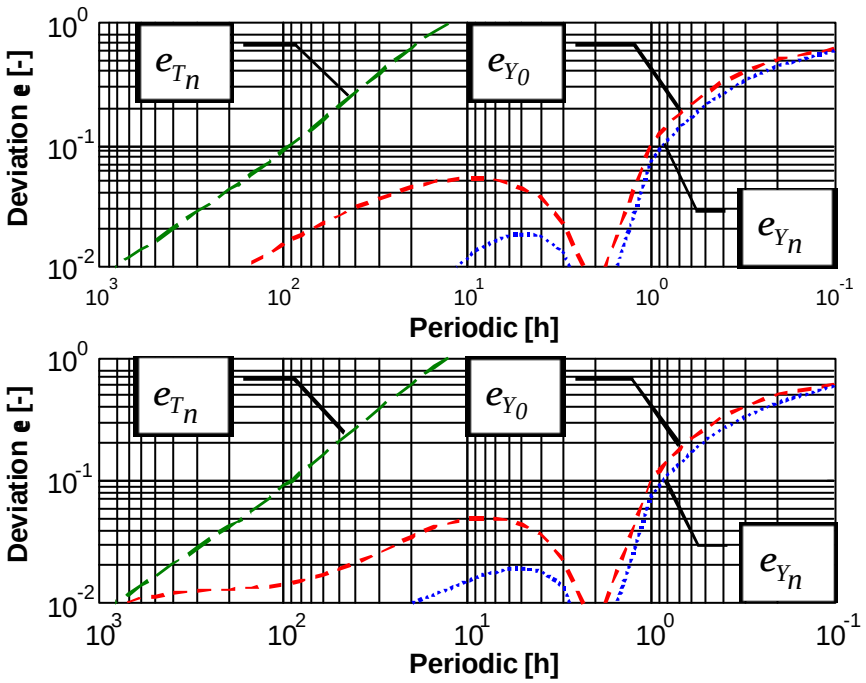

Figure 16: Model deviation $\boldsymbol{e}$ *for boundary conditions* $\tilde{q}_n = \tilde{q}_0$ *are plotted in the upper diagram. The lower diagram shows model deviation if the temperature is constant at either surface.*

6.3.3 Fields of application: State-of-the-art and future perspectives

One dimensional heat transfer in multilayer building components

ORCs have within this context been used to model heat transfer in multilayer components. As shown in paper 4, the 5-node ORC can be used within building simulation programs for thermal comfort, peak load and for energy prediction calculations. This ORC provides faster run time than FDMs that have the same (and worse) admittance characteristics. In a case study performed with the IDA/ICE building simulation application (Sahlin 1996, Bring et al 1999), several ORCs and FDMs were used to model building components in an office cell which was subjected to intermittent heating. Table 10 shows run results for the different cases. Table 11 shows calculated energy requirement for the last 12 of totally 19 simulated days.

Table 10: An office was simulated with IDA/ICE where building components were represented by different models. The first two columns show results when these were modelled with 3- or 5-node ORCs. In the simple FDM, discretisation was made such that cell size approximately 50 mm, unless the layer was thinner. In the detailed FDM, cell size was determined as half the value of with equation 37.

Simulated office with	3-node ORC	5-node ORC	Simple FDM	Detailed FDM
Amount of equations	115	139	163	280
Simulation time (s)	47.1	54.0	57.7	86.8
No. time steps	1825	1872	1865	1878

Table 11: The energy demand of the office during a 12-day winter period. "Electricity" is heat from lighting, appliances and a radiator The air handling units preheat supplied air and includes fan energy.

Simulated office with	3-node ORC	5-node ORC	Simple FDM	Detailed FDM
Electricity (Wh)	69 146.8	69 016.4	69 306.5	68 991.4
Air handling units (Wh)	24 706.4	24 801.3	24 821.5	24 818.6
Difference in sums related to Detailed FDM (Wh)	-43.2	7.7	318.0	0.0

On basis of table 11, all models can be used within energy prediction calculations. However, differences in results can be observed when temperatures and heat flows at the surfaces are studied. On plotting the heat flowing through the surface between 06:00 – 18:30 hours, there are notable discrepancies. The 3-node ORC has difficulties in representing fast changes – high frequencies are not well modelled. The simple FDM has a small cell at the surface, which models fast processes well. However, the adjacent cell is too large, which results in that medium-rate frequencies are not modelled well (see between 08:00 – 12:00 hours). The 5-node ORC has a curve that lies slightly above the detailed FDM curve (which is according to the Bode diagram most correct, see paper 4) before noon, and will thereafter lie slightly lower. This may be the effect of daily thermal transmittance, since the weakness of the 5-node ORC is modelling dynamic transmittance.

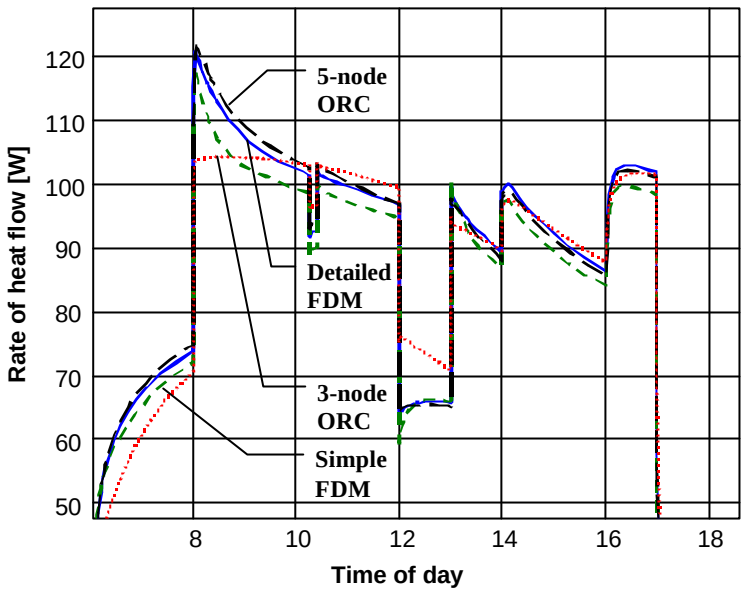

Figure 17: Heat flowing into the surface of an external wall.

From this study and an earlier analysis of ORCs (Akander 1995), it can be concluded that the 3-node ORC can model building components well within the frame of energy prediction of buildings. The 3-node ORC can only model lightweight building components in detailed calculations that require good accuracy below the 1-hour periodicity, such as external walls composed of a gypsum board, mineral wool and wood panelling. It is not suitable for representing massive components since the response of the semi-infinite solid is not well modelled for wide ranges of frequencies. The same applies to multilayer components that have more than one switching frequency.

The 5-node ORC is more reliable and gives a far better agreement with the analytical thermal performance. This is due to the parallel circuits, which give better semi-infinite solid response modelling than serially connected chains. However, dynamic transmittance is not represented well in this model, and this is a feature that has to be improved in the future. On the other hand, dynamic transmittance is of minor importance in Nordic countries for the reason that the components are well insulated.

Multidimensional heat transfer

The optimisation of an RC-network to model multidimensional heat transfer is the same as for one dimensional heat transfer, with the exception that the analytical performance is usually unknown. Analytical performance is instead approximated with a finite difference calculation in the frequency domain, for example as proposed by Andersson et al (1983). By using “the framework for equilibrium equations” (Strang 1986) to solve for the temperature field, iterative methods are avoided, thus giving the response of each frequency fast. The approximated response is now the basis for RC-optimisation.

ORCs have earlier been used for modelling multidimensional heat transfer. Mao (1997) used a 2-node ORC to simulate heat transfer in thermal bridges and ground loss on a stand-alone basis. Within building simulation programs, the modelled inaccuracy has to be reduced for high frequencies having an ORC with more nodes. Multidimensional heat transfer was modelled in one dimension by that ORC. In (Akander et al 1996), a simulation of an office was performed with IDA/ICE that modelled the dynamic thermal performance of thermal bridges. However, the ORC was here configured so that one branch modelled heat transfer from the upper part of an intermediate floor/wall joint to the exterior environment and another modelled the heat transfer process from the lower part of the joint. The purpose of this work was to ensure that the methodology worked. It also gave insights in the problems involved with the modelling of thermal bridges within the zone: where should the cut-off planes be situated, where do two- and three-dimensional thermal bridges meet and what component parts were to be modelled with heat transfer in one dimension? The complexity of this type of modelling demands skilled users, even though the modelling of the thermal bridge with the ORC works well.

The ORCs application can be extended as to have heat sinks or sources within the building components as well as passive components. With applications in borehole heat storage, Schmidt will use ORCs to study the interaction between building and heat storage.

In the future, the linking of CAD output and simulation programs will be a standard way of designing buildings. A problem is the redundant data generated by CAD and how to insert thermal parameters into the data. The ORC methodology promises the link between the sorted CAD data and the simulation program. As shown in figure 18, future work should be dedicated to establishing a format that makes CAD output compatible with thermal calculations.

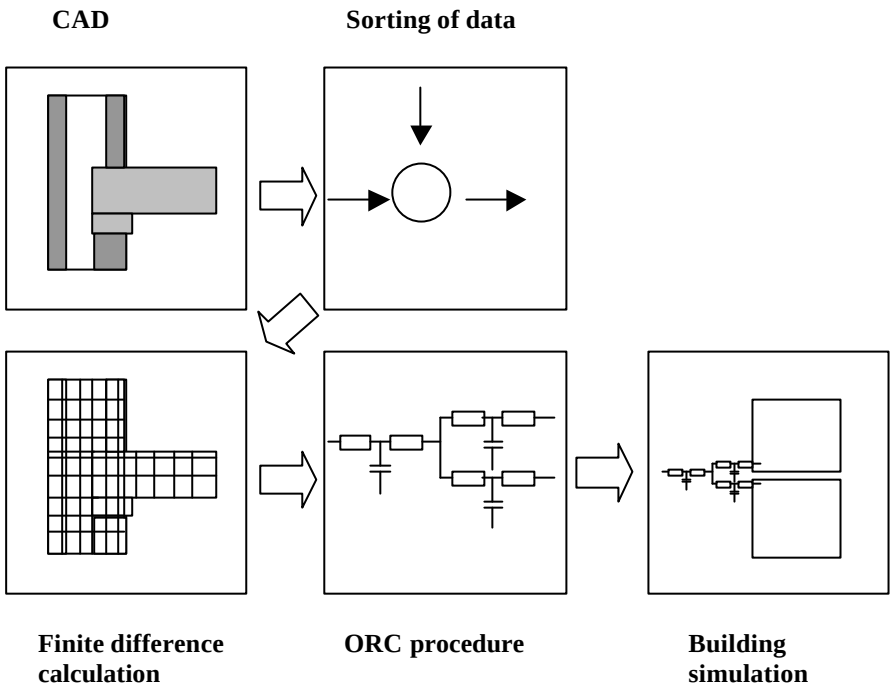

Figure 18: The flow of information from the CAD stage to the building simulation. The three lower blocks within the figure works today: the ORC Method.

7 Reference list

This reference list includes references from the whole thesis.

Abel E., Isfält E. and Ljungkrona I. (1992). Analysis of the dynamic energy balance in an occupied office room using simulations and measurements. *TRANS ASHRAE 92 Part 2:363*.

Akander J. (1995). *Efficient Modelling of Energy Flow in Building Components. Parts 1 and 2*. ISRN-KTH-BYT/AR--95/5--SE. KTH, Stockholm, Sweden.

Akander J. (1996). Controlling the Inaccuracy of Models that Represent Multilayer Constructions. *Proc. 4th Symp. on Building Physics in the Nordic Countries*, Espoo, Finland, pp. 59-66.

Akander J. (1997a). *Air tightness of the LECA-house at Röskär: Using the pressurized fan method – Test 4*. Division of Building Technology, Department of Building Sciences, KTH, Stockholm, Sweden.

Akander J. (1997b). *Measurements of the rate of air change in the LECA-house at Röskär – Test 1*. Division of Building Technology, Department of Building Sciences, KTH, Stockholm, Sweden.

Akander J. (1997c). *Measurements of the rate of air change in the LECA-house at Röskär – Test 2*. Division of Building Technology, Department of Building Sciences, KTH, Stockholm, Sweden.

Akander J. and Johannesson G. (1997). *The utilisation factor of two Swedish buildings.* Proceedings of Cold Climate HVAC '97, Reykjavik, Iceland. p. 117-122.

Akander J., Lacour C., Mao G., Johannesson G. (1994). *Ett elbaserat golvvärmesystem - Mätningar och beräkningsmodeller*. Dept. of Building Technology, KTH, Stockholm, Sweden. (In Swedish).

Akander J. and Levin P. (1997). *Air tightness of the LECA-house at Röskär: Using the pressurized fan method – Test 1*. Division of Building Technology, Department of Building Sciences, KTH, Stockholm, Sweden.

Akander J., Mao G. and Jóhannesson G. (1996). A Method for Modelling Two-Dimensional Heat Flow in Building Simulation Programs. *Proc. International Symp. of CIB W67 on Energy and Mass Flow in the Life Cycles of Buildings*, Vienna, Austria, pp. 575-580.

Anderlind G. (1992). Multiple Regression Analysis of In Situ Thermal Measurements - Study of an attic insulated with 800 mm loose fill insulation. *J. Thermal Insul. And Bldg. Ensv*. Vol. 16. pp.81-104.

Anderlind G. (1996). *Dynamic Thermal Models - Two Dynamic Models for Estimating Thermal Resistance and Heat Capacity from in Situ Measurements*. Report A16:1996. The Swedish Council for Building Research, Sweden.

Anderlind G. (1997). High Accuracy Heat Flow Calculation – A method to calculate the heat flow for an arbitrary wall with constant material properties in a natural climate. *Nordic Journal of Building Physics, Vol 1. Available at http://www.ce.kth.se/bim/bphy/*

Anderlind G. (1998). *Program Description DAVID-32*. http://www.gullfiber.se

Anderlind G. (1999). A new model for calculation the effects of two- and three-dimensional thermal bridges. *Proc. of the 5th Symp.on Building Physics in the Nordic Countries. CTH, Göteborg, Aug. 24-26*, 1999.

Andersson A.C. and Jóhannesson G. (1983). *Application of Frequency Response for Fast Analysis of Two-dimensional Heat Flow Problems*. Coden: LUTVDG/(TVBH-7072)/1-8/(1983), LTH, Lund, Sweden.

Andersson L.O., Bernander K.G., Isfält E. and Rosenfeld A.H. (1979). *Storage of Heat and Coolth in Hollow Core Concrete Slabs. Swedish Experience and Application to Large, American - Style Buildings.* Report LBL-8913. Lawrence Berkeley Laboratory, Berkeley, California.

Asan H. and Sancaktar Y.S. (1998). Effects of Wall's Thermophysical Properties on Time Lag and Decrement Factor. *Energy and Buildings Vol. 28 (1998)*, pp. 159-166.

ASHRAE HVAC2 Toolkit (1993). *HVAC2 Toolkit – Algorithms and Subroutines for Secondary HVAC Sytem Energy Calculations.* ASHRAE TC 4.7. Ed: M. Brandemuehl. Atlanta, Georgia, USA.

Athienitis A.K. (1989). A Computer Method for Systematic Sensitivity Analysis of Building Thermal Networks. *Building and Environment, Vol. 24, No. 2, (1989)* pp. 163-168.

Barnaby, C., Dean, E., Fuller, F., Nell, D., Shelley, T. and Wexler, T. (1980). *Utilizing the Thermal Mass of Structural Systems in Buildings for Energy Conservation and Power Reduction*. Lawrence Berkeley Laboratory, Berkeley. California.

Bland B.H. (1992). Conduction in Dynamic Thermal Models: Analytical Tests for Validation. *Building Serv. Eng. Res. Technol. Vol. 13(4)*, pp. 197-208.

Blomberg T. (1996). *Heat Conduction in Two and Three Dimensions - Computer Modelling of Building Physics Applications.* Report TVBH-1008. Department of Building Physics, LTH, Lund, Sweden. p.125-133.

Boverket (1997): *Vem bor hur och till vilket pris? – Hushållens boendeförhållanden och utgifter*. Boverket, Sweden (In Swedish).

Boverket (1995): *Boverkets Byggregler (BBR94)*. Boverket, Sweden (In Swedish).

Bunn J.P. (1983). The Thermal Response of a Homogeneous Slab to a Constant Heat Flux. *Building and Environment, Vol. 18 No. 1/2 (1983)*, pp. 61-64.

Bring A. (1983): Versatile System Simulation with the BRIS Program. *Proceedings of the Fourth Symposium on the Use of Computers for Environmental Engineering Related to Buildings.* Ed: Kenchiku Kaikan, Tokyo, Japan.

Bring A., Sahlin P. and Voulle M. (1999). Models for Building Indoor Climate and Energy Simulation. *A Report of International Energy Agency (IEA SHC)*, Task 22.

Bris Data AB (2000). http://home.swipnet.se/nmf.

Brown G. (1964). *A Method of Calculating on a Computer the Thermal and Light Radiation in a Room and also the Cooling and Heating Requirements*. National Swedish Institute for Building Research. Reprint No 4:1964.

Brown G. (1990). The BRIS Simulation Program for Thermal Design of Buildings and their Services. *Energy and Buildings Vol. 14*, pp. 385 - 400.

Brown G. and Isfält E. (1973). Proper use of the heat capacity of buildings to achieve low cooling loads. *Contribution to the CIB W 40 Birmingham meeting*. (Also published in the IHVE Journal, London).

Brown G. and Partheen K. (1980). *Värmelagring och temperatur i väggar och bjälklag vid rumstemperatursvängningar.* Teknisk Rapport SP-RAPP 1980:13. Statens Provningsanstalt, Borås, Sweden. (In Swedish.)

Burmeister H. and Keller B. (1998). Climate Surfaces: A Quantitative Building-specific Representation of Climates. *Energy and Buildings Vol. 28 (1998)*, pp. 167-177.

Carslaw H.S. and Jaeger J.C. (1959). *Conduction of Heat in Solids*, 2nd ed. Oxford University Press, London, United Kingdom.

Claesson J. (1999). Dynamic Thermal Networks. Application of a General Theory to a Ventilated Crawl Space. *Proc. of the 5th Symp. Building Physics in the Nordic Countries*, Vol. 1, CTH, Gothenburg, Sweden. Aug. 24-26, 1999, pp. 57-64.

Claesson J., Nevander L.-E. and Sandin K. (1984). *Värme*. Kompendium i byggnadsfysik. Institutionen för Byggnadsteknik, LTH, Sweden. (In Swedish).

Davies M.G. (1983). Optimum Design of Resistance and Capacitance Elements in Modelling a Sinusoidally Excited Building Wall. *Building and Environment, Vol. 18. No. 1/2*, pp. 19-37.

Davies M.G. (1994). The Thermal Response of an Enclosure to Periodic Excitation: The CIBSE Approach. *Building and Environment, Vol. 29, No. 2*, pp. 217-235.

Davies M.G. (1995). Solutions to Fourier's Equation and Unsteady Heat Flow through Structures. *Building and Environment, Vol. 30, No. 3*, pp. 309 - 321.

Danter E. (1973). Heat Exchange in a Room and the Definition of Room Temperatures. *IHVE Symposium*, June 1973.

Eftring B. (1990). *Numerisk beräkning av temperaturförlopp - Ett fysikaliskt betraktelsesätt*. Doctoral Dissertation. Rapport R81:1990. Byggforkningsrådet, Stockholm, Sweden. (In Swedish).

Graaf F. van der (1990). "Heat-flux Sensors." Chapter 8, Volume 4 of the multivolume work "*Sensors - A Comprehensive Series*" (Ed. W. Göpel et al.). VCH Verlagsellschaft mbh, Germany. p. 297-322

Gruber P. and Toedtli J. (1989). On the Optimal Thermal Storage Capability of a Homogeneous Wall Under Sinusoidal Excitations. *Energy and Buildings, Vol 13*, p. 177 - 186.

Isfält E. (1989). The Thermal Balance of Buildings. A basis for comparisons of computer programs for calculations of the room climate and the power and energy requirements for climate control of buildings. A detailed presentation of a number of BRIS simulations with comments. *IEA Annex 21 Subtask C*.

Isfält E. and Bröms G. (1992). *Effekt- och energibesparing genom förenklad styrning och drift av installationssystem i byggnader - Beräkningar.* Meddelande nr 22, Institutionen för installationsteknik, KTH, Sweden. (In Swedish).

Isfält E. and Johnsson H. (1986). *Stockholmsprojektet. Effekt- och energisimuleringar med datorprogrammen BRIS och DEROB.* Rapport No R59: 1986, Statens råd för byggnadsforskning, Sweden. (In Swedish).

Jensen L. (1978). *Digital reglering av klimatprocesser*. Doctoral Dissertation. Department of Automatic Control, LTH, Lund, Sweden. (In Swedish).

Jensen S.Ø. (1995). Validation of Building Energy Simulation Programs: A Methodology. *Energy and Buildings, Vol. 22*, No. 2, pp. 133-144.

Johannesson, C.M. 1994. KTH vidgar reviren med experimentlåda i fullskala. *Byggforskning, Vol. 94.3* Juni. (In Swedish).

Jóhannesson G. (1979). *Värmeflödesmätningar: Termoelektriska mätare, funktionsprinciper och felkällor.* (Eng: *Heat-Flow Measurements: Thermoelectrical Meters, Function Principles and Sources of Error.*) Rapport TVBH-3003, Division of Building Technology, LTH, Lund, Sweden. (In Swedish).

Jóhannesson G. (1981). *Active Heat Capacity - Models and Parameters for Thermal Performance of Buildings.* Doctoral Dissertation. Report TVBH-1003, LTH, Lund, Sweden.

Jóhannesson G., Leander U. and Hallgrimur G. (1982). *Mätning av värmeväxlareffekt och värmelagring i hålkanaler av betong*. LUTVDG/(TVHB-7069) 1-20/(1982), Division of Building Technology, LTH, Lund, Sweden. (In Swedish).

Johnsen, K. and Grau, K. (1994). *TSBI3 Computer Program for Thermal Simulation of Buildings. User's Guide* vers B.05. Danish Building Research Institute SBI.

Kalema T. and Haapala T. (1995). Effect of interior heat transfer coefficients on thermal dynamics and energy consumption. *Energy and Buildings Vol. 22*, pp. 101-113.

Khalifa A.J.N. and Marshall R.H. (1990). Validation of Heat Transfer Coefficients on Interior Building Surfaces Using a Real-sized Indoor Test Cell. *Int. J. Heat Mass Transfer, Vol 33*, No. 10, pp. 2219-2236.

Klein S.A., Beckman W.A. and Duffie J.A. (1976). TRNSYS - A Transient Simulation Program. *ASHRAE Trans, 1976, Vol. 82, Pt.2.* (http://www.engr.wisc.edu/centers/sel/trnsys/index.html).

Kossecka E. and Kosny J. (1996). Relationship between structural and dynamic thermal characteristics of building walls. *Proc. International Symp. of CIB W67 on Energy and Mass Flow in the Life Cycles of Buildings*, Vienna, Austria, pp. 627-632

Kre K. (1993). *On the Storage of Heat in Building Components*. Hochbau für Architekten und Entwefen. Technische Universität Wien, Austria.

Levin P. (1991). *Building Technology and Air Flow Control in Housing*. Document D16:1991. Swedish Council for Building Research, Sweden.

Lomas K., Eppel H., Martin C. and Bloomfield D. Empirical Validation of Building Energy Simulation Programs. *Energy and Buildings Vol 26*, pp. 253-275.

Magyari E. and Keller B. (1998). The Storage Capacity of a Harmonically Heated Slab Revisited. *Int. J. Heat Mass Transfer, Vol. 41, No. 10*, pp. 1199-1204.

Malcorps, H. (1981). Frequency-response of Heat Fluxmeters. *J. Phys. E. Sci. Instrum., Vol. 14*. Pp. 1054-1060.

Mao G. (1997). *Thermal Bridges - Efficient Models for Energy Analysis in Buildings.* Doctoral Dissertation. Bulletin no 173, TRITA-BYT 97/0173, Department of Building Sciences, KTH, Stockholm, Sweden.

Milbank N.O. and Harrington-Lynn J. (1974). Thermal response and the admittance procedure. *Building Services Eng., Vol. 42*, pp. 38-51.

Mitalas G.P. and Stephenson D.G. (1967). Room Thermal Response Factors. *ASHRAE Transactions Vol. 73, Part 1*.

Norberg C. (1990). *Husets Tidskonstanter*. Eleffektiviseringslaboratoriet i Marma, Vattenfall Utveckling AB, Sweden. (In Swedish).

Norén A., Akander J., Isfält E. and Söderström O. (1999). The Effect of Thermal Inertia on Energy Requirement in a Swedish Building – Results Obtained with Three Calculation Models. *Int. J. Low Energy and Sustainable Buildings, Vol 1*. Available at http://www.bim.kth.se/leas

Nylund, P.O. (1980). *Infiltration and ventilation*. Document D22:1980. Swedish Council for Building Research, Sweden. (In Swdish).

Panzhauser E. (1991). *Programmpaket WAEBRU*. Hochbau für Architekten und Entwefen. Technische Universität Wien, Austria.

Poloniecki J.G., Vianou A.V and Mathioulakis E. (1995). Steady-state analysis of the zero-balance heat-flux meter. *Sensors and Actuators, Vol. A 49*. Pp. 29-35.

Ramirez R. (1985). *The FFT - Fundamentals and Concepts*. Prentice-Hall, Inc., New Jersey, USA.

Sahlin, P. (1996). *Modelling and Simulation Methods for Modular Continuous Systems in Buildings.* Doctoral Dissertation. Bulletin No. 39, Building Services Engineering, Royal Institute of Technology, Stockholm.

Sahlin P., Bring A. and Sowell E.F. (1994). *The Neutral Model Format for Building Simulation*. Bulletin No. 32, Building Services Engineering, Royal Institute of Technology, Stockholm.

Sandin K. (1990). *Värme, luftströmning, fukt.* Kompendium i byggnadsfysik. Avdelningen för byggnadsfysik, LTH, Lund, Sweden. (In Swedish).

Seem J.E., Klein S.A., Beckman W.A. and Mitchell J.W. (1989). Transfer Functions for Effective Calculation of Multidimensional Transient Heat Transfer. *Journal of Heat Transfer, Vol. 111/5*, pp. 9-12.

Simmonds P. (1991). The Utilization and Optimization of a Building´s Thermal Inertia in Minimizing the Overall Energy Use. *TRANS ASHRAE 92 Part 2:1031*.

Skanska Software (1996). *VIP+ 1.3 Info*. Skanska Software, Malmö,Sweden.

Standeven M., Cohen R., Bordass B. and Leaman A. (1998). The best building ever? PROBE Team's verdict on the Elisabeth Fry Building. *Building Services Journal*, April 1998.

Strang G. (1986). *Introduction to Applied Mathematics*. Wellesly-Cambridge Press, Massachusetts, USA.

SP (1996). *Bestämning av värmekapacitet på lättklinker*. SP, Sveriges Provnings- och Forskningsinstitut (Swedish National Testing and Research Institute), Borås. Handläggare Fredrik Stenberg. (In Swedish).

Taesler R. and Isfält E. (1980). *Choice of Climatological Data for Testing of Computations of Energy Requirements in Buildings.* A4 - serien nr 28, Inst. för uppvärmnings- och ventilationsteknik, KTH, Sweden.

Walsh P.J. and Delsante A.E. (1983). Calculation of the Thermal Behaviour of Multi-Zone Buildings. *Energy and Buildings, Vol. 5*, pp. 231-242.

Winwood R., Wilkins R. and Edwards R. (1994). Modeling the thermal flywheel. *Building Services Journal*, October 1994.

Åström K.J. (1968). *Reglerteori*. Almqvist & Wiksell/Gerbers Förlag AB, Stockholm, Sweden. (In Swedish).

Standards

EN 832 (1998). Thermal performance of buildings - Calculation of energy use for heating - Residential buildings. European Committee for Standardisation (CEN), Brussels.

prEN ISO 13786 (1998). Thermal performance of building components- Dynamic thermal characteristics - Calculation methods. CEN/TC 89/WG 4/N176, Brussels.

EN ISO 13370 (1998). Thermal performance of buildings – Heat transfer via the ground – Calculation methods. European Committee for Standardisation (CEN), Brussels.

PAPER 1

The Thermal Performance of Multilayer Building Components - Applications of the Bode Diagram

The Thermal Performance of Multilayer Building Components - Applications of the Bode Diagram

SUBMITTED: November 1999.
REVISED: .
PUBLISHED: .

Jan Akander, Techn. Lic,
Department of Building Sciences, Kungl Tekniska Högskolan;
S – 100 44 Stockholm;
akander@bim.kth.se

Guðni Jóhannesson, Professor,
Department of Building Sciences, Kungl Tekniska Högskolan;
S – 100 44 Stockholm;
gudni@bim.kth.se

KEYWORDS*: building component, thermal performance, analytical thermal model, finite difference method, Bode diagram.*

SUMMARY*:*
The commonly used U-value is a quantification of the steady-state thermal performance of the thermal performance of a building component. It describes only one of endlessly many states that a building component can have. The dynamic performance is accordingly a matter that deserves more attention, which is mirrored in the standard prEN ISO 13786. A limitation is that the standard focuses only on diurnal thermal processes. In order to characterise the thermal performance for a wide range of frequencies, the Bode diagram can be utilised. The Bode diagram not only visualises thermal performance since it also gives quantitative and qualitative information on a given building component. This paper focuses on the application of the Bode diagram along with asymptotic values of thermal performance entity admittance and dynamic transmittance. By using switching frequencies that are based on surface material properties, the range of frequencies at which different types of responses occur can be approximated. Also, a method of thermal model performance evaluation (RC-networks and finite difference models) is presented along with a new procedure for finite difference model discretisation. Discretisation is based on model performance inaccuracy rather than on the traditional stability time step criterion. These are however closely related. This is the first part of a series of papers entitled "The Thermal Performance of Multi-Layer Building Components".

1 Scope

This paper focuses on an introduction to thermal frequency response of plane multi-layer building components and the application in the Bode diagram. A survey is made on how the Bode diagram qualitatively and quantitatively can be utilised when the analytical performance of the component is known. Thermal behavior can in terms of asymptotes of admittance easily be identified in the Bode diagram. On basis of surface layer material parameters, switching frequencies can be determined as to approximate frequency ranges where the thermal performance of the component is that of a thermal resistance, a simple mass and that of the semi-infinite solid.

This paper also presents how this theory can be used to determine the inaccuracy of one-dimensional finite difference models and RC-network models. A new criterion for cell size discretisation of building components

into a finite difference model is introduced. This criterion is based on model high frequency performance but is related to the commonly used stability time step criterion within explicit forward finite difference methods.

Being the first part of a series of papers entitled "The Thermal Performance of Building Components", the present work serves as a base for following parts. More details on this work are found in Johannesson (1981), Akander (1995,1996) and Mao (1997). With the exception of the Bode diagram, similar matter on frequency response is also found in (Davies 1994).

2 Introduction

A subject within building physics and the building industry that has increasingly been gaining understanding for is the dynamic thermal performance of building components. With the development and spreading of building simulation programs, such as for example BRIS (Brown 1990), TRNSYS (Klein et al. 1976), TSBI3 (Johnsen and Grau 1994) and IDA (Sahlin 1996), engineers and architects have the means of understanding and predicting thermal processes within buildings. What can be concluded is that well-known (and less well applied) steady state relationships do not simulate short-term processes very well for the reason that thermal inertia is not present in the calculations.

The importance of this subject is reflected by the existence a proposal to EN ISO standard (prEN ISO 13786:1998 E) with the title "Thermal performance of building components - Dynamic thermal characteristics - Calculation methods." The stated methods are based on frequency response. A main feature of the standard is the calculation of an effective heat capacity, which is a quantification of the dynamic performance of the building component in question. The effective heat capacity for a 24-hour process and the decrement factor (a factor that indicates the components ability to damp thermal processes coming from the external environment), along with the U-value are thought to give a fairly good picture of the thermal behaviour of a given building component. The question is if the information from two frequencies, those that correspond to the steady state and the 24-hour periodic, are enough to make a more detailed analysis on thermal performance. Information would certainly be preferred for a wider range of frequencies, and diagrams are the convenient means of exhibiting this information.

The most common way to express the thermal performance of insulated components is by using the U-value, but this entity is strictly limited to the performance at steady state. When it comes to dynamic performance, there are several means for expressing thermal performance. One way is to list a set of response factors. The response factors are derived analytically from a building component that undergoes the excitation of triangular pulses (Mitalas and Stephenson 1967). Another method is by letting the building component undergo a step change, for example a sudden drop of temperature in one or both environments. The step response is an exponentially decaying temperature and heat flux process, from which a Newtonian time constant can be calculated. The time constant is therefore a form of quantifying the thermal inertia of the component. This is also a common method used on whole buildings, as to experimentally or by simulations determine the time constant of a building, for example as done by Isfält and Bröms (1992). Norberg (1990) uses two time constants to describe measured decay in temperature of a building. Working within the frequency domain, Jóhannesson (1981) illustrated the frequency response of individual building components in the Bode diagram, which uses real numbers in terms of magnitude and phase shifts. The Bode diagram is a common tool used within the field of automation and theories of signal processing. If heat flux and temperature oscillations are considered to be signals within the frequency domain, the thermal response of constructions can be treated in a similar fashion. Also working within the frequency domain, Davies (1983) uses the polar diagram to plot analytical and model heat transfer functions. By defining a so-called cyclic thickness of a slab, Davies (1994) also plotted dynamic transmittance in a Bode diagram where magnitude and phase are shown as function of this definition. The calculation procedures of prEN ISO 13786 (1998) are related to the works of Jóhannesson and Davies, since these deal with frequency response. Thermal performance of the building component is in the standard characterised by the U-value, an effective heat capacity and the decrement factor at a certain frequency, more specifically the 24-hour periodic. Asan and Sancaktar (1998) have studied the effect of the thermal properties of a slab on the decrement factor and time lag. Time lag and the decrement factor are as functions of the heat capacity, the thermal condutivity and

thickness in various combinations plotted in 3-D diagrams. Burmeister and Keller (1998) characterise the performance of zones in a certain climate plotted in terms of the heat loss factor and a time constant in the form of so-called climatic surfaces. Climatic surfaces are used to predict energy use and heating/cooling power in buildings at design stages.

2.1 A solution of the heat conduction equation

For multi-layer plane building components, analytical heat transfer solutions can be solved from the general heat conduction equation. One method is by assuming that the boundary conditions are harmonic. If one frequency is considered and the system is linear, then the response of the construction can be determined for that frequency. Carslaw and Jaeger (1959) formulated a solution of the heat conduction equation with harmonic boundaries. For a homogeneous plane slab, the solution is such that

$$\begin{bmatrix} \tilde{\boldsymbol{q}}_n \\ \tilde{q}_n \end{bmatrix} = \begin{bmatrix} A_1 & B_1 \\ C_1 & D_1 \end{bmatrix} \begin{bmatrix} \tilde{\boldsymbol{q}}_0 \\ \tilde{q}_0 \end{bmatrix} \tag{1}$$

Sinusoidal surface heat flux (density of heat flow rate) and surface temperature oscillations are denoted by $\tilde{q}$ and $\tilde{\boldsymbol{q}}$. These are functions of *one* angular frequency $\boldsymbol{w}$, here depicted by the superscript ”~”. Surface *0* is the excited surface, whereas surface *n* is the obverse surface that is subject to different boundary conditions discussed later. The heat transfer matrix contains complex elements, here

$$A_1 = \cosh(k \cdot l(1+i))$$

$$B_1 = -\frac{\sinh(k \cdot l(1+i))}{\boldsymbol{l} \cdot k(1+i)}$$

$$C_1 = -\boldsymbol{l} \cdot k(1+i) \cdot \sinh(k \cdot l(1+i))$$

$$D_1 = \cosh(k \cdot l(1+i))$$

with

$$k = \sqrt{\frac{\boldsymbol{w}}{2 \cdot a}} \quad \text{and} \quad a = \frac{\boldsymbol{l}}{\boldsymbol{r} \cdot c}$$

For a multi-layer construction, a heat transfer matrix can be maintained through the successive multiplication of the heat transfer matrix of each layer. A construction with three material layers would give a heat transfer matrix based on the product of its components.

$$\begin{bmatrix} \tilde{\boldsymbol{q}}_n \\ \tilde{q}_n \end{bmatrix} = \begin{bmatrix} A_3 & B_3 \\ C_3 & D_3 \end{bmatrix} \begin{bmatrix} A_2 & B_2 \\ C_2 & D_2 \end{bmatrix} \begin{bmatrix} A_1 & B_1 \\ C_1 & D_1 \end{bmatrix} \begin{bmatrix} \tilde{\boldsymbol{q}}_0 \\ \tilde{q}_0 \end{bmatrix} = \begin{bmatrix} A & B \\ C & D \end{bmatrix} \begin{bmatrix} \tilde{\boldsymbol{q}}_0 \\ \tilde{q}_0 \end{bmatrix} \tag{2}$$

The heat transfer matrix can be re-arranged to give heat flux as functions of temperature oscillations.

$$\begin{bmatrix} \tilde{q}_0 \\ \tilde{q}_n \end{bmatrix} = \begin{bmatrix} -A/B & 1/B \\ C - A \cdot D/B & D/B \end{bmatrix} \begin{bmatrix} \tilde{\theta}_0 \\ \tilde{\theta}_n \end{bmatrix} \tag{3}$$

The first element in the second row can be replaced by the term $-1/B$ since the determinant of the heat transfer matrix is for a plane construction equal to one.

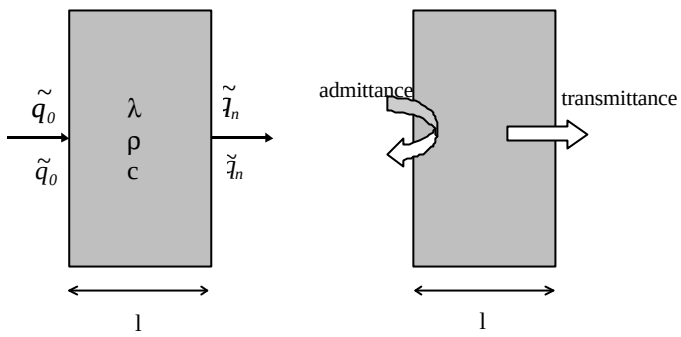

FIG. 1: To the left: Material parameters, temperature oscillation and heat flux direction for a homogeneous slab. To the right: Illustration of admittance and transmittance.

2.2 Thermal response, definitions

A way of characterising thermal performance within the frequency domain is by using the definition of admittance (Danter 1973) and that of dynamic transmittance. Admittance is the ratio between heat flux and temperature oscillation on one side of the construction. The temperature oscillation may be assumed to take place in a node that represents the environment, which is coupled to one of the surfaces of the component by means of a surface thermal resistance. Heat transfer is thus regarded on an "environment-to-environment" basis. However, since the surface thermal resistance varies due to different boundary conditions, geormetrical arrangements, the types of thermal process, etc, the thermal response of the component interacting with the thermal resistance cannot be considered to be the thermal performance of the component alone (see sectione 2.3.2). On the other hand, if the temperature oscillation at the surface of the component is considered, the thermal response of the component alone is found. This resonse is on a "surface-to-surface" basis, the true response of the building component. Admittance, denoted by Y_0, is for a surface 0 of the component defined as

$$Y_0 = -\frac{\tilde{q}_0}{\tilde{\theta}_0} \tag{4}$$

Admittance is defined as positive on exiting the component through the surface, see figure 1, hence the minus sign before the quotient. Depending on the boundary conditions, admittance can be determined from the heat transfer matrix. If the temperature is constant at surface n, then

$$Y_0 = \frac{A}{B} \quad \left(\tilde{q}_n = 0\right) \tag{5}$$

If the component is well-insulated, the heat flux at the non-excited side can be considered to be zero such that

$$Y_0 = \frac{C}{D} \quad (\tilde{q}_n = 0) \tag{6}$$

In the special case where $\tilde{q}_n = \tilde{q}_0$, admittance will be

$$Y_0 = \frac{A-1}{B} \quad (\tilde{q}_n = \tilde{q}_0) \tag{7}$$

The latter expression is in EN ISO-standard (prEN ISO 13786) chosen to be the definition of admittance of a construction for establishing the effective heat capacity of building components.

From the same calculation, the admittance at the other surface, here denoted by n, can be determined in a similar fashion. Depending on the boundary condition, admittance becomes

$$Y_n = \frac{D}{B} \quad (\tilde{q}_0 = 0); \quad Y_n = \frac{D-1}{B} \quad (\tilde{q}_n = \tilde{q}_0) \tag{8}$$

Dynamic transmittance T_D is defined as

$$T_D = \frac{\tilde{q}_n}{\tilde{q}_0} \tag{9}$$

and will for the boundary condition where temperature is constant at surface n be

$$T_D = \frac{1}{B} \quad (\tilde{q}_n = 0) \tag{10}$$

Dynamic transmittance has the same magnitude in both directions if either $\tilde{q}_0$ or $\tilde{q}_n$ is zero.

Admittance and dynamic transmittance are harmonic entities, composed of a real and imaginary part. It is more convenient to describe these entities in terms of magnitude and phase shift. Magnitude is determined by taking the absolute value of the entity. Here, magnitudes are denoted by r and phase shifts by $\boldsymbol{j}$.

$$r_{Y_0} = |Y_0|, \quad j_{Y_0} = \arg(Y_0); \quad r_{T_D} = |T_D|, \quad j_{T_D} = \arg(T_D) \tag{11}$$

2.2.1 Informative asymptotic values of admittance

Equation 4 contains asymptotic values for low and high frequency processes. Three different asymptotic values can be found. These are important approximations used to understand the thermal performance of building components in the Bode diagram.

Stage 1: The steady state condition.

Frequencies approaching the steady state condition where $w = 0$ will give that admittance approaches the value

$$Y_0 = -\frac{1}{R_t} \quad \left(\tilde{q}_n = 0\right) \tag{12}$$

The magnitude is $1/R_t$ W/(m^2·K) and the phase lag is 180°.

Stage 2: The response of a simple mass.

If a construction is composed of more than one layer, where one of the layers is insulation so that $\tilde{q}_n$ can be considered to be zero (adiabatic), and the thermal process is that of a low frequency type, i.e. w has a small value, then

$$Y_0 = -iw \cdot r_1 \cdot c_1 \cdot l_1 \tag{13}$$

Index 1 denotes the surface material layer. The magnitude of admittance is $w \cdot c_1$ W/(m^2·K) with a phase lag of 90°. Here, c_1 is the areic heat capacity of the surface layer.

Stage 3: The response of a semi-infinite solid.

Independently of boundary condition, high frequency processes where w approaches infinity result in an admittance with the value converging to

$$Y_0 = -\sqrt{\frac{l_1 \cdot r_1 \cdot c_1 \cdot w}{2}}\left(1 + i\right) \tag{14}$$

The magnitude of admittance is $\sqrt{l_1 \cdot r_1 \cdot c_1 \cdot w}$ W/(m^2·K) with a phase of 135° behind the temperature oscillation.

2.3 The Bode diagram

The Bode diagram is a tool for visualising transfer functions (Åström 1968). With this in mind, heat transfer functions of a component can be plotted, giving a picture on the thermal performance of that component as function of frequency. Below, an example is given. The Bode diagram has a logarithmic x-axis that represents the time period (inverse of frequency) of the thermal process. The y-axis of the upper diagram holds the

magnitude, with the unit W/(m^2·K), whereas the y-axis of the lower diagram shows the phase of the processes. The admittance and the dynamic transmittance of a roof with data according to table 1 are plotted.

TAB. 1: Material data for a roof. The innermost layer is listed first.

Material	l [m]	λ [W/(m·K)]	ρ [kg/m^3]	c [J/(kg·K)]	R [(m^2·K)/W]	χ [J/(m^2·K)]
Concrete	0.040	1.2	2400	880	0.0333	84480
Mineral wool	0.120	0.04	200	750	3.0000	18000
Roofing felt	0.004	0.26	1100	1500	0.0154	6600

For this component, the performance can be read for a wide range of frequencies, here corresponding to the range of a 1-hour to a 1000-hour time period. On the choice of a 24-hour process as shown in figure 2, admittance has the magnitude of $19.7/R_t$ (6.47 W/(m^2·K)) and a phase of -98°. The corresponding values for dynamic transmittance are $0.91/R_t$ (0.30 W/(m^2·K)) and -43°.

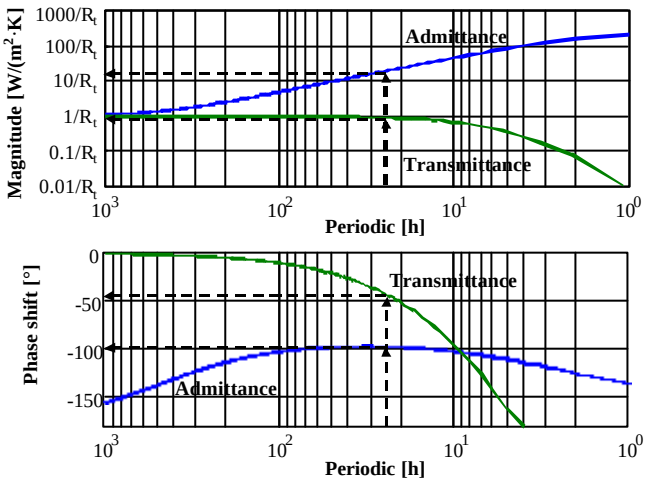

FIG. 2: The Bode diagram. The upper diagram plots admittance (r_{Y_0}) and dynamic transmittance (r_{T_D}) magnitude of the roof. The lower diagram shows admittance (j_{Y_0}) and dynamic transmittance(j_{Y_0}) phase shift. R_t is the thermal resistance of the component, here 3.049 m^{2}xK/W.

Figure 3 displays these processes in the time domain, where the component is subject to a temperature excitation of 1°C. Worth noting is that heat flow q_0 has a time lead of 5.5 hours ahead of temperature $\boldsymbol{q}_0$, which is not explicitly expressed in the Bode diagram. The reason is that admittance is defined as being positive in the direction surface-to-environment, whereas q_0 is positive in the direction environment-to-surface, thus having a difference in time shift of 12 hours (180°).

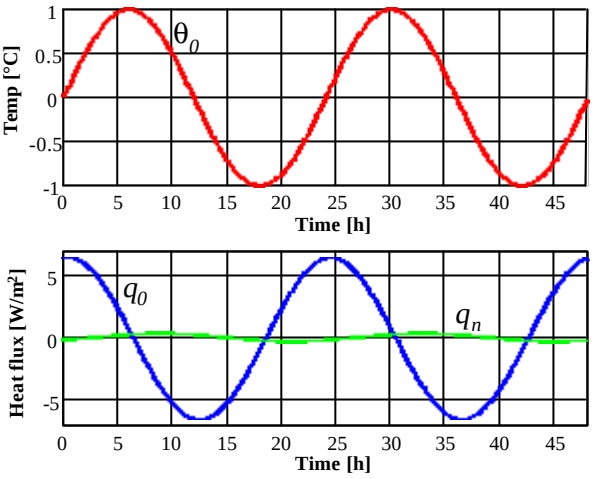

FIG. 3: Time domain representation of the 24-hour periodic with data from table 1.

As of now, quantitative aspects have been shown in the Bode diagram. Sometimes it is necessary to make a qualitative analysis of the thermal performance of a construction. Within this context, the asymptotic values for admittance are used. These are illustrated in figure 4, using the same component as above. For low-frequency processes that approach the steady-state condition, the magnitude of admittance and the dynamic transmittance converge to the inverse of the total thermal resistance of the construction. This was derived earlier as an asymptotic value of Stage 1.

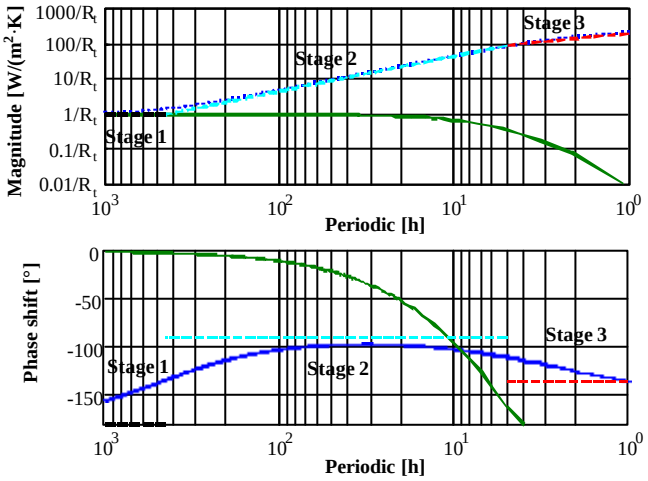

FIG. 4: Asymptotes of admittance (dashed) plotted in the Bode diagram. Stage 1, Stage 2 and Stage 3 qualitatively represent the steady state response, simple mass response and the response of a semi-infinite solid. R_t *is the thermal resistance of the roof, here 3.049* m^2*x K/W.*

As the dynamics of the construction start to dominate the performance of the construction, the magnitude of admittance starts to diverge from the magnitude of transmittance. When frequency increases, transmittance will successively be damped, whereas admittance merges with the asymptote having the slope of 1:1. The phase increases steadily from asymptotic value -180° to some -90°. This characterises the response of a simple mass. The plotted asymptotes of Stage 2 are -90° for phase shift and $\left|-iw \cdot c_1\right|$ for magnitude. Here, c_1 is the areic

heat capacity of the concrete slab at the surface of the construction. The range of periods for which this response is valid is roughly

$$2\pi \cdot R_1 \cdot c_1/3600 \le T_{mass} \le 2\pi \cdot R_t \cdot c_1/3600 \qquad (15)$$

The extreme value to the right is found at the intersection of the asymptote with the $1/R_t$ -line, whereas the value to the left is at the intersection between Stages 2 and 3. Equation 15 applies to components with one homogeneous surface next to the insulating layer (Akander, 1995 and 1999). These switching frequencies (periods) mark a change in behaviour for a given component.

After a short transitional region, often at the whereabouts of a frequency corresponding to

$$T_{semi} < 2\pi \cdot c_1 \cdot R_1/3600 \qquad (16)$$

the response changes to the behavior of the semi-infinite solid. For increasing frequencies, the magnitude of admittance has a slope of 1:2, a relationship that was derived at Stage 3. The phase converges to the constant value of -135°.

2.3.1 The influence of the boundary condition

In the previous section, an example of the performance of a construction with the boundary condition $\tilde{J}_n = 0$ was shown. The choice of boundary condition does influence the outcome of the performance. However, which boundary condition has been used can be revealed in the Bode diagram, since the performance follows a special pattern. This is demonstrated here with the example of a homogeneous concrete slab with data as shown in table 2.

TAB. 2: Material data of a concrete slab.

Material	l [m]	λ [W/(m·K)]	ρ [kg/m^3]	c [J/(kg·K)]	R [(m^2·K)/W]	χ [J/(m^2·K)]
Concrete	0.150	1.2	2400	880	0.125	316800

The performance of the slab has been calculated for three types of boundary conditions and is plotted in the Bode diagram of figure 5. The first thermal performance (filled curves) is from the condition where $\tilde{q}_n = 0$, where admittance is denoted by r_{Y_0} and j_{Y_0}. This boundary condition allows the calculation of dynamic transmittance (r_{TD} and j_{TD}). Analogous to the previous example, the response is resistive at low frequencies. However, at the switching frequency corresponding to $T_{semi} = 69.1\ h$ (which for slabs is equal to T_{mass}, see equations 15 and 16), admittance changes to the response of a semi-infinte solid. The response of the simple mass is never present.

The second thermal performance (dotted curves) is based on the condition that $\tilde{q}_n = \tilde{q}_0$. Admittance is with this condition denoted by r'_{Y_0} and j'_{Y_0}. Dynamic transmittance lacks relevance for this condition, since the slab can be regarded to be adiabatic for non-zero frequencies at the centre line. For high frequencies, the response is that of a semi-infinite solid with a magnitude having the slope of 1:2. As the frequency is lowered, a switching

frequency is found at the intersection of this curve and the line with half the value of $1/R_t$. For lower frequencies, admittance magnitude has the slope of 1:1 or explicitly $\left|\frac{-iw\cdot c_1}{2}\right|$. At this stage, the response is that of a simple mass with a phase that converges to -90°. The switching frequency is therefore $T_{semi} = 17.3\ h$, a value that is derived from equation 16 for half the slab.

The third thermal performance is that of the adiabatic slab, where $\tilde{q}_n = 0$. The performance is illustrated with dashed curves with the symbols r''_{Y_0} and j''_{Y_0}. High frequency processes have the response of the semi-infinite solid until the magnitude curve crosses the line with the value $1/R_t$. Again, the switching frequency is at $T_{semi} = 69.1\ h$. The curve continues to drop as frequency is lowered, now following the asymptote with the equation $\left|-iw\cdot c_1\right|$. Phase approaches -90°. For obvious reasons, there is no transmittance. Note the positioning of r'_{Y_0} and r''_{Y_0} ($r''_{Y_0} \approx 2\cdot r'_{Y_0}$) when these have the response of a simple mass. Lines representing heat capacity (slope 1:1) descend in value on traversing to the right in the Bode diagram.

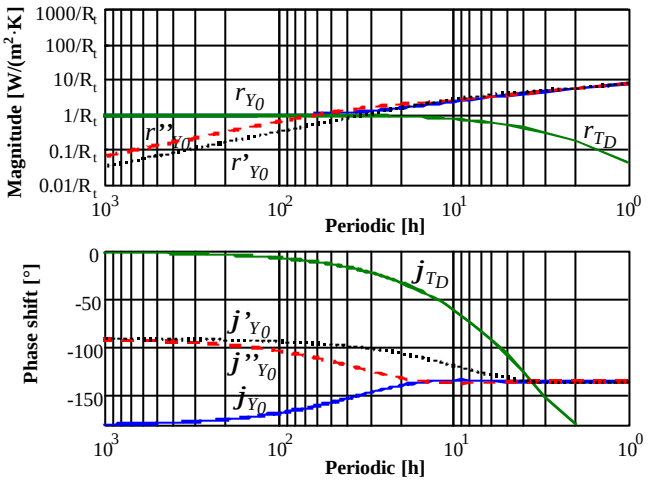

FIG. 3: The thermal performance of a concrete slab. The filled curves represent performance with the boundary condition $\tilde{q}_n = 0$, the dotted curves when $\tilde{q}_n = \tilde{q}_0$ and the dashed curve when $\tilde{q}_n = 0$. R_t = 0.125 m^2x K/W.

2.3.2 The influence of a surface thermal resistance

So far, the analysis has been limited to what happens at the surfaces of building components. However, it is often necessary to investigate heat transfer on an environment to environment basis. An environment, commonly represented by a node, is coupled to the component by means of a surface thermal resistance. The surface resistance will not only change the degree of insulation between the environments; it will also modify the dynamic interaction between of the component and the environments (see for example Brown and Partheen, 1980). Whereas the previous analysis can be used for analysis of for example solar radiation onto surfaces, the analysis here is focused on the effect of convection and long wave radiation (here linearized) on dynamic heat transfer. However, the aim is here to illustrate the *effect* of a surface thermal resistance more than to ponder on the value of the surface resistance and criterions on when this value can be regarded as being constant.

A new heat transfer matrix can be set up between the two environmental nodes. The surface thermal resistances R_{se} and R_{si} can each be treated as purely resistive material layers, such that

$$\begin{bmatrix} \tilde{q}_e \\ \tilde{q}_e \end{bmatrix} = \begin{bmatrix} 1 & -R_{se} \\ 0 & 1 \end{bmatrix} \begin{bmatrix} A & B \\ C & D \end{bmatrix} \begin{bmatrix} 1 & -R_{si} \\ 0 & 1 \end{bmatrix} \begin{bmatrix} \tilde{q}_i \\ \tilde{q}_i \end{bmatrix} \tag{17}$$

By using the definition of admittance on the product matrix, and allowing w approaching infinity, the magnitude of admittance will converge to the value of $1/R_{si}$. This implies that surface thermal resistances damp fast thermal processes within buildings, certainly in buildings with low levels of insulation where R_{si} is not much smaller than $R_t + R_{si}$. This applies to time periods that are lower than the switching frequency for which the surface thermal resistance starts influencing admittance, such that

$$T_{Rsi} \leq 2p \cdot R_{si} \cdot c_1 / 3600 \tag{18}$$

In the example above, the surface resistance curbs admittance for time periods that are faster than 19.2 hours. It should be noted that equation 18 is valid within the frequency range where the response is that of a simple mass.

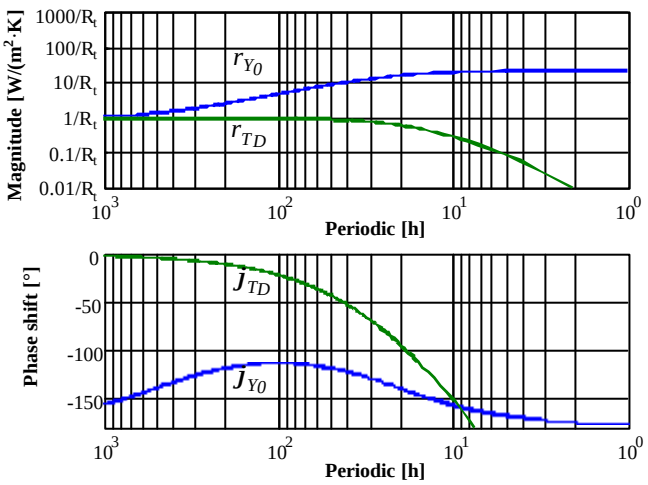

FIG. 4: The influence of a surface thermal resistance at each surface. R_t is the thermal resistance of the roof, here including R_{si} and R_{se} such that R_t = 3.219 m^2xK/W.

Surface resistances damp the magnitude of transmittance, both in the steady-state form and dynamically too, compare figures 2 and 6.

2.4 The order of material layers

It's well known that the order of material layers in a multi-layer construction influences the thermal performance of the construction. A rule of the thumb is that material layers on the inside of the insulation layer constitute the effective heat capacity of the construction. By doubling the thermal mass of a surface layer, twice the amount of heat can for some instances be stored without radically changing the temperature of the process. This can easily be shown in the Bode diagram. However, what is less self-evident is how the order of material layers affects the

dynamic transmittance of a construction. In prEN ISO 13786, dynamic transmittance is represented by the decrement factor f, defined such that

$$f = \frac{1}{|B| \cdot U} \tag{19}$$

This is in other words a ratio between the transmittance magnitude for one given frequency and the steady state U-value. Also, the influence of the surface thermal resistances is included - it is therefore not explicitly an entity of the building component itself.

The importance of the order of material layers will be shown with an example. Suppose a construction is to be built up of four material layers, whereof two are composed of a lightweight insulating material and the others of a heavyweight material. The order of the layers is varied and the thermal performance of each construction is calculated. The material layer parameters are shown in table 2. The boundary conditions are that $\tilde{q}_0 = 1$ °C and $\tilde{q}_n = 0$ °C.

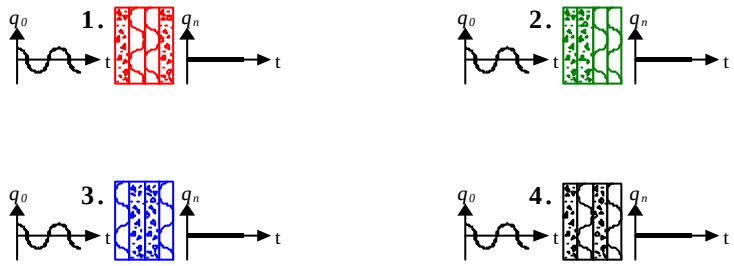

FIG. 5: Number and side of excitation for four different components.

TAB. 3: Material parameters for the lightweight and the heavyweight material layer.

Material	l [m]	λ [W/(m·K)]	ρ [kg/m^3]	c [J/(kg·K)]	R [(m^2·K)/W]	χ [J/(m^2·K)]
Concrete	0.050	1.8	2400	1000	0.028	120000
Mineral wool	0.050	0.04	30	1400	1.250	2100

The results on admittance are as expected. Construction 2 with double concrete layers at the inner surface allows the largest amount of heat to be pumped back and forth, and is in the Bode diagram situated farthest to the left in comparison to the admittance of the other constructions. The admittance is for this construction within Stage 2 twice the magnitude of admittance for constructions 1 and 4.

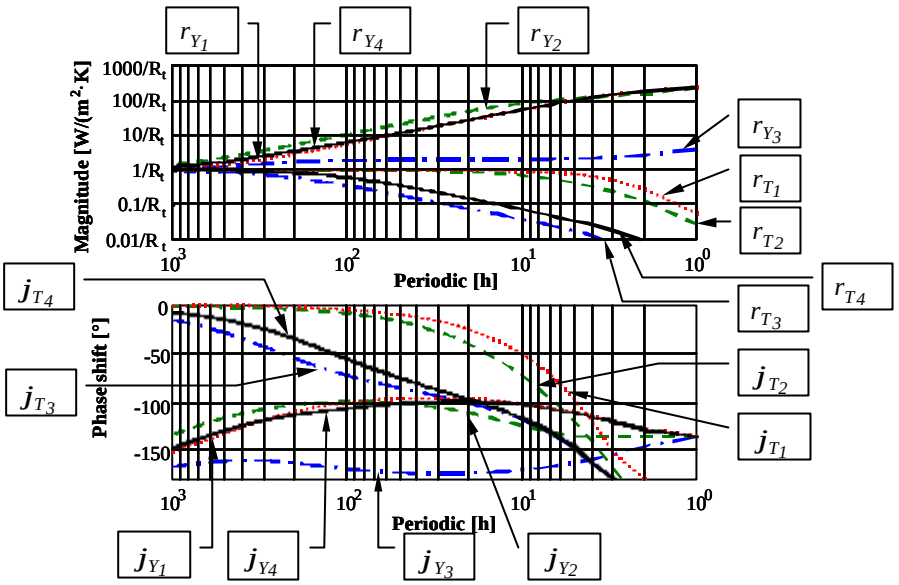

FIG. 6: Comparison of the thermal performance of four constructions with different material order. R_t *= 2.556* $m^2 \times K/W$*. The dotted curves are for construction 1, the dashed curves for construction 2, the dash-dotted curve for construction 3 and the filled curve represents the performance of construction 4.*

Note that for higher frequencies, the magnitudes converge to the response of the semi-infinite solid for constructions 1, 2 and 4. As for construction 3 with the insulation at the surface, the response is resistive for a periodic between 3 and 60 hours. The analogy with a surface thermal resistance is in this case evident. For a periodic lower than 3 hours, the response is that of a semi-infinite solid, caused by the insulation.

As for transmittance, the conclusion is that a heavyweight material inside the component, with insulation on both sides, has the greatest damping effect. Therefore, when designing a building envelope that is supposed to minimize the influence of the external climate variations on the internal climate as much as possible, a heavy slab with insulation on both sides is recommended. Of course, this conclusion applies to the boundary conditions where the external surface temperature oscillates and the internal surface temperature is constant, such as the envelope of a cold-storage building. The poorest dampening effect is caused by construction 1, which is the most common type of sandwich construction of today. For this example, diurnal external surface variations are literally dynamically undamped when transmitted to the inner surface.

3 Evaluation of thermal models

Shown thus far, the use of the Bode diagram has been of a qualitative type to express the thermal performance of building components. The calculated entities, admittance and dynamic transmittance, are analytical. These can be used to simulate building components or buildings as a whole, under the circumstance that the system is linear. Solutions of each frequency can be superposed, giving information on thermal processes within the time domain. However, some thermal processes are non-linear and cannot properly be within the frequency domain with sufficient accuracy. It therefore becomes necessary to perform the simulation within the time domain.

A common way of modelling heat conduction in solids is by using finite difference methods or linear RC-networks within the time domain. Both methods involve chains of heat capacities serially connected by thermal resistances. The means of establishing values to parameters in the chains (models) vary to some extent, but the concept in general is the same: a heat balance is performed at every node during simulation. Here, the explicit

finite difference method will be used to show the evaluation of such models. The evaluation is made within the frequency domain as opposed to validation tests which commonly are made within the time domain, for example as proposed by Bland (1992). However, the evaluation procedure shown here resembles the "qualifying density power spectra" used for experimental validation of building energy simulation programs; introduced by the Model Validation and Development Subgroup within PASSYS (Jensen 1995).

3.5 The finite difference method - theoretical analysis of inaccuracy

A building component is in this method discretised into cells by the sub-division of material layers. Depending on the chosen model cell configuration, the thermal mass of the cell is condensed into one or two mass nodes (see figure 8). The Central Capacity Cell (CCC) has the heat capacity of the cell placed in the geometrical center of the cell. The central node is coupled to each cell surface by a thermal resistance, which has the value of half the thermal resistance of the cell. In the case of the Edge Capacity Cell (ECC), the heat capacity of the cell is halved and placed at each surface of the cell. The thermal resistance of the cell couples these heat capacities. The choice of cell configuration influences the thermal performance of the model at high frequencies, as will be seen in the following section. For the moment, attention will be paid to the criterion of discretisation.

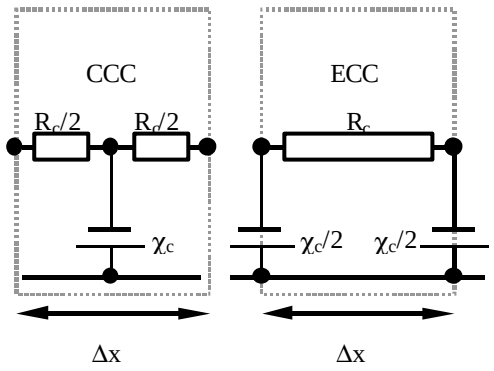

FIG. 7: Two different types of cell configurations that model heat flow in one dimension. To the left: Central Capacity Cell (CCC). To the right: Edge Capacity Cell (ECC). R_c is the thermal resistance and c_c is the areic heat capacity of the cell.

A method of discretisation, which is empirical to its nature, is by using rules of the thumb concerning the spatial size of cells of different materials. An example is that a cell of concrete should not exceed the size of 5 centimeters. Another is to use the stability time step criterion. The stability time step is the smallest time step that can be taken in a simulation (using explicit methods) and this is governed by the mathematical formulation of the heat balance of a node within the model. The heat balance of an arbitrary node is for the explicit forward method

$$q_j^{t+\Delta t} = \frac{\Delta t}{c_j} \cdot \left[\Phi_j + \frac{1}{R_j} q_{j-1}^t + \frac{1}{R_{j+1}} q_{j+1}^t + \left(\frac{c_j}{\Delta t} - \frac{1}{R_j} - \frac{1}{R_{j+1}} \right) \cdot q_j^t \right] \tag{20}$$

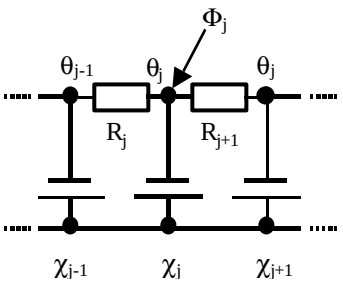

FIG. 8: Node number j in a thermal model.

Here, Δt is the time step of the simulation, θ_j^t is the temperature of node *j* at time *t* and $\theta_j^{t+\Delta t}$ is the temperature of node *j* at time $t+\Delta t$. Φ_j stands for an internal heat source at node *j*, which is commonly equal to zero for most conventional building components. The criterion for stability in the solution is that the term within the parenthesis is non-negative, if $\Phi_j = 0$. The largest time step that can be taken is therefore (Eftring 1990)

$$\Delta t_{stab,\ j} = \frac{\chi_j}{\frac{1}{R_j} + \frac{1}{R_{j+1}}} \tag{21}$$

Discretisation is often made by letting the smallest value of $\Delta t_{stab,\ j}$ be slightly larger than the simulation time step Δt such that $\Delta t = k \cdot \Delta t_{stab,\ j}$ $(k < 1.0)$. For a homogeneous slab with equidistant CCC's, the stability time step is smallest at the mass node next to the surface. The stability time step criterion gives

$$\Delta x \leq \sqrt{\frac{3 \cdot \lambda \cdot \Delta t / k}{\rho \cdot c}} \tag{22}$$

The stability time step criterion is not a discretisation in time that depends on boundary conditions and the thermal behaviour of the building component, but more so on the cell configuration and parameters of the simulation model itself.

3.6 The response of a thermal model

The product of the heat transfer matrix of each model component can establish the thermal performance of chain, where each model component is modelled as a material layer. A purely resistive layer with the thermal resistance R has a heat transfer matrix such that

$$\begin{bmatrix} 1 & -R \\ 0 & 1 \end{bmatrix} \tag{23}$$

A purely capacitive layer with the heat capacity χ has the following heat transfer matrix (Johannesson, 1981):

$$\begin{bmatrix} 1 & 0 \\ -i\omega c & 1 \end{bmatrix} \tag{24}$$

The sequential product of the chains' components determines the heat transfer matrix of the model as a whole. When the heat transfer matrix has been established, model admittance and dynamic transmittance can be calculated and compared with analytical admittance and dynamic transmittance. This procedure can be used to give a quality assurance of how well a chain models the thermal behavior of a building component. If the thermal performance of the model is poor, it may be wise to go farther with the discretisation and choose a finer mesh.

The choice if whether or not the performance of model is adequate is left to the user. What should be kept in mind is the following:

- Thermal surface resistances damp high frequency processes, these are "filtered" away in simulations;
- One-dimensional finite difference models, even with coarse cells, give good agreement with analytical performance at low frequencies;
- A fine mesh gives better accuracy at higher frequencies at the cost of larger computational expenses (memory and time) and should take the first point into consideration.

As an example, a 250 mm homogeneous slab of aerated concrete is discretised into 5 cells. Both cell types are modelled in two separate chains. The thermal performance is based on the assumption that $\tilde{q}_n = 0$ °C. Results are plotted in the Bode diagram of figure 10. As can be seen, the CCC (dashed) and the ECC (dotted) give a good approximation of the analytical solution (filled) at lower frequencies. At higher frequencies, the curves of admittance and transmittance start to diverge. For admittance, the ECC's dotted curves shoot up whereas the CCC's dashed curves drop off in comparison to the analytical curves. This phenomenon is more thoroughly discussed in the next section. As of now, a method for quantifying model inaccuracy is presented.

TAB. 4: Material data for a homogeneous slab of aerated concrete.

Material	l [m]	λ [W/(m·K)]	ρ [kg/m^3]	c [J/(kg·K)]	R [(m^2·K)/W]	χ [J/(m^2·K)]
Aerated concrete	0.250	0.12	600	1050	2.083	157500

If the surface of the building component and the model are excited such that $\tilde{q}_0 = 1$ °C, a heat flux, corresponding to the admittance, will arise. This model admittance may deviate from that of the analytical admittance. The difference will be a sinusoidal entity. By dividing the difference by the analytical admittance, the relative deviation in complex form is found for each frequency. On taking the absolute value of deviation, the magnitude of deviation of the thermal performance for each frequency is established. The maximal deviation of admittance at surface *0* is the dimensionless magnitude

$$e_{Y0}(\omega) = \left| \frac{Y_{0model} - Y_{0analyt}}{Y_{0analyt}} \right|_{\omega} \tag{25}$$

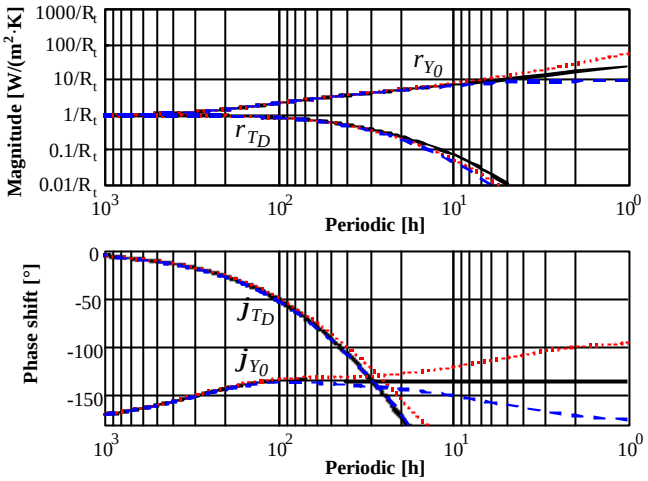

FIG. 9: Bode diagram for the aerated concrete slab. The response is plotted as a filled curve for the analytical result, dashed for the CCC model and dotted for the ECC model. $R_t = 2.083\ m^2 \times K/W$.

Similar expressions can be set up for admittance on the other surface and for the dynamic transmittance. Since model inaccuracy now is quantified, criteria can be set on a set of frequencies on how much model performance is allowed to deviate from analytical performance. Figure 11 illustrates the inaccuracy of the ECC and the CCC model for admittance and transmittance of the aerated concrete slab, each model composed of 5 cells. In this case, if the inaccuracy is judged to be too large at high frequencies, discretisation can be made with 6 or more cells until the criterion is fulfilled. An example of a criterion is as follows: all periodics larger than 3 hours should give deviations less than 0.10 and the 24 hour periodic deviation must be less than 0.01 ($e_{Y_0}(T \geq 3\,h) \leq 0.10$ and $e_{Y_0}(24\,h) \leq 0.01$) if the model is to be accepted. In essence, this method is a type of quality assurance that a model has a limited inaccuracy, independent of the boundary conditions in the simulation and numerical solver, which it is subject to.

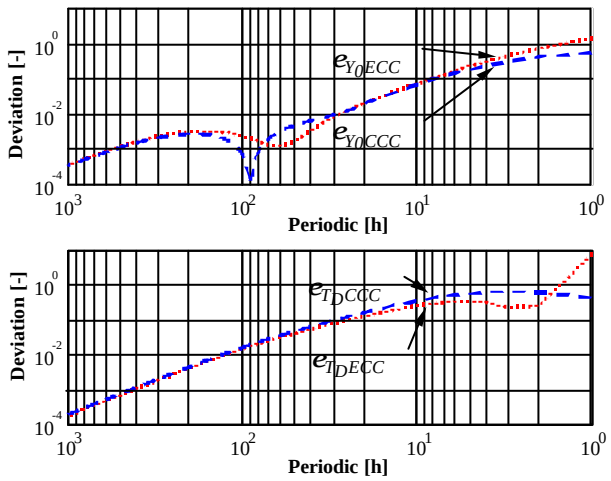

FIG. 10: The inaccuracy of the ECC (dotted) and the CCC (dashed) model compared to the analytical solution. The upper diagram shows deviation of admittance. The lower diagram shows deviation of dynamic transmittance.

3.7 The influence of cell configuration

Cell configuration influences the performance of models at higher frequencies, as seen in figure 10. As seen earlier in the section of the influence of surface thermal resistances, a thermal resistance R will lead to that high frequency admittance converges to the value $1/R$. This is also true for CCC-models, which have a thermal resistance as the outermost component of the chain. In the example of figure 10, the outermost thermal resistance has the numerical value of a 10th of R_t since the aerated concrete slab was discretised into 5 cells. The magnitude of admittance converges to this value with the slope of a horizontal line, and admittance phase shift converges to the value -180°.

The ECC-chain has an outermost component that is a heat capacity. For high frequency processes, model admittance will become asymptotic with $-i\omega c$, i.e. the response of a simple mass. The simple mass is in this case the outermost heat capacity. Therefore, model admittance magnitude is in the Bode diagram at high frequencies an ascending line with the slope 1:1. Model admittance phase shift converges to -90°.

3.7.1 The semi-infinite solid

The performance of all building components without surface thermal resistances will for increasing frequencies have the response of a semi-infinite. This is the most difficult response to model with chains of thermal resistances and heat capacities. As seen in the Bode diagram, the response of the semi-infinite solid has the magnitude with a slope of 1:2. Neither the thermal resistance nor the heat capacity can alone model this response. With the increase of frequencies, the component has to have a finer mesh to maintain a low inaccuracy. A question that can be posed is the following. Can a discretisation be made with the condition that the finite difference model gives small inaccuracies for periodics larger than a given time period? This question has a positive answer if asymptotes within the Bode diagram are used. The answer will be exemplified with the aerated concrete slab (5 cells) used earlier.

The admittance of the slab has the performance of a resistance for a periodic that is longer than $2\pi \cdot R_1 \cdot c_1/3600$ hours, in the example longer than 573 hours. For a shorter periodic, the response is as of stage 3, the response of a semi-infinite solid. The magnitude of admittance is for the slab

$$|Y_0| = \sqrt{\lambda_1 \cdot \rho_1 \cdot c_1 \cdot \omega} \tag{26}$$

The CCC-model has a high-frequency response corresponding to the inverse of the outermost thermal resistance, here called R_{CCC0} (in the example a 10th of R_t), such that

$$|Y_{CCC0}| = \frac{1}{R_{CCC0}} \tag{27}$$

The CCC-model has a switching frequency where the model's semi-infinite solid performance becomes resistive, in other words $|Y_0| = |Y_{CCC0}|$. The switching frequency corresponds to

$$T = 2\pi \cdot R_{CCC0}^2 \cdot \lambda_1 \cdot \rho_1 \cdot c_1 \tag{28}$$

In the example of the slab, T = 5.7 hours (see figure 11) since R_{CCC0} is given. However, a discretisation can be done with this equation if the model user gives a value for T, corresponding to the frequency where the model inaccuracy becomes large. Therefore, the sought entity is Δx, and this is found in the term R_{CCC0}, since

$$R_{CCC0} = \frac{\Delta x}{2 \cdot \lambda_1} \tag{29}$$

On inserting equation 29 into equation 28, an expression is found that gives cell size as function of the time period where the inaccuracy of the CCC-model starts to become large. The cell size is

$$\Delta x = \sqrt{\frac{\lambda_1}{\rho_1 \cdot c_1} \cdot \frac{2 \cdot T}{\pi}} \tag{30}$$

The solution actually becomes the same for the ECC-model, since

$$|Y_0| = |Y_{ECC0}| = \omega \cdot \varepsilon_{ECC0} \text{ and } \varepsilon_{ECC0} = \rho_1 \cdot c_1 \frac{\Delta x}{2} \tag{31}$$

The stability time step is for the outermost mass node of the CCC-chain

$$\Delta t_{stab,CCC\,0} = \frac{\rho_1 \cdot c_1}{\lambda_1} \cdot \frac{\Delta x^2}{3} \tag{32}$$

This expression is usually used to determine the cell size, having the largest value with the simulating time step Δt inserted in the place of $\Delta t_{stab,\,0}$. Thus k of equation 22 is set to have the value 1. On solving for the cell size as stated in equation 33, the solution does not match with equation 30.

$$\Delta x = \sqrt{\frac{\lambda_1}{\rho_1 \cdot c_1} \cdot 3 \cdot \Delta t} \tag{33}$$

On setting equation 30 equal to equation 33, the relationship between simulation time step and model inaccuracy switching time period is found, being

$$T = \frac{3\pi}{2} \Delta t \tag{34}$$

The meaning of this equation is that if a discretisation is made on basis of a given simulation time step (or stability time step), the frequency components within the simulation that are higher than the frequency corresponding to T may be inadequate in terms of accuracy. By discretising the building component on basis of model and analytical thermal performance, more reliable results will be achieved. Yet, the stability time step is

true when solving equation systems of the model with explicit methods, but discretisation should be made from the point of view of the thermal performance, not from the solver technique of the simulation. Table 5 shows difference in cell size depending on the choice of discretisation method for some common building materials. It should be noted that these materials are thick surface materials of multi- or single-layer components, as this discretisation assumes that the response is that of a semi-infinite solid. However it is important that the following is noted: by reducing the value of T, smaller simulation time steps will have to be taken with an explicit solving method.

As mentioned earlier, there will actually always exist frequency components within the simulation that are higher than the frequency corresponding to T. The higest frequency present in a simulation with the constant time step Δt is the Nyquist frequency, see for example (Ramirez 1985), corresponding to T_{Ny}, such that

$$T_{Ny} > 2 \cdot \Delta t \tag{35}$$

The inequality sign can be substituted by $\approx$ for large time series. Equation 34 can now be rewritten to the expression

$$T = \frac{3\pi}{4} T_{Ny} \tag{36}$$

so that T is a factor 2.36 greater than the shortest periodic T_{Ny} that is present in the simulation. As an example, if a simulation program uses the time step of half an hour, the Nyquist periodic will be one hour. A thermal performance for a process with a periodic between 1 hour and $3\pi/4$ hours will not be well modelled.

TAB. 5: Cell size of a central capacity cell (CCC) for several building materials using the two discretisation methods. The term $\Delta x_{\Delta t}$ depicts cell size based on the stability time step criterion whereas Δx_T represents cell size based on model performance criterion.

Material	λ [W/(m·K)]	ρ [kg/m³]	c [J/(kg·K)]	$\Delta x_{\Delta t}$ [m] when Δt =0.5 h	$\Delta x_{\Delta t}$ [m] when Δt = 1 h	Δx_T [m] when T = 1 h	Δx_T [m] when T = 6 h
Aerated concrete	0.12	600	1050	0.032	0.045	0.021	0.051
Concrete	1.8	2400	1000	0.064	0.090	0.041	0.102
Polystyrene	0.033	30	1400	0.068	0.096	0.044	0.109
Brick	0.60	1500	900	0.049	0.069	0.032	0.078
Wood	0.14	500	2300	0.026	0.036	0.017	0.041

4 Conclusions and discussion

Characterisation of the thermal performance of a building component can be done within the frequency domain. A mean of visualising the performance for a wide range of frequencies is with the Bode diagram, in which transfer functions can be plotted. Since the thermal performance can be expressed in terms of admittance and dynamic transmittance as function of frequency or time periods, these transfer functions can be followed in the

diagram. This offers qualitative information on performance characteristics of a building component, for example if the response for a given frequency is that of a semi-infinite solid, a simple mass or if the response is that of a resistance. Also, quantitative information is found for a given building component, allowing detailed analysis at design stages on the behaviour of components. From an example in this paper, it is shown that the greatest damping of dynamic transmittance is achieved by having a capacitive (heavy) material layer between two insulating layers.

Another important factor is how a building component interacts with the surrounding environments. The impact of surface thermal resistances is such that high frequency processes are damped in their presence. High frequency admittance is curbed to the value corresponding to the inverse of the surface thermal resistance. Dynamic transmittance is reduced for the reason that the building component can be regarded as a capacitive layer between two insulating layers.

The methodology also provides a mean of evaluation of thermal performance of models that are composed of serially connected thermal resistances and heat capacities. For such models, a heat transfer matrix can be established, thus can model admittances and dynamic transmittance be found. Since the analytical performance of multi-layer building components is known, an evaluation of the model performance can be done. The inaccuracy of the model can be expressed in terms of a frequency dependent relative deviation in comparison to the analytical performance. By establishing the over-all relative deviation for a set of pre-selected frequencies, a judgement can be made on whether the model, on basis of inaccuracy, should be accepted or has to be improved prior to a simulation. Having a finer mesh commonly decreases model inaccuracy. However, by minimising the over-all relative deviation of a model with a fixed configuration (fixed number of thermal resistances and heat capacities) the thermal components within an RC-network model can be optimised. This procedure is beyond the scope of this paper, but will be presented as a following part within this publication series. More on the subject can also be found in Johannesson (1981), Akander (1995) and Mao (1997).

A new platform for discretisation of building components within finite different techniques can be formulated. The essence of this procedure lies in asymptotes of thermal performance at high frequencies. For a chain (model), depending on whether the surface model component is a heat capacity or a thermal resistance, the performance will differ at high frequencies. A model switching frequency is found where the analytical response of the semi-infinite solid is intercepted by the response of the surface component of the chain, being either the response of a thermal resistance or the response of a simple mass (heat capacity). On using the model switching frequency as a criterion for discretisation rather than the stability time step of the chain, a control of model inaccuracy is implemented in the discretisation procedure. This means that a model user, prior to a simulation, has to decide the highest frequency for which the model has to be accurate and then determine the simulation time step. The relationship between the shortest period T (corresponding to the model switching frequency) and the simulation time Δt step for the explicit forward finite difference method with a central capacity cell is

$$T = \frac{3\pi}{2}\Delta t \tag{37}$$

The cell size of the surface material is then found to be

$$\Delta x = \sqrt{\frac{\lambda_1}{\rho_1 \cdot c_1} \cdot \frac{2}{\pi} \cdot T} \tag{38}$$

5 References

Akander J. (1995). *Efficient Modelling of Energy Flow in Building Components. Parts 1 and 2*. ISRN-KTH-BYT/AR--95/5--SE. KTH, Stockholm, Sweden.

Akander J. (1996). Controlling the Inaccuracy of Models that Represent Multilayer Constructions. *Proc. 4th Symp. on Building Physics in the Nordic Countries*, Espoo, Finland, pp. 59-66.

Asan H. and Sancaktar Y.S. (1998). Effects of Wall's Thermophysical Properties on Time Lag and Decrement Factor. *Energy and Buildings Vol. 28* (1998), pp. 159-166.

Bland B.H. (1992). Conduction in Dynamic Thermal Models: Analytical Tests for Validation. *Building Serv. Eng. Res. Technol. Vol. 13(4*), pp. 197-208.

Brown G. (1990). The BRIS Simulation Program for Thermal Design of Buildings and their Services. *Energy and Buildings Vol. 14*, pp. 385 - 400.

Brown G. and Partheen K. (1980). *Värmelagring och temperatur i väggar och bjälklag vid rumstemperatursvängningar.* Teknisk Rapport SP-RAPP 1980:13. Statens Provningsanstalt, Borås, Sweden. (In Swedish.)

Burmeister H. and Keller B. (1998). Climate Surfaces: A Quantitative Building-specific Representation of Climates. *Energy and Buildings Vol. 28* (1998), pp. 167-177.

Carslaw H.S. and Jaeger J.C. (1959). *Heat Conduction in Solids.* 2nd ed., Oxford University Press.

Davies M.G. (1983). Optimum Design of Resistance and Capacitance Elements in Modelling a Sinusoidally Excited Building Wall. *Building and Environment, Vol. 18*. No. 1/2, pp. 19-37.

Davies M.G. (1994). The Thermal Response of an Enclosure to Periodic Excitation: The CIBSE Approach. *Building and Environment, Vol. 29*, No. 2, pp. 217-235.

Danter E. (1973). Heat Exchange in a Room and the Definition of Room Temperatures. *IHVE Symposium*, June 1973.

Eftring B. (1990). *Numerisk beräkning av temperaturförlopp - Ett fysikaliskt betraktelsesätt. Doctoral Dissertation*. Rapport R81:1990. Byggforkningsrådet, Stockholm, Sweden. (In Swedish).

Isfält E. and Bröms G. (1992). *Effekt- och energibesparing genom förenklad styrning och drift av installationssystem i byggnader - Beräkningar.* Meddelande nr 22, Institutionen för installationsteknik, KTH, Sweden. (In Swedish).

Jensen S.Ø. (1995). Validation of Building Energy Simulation Programs: A Methodology. *Energy and Buildings, Vol. 22*, No. 2, pp. 133-144.

Johannesson G. (1981). *Active Heat Capacity - Models and Parameters for Thermal Performance of Buildings.* Doctoral Dissertation. Report TVBH-1003, LTH, Lund, Sweden.

Johnsen, K. and Grau, K. (1994): *TSBI3 Computer program for thermal simulation of buildings. User's Guide* vers B.05. Danish Building Research Institute SBI.

Klein S.A., Beckman W.A. and Duffie J.A. (1976). TRNSYS - A Transient Simulation Program. *ASHRAE Trans, 1976, Vol. 82*, Pt.2. (*Also* http://www.engr.wisc.edu/centers/sel/trnsys/index.html).

Mao G. (1997). *Thermal Bridges - Efficient Models for Energy Analysis in Buildings.* Doctoral Dissertation. Bulletin no 173, TRITA-BYT 97/0173, KTH, Stockholm, Sweden.

Mitalas G.P. and Stephenson D.G. (1967). Room Thermal Response Factors. *ASHRAE Transactions Vol. 73*, Part 1.

Norberg C. (1990). *Husets Tidskonstanter*. Eleffektiviseringslaboratoriet i Marma, Vattenfall Utveckling AB, Sweden. (In Swedish).

prEN ISO 13786: 1998 E. *Thermal Performance of Building Components - Dynamic thermal characteristics - Calculation methods.* CEN/TC 89/WG 4/N176, Brussels.

Ramirez R. (1985). *The FFT - Fundamentals and Concepts*. Prentice-Hall, Inc., New Jersey, USA.

Sahlin, P. (1996). *Modelling and Simulation Methods for Modular Continuous Systems in Buildings.* Doctoral Dissertation. Bulletin No. 39, Building Services Engineering, Royal Institute of Technology, Stockholm.

Åström K.J. (1968). *Reglerteori*. Almqvist & Wiksell/Gerbers Förlag AB, Stockholm, Sweden. (In Swedish).

Submitted to: Nordic Journal of Building Physics
Avaliable at http://www.ce.kth.se/bphys

PAPER 2

The Thermal Performance of Multilayer Building Components - A Method for Approximating the Effective Heat Capacity.

The Thermal Performance of Multilayer Building Components - A Method for Approximating the Effective Heat Capacity.

SUBMITTED: December 1999.
REVISED: .
PUBLISHED: .

Jan Akander, Techn. Lic.,
Dept of Building Sciences, Kungl Tekniska Högskolan;
S – 100 44 Stockholm;
akander@bim.kth.se

KEYWORDS*: heat capacity, effective heat capacity, thermal performance, thermal behaviour, building component.*

SUMMARY*:*
In order to establish the effective heat capacity of a multilayer building component, one has to perform calculations within the frequency domain. This involves calculations with complex numbers and preferably programming tools that can handle these numbers. However, it is shown in this paper that the effective heat capacity can be calculated from material parameters from layers in the component with acceptable accuracy. The simplified method comprises four equations that are derived from frequency response theory. The effective heat capacity of a component is calculated for a given periodic. Time constants, based on material layer parameters, are used to select which equation is appropriate to determine the effective heat capacity. Tools for performing calculations are common calculators or computational spreadsheet programs. This paper also brings forth a discussion on what the effective heat capacity is and how it may be quantified.

1. Scope

The work presented in this paper focuses on the thermal performance of multi-layer components; a means of characterising and classifying the performance in terms of time constants and suggests an approximate method for calculation of the areic effective heat capacity of a component without the use of complex numbers. A discussion on what the areic effective heat capacity is and how it may be modelled is also put forth.

The theory and application of the approximate method is made on plane homogeneous and multi-layer components that are typical for Swedish buildings, which to some degree are better insulated those in warmer climates. The methodology is however applicable to plane building components of all nations, independent of building material and building technology. This methodology can be regarded as a further development of the approximate methods stated in normative Annex A of standard proposal prEN ISO 13786 with the title "Thermal Performance of Building Components - Dynamic Thermal Characteristics - Calculation Methods."

This paper is the second part of the series "The Thermal Performance of Multilayer Building Components". The reader is advised to read the first part, in the current journal (Akander and Jóhannesson 2000), since several definitions used in this paper are presented in the first paper in more detail.

2. Introduction

The dynamic thermal performance of building components is an issue which is gaining attention, not only due to increasing demand on thermal comfort, increasing costs on heating fuels and sources, but also from a perspective

of the global environment in terms of availability of energy resources and pollutants. This is reflected in national building codes where criteria are set to reduce the energy requirement in new buildings. A common criterion is to lower the heat loss factor by means of lowering levels of U-values compared to older code versions. The heat loss factor is commonly used to compare one building design with another to evaluate which building gives the least predicted energy requirement.

The traditional method of calculating the energy requirement of a building is by means of a steady-state energy balance, where the heat loss factor of the building is multiplied by the difference in mean temperature between the interior and the exterior climates, and time duration. This method is somewhat reliable for very coarse energy requirement predictions, but it totally lacks account of heat that can be stored within building components. In the European standard EN 832 (1998), a calculation procedure using a traditional energy balance is made, however taking into consideration the dynamic thermal performance of the building by means of the utilisation factor. The utilisation factor accounts for how much of the heat gain (the sum of solar irradiation, household appliances and metabolic heat) actually relieves the heating system from meeting the whole energy requirement based on the heat loss factor. The variables that affect the size of the utilisation factor are limited to the heat loss factor, the ratio between heat gains and heat loss, and the effective heat capacity of the building. The effective heat capacity is the sum of the effective heat capacity of each building component, i.e. the dynamic thermal performance of each component.

The quantification of the areic effective heat capacity of a building component is established within the frequency domain. This involves calculations with complex numbers and matrix multiplication. If access to computers with suitable programs that can handle such calculations is not possible, progress in calculating an effective heat capacity is limited and rather tedious. There are, of course, rules of the thumb that are regarded as ”approximate methods” that avoid complex numbers. Results from these simplified methods can give great deviations from ”what-should-have-been” results. This is the case for normative Annex A of prEN ISO 13786 (1998): a simplified method is given, tagged with the comment that results are probably inaccurate and over-estimate values derived from analytical expressions. The simplified methods are based on the thermal penetration depth of a 24-hour periodic, for multi-layer components the sum of the heat capacities on the interior side within the insulation material or an effective thickness within massive homogeneous layers.

3. The response of multi-layer components

Frequency response is basically thermal behaviour in the sense that if the component is prone to a sinusoidal thermal change at a surface, the component will reply to this change. Carslaw and Jaeger (1959) put forth a frequency domain solution to the heat conduction equation. Many authors have done various works on frequency domain calculations applied to buildings, such as Milbank and Harrington-Lynn (1974), Walsh and Delsante (1983), Athienitis (1989), Panzhauser (1991) and Davies (1995). A special field that gained interest was optimising slab thickness to withhold a maximum heat given certain boundary conditions. Among these are work for example by Bunn (1983), Gruber and Toedtli (1989) and Magyari and Keller (1998). Accordingly, work has also been done by other authors within the subject of equivalent electrical circuits to model components in simulations, such as Davies (1983, 1994). The effective heat capacity is the simplest model for simulating dynamic effects, for example as shown in work by Jóhannesson (1981) and Krec (1993).

3.1 An analytical solution of the heat conduction equation

Carslaw and Jaeger (1959) put forth a solution to the heat conduction equation for a slab within the frequency domain. The solution can be formulated in terms of matrices for the heat transfer of a homogeneous slab such that

$$\begin{bmatrix} \tilde{\boldsymbol{q}}_n \\ \tilde{q}_n \end{bmatrix} = \begin{bmatrix} \boldsymbol{A}_1 & \boldsymbol{B}_1 \\ \boldsymbol{C}_1 & \boldsymbol{D}_1 \end{bmatrix} \begin{bmatrix} \tilde{\boldsymbol{q}}_0 \\ \tilde{q}_0 \end{bmatrix} \tag{1}$$

where

$$\boldsymbol{A}_1 = \cosh(k \cdot l(1+i))$$

$$\boldsymbol{B}_1 = -\frac{\sinh(k \cdot l(1+i))}{\boldsymbol{l} \cdot k(1+i)}$$

$$\boldsymbol{C}_1 = -\boldsymbol{l} \cdot k(1+i) \cdot \sinh(k \cdot l(1+i))$$

$$\boldsymbol{D}_1 = \cosh(k \cdot l(1+i))$$

with

$$k = \sqrt{\frac{\boldsymbol{w}}{2 \cdot a}} \quad \text{and} \quad a = \frac{\boldsymbol{l}}{\boldsymbol{r} \cdot c}$$

Sinusoidal surface heat flux and surface temperature oscillations are denoted by $\tilde{q}$ and $\tilde{\boldsymbol{q}}$. These are functions of *one* angular frequency, here depicted by the superscript ”~”. Surface *0* is the excited surface, whereas surface *n* is the obverse surface that is subject to different boundary conditions discussed later.

For a multi-layer component, a heat transfer matrix can be maintained through the successive multiplication of the heat transfer matrix of each layer. A component with three material layers would give a heat transfer matrix based on the product of its components.

$$\begin{bmatrix} \tilde{\boldsymbol{q}}_n \\ \tilde{q}_n \end{bmatrix} = \begin{bmatrix} \boldsymbol{A}_3 & \boldsymbol{B}_3 \\ \boldsymbol{C}_3 & \boldsymbol{D}_3 \end{bmatrix} \begin{bmatrix} \boldsymbol{A}_2 & \boldsymbol{B}_2 \\ \boldsymbol{C}_2 & \boldsymbol{D}_2 \end{bmatrix} \begin{bmatrix} \boldsymbol{A}_1 & \boldsymbol{B}_1 \\ \boldsymbol{C}_1 & \boldsymbol{D}_1 \end{bmatrix} \begin{bmatrix} \tilde{\boldsymbol{q}}_0 \\ \tilde{q}_0 \end{bmatrix} = \begin{bmatrix} \boldsymbol{A} & \boldsymbol{B} \\ \boldsymbol{C} & \boldsymbol{D} \end{bmatrix} \begin{bmatrix} \tilde{\boldsymbol{q}}_0 \\ \tilde{q}_0 \end{bmatrix} \tag{2}$$

3.2 Frequency response: Admittance.

The frequency response of a plane multi-layer component is the thermal behaviour of that component if it is subject to a sinusoidal excitation. This assumes that at least one of the surfaces is thermally excited, such as a surface temperature oscillation. The response is the heat flux that is induced at the excited surface and at the obverse surface. Provided that the temperature oscillates $\tilde{q}_0$ at surface *0* and the temperature at surface *n* is held constant, $\tilde{q}_n = 0$, the admittance Y_0 of surface *0* is defined as the ratio between the heat flux and temperature oscillation.

$$Y_0 = -\frac{\tilde{q}_0}{\tilde{\boldsymbol{q}}_0} = \frac{\boldsymbol{A}}{\boldsymbol{B}} \qquad (\tilde{q}_n = 0) \tag{3}$$

If temperature oscillations are the same at both surfaces, the admittance can be formulated such that

$$Y_0 = -\frac{\tilde{q}_0}{\tilde{\boldsymbol{q}}_0} = \frac{\boldsymbol{A-1}}{\boldsymbol{B}} \qquad \left(\tilde{q}_n = \tilde{q}_0\right) \tag{4}$$

When the obverse surface is adiabatic, the admittance can be formulated such that

$$Y_0 = -\frac{\tilde{q}_0}{\tilde{\boldsymbol{q}}_0} = \frac{\boldsymbol{C}}{\boldsymbol{D}} \qquad \left(\tilde{q}_n = 0\right) \tag{5}$$

3.3 The areic effective heat capacity

A building component is composed of materials that are continuums. A continuum is a ”melting pot” of continuously scattered thermal resistances and heat capacities. The effective heat capacity of the component is however a discrete value, that is supposed to represent the thermal performance (admittance) of the continuum. It must describe the combined effect of the scattered thermal resistances and heat capacities of the continuum.

Two discrete models can be set up to establish how the effective heat capacity may be defined and calculated. The first is a simple mass: the surface heat capacity model. The second is an RC-network that is composed of a thermal resistance in series with a heat capacity. Both have appeared in different versions of EN ISO standard proposals. In the following sections, the areic effective heat capacity will be denoted by χ and have the unit J/(m^2·K).

3.3.1 The surface heat capacity model

The effective heat capacity was in earlier proposals of European standard based on the model called the surface heat capacity. The surface heat capacity is calculated by means of analytical admittance of a component and the admittance of a model that represents a simple mass.

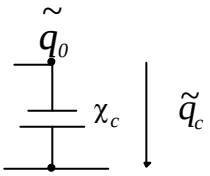

FIG. 1 The surface heat capacity model.

The heat transfer matrix of a heat capacity $\boldsymbol{c}_c$ is (Johannesson 1981)

$$\begin{bmatrix} \tilde{\boldsymbol{q}}_0 \\ 0 \end{bmatrix} = \begin{bmatrix} 1 & 0 \\ -i\boldsymbol{w}\boldsymbol{c}_c & 1 \end{bmatrix} \begin{bmatrix} \tilde{\boldsymbol{q}}_0 \\ \tilde{q}_c \end{bmatrix} \tag{6}$$

Therefore, this model has the admittance corresponding to

$$Y_c = -\frac{\tilde{q}_c}{\tilde{q}_0} = -i\omega c_c \tag{7}$$

By setting the amplitude of admittance of the model $|Y_c|$ equal to the amplitude of admittance of the component $|Y_0|$, a value for c_c can be determined. The effective heat capacity is the amplitude of admittance divided by the angular frequency.

$$c_c = \frac{|Y_0|}{\omega} \tag{8}$$

3.3.2 The RC-network model

In later European standard proposals, the effective heat capacity, here denoted by c_{rc}, is a part of a simple RC-network model, as shown in figure 2.

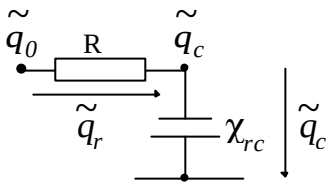

FIG. 2: The RC-network model.

The admittance of this model is

$$Y_{rc} = -\frac{\tilde{q}_r}{\tilde{q}_0} = -\frac{i\omega c_{rc}}{1 + R \cdot i\omega c_{rc}} \tag{9}$$

By setting the admittance of the model, Y_{rc}, equal to the admittance of the component, Y_0, the value of R and c_{rc} can be determined so that

$$R = -\mathrm{Re}\left(\frac{1}{Y_0}\right) \qquad \text{and} \qquad c_{rc} = \frac{1}{\omega \cdot \mathrm{Im}\left(\frac{1}{Y_0}\right)} \tag{10}$$

3.3.3 Differences in the two models

Jóhannesson (1981) analysed the thermal performance of the surface heat capacity and the RC-network. For a wide range of frequencies, the thermal performance of the RC-network agrees better with the analytical thermal

performance than does the surface heat capacity. The surface heat capacity models the amplitude of admittance for *one* given frequency very well but is inaccurate in describing the phase shift between the heat flux and temperature oscillation. The model emphasises on how much heat can be stored in a component, not when the storing takes place. The RC-network models not only the amplitude of admittance for the given component and frequency, but also models the phase shift. Information can be withheld on how much heat can be stored as well as when it takes place. The question is if the modelled phase shift has any greater importance within the level of detail in calculations with one of these two simple models.

The value of the heat capacity c_{rc} of the RC-network is always larger than the value of the surface heat capacity c_c. This is due to the "screening" effect that the thermal resistance in front of the heat capacity of the RC-model has on the model's thermal performance. So, which model gives the true effective heat capacity? In the author's opinion, c_c is more suited to be called the effective heat capacity for three reasons. The first is that the surface heat capacity is the amplitude of admittance divided by the frequency. It is therefore an informative value that explicitly gives the possibility of storing heat. The second is that the phase shift is often redundant in practical calculations, such as in EN 832. If the phase shift is needed, the analytical expressions in equations 1-3 can be used instead of the values from the RC-model since these are more accurate. The third reason is that the RC-network is complicated to understand since the thermal performance is modelled by the interaction between the thermal resistance and the heat capacity. Alone, c_{rc} can give no information on the amplitude and phase shift. Neither is it self-evident that the discrete model configuration with the thermal resistance and a heat capacity is a perfect representative of a continuum merely for the reason that admittance is composed of a real and an imaginary number.

4. The approximate method using the surface capacity model.

The new approximate method for determining the effective heat capacity is based on the surface heat capacity model, for reasons given in the previous section. The methodology, in more detail given in Appendix A, can be applied to various boundary conditions or to the RC-network model. The new method and applications will be shown as examples using typically Swedish multi-layer components. Also, it will be shown that the method is valid for a range of different frequencies including the important frequency corresponding to the 24-hour periodic. The approximative methods of the approximate prEN ISO standard will also be applied within the examples. First, these will be presented.

4.1 The approximate prEN ISO-methods.

Three different simplified methods are stated in Annex A of prEN ISO 13786. The methods are briefly reviewed below. These methods use a variable called the periodic penetration depth, but will within this context be reformulated in terms of time constants i.e. the product of thermal resistance and heat capacity of material layer parameters. See table 1 on the next page for nomenclature.

The thin layer approximation can be used for a thin surface layer next to insulation. If the time period T of the thermal process is

$$T \geq 4\pi \cdot R_1 \cdot C_1 \tag{11}$$

the effective heat capacity is determined from the material parameters of the surface layer so that

$$c = d_1 \cdot c_1 \cdot \rho_1 \tag{12}$$

The semi-infinite medium approximation can be used for a periodic T where

$$T \leq \frac{\pi}{4} R_1 \cdot C_1 \tag{13}$$

giving an effective heat capacity such that

$$c = \sqrt{\frac{\lambda_1 \cdot \rho_1 \cdot c_1}{\omega}} \tag{14}$$

Note that the validity ranges of equations 11 and 13 leave an interval that is not covered by an expression for determining the effective heat capacity. For this reason, and also to take into consideration multiple material layers between the insulation material and the interior surface, the *effective thickness method* can be applied. This method calculates the effective heat capacity on basis of the effective thickness d_e such that

$$c = \sum_i \rho_i \cdot d_i \cdot c_i \qquad \text{with} \qquad \sum_i d_i = d_e \tag{15}$$

The effective thickness d_e is calculated from material parameters for a concrete slab, and it is assumed that the effective thickness for the concrete slab is the same as for the actual component!

The effective thickness is the minimum value of either

- Half the total thickness of the component
- The thickness of materials between the surface and the first thermal insulating layer
- A maximum effective thickness depending on the period of the variations (1 hour uses 2 cm, 1 day uses 10 cm, 1 week with 25 cm).

4.2 The New Method.

The new method consists of 5 steps. These are to be followed in the order as stated below.

TAB. 1: Nomenclature and definitions.

Symbol	Unit	Comment
j	Index	Layer number. *1* is the internal surface material, *n* the external surface material.
d_j	m	Thickness of material layer *j*.
λ_j	W/(m·K)	Thermal conductivity of material layer *j*.
ρ_j	kg/m^3	Density of material layer *j*.
c_j	J/(kg·K)	Specific heat capacity of material layer *j*.
R_j	m^2·K/W	Thermal resistance of material layer *j*, $R_j = d_j / \lambda_j$
κ_j	J/(m^2·K)	Heat capacity of material layer *j*, $\kappa_j = d_j \cdot \rho_j \cdot c_j$
b_j	W·$\sqrt{s}$ /(m^2·K)	Thermal effusivity of material layer *j*, $b_j = \sqrt{\lambda_j \cdot \rho_j \cdot c_j}$

1. Acquire material data (λ_j , ρ_j and c_j) and geometry (d_j) of each material. Calculate R_j , κ_j and b_j for each layer *j*. Choose the time period T for which the areic heat capacity is to be calculated. The angular frequency ω (s^{-1}) is given by

$$\omega = 2\pi / T \tag{16}$$

2. Determine the maximum areic heat capacity κ_{c0} for the considered surface according to

$$\kappa_{c0} = \frac{1}{R_t} \cdot \left[\sum_{j=1}^{n} \kappa_j \left(\frac{R_j}{2} + \sum_{k=j+1}^{n+1} R_k \right) \right], \quad R_{n+1} = 0\,; \qquad R_t = \sum_{j=1}^{n} R_j \tag{17}$$

3. Calculate the effective thickness d_{eff} by means of κ_{c0} . The number of layers x at the inner side of the adiabatic plane is established.

$$\kappa_{c0} = \sum_{j=1}^{x} \rho_j \cdot c_j \cdot d_j \quad \text{such that} \quad \sum_{j=1}^{x} d_j = d_{eff} \tag{18}$$

The thickness of layer x can be adjusted to the length $d_{eff} - \sum_{j=1}^{x-1} d_j$.

4. Calculate time period values T_1 and T_2 (T_2 is omitted for slabs) according to

$$T_1 = 2\pi \cdot R_1 \cdot c_1 \qquad \text{and} \qquad T_2 = 4\pi \left[\frac{1}{b_2} \cdot \frac{(c_1 + c_2)^2 - c_1^2}{c_1 + \sqrt{2(c_1 + c_2)^2 - c_1^2}} \right]^2 \tag{19}$$

Selection of formula for c_c is based on fulfilment of criteria for the size of d_{eff}, T_1 and T_2 in table 2.

5. Calculate c_c. If c_c is greater than c_{c0}, then c_c is set equal to c_{c0}.

TAB. 2: Condition on the effective thickness and time period range of validity that gives the formula number for table 3.

Condition nr	Condition on d_{eff}	Condition on T_1 and T_2	Select formula
1	$d_{eff} \le d_1$	$T < 2\pi \cdot r_1 \cdot c_1 \cdot d_{eff}^2 / l_1$	Formula 1
2	$d_{eff} \le d_1$	$T \ge 2\pi \cdot r_1 \cdot c_1 \cdot d_{eff}^2 / l_1$	Formula 4
3	$d_{eff} > d_1$	$T < T_1$ and $T_2 > T_1$	Formula 1
4	$d_{eff} > d_1$	$T_1 < T < T_2$	Formula 2
5	$d_{eff} > d_1$	$T_2 < T_1$ and $T < T_1$	Formula 1
6	$d_{eff} > d_1$	$T_2 < T_1$ and $T \ge T_1$	Formula 3
7	$d_{eff} > d_1$	$T_2 > T_1$ and $T > T_2$	Formula 3

TAB. 3: Table for determination of the effective heat capacity. Formula number is given by condition fulfilment in table 2.

Formula nr	Effective heat capacity c_c	Max value
1	$c_c = b_1 / \sqrt{w}$	c_{c0}
2	$c_c = \sqrt{\dfrac{w \cdot c_1^2 + c_1 \cdot b_2 \sqrt{2w} + b_2^2}{w(1 + R_1 \cdot b_2 \sqrt{2w} + R_1^2 \cdot b_2^2 \cdot w)}}$	c_{c0}
3	$c_c = \sqrt{\dfrac{b_3^2(1 + (w \cdot R_2 c_1)^2) + b_3 \sqrt{2w}(c_1 + c_2)(1 + w \cdot R_2 c_1) + w(c_1 + c_2)^2}{w(1 + b_3^2 \cdot w(R_1 + R_2)^2 + b_3 \sqrt{2w}(R_1 + R_2)(1 + w \cdot R_1 c_2) + (w \cdot R_1 c_2)^2)}}$	c_{c0}
4	$c_c = c_{c0}$	c_{c0}

5. Application of the new method on examples

This section serves to show the application on the method on a step-to-step basis. The results of each step are commented. The core of the method lies in step 4, where effective thickness d_{eff} and periods T_1 and T_2 are the basis of the selection of formula. For this reason, there is no room left for intuition on behalf of a user to judge how many material layers actually participate in the heat transfer within the building component. The results in

the examples below are from a computational program with a source code based on conditions and relationships as expressed in the previous section.

5.1 Example 1

This first example is a sandwich construction with two material layers on the inside of the insulation layer.

TAB. 4: An exterior wall. The innermost layer is shown in the first row.

Wall 1	d [m]	λ [W/(m·K)]	ρ [kg/m³]	c [J/(kg·K)]	R [m²·K/W]	χ [J/(m²·K)]	b [W $\sqrt{s}$ /(m²·K)]
Mortar	0.01	1.0	1800	950	0.0100	17 100	1307.7
LECA*	0.10	0.25	1000	1050	0.4000	105 000	512.3
EPS	0.15	0.04	20	1400	3.7500	4 200	33.5
LECA*	0.05	0.25	1000	1050	0.2000	52 500	512.3
Mortar	0.01	1.0	1800	950	0.0100	17 100	1307.7

* LECA = Light Expanded Clay Aggregates

Step one is composed of acquiring material data and to determine the thermal resistance, heat capacity and thermal effusivity of each layer. These parameters are listed in the table of each example. The time periods of interest are for this example chosen to be totally four, namely 6, 12, 24 and 48 hours.

Step two is a straightforward calculation using equation 17 to determine c_{c0}, such that

$$c_{c0} = \frac{1}{R_t} \cdot \left[c_1 \left(\frac{R_1}{2} + R_2 + R_3 + R_4 + R_5 \right) + c_2 \left(\frac{R_2}{2} + R_3 + R_4 + R_5 \right) + \right. \\ \left. + c_3 \left(\frac{R_3}{2} + R_4 + R_5 \right) + c_4 \left(\frac{R_4}{2} + R_5 \right) + c_5 \left(\frac{R_5}{2} \right) \right] \tag{20}$$

In this example, c_{c0} = 120 380 J/(m²·K), which is the same as the analytical value for an annual periodic.

Step three is actually optional and helpful only for conditions 1 and 2 in table 2. In this example, d_{eff} = 0.1084 m. Therefore, d_{eff} indicates that the first two layers (x = 2) are on one side of the adiabatic plane, $d_{eff} > d_1$.

Step four is to determine the time constants. For the four chosen time periods, these will fulfil condition number 2 since insertion of data for T_1 and T_2 gives 0.30 h and 79.6 h, respectively. Since the four chosen periods fulfil the condition 0.30 h ≤ T ≤ 79.6 h (condition nr 2), formula 2 in table 3 has to be applied to determine c_c. In table 4 below, results are shown on values of c_c as well as deviation from analytical values. Also, values on the effective heat capacity determined by means of the prEN ISO effective thickness method are listed.

Step five is to assure that no value of c_c exceeds c_{c0}, which is the maximum value possible. Note that detailed calculations in step three were actually not needed.

TAB. 5: Results for the four chosen periods.

Time period [h]	6	12	24	48
New method c_c [J/(m^2·K)]	41 212	53 511	70 953	95 695
Deviation [%]	0.4	-3.8	-11.8	-7.9
EN ISO method c_c [J/(m^2·K)]	58 108	79 443	109 616	122 100
Deviation [%]	41.5	42.8	36.3	17.4

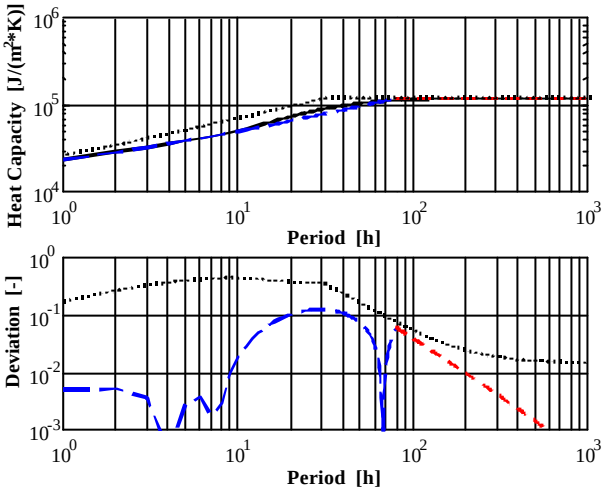

FIG. 3: Effective heat capacity from the various methods and deviation from the analytical solution. The filled curve is analytical, the dotted curve from prEN ISO, the dashed from the new method. The long dash curves are from formula 2 applied within the range 0.30 h ≤ T ≤ 79.6 h, the short dash curve from formula 3 since T > 79.6 h.

5.2 Example 2

This example is used to illustrate how the new method is used when applied to "homogeneous slabs".

TAB. 6: An exterior massive wall. The innermost layer is shown in the first row.

Wall 2	d [m]	λ [W/(m·K)]	ρ [kg/m^3]	c [J/(kg·K)]	R [m^2·K/W]	χ [J/(m^2·K)]	b [W $\sqrt{s}$ /(m^2·K)]
Aerated concrete	0.250	0.12	600	1050	2.083	157 500	275.0
Mortar	0.01	1.0	1800	950	0.01	17 100	1307.7

The results of s*tep one* are shown in table 5 and the time period is chosen to be T = 24 h. In s*tep two*, equation 17 gives the value c_{c0} = 79 167 J/(m^2·K). *Step three* gives an approximated effective thickness d_{eff} = 0.1257 m, so that $d_{eff} < d_1$. The calculations of time constants in *step four* are redundant, since $d_{eff} < d_1$ fulfils condition numbers 1 or 2. The time constant $2\pi \cdot r_1 \cdot c_1 \cdot d_{eff}^2 / l_1$ is found to be 144.7 hours. Condition 1 is therefore appropriate, thus is formula 1 to be used to determine c_c. The calculated value becomes 32 194 J/(m^2·K), deviating -5.7 % from the analytical value. *Step five* implies no change in the value of c_c.

On using the approximate methods of prEN ISO, equation 14 (applicable in this case) would give no differences in results compared to the new method. However, the prEN ISO method does have a limitation on the range of validity, which could lead to problems. Figure 4 illustrates the problem in terms of a ring, which shows where the range of validity ends. The value of the limit can be doubled without giving too large inaccuracies, since the doubled value marks the intersection with c_{c0}.

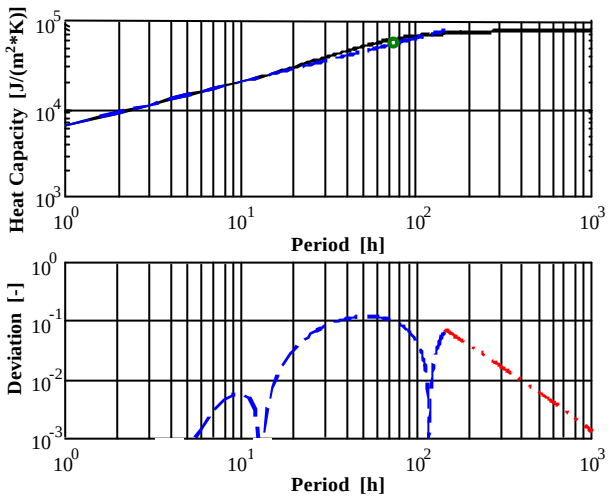

FIG. 4: Effective heat capacity and deviation from the analytical solution. The filled curve is analytical, the dashed is from the new method, here from formula 1. The dash -dot-dot is the line for c_{c0}. The ring marks the upper limit of the prEN ISO semi-infinite medium approximation validity range.

5.3 Example 3

Example 3 constitutes an external wall that has a thin interior surface material, here a gypsum board next to mineral wool. This type of lightweight component is very common in Swedish single family dwellings. Such a component is listed in table 7, with results plotted in figure 5.

On calculating with the new method, the maximal effective heat capacity (step 2) is established to be 13 601 J/(m^2·K); the same value as for an analytical annual cycle. The effective thickness is 0.1684 m, which reaches into the asphalt board (step 3). From the values calculated in step 4, where T_1 = 0.85 h and T_2 = 27.5 h, the condition used depends on the choice of T. For example, if the thermal process is diurnal, condition 4 of is fulfilled since 0.8 h $\leq T \leq$ 27.5 h and $d_{eff}>d_1$. The effective heat capacity is found with formula 2, 10 388 J/(m^2·K) (-9.3% deviation). On the other hand, if T is chosen to be 48 h, condition 7 is to be used since T > 27.5 h and $d_{eff}>d_1$. Condition 7 points to formula 3, which gives the value 11 232 J/(m^2·K) (-12.3% deviation). Step 5 of the calculation gives that the effective heat capacity has the value of c_{c0} for periodicities that are longer than 71 hours (see figure 5), where formula 3 actually gives larger results than the value of c_{c0}.

The prEN method gives one constant value for the displayed periods in figure 5. The reason is that the minimal penetration depth that is to be used in the calculation procedure is the distance between the surface and the insulation, here corresponding to the thickness of the gypsum board.

TAB. 7: An exterior lightweight wall. The innermost layer is shown in the first row.

Wall 3	d [m]	λ [W/(m·K)]	ρ [kg/m³]	c [J/(kg·K)]	R [m²·K/W]	χ [J/(m²·K)]	b [W √s /(m²·K)]
Gypsum board	0.013	0.216	740	840	0.0602	8 081	366.4
Mineral wool	0.150	0.040	23	750	3.7500	2 588	26.3
Asphalt board	0.012	0.065	400	1350	0.1846	6 480	187.3
Air cavity	0.020	0.133	1.2	1000	0.1504	24	12.6
Brick	0.120	0.60	1500	840	0.2000	151 200	869.5

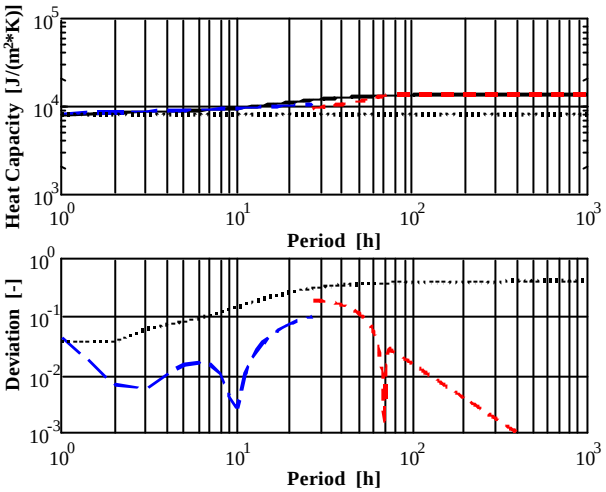

FIG. 5: Effective heat capacity from the various methods and deviation from the analytical solution. The filled curve is analytical, the dotted curve from prEN ISO, the dashed from the new method. The long dash curves are from formula 2, the short dash curves from formula 3.

5.4 Example 4

This is an example where a component has additional insulation at the interior surface: a common situation when a building is subject to retrofitting. Originally, the wall of this example is a heavy sandwich component. The additional insulation is placed at the interior surface along with a gypsum board.

The maximal effective heat capacity is c_{c0} = 147 576 J/(m²·K). The adiabatic plane of the new method is located at 0.1250 m, which is 0.0670 m into the third layer. Upon calculating the values T_1 = 0.87 h and T_2 = 2.91 h in *step 4*, conditions 4 or 7 are to be used depending on the choice of T. For T = 24 h, condition 7 is fulfilled such that formula 3 is used to determine the effective heat capacity. If T is greater than 383 h, step 5 of the calculation procedure gives the constant value of c_{c0} since formula 3 produces larger values, see figure 6. The effective thickness method of prEN underestimates the effective heat capacity as time periods increase. Due

to the criterion that the sum of layer thickness between surface and the first insulation layer is to be used, the material layers behind this insulation will not be taken into account.

TAB. 8: An exterior wall with additional insulation. The innermost layer is shown in the first row.

Wall 4	d [m]	λ [W/(m·K)]	ρ [kg/m^3]	c [J/(kg·K)]	R [m^2·K/W]	χ [J/(m^2·K)]	b [W $\sqrt{s}$ /(m^2·K)]
Gypsum board	0.013	0.21	740	840	0.0619	8 081	361.3
Mineral wool	0.045	0.036	20	800	1.2500	720	24.0
Concrete	0.100	1.7	2300	900	0.0588	207 000	1 875.9
EPS	0.100	0.04	23	1300	2.5000	3 220	35.9
Concrete	0.100	1.7	2300	900	0.0588	207 000	1 875.9

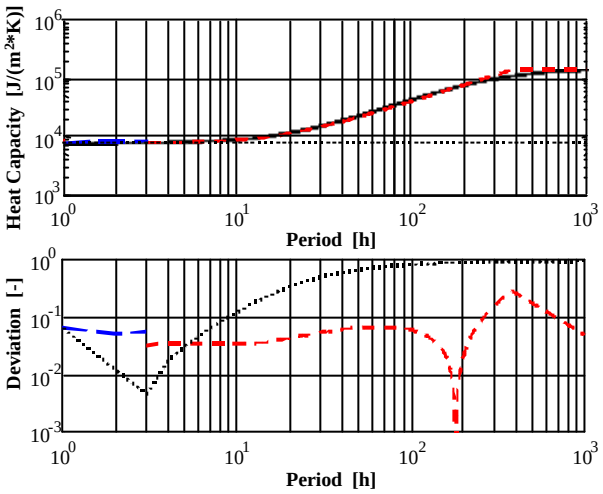

FIG. 6: Effective heat capacity from the various methods and deviation from the analytical solution. The filled curve is analytical, the dotted curve from prEN ISO, the dashed from the new method. The long dash curves are from formula 2, the short dash curves from formula 3.

5.5 Example 5

Example 5 serves to illustrate what is done if $T_2 < T_1$. For this purpose, the more or less non-conventional wall component is listed in table 9. Application of equation 17 of *step 2* gives the maximum value of the heat capacity to be 75 846 J/(m^2·K). The value of d_{eff} calculated in *step 3* is 0.0859 m, well into the third layer. In *step 4*, the time periods receive values such that T_1 = 5.73 h and T_2 = 0.01 h. On checking the conditions of table 2, d_{eff} is obviously larger than the first layer and $T_2 < T_1$. Now, the criterion depends on the magnitude of the chosen period *T*. If $T < T_1$, condition 5 pointing to formula 1 is convenient to use. Should *T* be chosen such that $T \geq T_1$, condition 6 thus formula 3 gives appropriate values to the effective heat capacity. In figure 7, results are shown for the choice of *T* ranging from periodicities of 1 hour to 1000 hours.

TAB. 9: An exterior wall with additional insulation. The innermost layer is shown in the first row.

Wall 5	d	λ	ρ	c	R	χ	b

	[m]	[W/(m·K)]	[kg/m^3]	[J/(kg·K)]	[m^2·K/W]	[J/(m^2·K)]	[W $\sqrt{s}$ /(m^2·K)]
Wood board	0.020	0.14	500	2300	0.1429	23 000	401.2
Air cavity	0.020	0.133	1.2	1000	0.1504	24	12.6
Massive wood	0.050	0.14	500	2300	0.3571	57 500	401.2
Mineral wool	0.150	0.040	23	750	3.7500	2 588	26.3
Air cavity	0.012	0.133	1.2	1000	0.0902	14	12.6
Wood façade	0.020	0.14	500	2300	0.1429	23 000	401.2

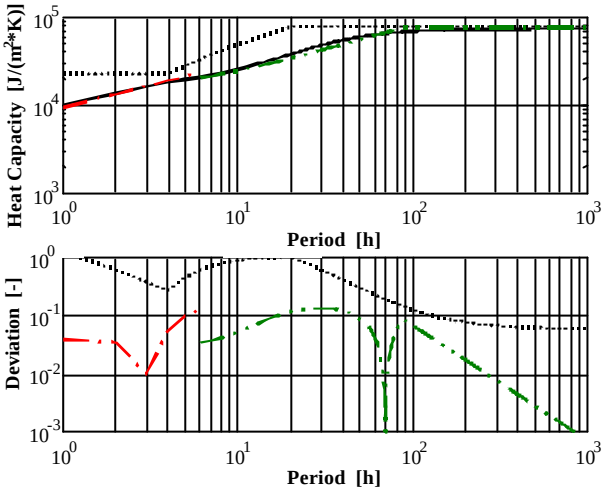

FIG. 7: Effective heat capacity from the various methods and deviation from the analytical solution. The filled curve is analytical, the dotted curve from prEN ISO, the dashed from the new method. The long dash-dot curves are from formula 1 for $T < T_1$*, the short dash-dot-dot curves from formula 3 were* $T \geq T_1$*.*

6. Conclusions and discussion.

The work presented in this paper has shown the application of a methodology for determining the effective heat capacity with equations that primarily require material data on the surface layer materials on one side of the multi-layer component. The method for determining the effective heat capacity presented in section 4.2 is similar to the simplified methods suggested in the normative Annex A of prEN ISO 13786. However, the new method is applicable for a wider range of frequencies and generally gives more reliable results for a number of comparable cases. This paper shows five cases of building components that are typical in northern climates. It is seldom that the deviation between the new method's solution and the analytical solution for one frequency is larger than ±20%. In fact, the deviations are some ±10% or lower. The approximate methods of prEN ISO 13786 consistently give results with larger deviations.

The equations use for determining the effective heat capacity are derived from the theory of frequency response with the assumption that temperature oscillations are identical at the surfaces of the building component. However, the methodology allows other boundary conditions to be considered, such as zero heat flux or constant temperature at one surface. Also, surface thermal resistances can be introduced in the calculation procedure.

The equations and comparisons made within the context of this paper assume that the effective heat capacity is defined on basis of a surface heat capacity model (equation 8). On the other hand, the methodology can be

applied for calculation of the effective heat capacity as defined by the simple RC-network (equation 10). For the reason that the author considers that the effective heat capacity is more conveniently quantified by the surface heat capacity model (section 3.3), the content of this paper focuses on the results from this model. Preliminary work has been done on the simplified method applied to the RC-network, which will be documented in a working report.

7. References

Akander J. (1995). *Efficient Modelling of Energy Flow in Building Components. Parts 1 & 2*. Licentiate Thesis. Department of Building Sciences, Kungliga Tekniska Högskolan, Stockholm, Sweden.

Akander J. and Jóhannesson G. (2000). The Thermal Performance of Building Components - Applications of the Bode Diagram. (*Submitted*) *Nordic Journal of Building Physics*, Available at http://www.bim.kth.se/bphys

Athienitis A.K. (1989). A Computer Method for Systematic Sensitivity Analysis of Building Thermal Networks. *Building and Environment, Vol. 24*, No. 2, pp. 163-168.

Bunn J.P. (1983). The Thermal Response of a Homogeneous Slab to a Constant Heat Flux. *Building and Environment, Vol. 18* No. 1/2, pp. 61-64.

Carslaw H.S. and Jaeger J.C. (1959). *Conduction of Heat in Solid*. 2nd ed. Oxford University Press, London, United Kingdom.

Davies M.G. (1983). Optimum Design of Resistance and Capacitance Elements in Modelling a Sinusoidally Excited Building Wall. *Building and Environment, Vol.18*, No. 1/2, pp. 19-37.

Davies M.G. (1994). The Thermal Response of an Enclosure to Periodic Excitation: The CIBSE Approach. *Building and Environment, Vol. 29*, No. 2, pp. 217-235.

Davies M.G. (1995). Solutions to Fourier's Equation and Unsteady Heat Flow through Structures. *Building and Environment, Vol. 30*, No. 3, pp. 309 - 321.

Gruber P. and Toedtli J. (1989). On the Optimal Thermal Storage Capability of a Homogeneous Wall Under Sinusoidal Excitations. *Energy and Buildings, Vol 13*, p. 177 - 186.

Johannesson G. (1981). *Active Heat Capacity - Models and Parameters for Thermal Performance of Buildings.* Doctoral Dissertation, Report TVBH-1003, LTH, Lund, Sweden.

Krec K. (1993). *On the Storage of Heat in Building Components*. Hochbau für Architekten und Entwefen. Technische Universität Wien, Austria.

Magyari E. and Keller B. (1998). The Storage Capacity of a Harmonically Heated Slab Revisited. *International Journal of Heat and Mass Transfer, Vol. 41*, No. 10, pp. 1199-1204.

Milbank N.O. and Harrington-Lynn J. (1974). Thermal response and the admittance procedure. *Building Services Eng., Vol. 42*, pp. 38-51.

Panzhauser E. (1991). *Programmpaket WAEBRU.* Hochbau für Architekten und Entwefen. Technische Universität Wien, Austria.

Walsh P.J. and Delsante A.E. (1983). Calculation of the Thermal Behaviour of Multi-Zone Buildings. *Energy and Buildings, Vol. 5*, pp. 231-242.

EN 832 (1998). *Thermal performance of buildings - Calculation of energy use for heating - Residential buildings.* European Committee for Standardisation (CEN), Brussels.

prEN ISO 13786 (1998). *Thermal performance of building components- Dynamic thermal characteristics - Calculation methods.* CEN/TC 89/WG 4/N176, Brussels.

APPENDIX A.

A1. The methodology

This appendix describes how the equations of tables 2 and 3 have been obtained. The methodology is to a great extent based on asymptotic values of admittance. These asymptotic values are dependent on whether the thermal process is that of a high or a low frequency, and on the boundary conditions. Therefore, the first part of this appendix focuses on the asymptotic values of admittance of a slab. The second part will to a greater extent show how the switching frequencies (time constants) and approximate equations for the effective heat capacity are derived.

A1.1 Informative asymptotic values of admittance

Equations 1 and 5 can be very informative and radically simplified by making a few of assumptions. The equations can roughly be said to be functions of two variables, namely the product of $k \cdot l$ and $\boldsymbol{l} \cdot k$. For a given slab, it is the thickness (l) and angular frequency (in k) which will dominate the response of the component. Therefore, the product of $k \cdot l$ becomes interesting with respect to its magnitude.

A1.1.1 The product of $k \cdot l$ is large.

For a process where the term $k \cdot l$ is large, it implies that l or $\boldsymbol{w}$ is "infinite". Approximations that can be used are $\tanh(k \cdot l) \approx 1$ and $\sinh(k \cdot l) >> k \cdot l$. It will be seen that equations 3 to 5 give the same value for the admittance, independent of the boundary condition used. The value is the response of a semi-infinite solid. For example, if $\tilde{J}_n = 0$, then the admittance becomes

$$Y_0 = \frac{\boldsymbol{A_1}}{\boldsymbol{B_1}} = -\frac{\cosh(k_1 \cdot l_1(1+i))}{\dfrac{\sinh(k_1 \cdot l_1(1+i))}{\boldsymbol{l}_1 \cdot k_1(1+i)}} = -\frac{\boldsymbol{l}_1 \cdot k_1(1+i)}{\tanh(k_1 \cdot l_1(1+i))} \approx -\sqrt{\frac{\boldsymbol{l}_1 \cdot \boldsymbol{r}_1 \cdot c_1 \cdot \boldsymbol{w}}{2}}(1+i) \qquad \text{(A1)}$$

This solution is also found if $\tilde{q}_n = 0$ and for $\tilde{J}_0 = \tilde{J}_n$.

A1.1.2 The product of $k \cdot l$ is small.

If the value of $k \cdot l$ is small, the surface layer is thin or the process is of a low frequency nature. The approximation used is that a small value $k \cdot l$ gives $\tanh(k \cdot l) \approx k \cdot l$. Also, the term $\sinh(k \cdot l) \approx k \cdot l$ is used.

A1.1.2.1 The admittance if $\tilde{J}_n = 0$.

The admittance of a component, where a surface temperature is fixed is according to equation 3

$$Y_0 = \frac{\boldsymbol{A}}{\boldsymbol{B}} = -\frac{\boldsymbol{l} \cdot k(1+i)}{\tanh(k \cdot l(1+i))} \approx -\frac{1}{R} \qquad \text{(A2)}$$

A1.1.2.2 The admittance if $\tilde{q}_n = 0$.

If the component can be considered to be adiabatic, for example if it is well insulated, the admittance is

$$Y_0 = \frac{\boldsymbol{C}}{\boldsymbol{D}} = -\boldsymbol{l} \cdot l(1+i) \cdot \tanh(k \cdot l(1+i)) \approx -i\boldsymbol{w} \cdot \boldsymbol{r} \cdot c \cdot l \tag{A3}$$

A1.1.2.3 The admittance if $\tilde{J}_0 = \tilde{J}_n$.

Components subject to the same thermal process at both surfaces have the admittance at surface *0* as being

$$Y_0 = \frac{\boldsymbol{A}-1}{\boldsymbol{B}} = -\frac{\boldsymbol{l} \cdot k(1+i)[\cosh(k \cdot l(1+i))-1]}{\sinh(k \cdot l(1+i))} \approx -i\boldsymbol{w}\frac{\boldsymbol{r} \cdot c \cdot l}{2} \tag{A4}$$

A1.2 Obtaining equations for the new method.

The sought effective heat capacity $\boldsymbol{c}_c$ is calculated from the analytical admittance that is a complex number (a real and an imaginary part). Therefore, it is determined by means of the absolute value of admittance by

$$\boldsymbol{w}\boldsymbol{c}_c = |Y_0| \tag{A5}$$

The value of $|Y_0|$ depends on the chosen boundary condition. For the reason that the proposed norm uses the boundary condition where temperature oscillation at both surfaces are the same, $\tilde{J}_0 = \tilde{J}_n$, admittance of the component is analytically found in the form of

$$|Y_0| = \left|\frac{\boldsymbol{A}-\boldsymbol{1}}{\boldsymbol{B}}\right| \tag{A6}$$

The use of this boundary condition creates an "adiabatic plane" within the building component for non-steady heat transfer. For example, in a symmetrical component, the adiabatic plane will be situated at the centre line of the component. Dynamic heat flux is zero at this point. This means that the boundary condition $\tilde{q} = 0$ can be used on a "thermal half" of the component; the part with the considered surface. It is therefore important within this context to establish where this plane is located, the so-called effective thickness d_{eff}, along with the maximum value of the effective heat capacity $\boldsymbol{c}_{c0}$ of the considered surface.

A1.2.1 Approximation of the maximum value of the effective heat capacity.

For a symmetrical component that is symmetrically excited on both sides, the maximum value of the effective heat capacity is half of the total heat capacity. The obviousness of this statement is seen in equation A4. However, it is more difficult to establish the effective heat capacity of a non-symmetrical component. An equation that gives good agreement with analytical values is expressed in equation A7, which is applicable to a component composed of n number of material layers. Equation A7 is derived from a chain of serially connected

thermal resistances and heat capacities where each material layer is represented by a central capacity cell (Akander and Jóhannesson 2000). The maximum value is found when ω approaches zero, here denoted by γ_{c0}.

$$\gamma_{c0} = \frac{1}{R_t} \cdot \left[\sum_{j=1}^{n} \gamma_j \left(\frac{R_j}{2} + \sum_{k=j+1}^{n+1} R_k \right) \right], \; R_{n+1} = 0 \qquad \text{(A7)}$$

The dummy resistance R_{n+1} is introduced merely to ease the mathematical formulation. Experience of use indicates that the inaccuracy of equation A7 is much less than 1% for common Swedish building components.

The effective thickness can be calculated from γ_{c0}. By finding how many material layers γ_{c0} is composed of, the effective thickness is found with the following two expressions.

$$\gamma_{c0} = \sum_{j=1}^{x} \rho_j \cdot c_j \cdot d_j \;\; \text{such that} \sum_{j=1}^{x} d_j = d_{eff} \qquad \text{(A8)}$$

This variable is important since it indicates where the adiabatic plane is situated. *The criterions of relationships stated in the following sections will therefore be based on the effective thickness and the material layers situated on the considered side of the adiabatic plane.*

A1.2.2 Single layer approximation.

A first hypothesis that can be formulated is that the surface layer completely dominates the thermal performance of the component. The component may be composed of one or more material layers. However, is necessary to set up two criterions since there are two types of heat transfers that depend on where the adiabatic plane is situated, as will be seen in the following text. These two are governed on whether $d_{eff} < d_1$ or $d_{eff} \geq d_1$.

A1.2.2.1 High frequency process.

A high frequency thermal process for a single-layer component results in the response of a semi-infinite solid, see equation A1. The effective heat capacity is for all boundary condition cases and effective thickness condition

$$\gamma_c = \frac{b_1}{\sqrt{\omega}} = \sqrt{\frac{\lambda_1 \cdot \rho_1 \cdot c_1}{\omega}} \qquad \text{(A9)}$$

A1.2.2.2 Low frequency process.

For a low frequency thermal process, it is important to establish where the effective thickness is situated in relation to the surface layer thickness. For a slab (single layer component) or a component with a thick surface layer, the condition $d_{eff} < d_1$ will hold true. The effective heat capacity, see equation A3, becomes

$$\gamma_c = \rho_1 \cdot c_1 \cdot d_{eff} \qquad \text{(A10)}$$

The switching frequency at which the response changes behaviour is found by setting equations A9 and A10 equal to each other. The switching period, which marks the transition from the semi-infinite response to the simple mass response, is

$$T = 2\boldsymbol{p} \cdot \frac{\boldsymbol{r}_1 \cdot c_1}{\boldsymbol{l}_1} d_{eff}^2 \qquad \left(\tilde{q}_n = \tilde{q}_0\right) \tag{A11}$$

If $d_{eff} \geq d_1$ for a surface layer next to a material layer that can be considered to be perfect insulation, an adiabatic plane exists behind the surface layer. Hereby, the asymptote of equation A3 can be used.

$$\boldsymbol{c}_c = \boldsymbol{r}_1 \cdot c_1 \cdot l_1 \qquad \left(\tilde{q}_n = 0\right) \tag{A12}$$

The switching period, which marks the transition from the semi-infinite response to the simple mass response, is

$$T_1 = 2\boldsymbol{p} \cdot R_1 \cdot \boldsymbol{c}_1 \qquad \left(\tilde{q}_n = 0\right) \tag{A13}$$

Equations A10 and A12 give the same results as stated in Annex A of the prEN ISO norm (here called equations 12 and 14). However, a new range of validity can be formulated thus covering the whole range of possible time periods for the single layer approximation. These are equations A11 and A13, to be compared with equations 11 and 13.

A1.2.3 Double layer approximation.

If the analytical effective heat capacity for a multi-layer component is larger than the heat capacity of the surface layer, the previous expressions will prove to be inadequate. In order to improve the method, the layer behind the surface layer will be taken into consideration. The heat transfer matrix will now include the second layer, giving

$$\begin{bmatrix} \boldsymbol{A} & \boldsymbol{B} \\ \boldsymbol{C} & \boldsymbol{D} \end{bmatrix} = \begin{bmatrix} \boldsymbol{A}_2 & \boldsymbol{B}_2 \\ \boldsymbol{C}_2 & \boldsymbol{D}_2 \end{bmatrix} \begin{bmatrix} \boldsymbol{A}_1 & \boldsymbol{B}_1 \\ \boldsymbol{C}_1 & \boldsymbol{D}_1 \end{bmatrix} \tag{A14}$$

The admittance is here C/D since the two material layers are in front of the adiabatic plane at d_{eff}. The admittance will after some mathematics have the form

$$Y_0 = \frac{\boldsymbol{C}}{\boldsymbol{D}} = \left(\frac{\dfrac{\boldsymbol{C}_1}{\boldsymbol{D}_1} + \dfrac{\boldsymbol{C}_2}{\boldsymbol{D}_2}}{\dfrac{\boldsymbol{B}_1}{\boldsymbol{A}_1} \cdot \dfrac{\boldsymbol{C}_1}{\boldsymbol{D}_1} + 1} \right) \tag{A15}$$

A1.2.3.1 High frequency processes.

On using the relationships from equations A1 - A3, the following expressions can be used with the assumption that the thermal process in the second layer resembles that of a semi-infinite solid. The frequency is assumed to be low enough as to totally penetrate the first layer.

$$\frac{\boldsymbol{C}_1}{\boldsymbol{D}_1} = -i\boldsymbol{w}\boldsymbol{c}_1\,;\ \frac{\boldsymbol{B}_1}{\boldsymbol{A}_1} = -R_1\,;\ \frac{\boldsymbol{C}_2}{\boldsymbol{D}_2} = -b_2\sqrt{\frac{\boldsymbol{w}}{2}}(1+i) \tag{A16}$$

Insertion of the expressions in A16 into equation A15 gives formula 2 as expressed in table 3. The lower limit of the range of validity is determined by the switching period that marks semi-infinite from the simple mass response (equation A13). The upper limit has to be calculated by setting the effective heat capacity to be the sum of the heat capacities of the two layers, which in turn is set equal to formula 2. The denominator of formula 2 is approximated to be 1 (the other terms can be neglected) to decrease the number of roots (solutions). The switching period is then given by

$$T_2 = 4\boldsymbol{p}\left[\frac{1}{b_2}\cdot\frac{(\boldsymbol{c}_1+\boldsymbol{c}_2)^2-\boldsymbol{c}_1^2}{\boldsymbol{c}_1+\sqrt{2(\boldsymbol{c}_1+\boldsymbol{c}_2)^2-\boldsymbol{c}_1^2}}\right]^2 \tag{A17}$$

A1.2.3.2 Low frequency processes.

For low frequency processes, the term for the second layer can be assumed to be

$$\frac{\boldsymbol{C}_2}{\boldsymbol{D}_2} = -i\boldsymbol{w}\cdot\boldsymbol{c}_2 \tag{A18}$$

The solution becomes

$$\boldsymbol{c}_c = \frac{\boldsymbol{c}_1+\boldsymbol{c}_2}{\sqrt{1+(\boldsymbol{w}\cdot R_1\cdot\boldsymbol{c}_2)^2}} \tag{A19}$$

This formula is not shown in table 3, for the reason of reducing the total amount of formulas. Formula 3 replaces the formula of equation A19 with the risk of giving a somewhat larger inaccuracy.

A1.2.4 Triple layer approximation.

For the triple layer approximation, only the high frequency process equation has been put forth within this context. The heat transfer matrix is for the triple layer

$$\begin{bmatrix}\boldsymbol{A} & \boldsymbol{B}\\ \boldsymbol{C} & \boldsymbol{D}\end{bmatrix} = \begin{bmatrix}\boldsymbol{A}_3 & \boldsymbol{B}_3\\ \boldsymbol{C}_3 & \boldsymbol{D}_3\end{bmatrix}\begin{bmatrix}\boldsymbol{A}_2 & \boldsymbol{B}_2\\ \boldsymbol{C}_2 & \boldsymbol{D}_2\end{bmatrix}\begin{bmatrix}\boldsymbol{A}_1 & \boldsymbol{B}_1\\ \boldsymbol{C}_1 & \boldsymbol{D}_1\end{bmatrix} \tag{A20}$$

The admittance can be reformulated such that

$$Y_0 = \frac{\boldsymbol{C}}{\boldsymbol{D}} = \left(\frac{\frac{\boldsymbol{C}_3}{\boldsymbol{D}_3}\left(1 + \frac{\boldsymbol{B}_2}{\boldsymbol{A}_2} \cdot \frac{\boldsymbol{C}_1}{\boldsymbol{D}_1}\right) + \frac{\boldsymbol{C}_1}{\boldsymbol{D}_1} + \frac{\boldsymbol{C}_2}{\boldsymbol{D}_2}}{\frac{\boldsymbol{C}_3}{\boldsymbol{D}_3}\left(\frac{\boldsymbol{B}_1}{\boldsymbol{A}_1} + \frac{\boldsymbol{B}_2}{\boldsymbol{A}_2}\right) + \frac{\boldsymbol{B}_1}{\boldsymbol{A}_1} \cdot \frac{\boldsymbol{C}_2}{\boldsymbol{D}_2} + 1} \right)_{approx} \tag{A21}$$

Again, it is assumed that the sinusoidal completely penetrates the first two layers, but not the third. Therefore, the terms of equation A21 will be

$$\frac{\boldsymbol{C}_1}{\boldsymbol{D}_1} = -i\boldsymbol{w}\boldsymbol{c}_1 ;\ \frac{\boldsymbol{C}_2}{\boldsymbol{D}_2} = -i\boldsymbol{w}\boldsymbol{c}_2 ;\ \frac{\boldsymbol{B}_1}{\boldsymbol{A}_1} = -R_1 ;\ \frac{\boldsymbol{B}_2}{\boldsymbol{A}_2} = -R_2 ;\ \frac{\boldsymbol{C}_3}{\boldsymbol{D}_3} = -b_3\sqrt{\frac{\boldsymbol{w}}{2}}(1+i) \tag{A22}$$

The result is found as formula 3 in table 3. For the correct switching period, formula 3 would have to be equal to the formula of equation A19. This would mean solving a 6th degree polynomial, which would give roots that are too complicated for an application of an approximate method.

PAPER 3

The Thermal Performance of Multilayer Building Components - Experimental Assessment of the Effective Heat Capacity.

The Thermal Performance of Multilayer Building Components - Experimental Assessment of the Effective Heat Capacity.

SUBMITTED: February 2000.
REVISED: .
PUBLISHED: .

Jan Akander, Techn. Lic.,
Dept of Building Sciences, Kungl Tekniska Högskolan;
S – 100 44 Stockholm;
akander@bim.kth.se

KEYWORDS*: Effective heat capacity, building component, frequency response, heat flux sensor.*

SUMMARY*:*
Measurements of a full-scale experimental building have been carried out with the purpose of establishing the effective heat capacity of various building components. The conventional auxiliary wall method was utilised, and excitation performed with electrical radiators according to a Pseudo Random Binary Sequence (PRBS). Acquired data was handled in various FFT windows, but the experimental results show a systematic deviation from expected analytical values at higher frequencies. The reason is explained with a numerical study, which shows that heat flux sensors with thermopiles have a frequency-dependent inaccuracy. This inaccuracy has the same size as the systematic deviation of the measurement results. Agreement is better at low frequencies, corresponding to periodicity above 10 hours. This paper also focuses on the influence of boundary conditions on the effective heat capacity.

1. Purpose

This paper demonstrates that in-situ measurement of the effective heat capacity of a building component is possible. Measurement methodology and the means of treating acquired data are validated with theoretical results. At a first glance, it appears that deviations between expected theoretical and measured results are large. On analysing sources of errors, one finds that heat flux sensors of the type "wound wire thermopiles" are inaccurate for measurement of high frequency dynamic heat flow. Hence, another purpose of this paper is to bring forth a discussion whether or not thermopile heat flux sensors only are suitable for measurements of steady-state entities.

2. Introduction

The heat capacity of a construction is a matter that is increasingly coming to focus within the field of building design. Heat capacity has a dominating role in the thermal performance of a building, and can therefore affect thermal comfort in the internal environment, energy requirement and peak loads. Within the frame of European building standards, there are requirements on that a building component’s thermal transmission is quantified in terms of a U-value and the dynamic thermal performance in terms of an effective heat capacity and decrement factor (prEN ISO 13786).

The calculation procedure for determining the effective heat capacity of a multi-layer construction is based on the assumption that the boundaries (surfaces of walls) are subject to sinusoidal excitations of temperatures and rates of heat flow density (heat fluxes). This calculation procedure is related or similar to work done by a number of scientists, some mentioned in previous parts of this series of papers with the title "The Thermal Performance of Multilayer Building Components" (Akander and Jóhannesson 2000), (Akander 2000).

The work within this paper deals with an empirical assessment in accordance to such a calculation procedure. It serves to experimentally validate theoretical calculations of the effective heat capacity. Furthermore, a study is made on how boundary conditions of natural climates influence the magnitude of the effective heat capacity.

3. The Nature of Continuous Signals.

Given any signal in terms of a set of discrete points in the time domain, the signal can be represented as the sum of an infinite harmonic series. This, of course, assumes that the system is linear so that each frequency component and the steady-state solution can be superposed. Now, if the signals in question are temperature and heat flux at the surface of a building component, the system is the building component itself. This system is linear if the material properties and the thickness of each material layer are constant. The density of heat flow rate (heat flux) q and the temperature $\boldsymbol{q}$ can be expressed as follows:

$$q = \bar{q} + \sum_{j=1}^{\infty} \tilde{q}_j \tag{1}$$

and

$$\boldsymbol{q} = \bar{\boldsymbol{q}} + \sum_{j=1}^{\infty} \tilde{\boldsymbol{q}}_j \tag{2}$$

Here, $\bar{q}$ and $\bar{\boldsymbol{q}}$ depict the steady state component (mean value of a longer time series). The terms $\tilde{q}_j$ and $\tilde{\boldsymbol{q}}_j$ represent heat flux and temperature oscillation for *one* frequency. If the considered series is time limited, ∞ is substituted by an integer.

Carslaw and Jaeger (1959) provide the analytical solution of the heat equation for solid materials in terms of a heat transfer matrix. The relationship between heat flux and temperature oscillation on one side of a homogenous slab, with index *0*, and the same entities on the other, here with the index *n*, is

$$\begin{bmatrix} \tilde{\boldsymbol{q}}_n \\ \tilde{q}_n \end{bmatrix} = \begin{bmatrix} A & B \\ C & D \end{bmatrix} \begin{bmatrix} \tilde{\boldsymbol{q}}_0 \\ \tilde{q}_0 \end{bmatrix} \tag{3}$$

where

$$A = \cosh\left(k \cdot l(1+i)\right),\ B = -\frac{\sinh\left(k \cdot l(1+i)\right)}{\boldsymbol{l} \cdot k(1+i)},\ C = -\boldsymbol{l} \cdot k(1+i) \cdot \sinh\left(k \cdot l(1+i)\right),\ D = \cosh\left(k \cdot l(1+i)\right)$$

with

$$k = \sqrt{\frac{\boldsymbol{w}}{2 \cdot a}} \quad \text{and} \quad a = \frac{\boldsymbol{l}}{\boldsymbol{r} \cdot c}$$

For a multi-layer component, the heat transfer matrix of each material layer is successively multiplied in material layer order. The product is a heat transfer matrix with four complex-numbered elements *A, B, C* and *D.*

$$\begin{bmatrix} \tilde{\boldsymbol{q}}_n \\ \tilde{q}_n \end{bmatrix} = \begin{bmatrix} A_n & B_n \\ C_n & D_n \end{bmatrix} \cdot \begin{bmatrix} A_{n-1} & B_{n-1} \\ C_{n-1} & D_{n-1} \end{bmatrix} \cdot \ldots \cdot \begin{bmatrix} A_1 & B_1 \\ C_1 & D_1 \end{bmatrix} \begin{bmatrix} \tilde{\boldsymbol{J}}_0 \\ \tilde{q}_0 \end{bmatrix} = \begin{bmatrix} A & B \\ C & D \end{bmatrix} \begin{bmatrix} \tilde{\boldsymbol{q}}_0 \\ \tilde{q}_0 \end{bmatrix} \tag{4}$$

3.1 Definition of admittance.

The heat transfer matrix contains information that quantifies admittance. Admittance is the ratio between heat flux and temperature oscillation on *one* side of the construction. A plane building component has two admittances, one for each surface. The definition of admittance of the surface with index 0 is

$$Y_0 = -\frac{\tilde{q}_0}{\tilde{\theta}_0} \tag{5}$$

Now, given the heat transfer matrix of the building component, and assumptions on the boundary condition type at the exterior surface, admittance at the interior surface can be established such that

$$Y_0\Big|_{\tilde{q}_n=0} = \frac{A}{B}; \quad Y_0\Big|_{\tilde{\theta}_n=0} = \frac{C}{D}; \quad Y_0\Big|_{\tilde{q}_n=\tilde{q}_0} = \frac{A-1}{B} \tag{6}$$

More on this subject is found within this series of papers (Akander and Jóhannesson 2000) and Akander (2000).

Special attention is in this context focused on the first term of equation 6, since the applied measurement technique is of the auxiliary wall method. Since there is a recommendation that heat flux sensors should not be placed directly on the external surface of building components ($\tilde{q}_n$ is not measured), admittance will according to equation 3 be

$$-\frac{\tilde{q}_0}{\tilde{\theta}_0} = \frac{A}{B} - \frac{1}{B}\cdot\frac{\tilde{\theta}_n}{\tilde{\theta}_0} \tag{7}$$

This equation can be used to find the ratio A/B if a value of $1/B$ is theoretically estimated.

3.2 The Effective Heat Capacity.

The simplest model that can represent the dynamic thermal performance of a construction is a surface heat capacity, see for example (Jóhannesson 1981) and (Akander 2000). If the absolute value of model admittance is set equal to the absolute value of analytical admittance, χ can be determined, where

$$|c| = \frac{|Y_0|}{w} \tag{8}$$

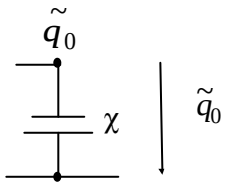

FIG. 1: Model of the surface heat capacity.

3.3 Application of the theory on the measured objects

AB Svensk Leca is a manufacturer of light expanded clay aggregate (LECA) products. The products are composed of clay aggregates, which are affixed by a thin layer of concrete. Depending on clay aggregate diameter, thus density, the building material as a whole can have different material properties.

3.3.1 The external wall

In table 1, a list of material layers, thickness and material properties are shown for an external wall, in the order of interior surface layer first. SP (1996) measured the thermal properties of the first three layers whereas the properties of the outermost layer have been assumed.

TAB. 1: Layer thickness and material properties of a wall specimen. The light expanded clay aggregate (LECA) material properties have been measured. The values of material properties of mortar are assumed.

Material layer	l [m]	λ [W/(m·K)]	ρ [kg/m³]	c [J/(kg·K)]
LECA high density	0.02	0.25	970	1040
LECA low density	0.30	0.16	540	1190
LECA high density	0.03	0.25	970	1040
Mortar	0.02	1.00	1800	950

Layer thickness can vary due to production method and clay aggregate diameter. The first layer can, for example, according to the manufacturer have a tolerance of ± 5 mm.

Figure 2 shows results on the application of heat capacity calculations. High frequency processes involve only heat exchange with the surface material since the heat pulse cannot penetrate deeper into the construction. Note the switching frequency (Akander and Jóhannesson 2000) corresponding to 1.6 hours, where the effective heat capacity starts to be influenced by the second material layer. Lower frequency processes allow heat waves to penetrate farther into the construction and will therefore permit larger quantities of heat to be stored, however influenced by the choice of boundary condition at the external surface.

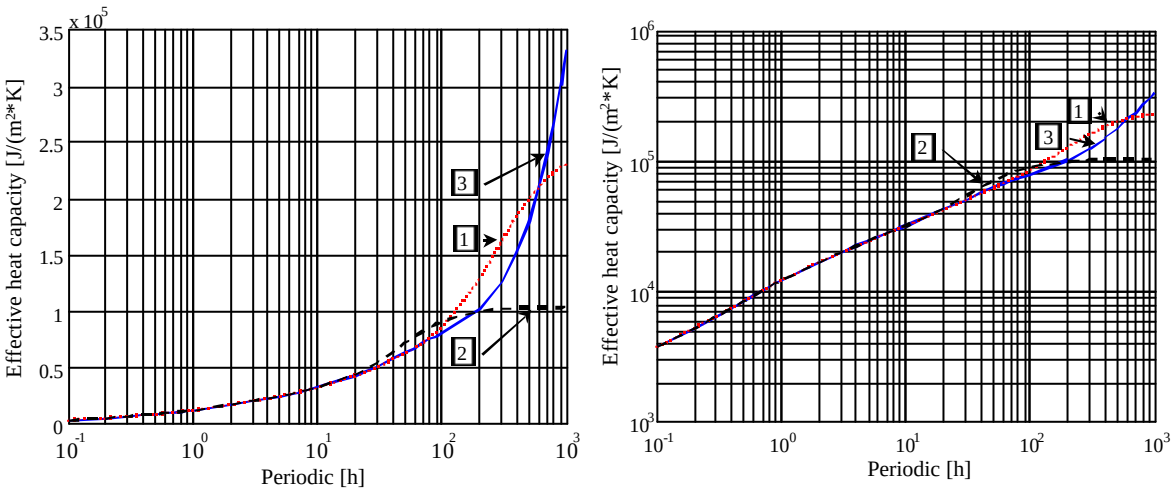

FIG. 2: The analytical effective heat capacity (equation 8) of the wall as function of periodic: <u>to the left</u> on a log-linear scale, <u>to the right</u> on a log-log scale. Curve [1](dotted) is derived when the boundary condition $\tilde{q}_n = 0$ *is assumed, curve [2](dashed) when* $\tilde{q}_n = \tilde{q}_0$ *and curve [3](filled) when* $\tilde{q}_n = 0$.

On plotting results in the Bode diagram (see Akander and Jóhannesson 2000), dynamic transmittance can be observed, as well as the earlier mentioned switching frequency of admittance. The steady-state transmittance can be considered as valid for time periods that are longer than 100 hours.

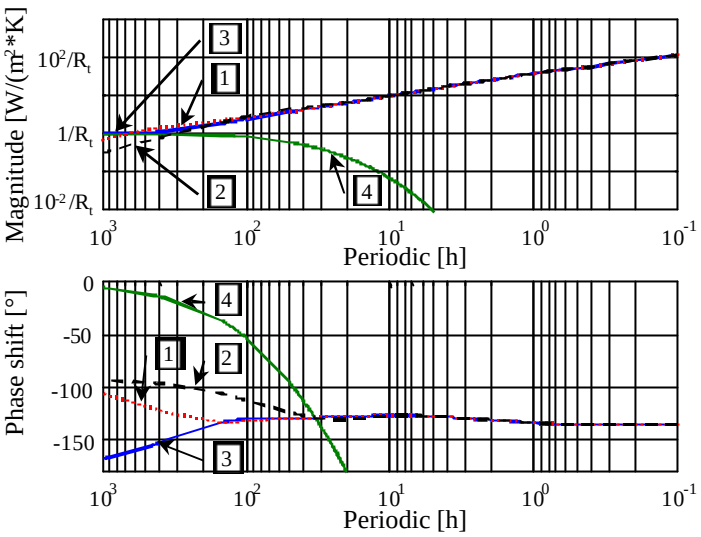

FIG. 3: The Bode diagram for the building component. Curve [1](dotted) is admittance when the boundary condition $\tilde{q}_n = 0$ *is assumed, curve [2](dashed) when* $\tilde{q}_n = \tilde{q}_0$ *and curve [3](filled) when* $\tilde{q}_n = 0$ *. Curve [4] represents dynamic transmittance. The calculated thermal resistance of the building component is* R_t *= 1.7938* $m^2 \times K/W$.

Dynamic transmittance has an influence on the effective heat capacity, as seen in equation 7. To check the influence of dynamic transmittance, the following assumption was made: the temperature oscillation at the internal surface is 1 °C, whereas the external surface temperature oscillation, also having an amplitude of 1 °C, is shifted in time as listed in table 2. The results are plotted in figure 4 in terms of a deviation defined as

$$\boldsymbol{d} = \left(\left| \frac{\tilde{q}_0}{\tilde{q}_0} \right| - \left| Y_0 \right|_{\tilde{q}_n = 0} \right) \Big/ \left| Y_0 \right|_{\tilde{q}_n = 0} \tag{9}$$

The shift in $\tilde{q}_n / \tilde{q}_0$ has an enormous influence on the effective heat capacity at low frequencies. For time periods larger than 10 hours, external temperature variations will start to influence admittance at the interior surface. An increase in amplitude of the external surface temperature oscillation will raise this effect, since the magnitude of the temperature ratio of this example is unity.

TAB. 2: Case number and boundary condition for figure 4.

Case no.	1	2	3	4	5	6	7	8
$\tilde{q}_n / \tilde{q}_0$	1	$(1+i)/\sqrt{2}$	i	$(-1+i)/\sqrt{2}$	-1	$-(1+i)/\sqrt{2}$	$-i$	$(1-i)/\sqrt{2}$

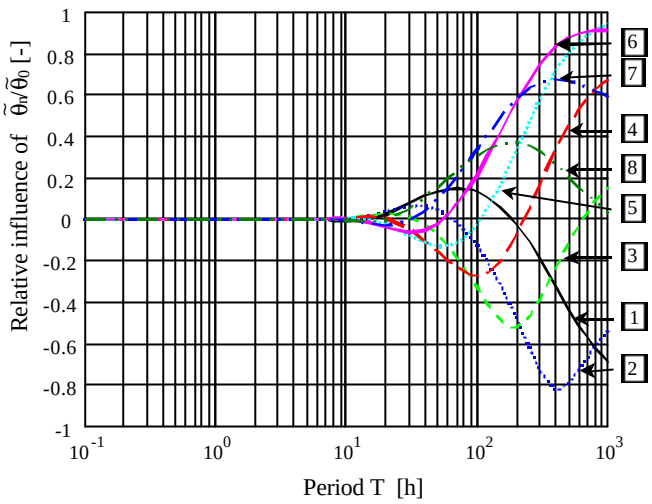

FIG. 4: The relative influence $\mathbf{d}$ *(equation 9) of* $\tilde{q}_n/\tilde{q}_0$ *on admittance as defined in equation 7. Case number associated with each curve is defined in table 2. The amplitude of* $\tilde{q}_n/\tilde{q}_0$ *is here assumed to be unity.*

3.3.2 The ceiling

Another building component that was subject to measurement was the tilted ceiling of the building. At first, this building component had no insulation material. After a series of measurements, insulation was attached at the external surface. The building components are listed in table 3.

TAB. 3: Layer thickness and material properties of the ceilings. LECA material properties have been measured. The values of material properties of the expanded polystyrene (EPS) layer are assumed.

Material layer	l [m]	λ [W/(m·K)]	ρ [kg/m³]	c [J/(kg·K)]
LECA high density	0.02	0.7	1650	990
LECA medium density	0.200	0.32	960	1040
LECA high density	0.03	0.7	1650	990
EPS	0/0.135	0.036	24	1400

The Bode diagrams and effective heat capacities are plotted for each type of ceiling in figures 5 and 6. The insulation has little influence on the effective heat capacity at higher frequencies since the ceiling has a thick core of LECA. However, the insulation screens thermal processes at the external surface, which has the effect that the effective heat capacity is less dependent of the type of boundary condition in comparison with the bare ceiling. The bare ceiling has more scattered heat capacities (boundary condition dependent) at corresponding low frequencies. This can also be seen in the Bode diagram: the insulation increases admittance and decreases dynamic transmittance for a given time period, and at the same time, the admittance curves are less apart.

A matter, which deserves special attention, is the effective heat capacity with the boundary condition $\tilde{J}_n = 0$ (curves [3] of figures 2 and on the left-hand side of 6). Note the steady rise in value at low frequencies. This rise is due to that the surface heat capacity model "interprets" the boundary condition as an extremely heavy thermal mass that damps temperature oscillation at the exterior surface to zero. Admittance converges to the value

$-1/R_t$ whereas the effective heat capacity is admittance divided by angular frequency, which approaches zero at lower frequencies. This actually gives effective heat capacities that are larger than what is physically present in the building component. The wall has a total heat capacity, c_t, of 277 420 J/(m^2·K), and the bare ceiling 281 355 J/(m^2·K). These values are passed at the switching frequencies (here $T_{switch} = 2\pi \cdot R_t \cdot c_t$) corresponding to time periods 869 h and 342 h, respectively.

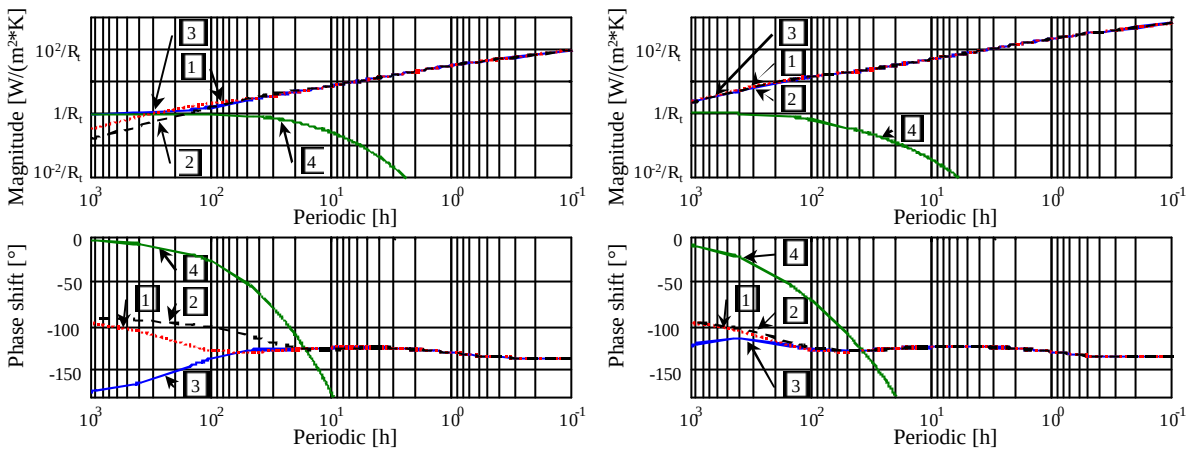

FIG. 5: Bode diagrams for the ceilings. See the caption of figure 3 for notations. <u>To the left</u>: The bare ceiling with R_t = 0.6964 m^{2}xK/W. <u>To the right</u>: Ceiling with insulation with R_t = 4.4464 m^{2}xK/W.

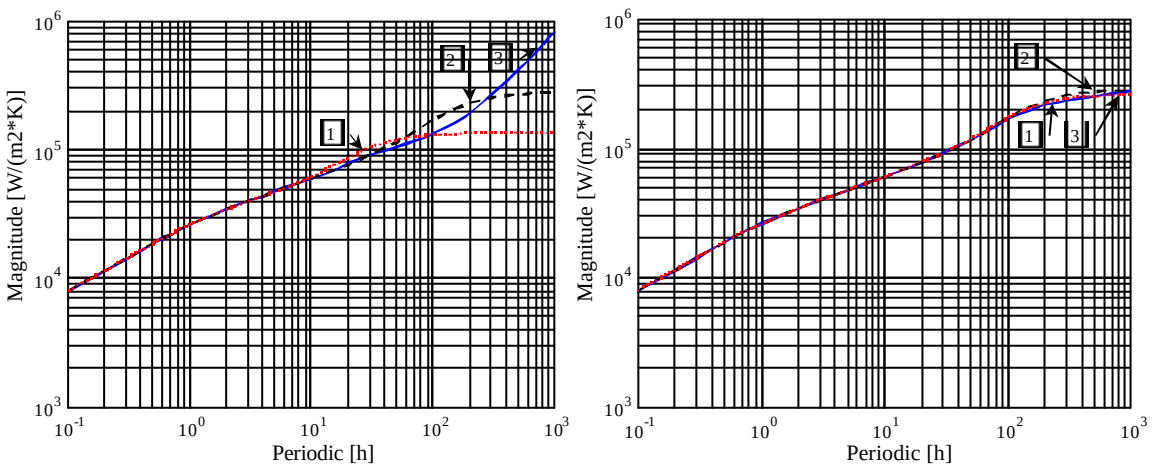

FIG. 6: Effective heat capacity for the ceilings. See the caption of figure 2 for notations. <u>To the left</u>: The bare ceiling. <u>To the right</u>: Ceiling with insulation.

4. Measurement methodology

The numerical calculations for determination of the effective heat capacity were performed within the frequency domain. However, measurements cannot directly be performed within the frequency domain for obvious reasons. Nevertheless, there exist two valuables tool that can be used, one to excite a surface and another that transforms collected time domain data into frequency domain data. These tools are called PRBS and FFT.

4.1 PRBS.

Pseudo Random Binary Sequence (PRBS) is a series of pre-determined pulses (zeros and ones). The series creates an excitation signal that contains a range of discrete frequencies with a given spectral density. The aim is to excite heat sources with this sequence so that the frequencies present in the system are known and controlled. An example of a sequence segment is illustrated in figure 7. Jenssen (1978), Jóhannesson et al (1982), Akander et al (1994), for example, have earlier used PRBS in measurements within building applications.

PRBS fulfils the requirement of continuous excitation of all modes in a system (Jenssen 1978).

- The signal changes value (0 or 1) at a time point that is a multiple of the pulse period T;
- The shortest pulse is T time units and the longest is $n \cdot T$ time units;
- Period T harmonises with the fundamental period of the sequence, $N \cdot T$, where N is determined from the sequence order number n according to $N = 2^n - 1$;
- The smallest and the largest time constants that can be determined are $T_{\min} = 2 \cdot T$ and $T_{\max} = N \cdot T/5$;
- By using a sampling interval T_s that is smaller than T, the smallest time constant (Nyquist frequency) becomes $T_{\min} = 2 \cdot T_s$;
- The mean value of the sequence is 0.5.

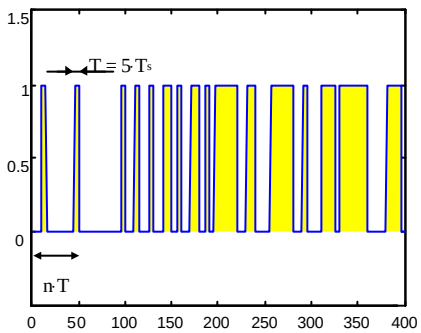

FIG. 7: The first 400 samples of a PRBS with the order number n = 10. Here, the shortest pulse length T is here 5 samples.

4.2 FFT

FFT is short for Fast Fourier Transform, a well-known Fourier analysis tool that splits a sampled time domain signal into harmonic components. The outcome of an FFT procedure is often plotted in a power spectrum, which visualises magnitude ("energy") of harmonic entities within the considered process as function of frequency. The power spectrum for the used PRBS sequence use is illustrated below. An important aspect is how the data is windowed (Ramirez 1985). The most common window used is the rectangle, but other types can be used. The effect of a sampling window is shown in the next section.

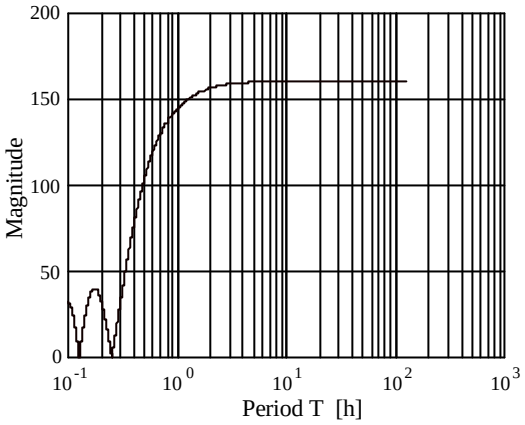

FIG. 8: Spectral density of a rectangular windowed PRBS with the order number 10 and 5 samples per pulse. The shortest pulse is 15 minutes: thereof the minima at the periodic 0.25 h.

4.3 Application of the methodology

The measurement objects are external walls, the ceiling (bare and insulated) and the intermediate floor of an experimental full-scale building constructed by AB Svensk Leca situated in the Stockholm region (Akander and Jóhannesson 1997). The external wall construction is listed in table 1. The bare ceiling and the intermediate floor are both made of the same building element, as listed in table 3.

For measurements of the rate of heat flow densities, the auxiliary wall method was practised. Totally seven heat flux sensors where mechanically attached with two small screws and tape on interior surfaces. To ensure good contact between the sensor and surface, a heat transfer compound was applied. A thermocouple was fastened next to each sensor, at a distance 10 cm away as to avoid disturbances from the sensor. For three of the measurement locations, thermocouples were also place at external surfaces.

To excite the building component surfaces, four radiators (each 600W) were utilised. The measurement objects were exposed to a number of excitation sources such as the radiators, opaque external building component and windows. Windows were externally covered with aluminium foil to decrease the influence of solar and downward long wave irradiation. Being of the type exhaust fan, the ventilation system had no heat recovery. Air was supplied by means of infiltration through cavities in the envelope (no inlets were present) at a rate of 0.4 air changes per hour.

4.3.1 Measurement Equipment.

The heat flux sensors used in the experiment were of the type TNO P40 and an older type from Mekanisk värmeteori, KTH. Thermocouples of type T (premium) measured the temperature difference between wall surface and a reference temperature in an aluminium block, which was placed in a well-insulated box. The reference temperature was measured with a pt-100 gauge. The data acquisition equipment was the DATASCAN 7000 series.

4.3.2 Time Samples, Periods and Ranges of Validity.

The interval between every scan was 6 seconds. The average of 30 scans was saved, giving a sampling time of 180 seconds (3 minutes). The length of a PRBS pulse was 5 samples or 900 seconds (15 minutes). With a PRBS

with the order n = 10, the sequence duration is 255.75 hours. The Nyquist frequency (Ramirez 1985) corresponds to 6 minutes, whereas the longest periodic that with certainty gives information is 2.13 days.

4.3.3 Determining the effective heat capacity of building components.

The effective heat capacity is earlier defined as the absolute quotient of admittance and angular frequency.

$$|c| = \frac{|Y_0|}{w} \tag{8}$$

Admittance is by definition defined as the ratio between heat flux $\tilde{q}_0$ and temperature $\tilde{q}_0$. These are measured and necessary to experimentally determine admittance. Equation 3 is used to arrive to equation 7, where

$$Y_0 = -\frac{\tilde{q}_0}{\tilde{q}_0} = \frac{A}{B} - \frac{1}{B} \cdot \frac{\tilde{q}_n}{\tilde{q}_0} \tag{7}$$

Now, a comparison can be made between experimental and theoretical values if the external surface temperature $\tilde{q}_n$ is recorded. Equation 7 can be re-written as function of heat transfer matrix elements A and B so that

$$Y_0\big|_{\tilde{q}_n=0} = \frac{A}{B} = -\frac{\tilde{q}_0}{\tilde{q}_0} + \frac{1}{B} \cdot \frac{\tilde{q}_n}{\tilde{q}_0} \tag{10}$$

Note that $1/B$ has to be known if A/B is to be solved. In practical in-situ measurements, this term would be undetermined unless a second heat flux sensor were placed at the external surface. Two measured effective heat capacities will be studied and compared. These are c_0^* and $c_{A/B}^*$ as defined below. The analytical value is called $c_{A/B}$.

$$c_0^* = \left| -\frac{\tilde{q}_0}{\tilde{q}_0} \right| \Big/ w; \qquad c_{A/B}^* = \left| -\frac{\tilde{q}_0}{\tilde{q}_0} + \frac{1}{B} \cdot \frac{\tilde{q}_n}{\tilde{q}_0} \right| \Big/ w; \qquad c_{A/B} = \left| \frac{A}{B} \right| \Big/ w; \qquad c_{(A-1)/B} = \left| \frac{A-1}{B} \right| \Big/ w \tag{11}$$

The first measured effective heat capacity, c_0^*, is the actual effective heat capacity of a building component in natural conditions. The second type, $c_{A/B}^*$, has a compensation for dynamic transmittance to make this measured entity comparable to $c_{A/B}$. The deviations of measured values will be related to the analytical value, such that

$$d_0 = \left(c_0^* - c_{A/B}\right) \Big/ c_{A/B}\ ; \qquad d_{A/B} = \left(c_{A/B}^* - c_{A/B}\right) \Big/ c_{A/B} \tag{12}$$

5. Results and analysis

5.1 Results with the rectangular window

A set of measured data on an external wall facing North was sampled in a rectangular window. The power spectrum of this data is shown on the left-hand side of figure 9. The power spectrum of heat flux resembles that of the PRBS signal, whereas the power spectrum of the internal surface temperature is more "noisy". The fact that the temperature power spectrum is not at a minimum at 0.25 hours indicates that something is not correct (this is dealt with later on). The power spectrum of the external surface temperature is stronger than the internal one for periods larger than 5 - 10 hours. This may result in problems in terms of influence of dynamic transmittance. To the right in figure 9, the experimental effective heat capacities are plotted along with two theoretical curves. On checking the deviations of experimental and theoretical values, as on the left-hand side of figure 10, one finds these turn out to be large, in general scattered around values below the zero line. The reason that the scattering increases for periods larger than 10 hours is the dynamic transmission. The power of the external surface temperature oscillation is so large that even if the building component has a damping effect on this transmittance (see the Bode diagram), it has a large influence on the internal surface performance. This phenomenon will be commented more in the following sections.

At a first glance, the scattered values of the measured results seem to give large discrepancies. For this reason, it is necessary to study what has been measured and how this data can be handled to give more precise results.

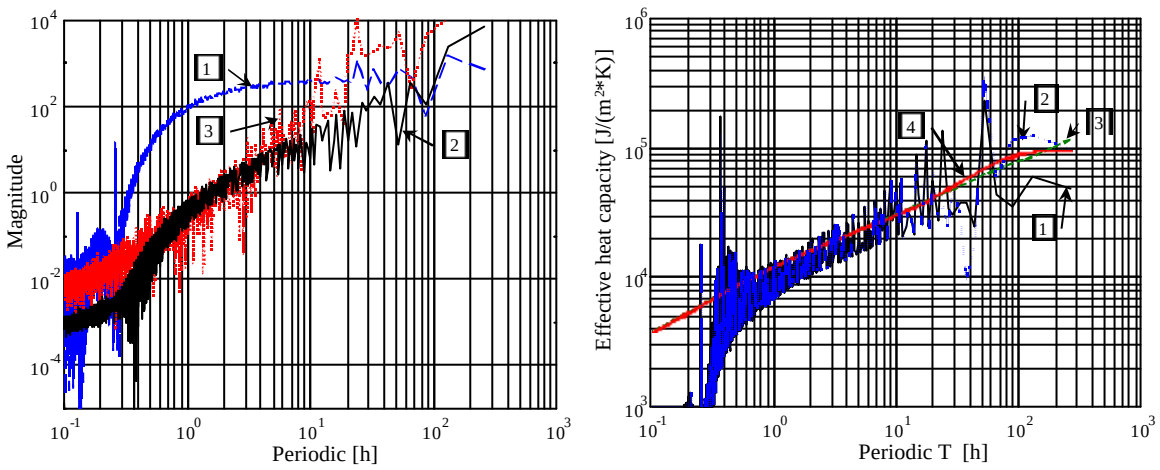

FIG. 9: <u>To the left</u>: Power spectrum of heat flux (1), internal surface temperature (2) and external surface temperature (3). <u>To the right</u>: Measured effective heat capacities c_0^* [1] and $c_{A/B}^*$ [2]; analytical effective heat capacities $c_{A/B}$ [3] and $c_{(A-1)/B}$ [4] as defined in equation 11.

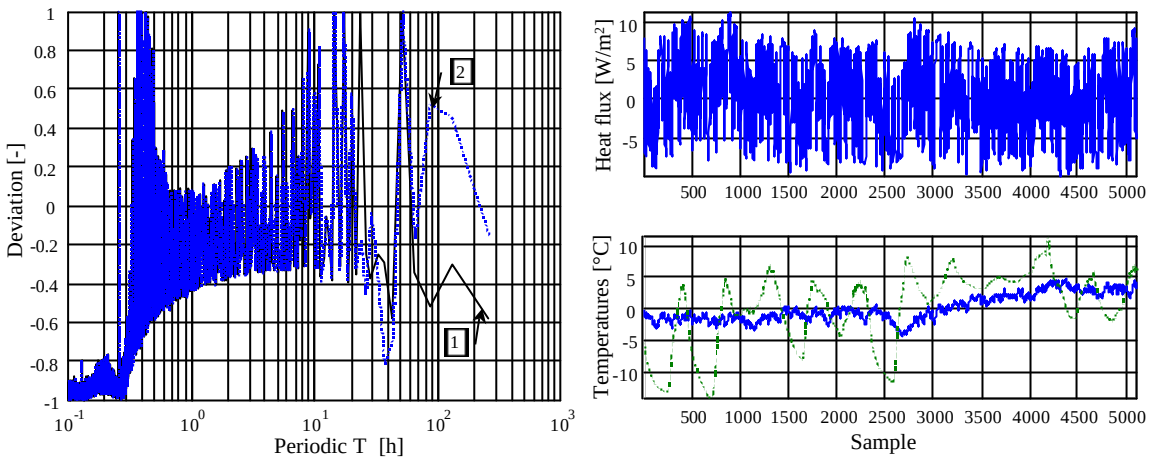

FIG. 10: <u>To the left</u>: Deviation between experimental and theoretical values, d_0 [1] and $d_{A/B}$ [2] (equation 12).

<u>To the right</u>: Measured heat flux and temperatures at the wall surfaces (external dashed, internal filled). The mean value of each series has been subtracted.

5.2 Sources of error

5.2.1 The heat flux sensor and the thermocouple.

How a heat flow sensor (HFS) behaves at steady-state conditions has been studied by a number of scientists, Johannesson (1979), van der Graaf (1990) and Poloniecki et al (1995) to name a few. Johannesson (1979) and Malcrops (1981) made frequency response studies, however only with 1-D heat transfer equations. Nonetheless, the conclusion from the steady-state studies is that 3-D effect should not be neglected. For this reason, and to trace what is being measured and what data is registered, two separate frequency domain finite difference programs were produced. One uses cylindrical co-ordinates to model a circular HFS. This program was used to study how the HFS disturbs the heat flow pattern at the surface of the building component and to investigate how different values of surface thermal resistances at the HFS and the thermocouple influence the size of the "measured" effective heat capacity. The second, a three-dimensional heat transfer program with Cartesian co-ordinates was made to model a small midsection of a wound wire thermopile HFS placed on a building component. The half-plated wound constantan wire, which measures temperature difference across the HFS, conducts heat faster than the filling material of the sensor (here polyurethane). This will give an error in measurements of dynamic heat transfer since the sensor is calibrated under steady-state conditions. Briefly, the theories behind the programs are stated below.

The modelled building component is a cylindrical section of the component with a HFS placed perpendicular to the axis of the cylinder. The cylindrical building component section is composed of circular material layer slabs that are adiabatic at the mantle surface in the radial direction. Each slab is composed of ring-shaped cells that have a representative temperature in the geometrical midpoint, as displayed in figure 11.

The component surface is coupled to a node that represents the environment's temperature by means of a thermal resistance with a constant value. The boundary condition used in the program is that the interior environment's node undergoes a sinusoidal excitation corresponding to 1 °C, whereas the outdoor temperature is assumed constant. The calculation method was developed by Andersson and Jóhannesson (1983) and has been applied by Mao (1997).

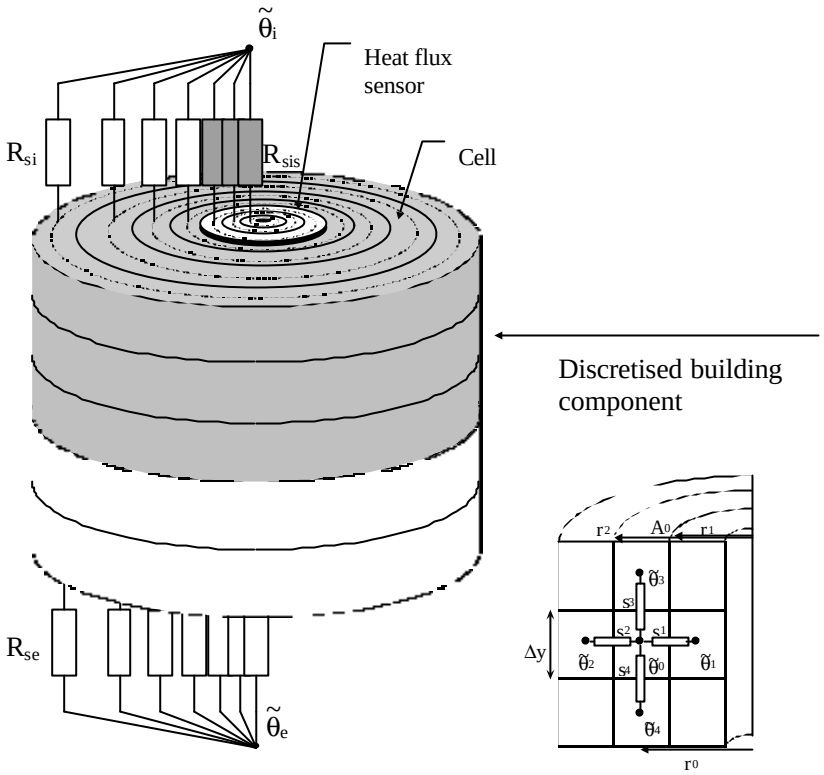

FIG. 11: <u>To the left</u>: A schematic sketch of the circular heat flow sensor mounted on a cylindrical wall section. <u>To the right</u>: A blow-up of a cell node with adjacent cell nodes, each linked by conductance s_i.

The thermopile within the HFS is omitted in this calculation, but its effects are studied in more detail in the following section. Here, the HFS is a slab of polyurethane (λ = 0.21 W/(m·K), ρ = 1280 kg/m^3 and c = 1400 J/(kg·K)) with a diameter of 100 mm and a thickness of 3mm. The sensor is in the axial direction subdivided in 3 layers and 10 cells along the radius. The radius (400 mm) of the building component of table 1 is divided into 80 cells. Consecutively counted from the interior surface layer, each layer was split to 6, 30, 5 and 3 sublayers.

On supposing that the mean temperature difference $\Delta q_{sensitive}$ of the 5 innermost cells (the sensitive part of the HFS) at a distance 0.5 mm from each sensor surface is recorded, how large would be the "measured" heat flux be? By hypothetically assuming that the HFS is *calibrated at steady state*, the calibration constant is calculated according to Fourier's law such that

$$E_{calib} = \bar{q}_{sensitive} \big/ \Delta\bar{q}_{sensitive} \tag{10}$$

For non-zero frequencies, the "measured" temperature difference and the calibration constant give the "measured" heat flux at the sensitive area such that

$$\tilde{q}_{measured} = E_{calib} \cdot \Delta\tilde{q}_{sensitive} \tag{11}$$

At the undisturbed wall surface, the "true" heat flux $\tilde{q}_{wall}$ is the sought value. The deviation $\boldsymbol{e}$ between the measured heat flux and what should have been expected is

$$\boldsymbol{e} = \frac{\left|\tilde{q}_{measured}\right| - \left|\tilde{q}_{wall}\right|}{\left|\tilde{q}_{wall}\right|} \tag{12}$$

This deviation also applies to the effective heat capacity, if the temperature measurement is perfectly made and the surface thermal resistances are identical at the HFS and the thermocouple.

Three sets of calculations are performed, where the surface thermal resistances at the surface of the HFS and the thermocouple are varied. In the first case, the thermal resistance R_{sis} at the HFS is equal to the thermal resistance R_{si} at the thermocouple, such that $R_{sis} = R_{si}$. This may likely be untrue since the HFS is thicker than the thermocouple; the 3-mm thick HFS might disturb the convection pattern. Also, the long wave radiation emissisivity may be different for the thermocouple, the HFS and the surface of the building component.

Three cases are set up, where the nominal convective heat transfer coefficient value of 2.4 W/(m^2·K) is varied with one unit[1]. The radiative heat transfer coefficient is assumed constant 5.2 W/(m^2·K) for all surfaces. However, since the programs have surface thermal resistances as input, there is no difference in whether or not heat is transferred by means of convection or radiation - this simulation merely serves to study how differences at gauges affect the results. Calculations were also performed with the analytical 1-D heat transfer equations (equation 3) as to study discrepancies from frequency dependency of multi-dimensional heat transfer in association with the HFS.

The results of figure 12 reveal that the 1-D analytical theory can in this application be used for cases 1 and 2 with an inaccuracy of some 4%. The discrepancies between the analytical and the numerical results at faster periods are likely due to discretisation and numerical errors in the finite difference model. However, as the periodicity increases, the deviations become larger for the reason that multi-dimensional heat transfer takes place, certainly at the guard zone. Another important issue is surface thermal resistances. If these are not the same at the sites of the heat flow and the temperature gauge, deviations are likely to increase, especially if the value of heat transfer coefficient at the HFS is less than the one at the thermocouple.

TAB. 4: Three cases to analyse the influence of surface thermal resistances at gauge surfaces. The heat transfer coefficient for long wave radiation is 5.2 W/(m^2·K) in all cases.

	h_c surface W/(m^2·K)	h_c sensor W/(m^2·K)	R_{si} m^2·K/W	R_{sis} m^2·K/W
Case 1	2.4	2.4	0.132	0.132
Case 2	1.4	2.4	0.152	0.132
Case 3	2.4	1.4	0.132	0.152

[1] The convective heat transfer coefficient was calculated from $h_c = 2.03(\Delta\boldsymbol{q})^{0.14}$ (Khalifa and Marshall 1990) with a mean temperature difference between the surface and bulk air temperature of approximately $\Delta\boldsymbol{q}$ =3.1 °C. Estimation on basis of this experiment lie in the range of 2.0-2.4 W/(m^2·K).

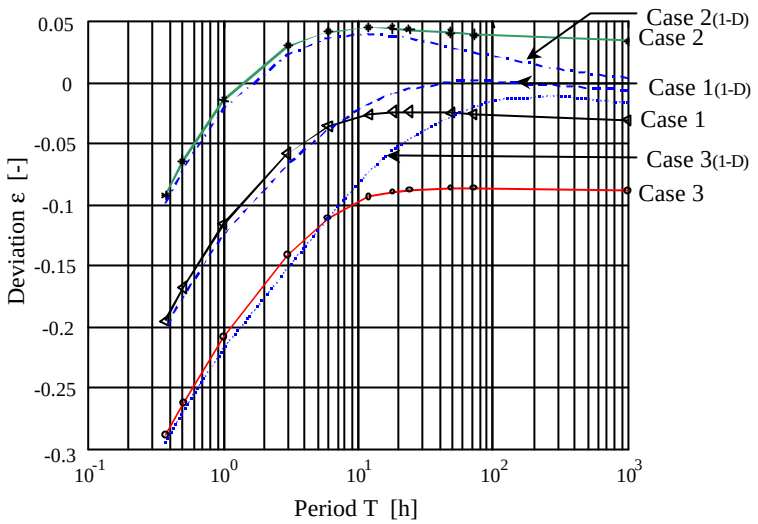

FIG. 12: Simulated deviations ε *between "measured" heat flux through a circular HFS and undisturbed heat flux through the surface of a building component (equation 12). Surface thermal resistances are varied for cases 1(<), 2(*) and 3(o) according to table 3. The dashed lines represent results for the same cases, as calculated using analytical equations for one-dimensional (1-D) heat transfer.*

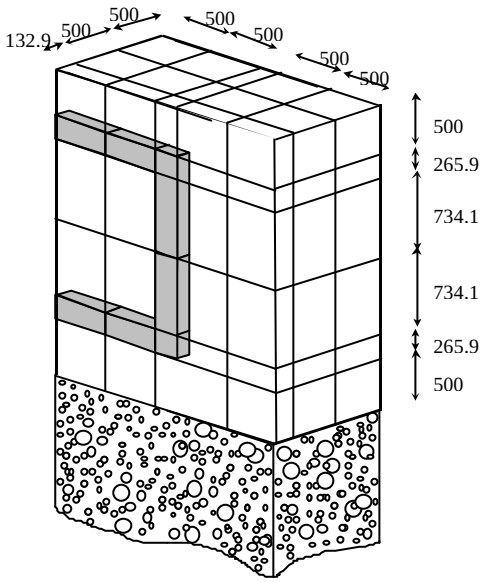

FIG. 13: Modelled section of a half-plated wound wire HFS. The shaded sections depict the wire, the white fields are plastic fillings and the spotted section the surface material. The length unit is mm.

HFSs that are composed of thermopiles and plastic filling are commonly of the "half-plated wound wire" technique, see for example (Jóhannesson 1979) and (van der Graaf 1990). Temperature difference is measured at the junctions between copperplated and bare parts of constantan wire. Now, during dynamic measurements, a heat wave is liable to be conducted faster in the wire than in the plastic filling. This may lead to problems since the HFS is calibrated at steady-state conditions: overlapping heat waves due to time shift are not present during calibration. Therefore, a computational investigation was made on how this phenomenon influences measurement results. Since the designs of heat flux sensors used within the experiment are unknown, a hypothetical model is set up as shown in figure 13. This small section of a HFS is attached to a building

component. The shaded part represents the wire, which measures temperature at the ends of the "⊃" section. The diameter of the wire is assumed to be 0.3 mm, but has for the reason that only rectangular cells are modelled been converted as to give a cross-section area that is the same as for the cylindrical wire. The constantan wire is modelled with the following material properties: λ = 22.6 W/(m·K), ρ = 8800 kg/m^3 and c = 383 J/(kg·K).

The calibration constant E_{calib} was calculated for the angular frequency ω = 0. The heat flux of the sensor section $q_{section}$ was computed as well as the temperature difference Δq_{wire} at the top and bottom of the wire, such that

$$E_{calib} = \bar{q}_{section} / \Delta\bar{q}_{wire} \tag{14}$$

For other angular frequencies, the measured heat flux (signal from the modelled heat flux sensor) is calculated from the "measured" temperature difference at the wire junctions, giving

$$\tilde{q}_{measured} = E_{calib} \cdot \Delta\tilde{q}_{wire} \tag{15}$$

Then again, the sought undisturbed value is $\tilde{q}_{wall}$, here calculated by means of the analytical solution of equation 3. Results are shown in figure 14. Worth commenting is that three-dimensional effects at the peripheral parts of HFS are not present in this calculation: these may cause greater deviations at low frequencies in comparison to these results. Nor is the calibration error (± 5%) included here, since the calibration constant is "calibrated" on the measurement object at steady state. It should also be noted that the finite difference methods are numerical approximations, not true solutions. However, these approximations can be used to analyse the reason for deviations and deviation magnitude that measurement gauges give rise to within the thermal domain.

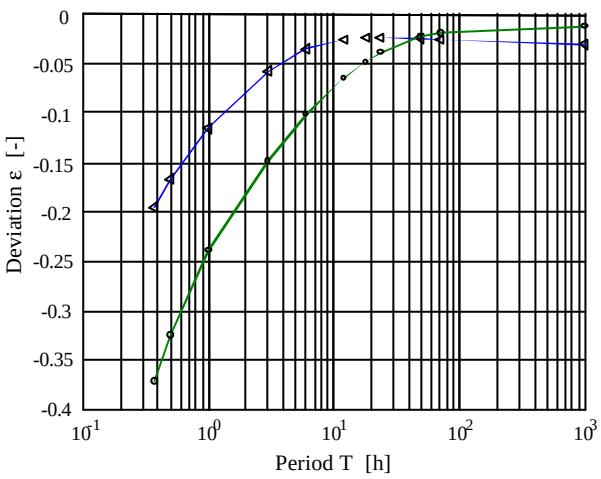

FIG. 14: The curve with rings displays deviation ε between heat flux "measured" at a simulated central section of a HFS containing constantan wire (thermopile) and the undisturbed heat flux at the building component surface (equation 12). The curve with triangles represents deviations from Case 1 in figure 12, where no thermopile is modelled within the HFS. Thus, the thermopile itself stands for a substantial part of deviations.

5.2.2 FFT

When handling data with FFT, there are some problems that may arise. Among these are aliasing and leakage (Ramirez 1985).

Aliasing is a phenomenon that may occur if the sampling rate is slower than frequencies within the monitored process. Aliasing occurs when the sampling rate is less than twice the highest frequency component and is quite treacherous since it gives rise to two problems. The first is that frequencies that are not present in the signal may be found in the power spectrum. The second is that the powers of present frequencies become larger than they ought to be. The reason is that the power of frequency components with frequencies higher than the Nyquist frequency is "folded over" to lower frequency components. Aliasing is most likely present if the lobes of the power spectrum next to the Nyquist frequency are not close to zero.

Leakage occurs when the number of cycles of a frequency component is a non-integer within the sampling window. This is seen in the temperatures of the left-hand side of figure 10: values of the first and the last samples are not the same. What happens in the FFT procedure is that the power of a frequency component "leaks" from the frequency to adjacent frequencies, as seen in the power spectrum of the internal surface temperature in figure 9. The reason for using the PRBS is that all frequencies within the pulse train are multiples of the fundamental frequency; the frequencies harmonise with the sampling window. In essence, the frequencies of the monitored process are known. However, frequencies are difficult to control in field measurements. With the introduction of new frequency components that appear in non-integer number of cycles in the window, leakage is unavoidable. Changing the shape of the window can reduce leakage.

5.3 Results with the Hanning window

A number of different sampling windows have been tested, and results from utilisation of the Hanning window are shown in figures 15 - 18. The Hanning window results are less noisy than rectangular window results, with the exception of periodicity that is faster than 0.3 hours. What also can be noticed is the systematic deviation from the analytical solution for periods less than 10 hours. This is due to the HFS, and the magnitude of deviation is of the order as shown in the numerical study in the previous section. At the period where the inaccuracy of the dynamic performance of the HFS is some 10% (around 10 hours), the two measured effective heat capacities c_0^* and $c_{A/B}^*$ start to diverge. The dynamic transmittance from thermal processes at the external surface starts to influence the thermal performance of the internal surface. The effective heat capacity c_0^*, without compensation for transmittance, has deviations that are comparable with those of the external wall in figure 4. On compensating for dynamic transmittance, $c_{A/B}^*$ is the measured effective heat capacity that corresponds to the analytical ratio between $|A/B|$ and w. It is therefore expected that $c_{A/B}^*$ should have better agreement with the analytical results than c_0^*. This is according to figure 15 not the case, and the reason is probably that the power spectrum of the external surface temperature is subject to leakage. The actual frequencies present outdoors do not correspond to the indoor frequencies, giving rise to a distorted power spectrum at low frequencies. The same applies to the bare ceiling (figure 16), and to a greater extent. This is motivated by a comparison in Bode diagrams of figures 3 and 5, where the bare ceiling has less ability to damp thermal transmittance at same frequencies. Also, thermal loads are larger at the external surface of the ceiling.

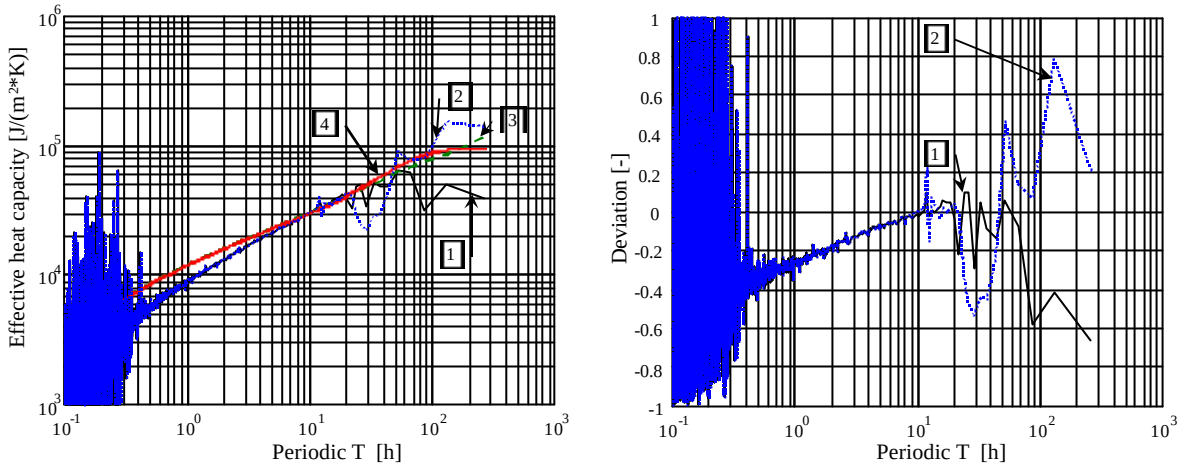

FIG. 15: Results for the external wall after using the Hanning window. <u>To the left</u>: Measured effective heat capacities c_0^* *[1] and* $c_{A/B}^*$ *[2] and analytical effective heat capacities* $c_{A/B}$ *[3] and* $c_{(A-1)/B}$ *[4] as defined in equation 11. <u>To the right</u>: Deviation between experimental and theoretical values,* d_0 *[1] and* $d_{A/B}$ *[2] (equation 12).*

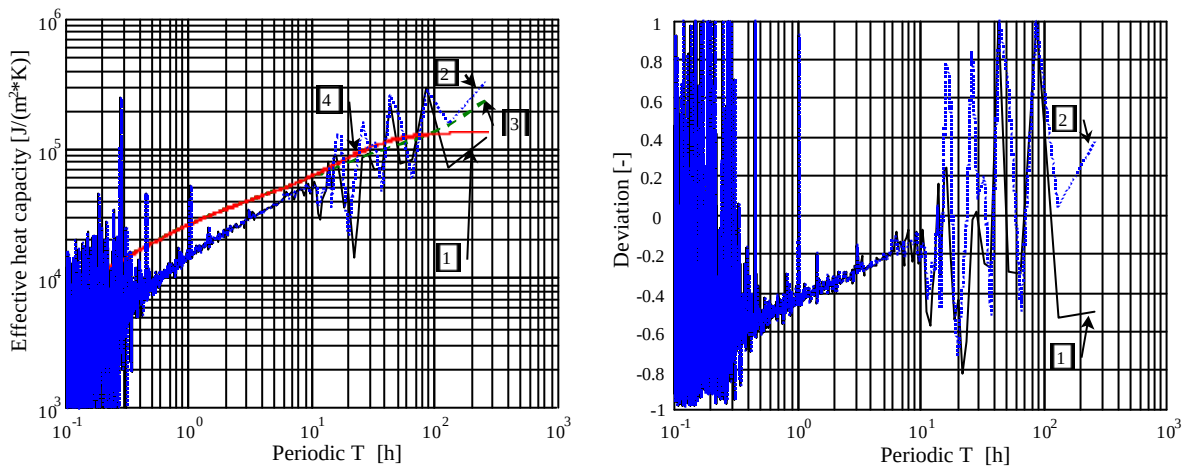

FIG. 16: Results for the bare ceiling after using the Hanning window. <u>To the left</u>: Measured effective heat capacities c_0^* *[1] and* $c_{A/B}^*$ *[2] and analytical effective heat capacities* $c_{A/B}$ *[3] and* $c_{(A-1)/B}$ *[4] as defined in equation 11. <u>To the right</u>: Deviation between experimental and theoretical values,* d_0 *[1] and* $d_{A/B}$ *[2] (equation 12).*

Figure 17 shows the effective heat capacities of the insulated ceiling. The measured curves have the best agreement for long time periods among the studied building component. This is due to dynamic transmittance characteristics as seen in the Bode diagram of figure 5.

Measurements were also conducted on a section of an intermediate floor above a crawlspace. The floor element is exactly the same as the bare ceiling. For the first time, as shown in figure 18, the values of the measured effective heat capacity are larger than the theoretical values. As shown in case 2 of figure 12, the natural convection is probably the reason why the measured curves are "shifted upwards". The HFS, being 3 mm in height, protrudes into air boundary layer whereas the thermocouple remains well beneath this layer. This

phenomenon would also be expected for the ceiling, but the ceiling is inclined and has exhaust air terminals at the highest level. This prevents stable stratification of air and leads to larger convective heat transfer coefficients.

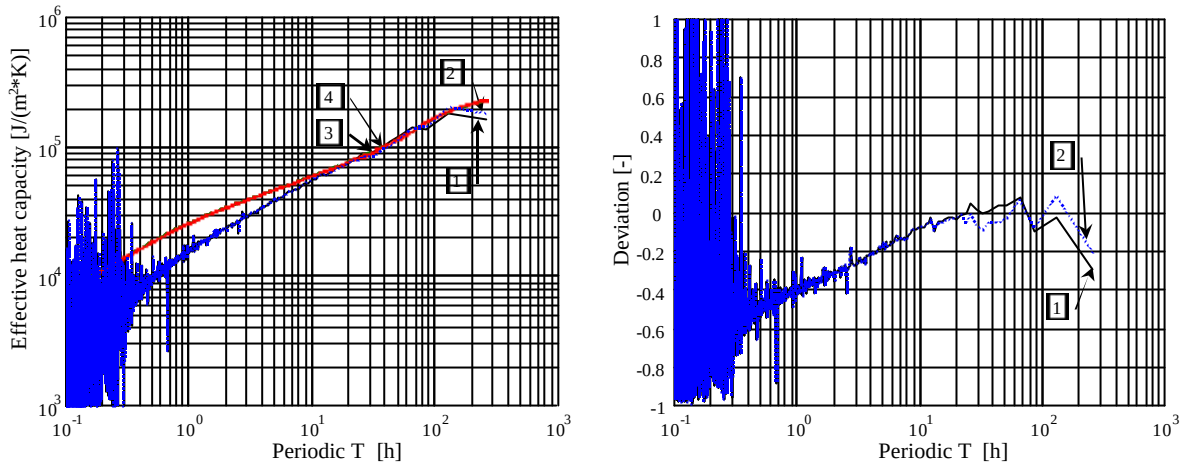

FIG. 17: Results for the insulated ceiling after using the Hanning window. To the left: Measured effective heat capacities c_0^* *[1] and* $c_{A/B}^*$ *[2] and analytical effective heat capacities* $c_{A/B}$ *[3] and* $c_{(A-1)/B}$ *[4] as defined in equation 11. To the right: Deviation between experimental and theoretical values,* d_0 *[1] and* $d_{A/B}$ *[2] (equation 12).*

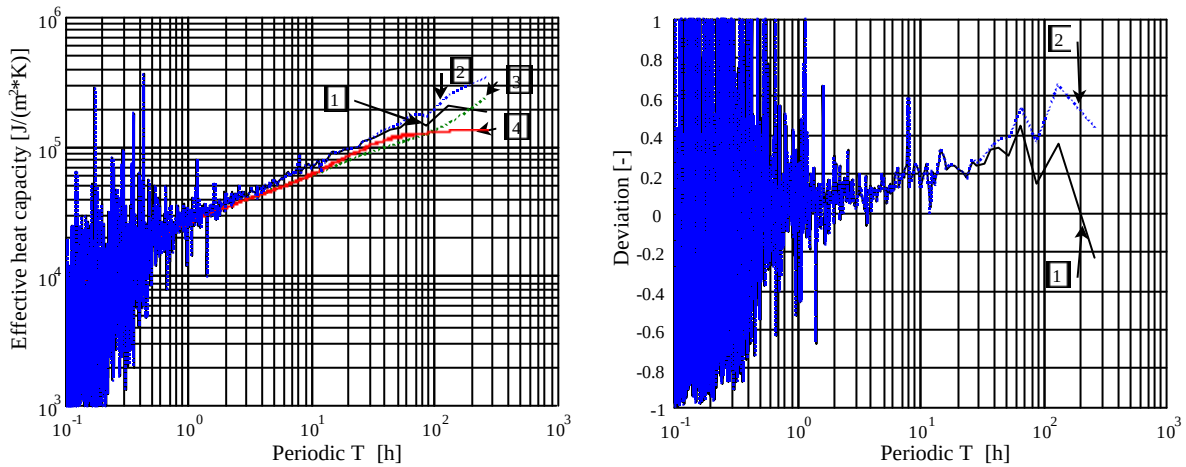

FIG. 18: Results for the intermediate floor after using the Hanning window. To the left: Measured effective heat capacities c_0^* *[1] and* $c_{A/B}^*$ *[2] and analytical effective heat capacities* $c_{A/B}$ *[3] and* $c_{(A-1)/B}$ *[4] as defined in equation 11. To the right: Deviation between experimental and theoretical values,* d_0 *[1] and* $d_{A/B}$ *[2] (equation 12).*

5.4 The thermal resistance of each component.

Having measured heat flux and temperature difference over various envelope building components for a longer time, the mean value of the considered measurement series should give the steady-state variables (see equations 1 and 2). The thermal resistance can therefore be calculated, and this is actually the common application of HFS within building physics. The duration of the PRBS was 255.75 hours. According to the Bode diagram of the

various building components, with exception of the insulated ceiling, this time lapse is enough to determine the steady-state heat transmission. If the aim of this experiment had only been to determine thermal resistance, the lapsed time could have been shorten by using multiple regression analysis as proposed by Anderlind (1992), where the influence of heat capacity is eliminated. Anderlind (1996) also introduced the Pentaur method, which for short measurement series estimates the thermal resistance and the total heat capacity of a building component. This method also coarsely estimates the thermal resistance and heat capacity of each material layer.

TAB. 5: Thermal resistances determined from material data and measured data.

Component	Calculated thermal resistance [$m^2 \cdot K/W$]	Measured thermal resistance [$m^2 \cdot K/W$]	Deviation [%]
External wall	1.7625	1.6840	-4.45
Bare ceiling	0.6964	0.6857	-1.55
Insulated ceiling	4.4464	4.2206	-5.08
Intermediate floor	0.6964	0.5454	-21.69

The measured results are in quite good agreement with calculated results, keeping in mind that the calibration inaccuracy is ±5%. The largest deviation is found for the intermediate floor, and the reason is found in figure 19. An increase in outdoor temperature leads to a long-term rise in surface temperature. If the first 2500 samples are used, the measured value becomes 0.5981 $m^2 \cdot K/W$ (-14.1%) and for the first 1500 samples, 0.6077 $m^2 \cdot K/W$ (-12.7%). These deviations are probably due to different heat transfer coefficients at the HFS and thermocouple. The HFS has a larger overall heat transfer coefficient and will measure a larger heat flux than what flows through the floor surface, see figure 12. Since thermal resistance is temperature difference divided by heat flux, the measured value will be lower than expected.

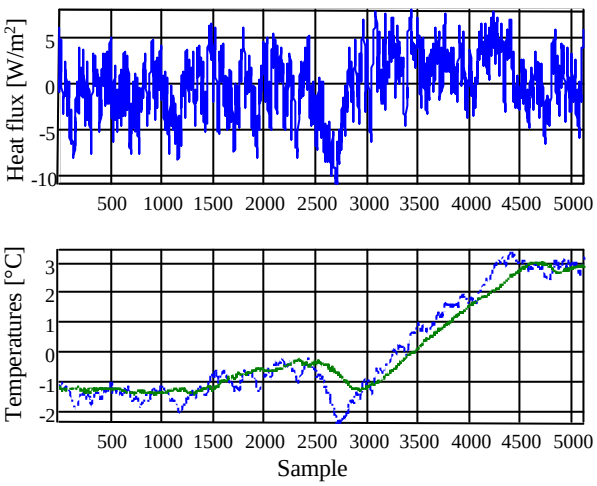

FIG. 19: Figures on heat flux and temperatures(the noisy at the internal surface, the smoother in the crawlspace) at the intermediate floor. Mean values have been subtracted.

6. Conclusions and discussion

In situ measurements of the effective heat capacity of multi-layer components by means of the auxiliary wall method have been performed. A comparison between experimental and analytical effective heat capacities shows a systematic frequency-dependent discrepancy caused by the heat flux sensors. For periodicity longer than 10 hours, the agreement is quite good.

What is required to achieve reliable results is to control the excitation of temperature and heat flux at the component surfaces. In the internal environment, this can be achieved by means of a Pseudo Random Binary Sequence (PRBS), which fulfils the requirement of a continuous excitation with known frequency input. Also, the number of cycles that each frequency component has within the sequence is an integer. A problem that may arise in in-situ measurements is the introduction of other frequencies, primarily generated by the external climate. The length of the PRBS should be chosen to be an integer multiple of the diurnal cycle (which was not done in the current application). Otherwise, the risk that the power spectrum of the external environment's signals is not correct with respect of the frequencies present in the internal environment increases. The processing of data with FFT gives clearer results for non-rectangular windows, but to interpret power spectrums for multiple frequencies that are subject to aliasing and leakage is difficult.

Two types of effective heat capacities were calculated from measured data, as it is evident that boundary conditions (dynamic transmittance) influence the size of this entity. The first is the straightforward application where the quotient of heat flux and temperature oscillation is divided by angular frequency, which can be considered to be the effective heat capacity during natural running conditions. The second is by compensating for dynamic transmittance from the external surface, as if to theoretically assume that the external temperature is constant. Though results of the second type are directly comparable to analytical values, these could actually give larger deviations than the results from the straightforward application. This implies that frequencies in the external environment are not all the same as those generated by the PRBS, thus yielding leakage in the power spectrum of external surface temperatures. This can lead to erroneous estimations of dynamic transmittance. A means of achieving more comparable results is to generate oscillations in temperature and heat flux at the internal surface that have greater magnitude than those on the outside, as to make dynamic transmittance negligible. This measured effective heat capacity will, however, not be the same as for the building in normal running conditions.

The heat transfer process is dynamic, which poses a practical problem when it comes to the measurements of heat fluxes. Within building physics, the most commonly used heat flux sensors are calibrated for measurement of steady-state entities, such as thermal resistance of building components. This worked well in this experiment. However, a systematic frequency-dependent deviation was noticed in processed measured data. A numerical frequency analysis of a heat flux sensor with a built-in thermopile indicates that the measured heat flux is less that what should be expected at higher frequencies. Within the thermal domain (this excludes inaccuracies in calibration, electronic equipment, surface contact etc), the inaccuracy may be some 10 % for a 6-hour periodic and 25 % for a 1-hour periodic for a 3-mm thick heat flux sensor. Analytical one dimensional heat transfer equations underestimate these inaccuracies.

Since the inaccuracy is frequency-dependent, measured heat flux series could be transformed into frequency domain data. Here, compensations could be done. Then, the data is transformed back into the time domain. The core of this compensation method is to calibrate the heat flux sensor for a spectrum of frequencies. PRBS can be used to achieve this type of calibration in a Lange apparatus. A set-up could be such that the heat flux sensor is embedded in a solid with known thermal properties. The solid is chilled on one side (constant temperature), but excited on the other with an electrical heater. Temperature measurements at the surface and in the solid will indicate the heat flux through the sensor, while the sensor output is recorded.

7. References

Akander J. (2000). The Thermal Performance of Multilayer Building Components - A Method for Approximating the Effective Heat Capacity. *(Submitted to) Nordic Journal of Building Physics, Vol 2*. Available at http://www.ce.kth.se/bphys

Akander J. and Johannesson G. (1997). The utilisation factor of two Swedish buildings. *Proceedings of Cold Climate HVAC '97*, Reykjavik, Iceland. p. 117-122.

Akander J. and Jóhanneson G. (2000). The Thermal Performance of Multi-Layer Components - Applications of the Bode Diagram. *(Submitted to) Nordic Journal of Building Physics, Vol 2*. Available at http://www.ce.kth.se/bphys

Akander J., Lacour C., Mao G., Johannesson G. (1994). *Ett elbaserat golvvärmesystem - Mätningar och beräkningsmodeller*. Dept. of Building Technology, KTH, Stockholm, Sweden. (In Swedish).

Anderlind G. (1992): Multiple regression analysis of in situ thermal measurements - Study of an attic insulated with 800 mm loose fill insulation. *J. Thermal Insul. And Bldg. Ensv. Vol. 16*. pp.81-104.

Anderlind G. (1996). *Dynamic Thermal Models - Two Dynamic Models for Estimating Thermal Resistance and Heat Capacity from in Situ Measurements*. Report A16:1996. The Swedish Council for Building Research, Sweden.

Andersson A.C. and Jóhannesson G. (1983). *Application of Frequency Response for Fast Analysis of Two-dimensional Heat Flow Problems*. Coden: LUTVDG/(TVBH-7072)/1-8/(1983), LTH, Lund, Sweden.

Carslaw H.S. and Jaeger J.C. (1959). *Conduction of Heat in Solids.* 2nd ed. Oxford University Press, London, United Kingdom.

Graaf F. van der (1990). "Heat-flux Sensors." Chapter 8, Volume 4 of the multivolume work "*Sensors - A Comprehensive Series*" (Ed. W. Göpel et al.). VCH Verlagsellschaft mbh, Germany. p. 297-322

Jensen L. (1978*). Digital reglering av klimatprocesser*. Doctoral Dissertation. Department of Automatic Control, LTH, Lund, Sweden. (In Swedish).

Jensen S.Ø. (1995). Validation of Building Energy Simulation Programs: A Methodology. *Energy and Buildings*, Vol. 22, No. 2, pp. 133-144.

Jóhannesson G. (1979). *Värmeflödesmätningar: Termoelektriska mätare, funktionsprinciper och felkällor.* (Eng: Heat-Flow Measurements: Thermoelectrical Meters, Function Principles and Sources of Error.) Rapport TVBH-3003, Division of Building Technology, LTH, Lund, Sweden. (In Swedish).

Jóhannesson G. (1981). *Active Heat Capacity - Models and Parameters for the Thermal Performance of Buildings.* Doctoral Dissertation. Report TVBH-1003, Division of Building Technology, LTH, Lund, Sweden.

Jóhannesson G., Leander U. and Hallgrimur G. (1982). *Mätning av värmeväxlareffekt och värmelagring i hålkanaler av betong*. LUTVDG/(TVHB-7069) 1-20/(1982), Division of Building Technology, LTH, Lund, Sweden. (In Swedish).

Khalifa A.J.N and Marshall R.H. (1990). Validation of heat transfer coefficients on interior building surfaces using a real-sized indoor test cell. *Int. J. Heat Mass Transfer*, Vol 33, No. 10, pp. 2219-2236.

Mao G. (1997). *Thermal Bridges - Efficient Models for Energy Analysis in Buildings.* Doctoral dissertation. TRITA-BYT 97/0173. KTH, Stockholm, Sweden.

Malcorps, H. (1981). Frequency-response of heat fluxmeters. *J. Phys. E. Sci. Instrum., Vol. 14*. Pp. 1054-1060.

Poloniecki J.G., Vianou A.V and Mathioulakis E. (1995). Steady-state analysis of the zero-balance heat-flux meter. *Sensors and Actuators, Vol. A 49*. Pp. 29-35.

Ramirez R. (1985). *The FFT - Fundamentals and Concepts*. Prentice-Hall, Inc., New Jersey, USA.

SP (1996). *Bestämning av värmekapacitet på lättklinker*. SP, Sveriges Provnings- och Forskningsinstitut (Swedish National Testing and Research Institute), Borås. Handläggare Fredrik Stenberg. (In Swedish).

prEN ISO 13786 (1998). *Thermal performance of building components- Dynamic thermal characteristics - Calculation methods.* European Committee for Standardisation (CEN), Brussels.

Submitted to: Nordic Journal of Building Physics
Available at http://www.ce.kth.se/bphys

PAPER 4

The Thermal Performance of Multilayer Building Components - The Methodology of ORC and Applications.

The Thermal Performance of Multilayer Building Components - The Methodology of ORC and Applications.

SUBMITTED: February 2000.
REVISED:
PUBLISHED:

Jan Akander, Techn. Lic.,
Dept of Building Sciences, Kungl Tekniska Högskolan;
S – 100 44 Stockholm;
akander@bim.kth.se

KEYWORDS*: Building physics, building component, building simulation, heat conduction, thermal modelling.*

SUMMARY*:*
RC-networks can be used in building simulation programs to model building components. In having a fixed configuration, a 5-node optimised RC-network (ORC) can effectively model both lightweight and heavyweight multilayer or massive components. Thermal performance is optimised in the frequency domain, but the use of the ORC is in time domain simulations. In this work, various RC-networks are shown and commented with respect to their fields of application. An application within the build simulation program IDA/ICE is presented, where results of the use of two ORC's are compared with results when the building components were modelled by means of the finite difference method. The 5-node ORC proved to be accurate in comparison to a detailed finite finite difference model, and it gave a shorter computational run time.

1. Purpose

This paper focuses on the modelling of thermal performance of a multilayer building component with Optimised RC-networks (ORCs) and finite difference models (FDMs). These models are implemented in the general simulation tool IDA within the Indoor Climate and Energy (IDA/ICE) application. A study is made on how the two models differ in performance, in terms of accuracy and computational time and memory. This serves to give an answer to whether or not ORCs are more efficient than conventional finite differences within the IDA simulation environment. In the first part of this paper, the optimisation of various ORC-configurations are shown along with a motivation to why ORCs where chosen as alternative to model multilayer building components. The second part shows results from simulations of an office room where building components are modelled with various ORC's and FDM discretisations.

The reader is kindly advised to examine the other three parts of this series with the title "The Thermal Performance of Multilayer Building Components", especially part one with the sub-title "Application of the Bode Diagram" (Akander and Jóhannesson 2000). That paper contains definitions and methodology that are fundamental to this paper.

2. Introduction

2.1 RC-networks in general

RC-networks, sometimes called lumped parameter models, have to a large degree been used as simplified models to establish the thermal performance of buildings or enclosures (rooms). During the 50's to the early 80's, prior to the rapid development of personal computers and numerical techniques, these networks were comprehensive and numerically manageable in terms of calculations by the hand. The introduction of computers within building physics allowed more detailed networks and other building component models to be implemented, with development leading to modern building simulation programs (BSPs) of today. This does not

mean that the simplified models of yesterday are obsolete. In terms of efficiency, these may still be competitive. What is meant by efficiency within this context is an optimum where the level of detail in models to obtain accurate results is put against "work" in terms of computational resources (time and memory). This trade-off depends on the purpose of the simulation, for example if the simulation serves to predict the annual energy requirement of a building or if the aim is to study thermal comfort or peak loads in a room for the warmest or coldest days of a year.

Here, the intent is to use RC-networks to model the performance of building components within the frame of energy prediction and also thermal comfort calculations. The idea is that the thermal performance of a RC-network is optimised within the frequency domain but is used within a modular simulation program working in the time domain. Commonly requiring fewer nodes than regular finite difference models, these may yet maintain an "adequate" level of inaccuracy (Akander 1995). This allows more computational resources left to other models, such as detailed controls, non-linear transfer mechanism, more zones, etc.

The idea of letting an RC-network model the thermal performance of a slab or multilayer building components in not by any means new. Jóhannesson (1981) studied modelling of multilayer building components by means of the surface heat capacity and the simple RC-configuration. With Jóhannesson's work as basis, an R-C-R-C-R network (a 2-node ORC) was developed to model external building component, such as walls and roofs. This network was implemented in the uni-zone energy prediction program VIP+ (Skanska Software 1996). In turn, Mao (1997) used this configuration to perform time domain simulation of multidimensional heat transfer in thermal bridges and ground heat loss. The performance of the network was optimised with respect to frequency response of the modelled component, which was calculated by means of frequency domain finite differences (Andersson and Jóhannesson 1983). Davies (1983) proposed the use of RC-networks that are build up of one or several serially connected "T-chain" or "Π-chain" units. These are optimised with respect to one frequency by means of a minimising the sums of squares of the differences between the corresponding pairs of the four elements of the analytical and the model heat transfer matrix. Davies' paper contains references on earlier work done by authors, limited to the modelling of a slab.

2.2 Brief description of IDA and NMF

IDA is a general modular simulation environment, with several fields of applications; for example the spreading of fire in ventilation systems and dispersion of pollutants in road traffic tunnels. The largest and most extensive application is the building simulation program called Indoor Climate and Energy (IDA/ICE). In being modular, IDA libraries contain precompiled models of building components and systems. The user chooses suitable components and connects them into a complete system(s), zone(s) or building. IDA has other features that are required of modern simulation tools. Having variable time steps, IDA regulates time steps depending on events within the modelled processes. Discontinuities are handled, such as the performance of thermostats. A descriptive list over IDA/ICE models is found in (Bring et al 1999). For example, the complete ASHRAE HVAC2 Toolkit (ASHRAE 1993) has for example been implemented. IDA has a fully developed air infiltration scheme implemented. Zone models have a fully non-linear long-wave radiation exchange between surfaces and temperature dependent convective heat transfer coefficients between surfaces and zone air node.

The models are documented in the Neutral Model Format (NMF) which is an ASHRAE standard for documentation of models (Sahlin 1996). This format simply states the model, but does not prescribe any solution method. By means of a translator (Bris Data AB 2000), a model stated in NMF can be used for several simulation environments, such as TRNSYS, HVACSIM+ and IDA.

2.3 On the choice of building component model for IDA

The work presented in this paper has to a great extent been carried out to implement a building component model within IDA (but can also be used in other simulation environments or as stand-alone models/programs). There

were, during the early 90's, several reasons for choosing RC-networks to model building components. The first was that NMF did not allow an automatic discretisation of material layers during parameter processing prior to the actual simulation calculation (in NMF terms: Computed Model Parameters cannot have the role of Supplied Model Parameters). In that event, discretisation had to be performed prior to input of data, a reason that was against the use of FDM. To avoid pre-processing units for this purpose, the FDM was ruled out. With this in mind, an RC-network with a fixed configuration was preferred, where the values of thermal resistances and heat capacities are optimised as to agree with the analytical thermal performance for a wide range of frequencies. Another reason is that the FDM has cell size that is restricted by the thickness of material layers. A thin steel sheet at the surface of a building component can result in numerical stability problems within the simulation solver. Layer thickness does not restrict the size of the constituents of ORCs. However, IDA Solver uses robust implicit methods that are commonly stable for small cell size. An FDM exist within IDA, but discretisation is not performed automatically; it has to be done by the user. The module (model) can be used by either advanced users or in the event that the standard 3-node ORC of IDA is not sufficiently accurate. This FDM module is used within the current work.

Furthermore, since IDA is a general simulation tool, it has a run-time that is somewhat longer than special purpose (monolithic) BSPs (Sahlin 1996). For this reason, it is beneficial to have as few nodes as possible, however with sustained accuracy in performance. Response factors are advantageous in this manner, since no information is calculated for state variables inside the building component: only surface to surface heat transfer is calculated. However, IDA uses variable time steps whereas response factor theory usually assumes a constant simulation time step.

Another application field for ORCs is to model multi-dimensional heat transfer in building simulation programs. A common way of modelling multi-dimensional heat transfer is with finite differences, however not directly in the simulation program. An efficient way is by calculating the thermal response with a finite difference program working in the frequency domain, adapting the RC-network model to have the same response, and implement this in the simulation program. This has within IDA been tested by Akander et al (1996). Similar methodology was done by Seem et al (1989) using response factors, with implementation in TRNSYS. Kossecka and Kosny (1996) model equivalent thermal walls, that give the same response factors as, for example, thermal bridges. Claesson (1999) uses a type of RC-network combined with response factors from square pulses. Applications of the method have been made on a heat underfloor space. Multidimensional heat transfer is beyond the scope of this paper, but is relevant in showing the fields of application of RC-networks.

3. Optimisation of ORCs

First of all, a few comments will be made on the performance of FDMs and ORCs and how performance is calculated. These are in this context composed of serially connected thermal resistances and heat capacities, or in parallel. An essential criterion is the total thermal resistance of the model is the same as that of the multilayer component. This criterion is only alleviated for the special boundary condition where the thermal processes can be assumed to be identical on both sides of the building component (an adiabatic component).

At high frequencies, the model performance will converge to the thermal performance of the outermost model component (see part 1 of this series of paper by Akander and Jóhannesson (2000)). In this work, the outermost component will be a thermal resistance; motivated by the fact that IDA does not handle differentiated variables at the links between models, as is the case of a surface heat capacity.

As the last comment, the thermal performance that requires most resources to model in terms of serially connected thermal resistances and heat capacities (ORCs and FDMs) is the response of the semi-infinite solid. The reason is seen in the Bode diagram (Akander and Jóhannesson 2000). This performance can neither be modelled with a pure resistance or capacity at the surface of model. The response can only be modelled by the

combined interaction between one or more RC-components. Obviously, the response of a simple mass can be modelled with a surface heat capacity.

The optimisation of an ORCs for building component performance is the following:

The level of detail of the simulation is first to be determined. An important factor to take into account is the Nyquist frequency of the process, in essence the frequency at which the thermal process in question is accurate. In short term simulations where fast thermal processes are to be studied, time steps down to minutes may be required. For annual energy requirement simulations, time steps more than an hour may be used.

- The network is optimised within the frequency domain as to give a performance that has the same transfer function as an analytical solution, or a multidimensional finite difference or finite element calculation. The networks can be optimised with regard to boundary conditions. The frequency response, in terms of admittance and dynamic transmittance, is essential to the optimisation;
- The number of nodes depends on the range of frequencies for which the network performance should be valid, and the thermal performance of the building component that is going to be modelled. The total thermal resistance of a model should be the same as for the modelled building component and this also applies to the total heat capacity;
- The ORC is to be used in time domain simulations. In work by other scientists, such as by Davies (1994), the network can be used in frequency domain simulations, which allows a model component to be impedance.

Evaluation of model performance is done against the analytical frequency domain solution of the heat conduction equation. In the first paper of this series, Akander et al (2000), a method for evaluating model performance in relation to analytical performance is proposed. The maximal model deviation is for admittance, Y, is the magnitude of the difference between model and analytical admittance divided by analytical admittance magnitude, as such

$$e_Y = \left| Y_{model} / Y_{analyt} - 1 \right| ; \qquad e_{T_D} = \left| T_{D\,model} / T_{D\,analyt} - 1 \right| \tag{1}$$

The latter expression applies to dynamic transmittance, T_D. Davies (1983) used similar equations as basis of a least square method to optimise component of complex RC-networks. The deviation was the sum of deviation of each transfer matrix element (totally four). He also proposed the use of two other deviations, one depicting deviation between model and analytical magnitude, and the other indicating phase shift deviation. These two were applied on ORCs in (Akander 1995), but the expressions of equation 1 indicates the combined effect of magnitude and phase shift deviation, see (Akander 1996).

4. Modelling multilayer building components with ORCs

In the following sections, several RC-configurations are shown. The number of nodes and thermal components (resistances and heat capacities) depends on the model application, boundary conditions and also range of validity in terms of frequency. In this paper, the concern is to optimise frequencies from zero and up to a higher frequency. If the inaccuracy of model performance is too large, it can be improved by inserting more nodes in the RC-network. In order to show a result of the application, an example is made using an external wall. Table 1 lists layer thickness and material properties.

TAB. 1: Layer thickness and material properties of an external sandwich wall .The layers are of light expanded clay aggregates (LECA), expanded polystyrene (EPS) and mortar, giving the U-value 0.219 W/(m2·K).

Material layer	d [m]	λ [W/(m·K)]	ρ [kg/m^3]	c [J/(kg·K)]
Mortar	0.01	1.00	1800	950
LECA LK8	0.1	0.30	1050	1020
EPS	0.15	0.039	30	1300
LECA LK5	0.05	0.25	1000	1050
Mortar	0.02	1.00	1800	950

4.1 The thermal resistance.

The simplest and most widely used model is the total thermal resistance of a building component. The model is strictly limited to steady state calculations ($w = 0\ s^{-1}$) and can only be used for calculations, for example on a month-wise basis, depending on the type of component (excluding ground heat loss). Dynamic behaviour is not present in this model.

4.2 The surface heat capacity.

The simplest model that is capable of approximating admittance is the surface heat capacity. The surface heat capacity can well approximate the amplitude of admittance, it is exact for the optimisation frequency and well modelled for a wider range of frequencies if the response of the component is that of a simple mass. A serious drawback is that dynamic transmittance does not exist. Another is that the response of the semi-infinite solid can only be modelled for the chosen optimisation frequency, as shown in figure 2. The surface heat capacity model is determined as such

$$c_1 = \frac{|Y_0|}{w} \tag{2}$$

How this equation is derived is found in Jóhannesson (1981) or (Akander and Jóhannesson 2000). This equation has appeared in earlier versions of prEN ISO 13786 for determination of the effective heat capacity of a building component. This type of model can appear in energy requirement calculations, such as in EN 832.

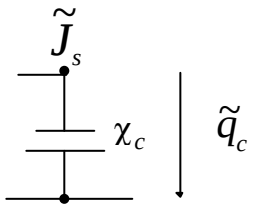

FIG. 1: The surface heat capacity model.

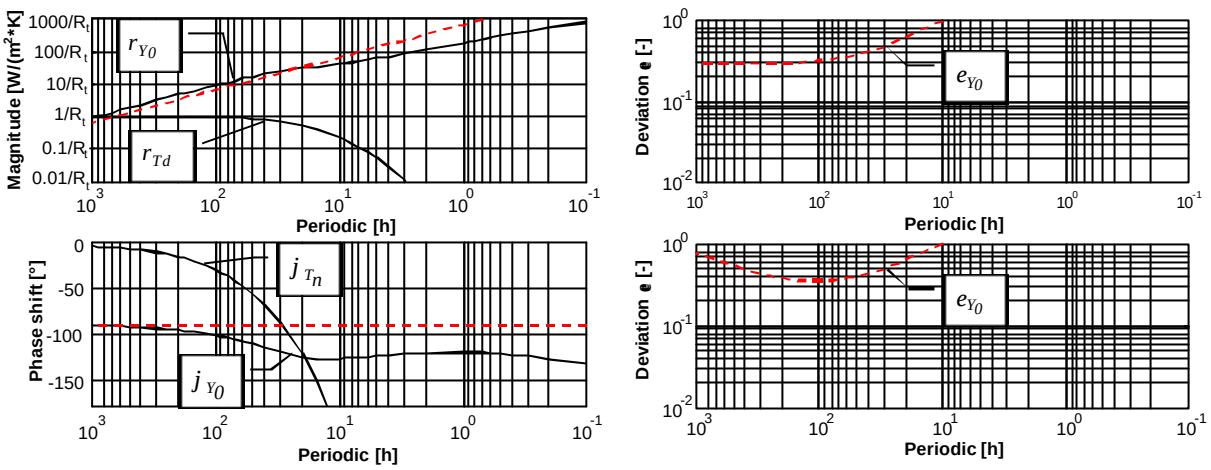

FIG. 2: To the left: The Bode diagram of the external wall of Table 1 as modelled with surface heat capacity, here for a periodicity of 24 hours and the boundary condition $\tilde{J}_n = \tilde{J}_0$. Admittances are plotted for this boundary condition. To the right: Model deviation e as defined in equation 1. The results for boundary conditions $\tilde{J}_n = \tilde{J}_0$ are plotted in the upper diagram. The lower diagram shows model deviation if the temperature is constant at either surface.

4.2.1 The simple RC-network

On increasing the number of components in the model, accuracy will increase. The RC-network is next in line, illustrated in figure 3. The values of R_1 and c_1 are determined as stated in equation 3

$$R_1 = \frac{1}{\mathrm{Re}(1/Y_0)}; \qquad c_1 = \frac{1}{w \cdot \mathrm{Im}(1/Y_0)} \tag{3}$$

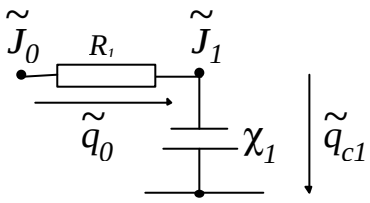

FIG. 3: The RC-network model.

This model gives possibilities to represent admittance of the semi-infinite solid. The configuration gives the exact solution to the optimised frequency, for magnitude and phase lag of admittance. This model alone does not handle transmittance. This network is effective to use for simulations where a component can be considered to be adiabatic in the sense that dynamic transmittance is not present, but can only handle one switching frequency, where the response switches from that of the simple mass to the semi-infinite solid. Otherwise, the extents of application are limited to those of the surface heat capacity. Thin or lightweight adiabatic components can be simulated.

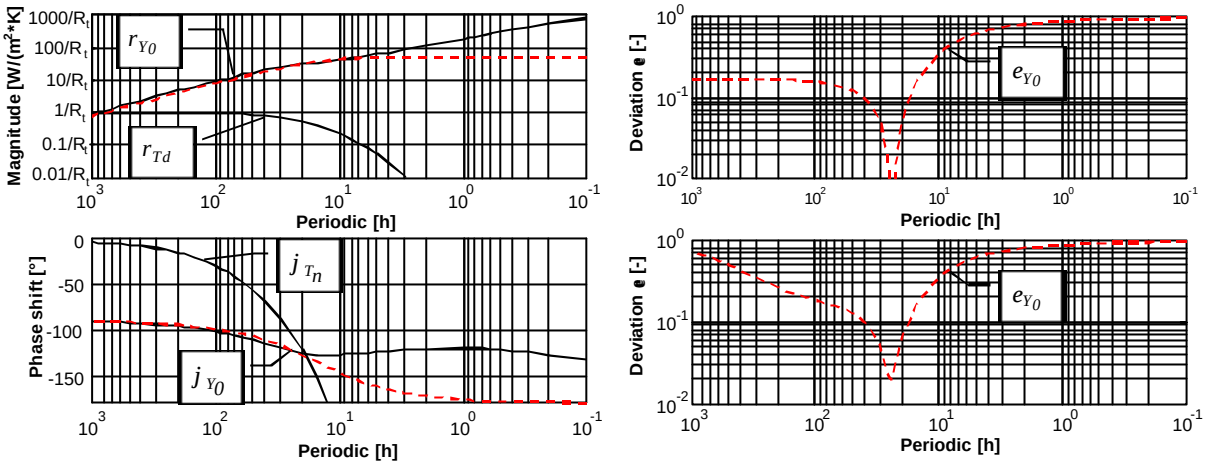

FIG. 4: <u>To the left</u>: The Bode diagram of the external wall of Table 1 as modelled with the simple RC-configuration, here for a periodicity of 24 hours and the boundary condition $\tilde{J}_n = \tilde{J}_0$. Admittances are plotted for this boundary condition. <u>To the right</u>: Model deviation $\boldsymbol{e}$ as defined in equation 1. The results for boundary conditions $\tilde{J}_n = \tilde{J}_0$ are plotted in the upper diagram. The lower diagram shows model deviation if the temperature is constant at either surface.

4.3 The T-chain

The T-chain allows admittance and transmittance to be approximated. In order to determine values, three equations have to be found. These are the real and the complex part of admittance for one frequency and the important steady state transmittance. The latter equation is that $R_1 + R_2 = R_t$. The heat transfer matrix, along with the boundary conditions, give the equations such that

$$\begin{bmatrix} 0 \\ \tilde{q}_n \end{bmatrix} = \begin{bmatrix} 1 & -R_2 \\ 0 & 1 \end{bmatrix} \begin{bmatrix} 1 & 0 \\ -i\boldsymbol{w}\boldsymbol{c}_1 & 1 \end{bmatrix} \begin{bmatrix} 1 & -R_1 \\ 0 & 1 \end{bmatrix} \begin{bmatrix} \tilde{J}_0 \\ \tilde{q}_0 \end{bmatrix} \tag{4}$$

$$R_2 = 1 \Big/ \mathrm{Re}\left(\frac{1}{R_t + 1/Y} \right); \qquad R_1 = R_t - R_2; \qquad \boldsymbol{c}_1 = 1 \Big/ R_2^2 \cdot \boldsymbol{w} \cdot \mathrm{Im}\left(\frac{1}{R_t + 1/Y} \right) \tag{5}$$

The T-chain models admittance with the performance of a simple mass very well. This assumes one switching frequency. Dynamic transmittance is poorly modelled.

4.4 The two-node ORC.

By coupling two T-chains, the Π-chain is formed. Containing five components, the two-node ORC needs five equations. The optimisation can now be done in two ways. The first is to optimise admittance on one side (preferably on the interior surface) and dynamic transmittance. For this optimisation, equations can be solved from the heat transfer matrix elements A and B as function of one frequency. The frequency that gives the best agreement is usually low, often corresponding to the time constant larger than the product of the total thermal resistance and the total heat capacity of the component (Akander 1995). The second is to optimise both admittances. The second type of optimisation is to achieve a good agreement for both admittances. The two-node ORC can be decomposed to two T-chains, which model admittance at either side of the component by means of

equations 4 and 5. The two T-chains are then superposed, and the resistances and capacities of the superposed 2-node ORC that gives the least over-all inaccuracy are saved as optimal parameters.

4.5 The 3-node ORC

The 3-node ORC can be used for conventional building components with application on energy prediction programs. The model may be inadequate for building components that contain many material layers with dissimilar thermal diffusivity or massive material layers, for the reason that the best agreement in performance may be obtained when one of the model constituents has a negative value. Then, the solution with all-positive values gives a poor agreement. Davies (1983) also experiences this.

The optimisation of the 3-node ORC is iterative. A 2-node ORC is first determined, as to optimise model admittances. Then, the central capacity, which fulfills the requirement of having a total heat capacity that is equal to that of the building component, is allowed to transverse between the capacities at the surfaces. The sets of model parameters that give the least over-all deviation are recognised as being optimal.

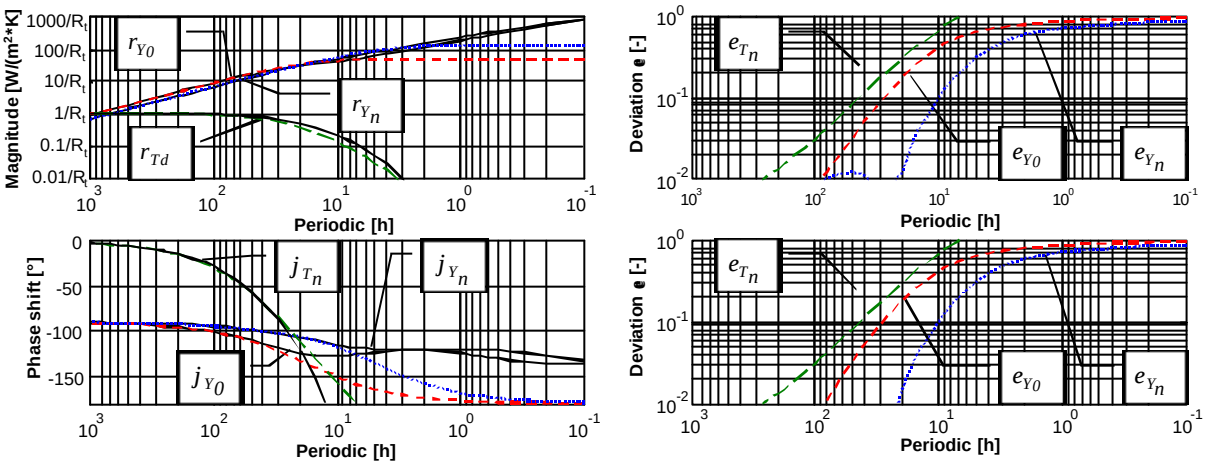

FIG. 5: <u>To the left</u>: The Bode diagram of the external wall of Table 1 as modelled with the 3-node ORC. Admittances are plotted for the boundary condition $\tilde{J}_n = \tilde{J}_0$. <u>To the right</u>: Model deviation $\boldsymbol{e}$ (equation 1) is for the boundary condition $\tilde{J}_n = \tilde{J}_0$ plotted in the upper diagram. The lower diagram shows model deviation if the temperature is constant at either surface.

4.6 The 5-node ORC

A further insertion of serially connected nodes into the 3-node chain leads to difficulties in performance optimisation; there are too many variables to determine by means of iterative methods. Admittance of the 3-node configuration can be improved by inserting a T-chain in parallel with the three model components at the surface, as displayed in figure 6. Since admittance is an additive entity, the admittance of the two T-chains at a surface can be added as to give the correct admittance of the whole model. The heat transfer matrix for two parallel T-chains, without the heat capacity $\boldsymbol{c}_5$, is expressed as

$$\frac{B_1 \cdot B_2}{B_1 + B_2}\begin{bmatrix} \left(\frac{A_1}{B_1}+\frac{A_2}{B_2}\right) & 1 \\ \left(\frac{A_1}{B_1}+\frac{A_2}{B_2}\right)\left(\frac{D_1}{B_1}+\frac{D_2}{B_2}\right)-\left(\frac{B_1 \cdot B_2}{B_2+B_2}\right)^2 & \left(\frac{D_2}{B_2}+\frac{D_2}{B_2}\right) \end{bmatrix} \tag{6}$$

Here, index *1* represents parameters of the upper T-chain in the parallel circuit on the left-hand side of figure 6; index *2* is for the lower T-chain. Note the first matrix element and the last, which are the sums of admittance of each T-chain.

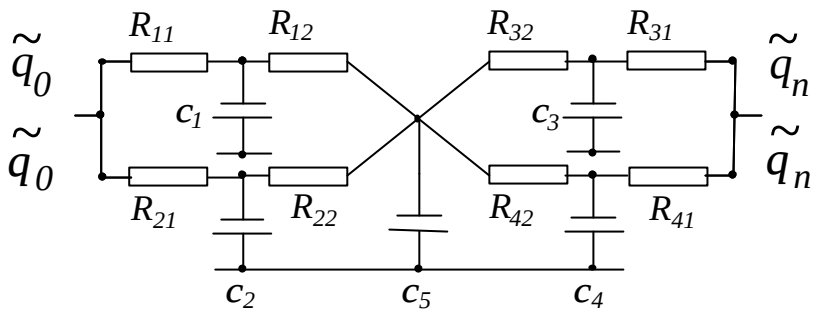

FIG. 6: The 5-node ORC is composed of a two sets of parallel T-chains in series with a central heat capacity.

In the same manner as the 3-node ORC, the boundary conditions where $\tilde{J}_n = \tilde{J}_0$ is assumed to find the adiabatic plane in the building component. The heat capacity c_5 is placed at that plane, and this allows the determination of the sum of thermal resistances for each T-chain. For a symmetrical building component with the total thermal resistance R_t, the sum is $R_{t1} = R_t$, for example $R_{11} + R_{12} = R_{t1} = R_t$.

The optimisation is primarily made at each side of the adiabatic plane. As two iterative loops are made to determine values for the T-chains, the combination of values that give the smallest deviations are saved. The calculation procedure is as follows. Let the T-chain with index *1* model high frequency processes and the T-chain with index *2* lower frequencies. Angular frequency w_1 is a high frequency, ranging for periodicity corresponding from, for example 0.1 hours to, say, 2 hours. Within the w_1-loop, a loop with w_2 steps from a periodicity of 2 hours to 30 hours. The equations that have to be solved are

$$Y_1(w_1) = Y_0(w_1) - \frac{1 + R_{22} \cdot i w_1 c_2}{-R_{t2} - R_{21} \cdot R_{22} \cdot i w_1 c_2}; \qquad Y_2(w_2) = Y_0(w_2) - \frac{1 + R_{12} \cdot i w_2 c_1}{-R_{t1} - R_{11} \cdot R_{12} \cdot i w_2 c_1} \tag{7}$$

These two equations are iteratively solved, and suitable initial values are calculated from

$$Y_1(w_1) = Y_0(w_1); \qquad Y_2(w_2) = Y_0(w_2) \tag{8}$$

Admittances $Y_1(w_1)$ and $Y_2(w_2)$ are used for determining the values of the parameters within each T-chain, such as

$$R_{12} = 1\Big/ \mathrm{Re}\left(\frac{1}{R_{t1} + 1/Y_1(\omega_1)}\right); \qquad R_{11} = R_{t1} - R_{12}; \qquad c_1 = 1\Big/ R_{12}^2 \cdot \omega_1 \cdot \mathrm{Im}\left(\frac{1}{R_{t1} + 1/Y_1(\omega_1)}\right) \tag{9}$$

$$R_{22} = 1\Big/ \mathrm{Re}\left(\frac{1}{R_{t2} + 1/Y_2(\omega_2)}\right); \qquad R_{21} = R_{t2} - R_{22}; \qquad c_1 = 1\Big/ R_{22}^2 \cdot \omega_2 \cdot \mathrm{Im}\left(\frac{1}{R_{t2} + 1/Y_2(\omega_2)}\right) \tag{10}$$

Finally, the central heat capacity c_5 is calculated by subtracting c_1 and c_2 from the total heat capacity of the considered thermal half of the component. A similar calculation is performed on the other side of the adiabatic plane, and the optimal parameters of each half are saved.

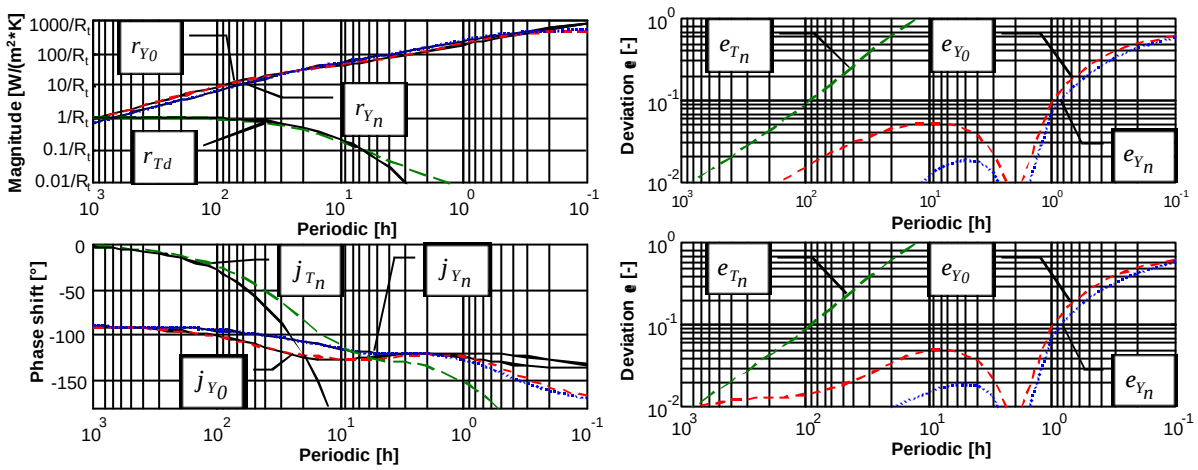

FIG. 7: <u>To the left</u>: The Bode diagram of the external wall of Table 1 as modelled by the 5-node ORC. Admittances are plotted for the boundary condition $\tilde{J}_n = \tilde{J}_0$. <u>To the right</u>: Model deviation e (equation 1) for boundary conditions $\tilde{J}_n = \tilde{J}_0$ are plotted in the upper diagram. The lower diagram shows model deviation if the temperature is constant at either surface.

This optimisation procedure has been found to be capable of modelling the thermal performance of lightweight gypsum-air cavity-gypsum internal walls and massive or multi-layer envelope building components. The ORC has one weakness, and this is that the modelling of dynamic transmittance may be relatively poor. The reason is that there is basically only one model component, c_5, that models this feature. An improvement would be to insert an extra heat capacity next to c_5, separated a thermal resistance. However, this would create a six-node model. For the time being, the five-node model will be tested as to study if the agreement of dynamic transmittance bears a great significance in a simulation. Two facts should be observed: dynamic transmittance is a damped phenomenon and the thermal resistance of envelope components is relatively large in Nordic countries. This makes transmitted heat is relatively small in comparison to admitted heat.

5. Time domain simulations

In order to test these models within the time domain, several simulations have been performed with IDA/ICE. A set of simulations was made for a cold winter period of 12 days plus previous 7 days to allow the effect of initial values to be diminished. The simulated object was a business office with a floor area of 12 m^2. A triple-glazed window (1.8 m^2) faces South, above an electrical radiator situated at the southern external wall (8.6 m^2) of the type as described in table 1. The radiator has a dead-band between 20 and 21ºC. Another external wall (table 1), 7.8 m^2, faces west. The internal walls are adiabatic, where the whole walls are composed of 100-mm light

expanded clay aggregate blocks LECA LK5 with material properties as listed in table 1. The roof, with the U-value 0.12 W/(m^2·K), has gypsum board and wooden panelling with air cavities; the rest is insulation (and wooden frames). Composed of a linoleum sheet (5 mm) on 150 mm concrete, the floor has a constant temperature of 18 ºC at the lower surface. Thermal bridges are not modelled. Air is supplied at a rate of 2.0 l/(s·m^2) with a constant temperature of 17 ºC, whereas air infiltration corresponds to 0.2 air changes per hour. A computer (160 W) and lights (200 W) are turned on at 08:00 hours when the occupant arrives, shut off during lunch (12:00 – 13:00) and when the occupants (two in the afternoon) leave at 17:00. Night setback control was used. The radiator and air supply was turned on at hours 06:00 and off at 16:00. At night, no internal gains were present.

In order to evaluate the performance of the various models, all building components were modelled as follows:

- Case 1: The 3-node ORC optimised as to give accuracy in both admittances and transmittance for periodicity corresponding to steady-state and down to as high-a-frequency as possible. The simple RC-network represented the adiabatic internal wall, optimised for the 24-hour periodic.
- Case 2: The 5-node ORC optimised on basis of admittance at both surfaces. Agreement was desired for steady state down to the 1-hour periodicity.
- Case 3: The FDM based on a discretisation on “rules of the thumb” where cell size is approximately 5 cm or less. The external wall was discretised into totally 7 cells (1, 2, 2, 1 and 1 in the order of table 1), and the same applies to the roof. The floor was modelled with totally 3 cells (here, the linoleum layer is neglected as sometimes done in modelling). Two cells represented the internal adiabatic wall half.
- Case 4: The FDM based on the discretisation rule as suggested by Akander and Jóhannesson (2000). The period is chosen to be 0.3 hours. The results give a discretisation that divides each material layer into 1, 7, 6, 4 and 2 central capacity cells, with the order starting at the internal surface material. The floor was modelled with 1 and 7 cells, respectively. Four cells modelled the adiabatic internal wall half and totally 13 cells were used for the roof.

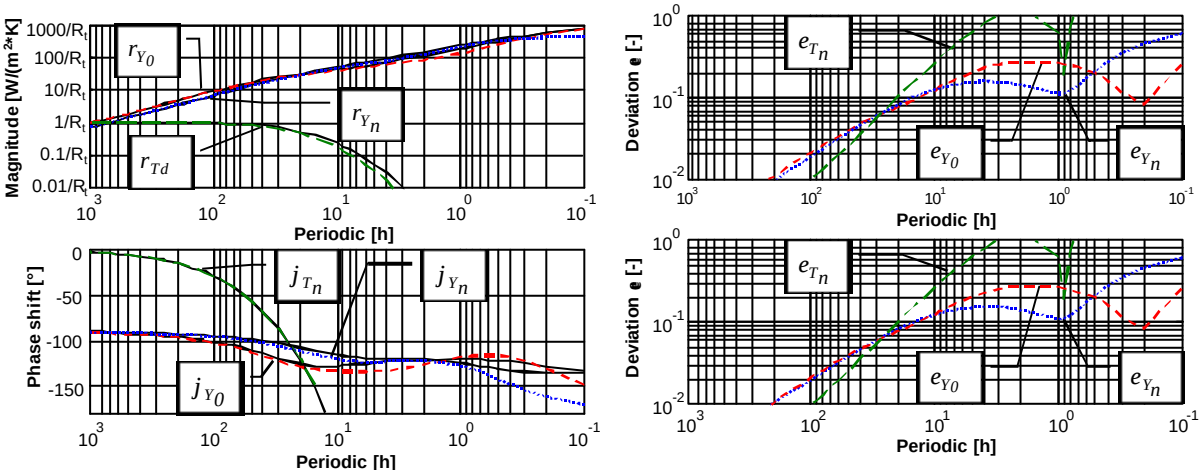

FIG. 8: <u>To the left</u>: The Bode diagram of the external wall of Table 1 as modelled in case 3. Admittances are plotted for the boundary condition $\tilde{J}_n = \tilde{J}_0$. <u>To the right</u>: Model deviation $\boldsymbol{e}$ *(equation 1) for boundary conditions $\tilde{J}_n = \tilde{J}_0$ are plotted in the upper diagram. The lower diagram shows model deviation if the temperature is constant at either surface.*

Case 4 has the best over-all agreement in terms of building component performance and is expected to give the most “exact” results within this context. The Bode diagrams for two FDMs are shown in figures 8 and 9 on the external wall.

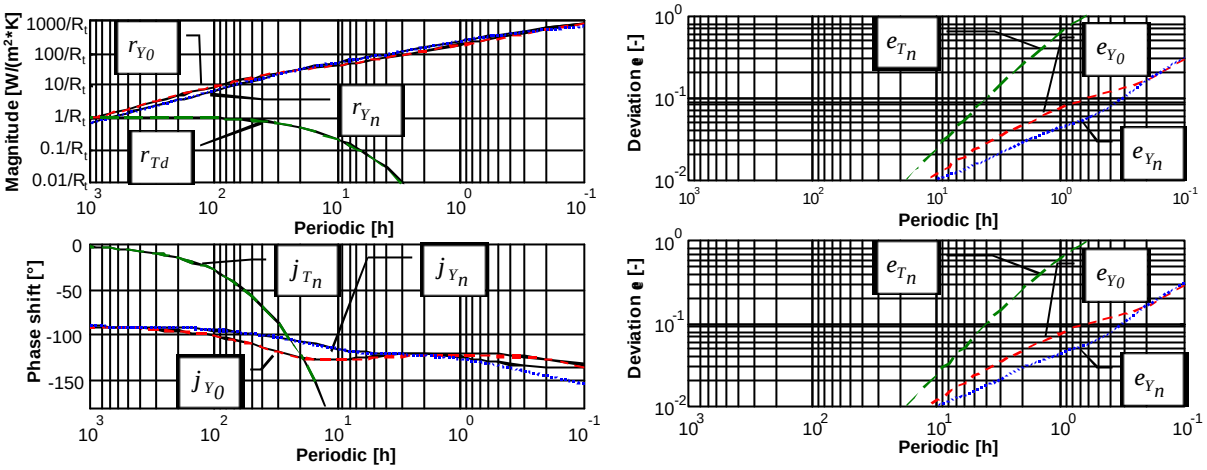

FIG. 9: <u>To the left</u>: The Bode diagram of the external wall of Table 1 as modelled in case 4. Admittances are plotted for the boundary condition $\tilde{J}_n = \tilde{J}_0$. <u>To the right</u>: Model deviation $\boldsymbol{e}$ *(equation 1) for boundary conditions $\tilde{J}_n = \tilde{J}_0$ are plotted in the upper diagram. The lower diagram shows model deviation if the temperature is constant at either surface.*

5.1 Simulation results and interpretation

Results for the last day of totally three weeks are shown in figure 10, with building components simulated by means of the 3-node ORC. The pattern of heat loads is seen, since intermittent heating is applied.

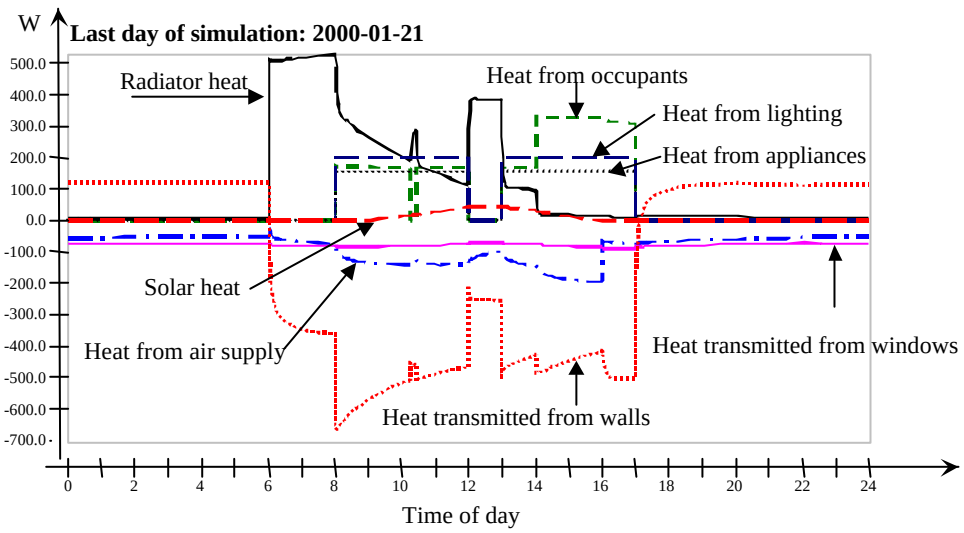

FIG: 10: Result output from IDA/ICE from the simulation of an office room where the building components were modelled with the 3-node ORC. "Heat transmitted from walls" includes all building components. Not shown is heat transmitted from furniture, which is small in all cases.

The mean air temperature of the zone and an operative temperature for the last day of simulation are shown in figure 11. These are from detailed FDM calculation (Case 4). It is needless to plot the same variables for the

other cases; the curves differ extremely little and the largest discrepancy is no more than 0.1°C (a contributing reason for this is that the temperature of the lower surface of the floor was fixed at 18ºC).

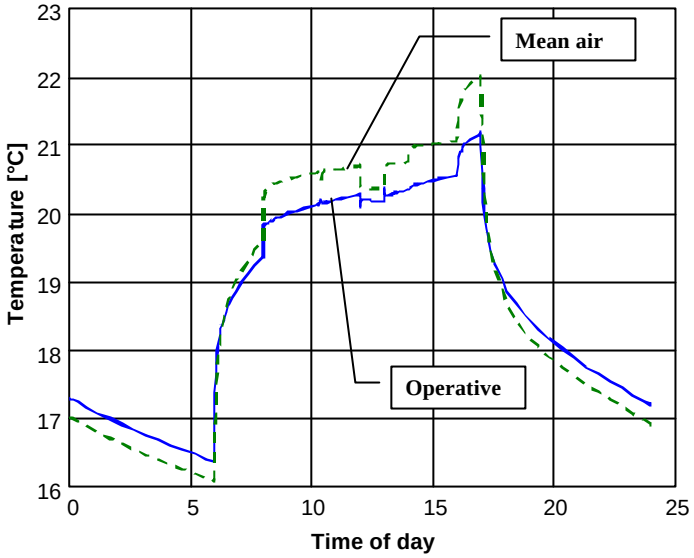

FIG. 11: The mean air temperature and an operative temperatue within the zone, as calculated with the detailed FDM (Case 4).

On zooming into the surface temperature of an external wall of figure 12, the various models give different results. The coarser models (Cases 1 and 3), as seen in the Bode diagram, cannot model high frequency processes well. This results in more damped curves, certainly for the 3-node ORC. What's happening is that the outermost resistance of the model is too large for this process, and as seen in the Bode diagram of figure 5, the magnitude of admittance is curbed, as seen in figure 13. This works vice-versa during the lunch hour. As for Case 3, the fine surface cell responds fast at 08.00 hours, but further penetration of heat is hampered by the large cell, corresponding to 5 cm LECA, behind it. The results of Case 2 agree better with those of Case 4, as seen in the Bode diagram of figure 6.

In table 2, the heating requirement (heat from the radiator, appliances and lighting) is listed for the four cases, based on the last ten days of the simulated period. The tendency is that the coarser models give an increased heating requirement.

TAB. 2: Energy requirement for a 12-day winter period. Electricity requirement for the radiator, appliances and lighting are here depicted by electricity. The air handling units require energy for fans and to preheat supply air. These are not the same for all cases due to the presence of a heat exchanger.

Simulated office with	Case 1	Case 2	Case 3	Case 4
Electricity (Wh)	69 146.8	69 016.4	69 306.5	68 991.4
Air handling units (Wh)	24 706.4	24 801.3	24 821.5	24 818.6
Difference in sums related to Case 4 (Wh)	-43.2	7.7	318.0	0.0

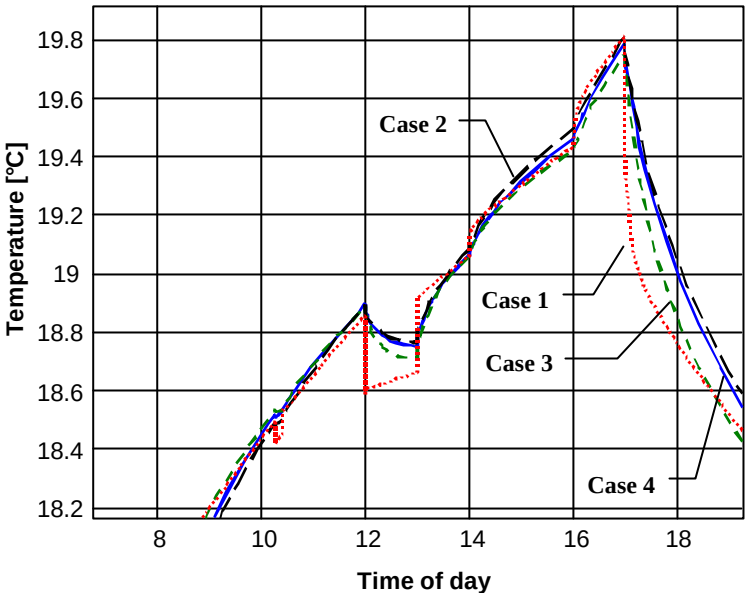

FIG. 12: A zoom into a figure that shows surface temperature of the western external wall as modelled with the various cases. The curves: Case 1 (3-node ORC, dotted), Case 2 (5-node ORC, long dash), Case 3 (simple FDM, short dash) and Case 4 (detailed FDM, filled).

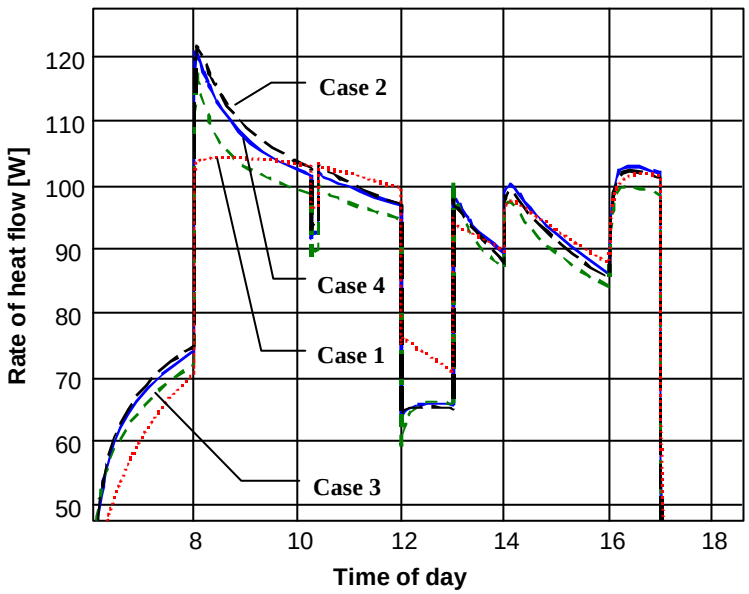

FIG. 13: The rates of heat flow into the external wall that faces west. See figure 12 for curve type.

The effect of the outermost thermal resistance will for a high frequency process prevent (damp) heat exchange between the surface and the nearest heat capacity of the model. As it turns out here, it stops some of the heat gains during the day from being stored in building components, to later be dissipated back into the room during night setback. This effect is seen in table 2, “electricity” which here is synonymous with heating requirement of the zone. Convective and radiative heat transfer coefficients have the same influence. The importance of the heat transfer coefficient of air convection on energy and peak loads is pointed out by Kalema et al (1995) who found

a 5-15% difference using two sets of correlation equations for their simulated office and on air temperature variations.

5.2 Simulation time and memory use

IDA Solver performs the numerical solving of the systems of equations. Using implicit methods with variable time steps, it is of interest to study the amount of equations that have to be solved, and the integration time these require. IDA Solver was configured with standard settings: a tolerance of 0.01 and a maximum time step of 0.5 hours. For this simulated office, the number of equations and simulation time are listed in table 3. The FDM with fine mesh has the most amounts of equations and takes longest simulation time. Note that the number of time steps taken are fairly much the same for all cases.

TAB. 3: Total amount of equations, simulation time and number of time steps depending on model used to represent the external walls.

Simulated office with	Case 1	Case 2	Case 3	Case 4
Amount of equations	115	139	163	280
Simulation time (s)	47.1	54.0	57.7	86.8
No. time steps	1825	1872	1865	1878

The 5-node ORC requires somewhat less computational time than Case 3, though more time steps have been used. The reason is that the 5-node ORC has a finer discretisation of the surface model components, but more calculation time is needed to solve Case 3, where more equations are used. Since IDA has variable time steps, these are shortened as to prevent instabilities at the nodes of Case 2. Yet, the amount of time steps is almost the same as for Case 4 with the detailed FDM.

6. Conclusions and discussion

This paper shows various RC-networks that model the thermal performance of building components. The performance of these networks can be optimised with respect to boundary conditions expected in simulations, the type of building components these are to represent, and with respect to accuracy as opposed to computational time and resources. Results in this paper shows that the use of ORC's decrease computational time and increase accuracy in results in comparison to FDM's that have the same amount of mass nodes or more. The 3-node ORC can be used to model lightweight building components, since inaccuracies may be too high or negative valued resistances or capacities may be obtained for heavyweight or massive building components. The 5-node ORC is more reliable in this sense. In being written in NMF, the model is available for object-oriented simulation environments.

The 5-node ORC has a configuration of thermal resistances and heat capacities that are advantageous if the configuration (and amount of nodes) is to be fixed and independent of boundary conditions and building component types. As shown in this paper, the 5-node ORC gives accurate results for an office cell simulated during a short cold period in a Nordic climate. In comparison with an FDM that has the same admittance qualities, the 5-node ORC gives a poorer modelling of dynamic transmittance, as seen in the Bode diagram. The reason is that the model configuration only has one heat capacity that damps low-frequency transmitted heat. Further development of this model can be made on this point, and it is likely that an extra central mass node has to be implemented. However, this action will mean that the model will be composed of six mass nodes (totally 15 model components) and an extension of optimisation procedure that improves the accuracy of high-frequency dynamic transmittance. On the other hand, the time domain simulations show that the 5-node ORC models

dynamic transmittance sufficiently accurately for well-insulated external building components in a Nordic climate. The correct modelling of admittance when heat gains are large should be of first priority.

The 5-node ORC has within this context been shown in an application on multilayer building components. In the same manner as mentioned in this paper, the ORC can be used to model multidimensional heat transfer, such as in thermal bridges and within the field of ground heat loss. Akander et al (1996) and Mao (1997) have practised the methodology, where 2 and 3-node ORCs were used. The methodology remains the same: the heat transfer within a building component is prior to a building simulation calculated by means of a frequency domain finite difference program. Implementation of "the framework for equilibrium equations" (Strang 1986) into the solving procedure of the finite difference program avoids iterative method, and thereby provides fast solutions. The thermal performance is found for a number of pre-chosen frequencies, and from this, the parameters of the ORC are optimised. In a time domain simulation, the ORC will model the sum of heat flow through the surface of a building component, and the surface temperature represents an area-weighted mean surface temperature.

7. References

Akander J. (1995). *Efficient Modelling of Energy Flow in Building Components. Parts 1 & 2.* Licentiate Thesis. Department of Building Sciences, KTH, Stockholm, Sweden.

Akander J. (1996). Controlling the Inaccuracy of Models that Represent Multilayer Constructions. *Proc. 4th Symp. on Building Physics in the Nordic Countries*, Espoo, Finland, pp. 59-66.

Akander J. (2000). The Thermal Performance of Multilayer Building Components - A Method for Approximating the Effective Heat Capacity. *(Submitted to) Nordic Journal of Building Physics, Vol 2*. Available at http://www.bim.kth.se/bphys

Akander J. and Jóhannesson G. (2000). The Thermal Performance of Building Components - Applications of the Bode Diagram. (*Submitted to*) *Nordic Journal of Building Physics, Vol 2*. Available at http://www.bim.kth.se/bphys

Akander J., Mao G. and Jóhannesson G. (1996). A Method for Modelling Two-Dimensional Heat Flow in Building Simulation Programs. *Proc. International Symp. of CIB W67 on Energy and Mass Flow in the Life Cycles of Buildings*, Vienna, Austria, pp. 575-580.

Andersson A.C. and Jóhannesson G. (1983). *Application of Frequency Response for Fast Analysis of Two-dimensional Heat Flow Problems.* Coden: LUTVDG/(TVBH-7072)/1-8/(1983), LTH, Lund, Sweden.

ASHRAE HVAC2 Toolkit (1993). *HVAC2 Toolkit – Algorithms and Subroutines for Secondary HVAC Sytem Energy Calculations.* ASHRAE TC 4.7. Ed: M. Brandemuehl. Atlanta, Georgia, USA.

Bring A., Sahlin P. and Voulle M. (1999). Models for Building Indoor Climate and Energy Simulation. *A Report of International Energy Agency (IEA SHC)*, Task 22.

Bris Data AB (2000). http://home.swipnet.se/nmf.

Claesson J. (1999). Dynamic Thermal Networks. Application of a General Theory to a Ventilated Crawl Space. *Proc. of the 5th Symp. Building Physics in the Nordic Countries*, Vol. 1, CTH, Gothenburg, Sweden. Aug. 24-26, 1999, pp. 57-64.

Davies M.G. (1994). The Thermal Response of an Enclosure to Periodic Excitation: The CIBSE Approach. *Building and Environment, Vol. 29, No. 2*, pp. 217-235.

EN 832 (1998). Thermal performance of buildings - Calculation of energy use for heating - Residential buildings. European Committee for Standardisation (CEN), Brussels.

Kalema T. and Haapala T. (1995). Effect of interior heat transfer coefficients on thermal dynamics and energy consumption. *Energy and Buildings Vol. 22*, pp. 101-113.

Kossecka E. and Kosny J. (1996). Relationship between structural and dynamic thermal characteristics of building walls. *Proc. International Symp. of CIB W67 on Energy and Mass Flow in the Life Cycles of Buildings*, Vienna, Austria, pp. 627-632

Klein S.A., Beckman W.A. and Duffie J.A. (1976). TRNSYS - A Transient Simulation Program. *ASHRAE Trans., 1976, Vol. 82, Pt.2*. (*Also* http://www.engr.wisc.edu/centers/sel/trnsys/index.html).

Mao G. (1997). *Thermal Bridges - Efficient Models for Energy Analysis in Buildings.* Doctoral Dissertation. Bulletin no 173, TRITA-BYT 97/0173, Department of Building Sciences, KTH, Stockholm, Sweden.

prEN ISO 13786: 1998 E. *Thermal Performance of Building Components - Dynamic thermal characteristics - Calculation methods.* CEN/TC 89/WG 4/N176, Brussels.

Sahlin, P. (1996). *Modelling and Simulation Methods for Modular Continuous Systems in Buildings.* Doctoral Dissertation. Bulletin No. 39, Building Services Engineering, Royal Institute of Technology, Stockholm.

Seem J.E., Klein S.A., Beckman W.A. and Mitchell J.W. (1989). Transfer Functions for Effective Calculation of Multidimensional Transient Heat Transfer. *Journal of Heat Transfer, Vol. 111/5*, pp. 9-12.

Skanska Software (1996). *VIP+ 1.3 Info*. Skanska Software, Malmö ,Sweden.

Strang G. (1986). *Introduction to Applied Mathematics*. Wellesly-Cambridge Press, Massachussettes, USA.

Submitted to Nordic Journal of Building Physics
Available at http://www.ce.kth.se/bphys

PAPER 5

The Effect of Thermal Inertia on Energy Requirement in a Swedish Building - Results Obtained with Three Calculation Models

The Effect of Thermal Inertia on Energy Requirement in a Swedish Building - Results Obtained with Three Calculation Models

SUBMITTED: August 1998
REVISED: March 1999
PUBLISHED: April 1999

Asima Norén, PhD
Jan Akander, PhD-student
Engelbrekt Isfält, PhD
Ove Söderström, Research Professor
Department of Building Sciences,
Kungliga Tekniska Högskolan (Royal Institute of Technology),
S-100 44 STOCKHOLM, Sweden
E-mail: ovesoder@ce.kth.se

KEYWORDS: *Building material, Thermal inertia*

SUMMARY: *Three different types of building constructions have been used in a study of the annual energy requirement. The buildings have identical exterior dimensions and the calculated steady state thermal transmittance is exactly the same but the thermal inertia of the chosen building materials differs. The study consists of computer simulations of the thermal processes in buildings during a heating season in Stockholm. Three different simulation programs have been used and they all show that the system with the highest thermal inertia has the lowest energy requirement and that a small change of the thermal inertia has a relatively large influence. Wood is an example of a building material with a large thermal inertia and with a fairly low weight. It gives a lower energy requirement than a traditional lightweight construction, but not as low as a heavyweight concrete construction.*

1. Introduction

The energy requirement for heating of a building located in a Nordic country is a parameter of high economic importance. In Sweden, the housing cost for standard inhabitants in different households is estimated to be between 20 and 30 % of the net income (Boverket 1997). A substantial part of the dwelling cost is heating. The thermal inertia of a building allows energy in a building zone, in times of abundance due to solar irradiation and heat from electrical appliances, to be stored in internal and external building constructions. This energy is transferred back into the zone when the indoor temperature decreases, thus limiting heat needed from the heating system without significantly affecting the thermal comfort. This issue has been studied earlier (Brown and Isfält 1973, 1983; Andersson et al 1979; Barnaby et al 1989; Simmonds 1991; Abel et al 1992; Gorman 1995; Burmeister and Keller 1996; Johannesson 1981; Akander 1995). There is an increasing interest of this subject, which is mirrored in recent publications (Winwood et al 1994; Standeven et al 1998).

The latest Swedish building code, BBR98 (Boverket 1998), allows the thermal inertia to influence the energy requirements, unlike earlier codes that solely recommended low U-values in the building envelope construction. This can only be done by means of simulations.

1.1 Research aim

The present paper is focused on three external constructions with the same steady state thermal transmittance (U-value) and computer simulations are performed with three independent programs. The indoor temperature is allowed to vary within a narrow field. The outdoor climate and the air exchange rate are the same for all cases. The aim of this research is, from these prerequisites, the identification of a considerable potential in reduction of energy requirement in buildings by choice of different building materials.

1.2 Simulation tools

Three simulation tools have been used, for the reason that results are more reassuring if these are withheld by different means. Two of the computational programs are detailed, both in modelling and input as well as the hourly calculations made. These programs are TSBI3 from the Danish Building Board and BRIS from the Swedish Council for Building Research. The third simulation tool is based on a standardised calculation procedure, EN 832, made to predict energy requirement of residential buildings as proposed by the European Committee for Standardisation (CEN). The calculation procedure is based on monthly calculations with a level of detail that is far simpler than the other two programs. An interesting aspect within this study is to compare if the results from the proposed code agree well with results from the more detailed programs.

The simulated building is described below and modelled as a whole with TSBI3 and EN 832. In BRIS, a separate apartment is simulated and is more thoroughly described in section 4.2. The results from BRIS can therefore not directly be compared with results from the other two programs; what is of importance is to study the tendency of the relationship between energy requirement and the thermal inertia of the building.

2. Building description

The building comprises two floors with six apartments, an unheated garage and attic, see Figure 1. The gross floor area of each storey is approximately 240 m^2. The building has totally 26 windows with three different areas. Each storey has 13 windows, five are facing North, and six are facing South, one to the West and the last one to the East. The balcony doors are facing South. The total window area is approximately 33 m^2 corresponding to 15 - 16 % of the net floor area.

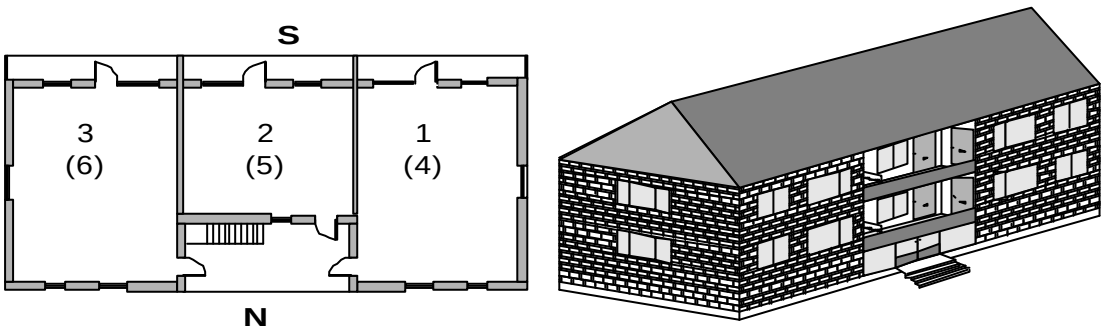

Figure 1. Plan and perspective of the building.

The building has been simulated with the following three different types of constructions, on condition that each building component has the same U-value in all three types of constructions.

2.1 Construction types

2.1.1 Lightweight construction

The exterior walls are provided of 20-mm boarding on the outside and gypsum boards interior and insulated with 175-mm mineral wool insulation (Figure 2). The interior walls are stud walls of gypsum boards. The roof is a light

wood construction with interior gypsum boards and insulated with 400-mm mineral wool insulation. The floor is provided of mineral wool insulation between two gypsum boards.

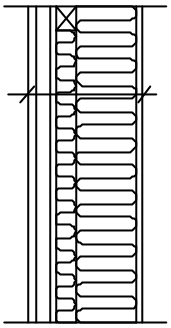

20	boarding
23	cavity
9	gypsum board
45	mineral wool
130	mineral wool
13	gypsum board

Figure 2. Exterior walls for lightweight construction (in mm).

2.1.2 Massive wood construction

The exterior walls are provided of 95-mm massive wood on the inside and gypsum boards on the outside and are insulated with 150-mm mineral wool (Figure 3). The interior walls are of 75-mm massive wood with gypsum boards on the surface layers. The roof is provided as a sandwich construction of wood and 395-mm mineral wool insulation, with an interior gypsum board. The floor is made of chipboards and wood fibreboard insulated with 95-mm mineral wool, and is situated 145-mm massive wood and gypsum boards. The reason for having gypsum boards as surface material rather than massive wood is for fire protection.

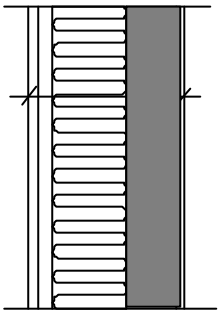

20	boarding
23	cavity
150	mineral wool
95	boarding
13	gypsum board

Figure 3. Exterior walls for massive wood construction (in mm).

2.1.3 Heavyweight construction

The exterior walls are provided with 180-mm load-bearing concrete on the inside and facing brick on the outside. The walls are insulated with 173-mm mineral wool (Figure 4). The interior walls are provided as a stud wall of gypsum boards. The roof has boarding exterior and 200 mm aerated concrete interior and is insulated with 395-mm mineral wool. The floor is composed of 200-mm concrete and mineral wool.

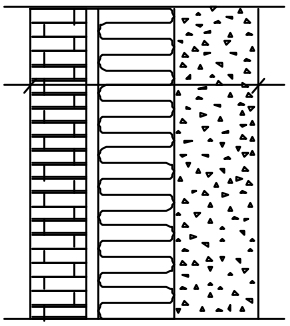

120	brick
23	cavity
173	mineral wool
180	concrete

Figure 4. Exterior walls for heavyweight construction (in mm).

The calculated U-value for building requirement and for all construction types has been:

U = 0.20 W/ (m^2 K), for exterior walls
U = 0.23 W/ (m^2 K), for intermediate floors
U = 0.097 W/ (m^2 K), for curved roof
U = 2.18 W/ (m^2 K), for interior walls
U = 1.28 W/ (m^2 K), for the garage floor

2.2 Windows

The windows are nominally triple-glazed with the U-value 1.7 W/ (m^2 K). Calculations have also been made using double-glazed windows with the U-value 2.3 W/ (m^2 K). The U-values account for the glazed part and wooden frames. Solar transmission is allowed only through the glazed part; the solar transmission factor is for triple-glazed windows 0.67 and for double-glazed windows 0.76. The windows gross areas are 1.17, 1.56 and 2.34 m^2 with a glazed area of 0.77, 0.99 and 1.32 m^2, respectively.

2.3 Heating and ventilation

Heating season is from the 15th of September to the 15th of May. The hydronic radiators have thermostats with a set point temperature at 21ºC. The rate of ventilation is set to be 0.5 ACH (**A**ir **C**hanges per **H**our) and is always turned on with a heat exchanger efficiency of 85 % as the maximum value. The efficiency may seem high, but is not unlikely since the exchanger is a regenerative type. The air leakage was assumed to correspond to a constant rate of 0.1 ACH.

For all simulations hourly weather data for a whole year was needed. The climate data file chosen was for Stockholm 1971, which is often used as a test in Sweden (Taesler and Isfält 1980).

2.4 Heated floor areas, specific energy requirement and specific bought energy

The heat capacity of each type of construction will evidently vary, hence resulting in the so-called lightweight, the massive wood and the heavyweight building. It should be noted that the influence of the thermal inertia of furniture is excluded in all calculations.

The simulation results will give the building or the modelled zone's energy requirement during the heating season. Since the volumes and floor areas within the building envelopes are different due to the thickness of exterior walls in each construction type (see Table 1), it is more convenient to define specific entities which are related to the heated (net) floor areas. Two entities are relevant in this study.

Specific energy requirement is the heat delivered from the heating system divided by the net floor area, i.e. the heated floor area within the exterior walls.

Specific bought energy is the sum of heat delivered from the heating system and electricity utilisation divided by the net floor area, i.e. the heated floor area within the exterior walls. The specific bought energy does not include the heating of domestic hot water.

Building type	Gross area [m^2]	Net floor area [m^2]	Ratio [-]
Lightweight	480	444	1.00
Massive Wood	480	435	0.98
Heavyweight	480	412	0.92

Table 1. Floor areas for the heated spaces of the three building types

A drawback for the heavier buildings is that the living space is smaller than in the lighter buildings. Under these circumstances, the heavyweight building offers a net floor area that is 8% less than that of the lightweight building, whereas the massive wood building's net floor area has a reduction of modest 2%.

3. Simulations using the TSBI3 program

A commonly used program for building energy simulation is TSBI3 (Thermal Simulations of Buildings and Installations), developed by the Danish Building Research Institute (Johnsen and Grau 1994). The program TSBI3 is a flexible PC program for dynamic analysis of energy consumption and indoor climate in a building divided into multiple thermal zones. By creation of a detailed mathematical description of the physical spaces, structures and systems, it is possible to simulate even very complex buildings with advanced heating and ventilation systems and varying operational strategies over a day, a week and a whole year.

The program calculates all power outputs and energy flows through structural parts, between zones as well as between the building and the surroundings. For all rooms or zones, which are simulated, the program will thus calculate heat loss by transmission, infiltration and ventilation. The program calculates all thermal gains in the form of solar heat, heat given off by people, equipment, lighting, etc. as well as the power demands and energy consumption for all components of heating, cooling and ventilation for each zone.

3.1 Parametric studies

The building has been modified to the standard input procedure for the TSBI3 program. It has been divided totally into eight thermal zones, each apartment as one separate zone, the garage and the attic. The building has been simulated in three different construction types and all types were tested in two cases. In case A the windows were triple-glazed and in case B double-glazed.

For TSBI3 program simulation the heating system was turned on during whole heating season and was 100 % effective and perfectly controlled. The maximum heating power (P_{max}) was reached when the outdoor temperature is at the design level (te_{design}) and at outdoor temperatures below the design temperature the maximum power output was available. The heating power decreased to the minimum level (P_{min}) when the outdoor temperature increased to (te_{min}) and at temperatures above (te_{min}) under all heating season. At outdoor temperatures (te) below (te_{min}) and above (te_{design}) the available power ($P_{heating}$) followed a linear curve according to the following formula:

$$P_{heating} = P_{\max} + (P_{\min} - P_{\max}).\frac{te - te_{design}}{te_{\min} - te_{design}} \qquad (1)$$

$$te_{design} \le te \le te_{\min}$$

The totally maximum heat power for the whole building was 8.0 kW. It has been used 1.0 kW for small apartments and 1.5 kW for larger apartments. The totally minimum power was 3.0 kW, for each apartment 0.5kW. The used values are shown in Figure 5, where the heat control curve shows that the available radiator power is linear between the maximum and minimum values.

The mean values of heat gains per day for the whole building are:

38.4 kWh, from house equipment
34.5 kWh, from people

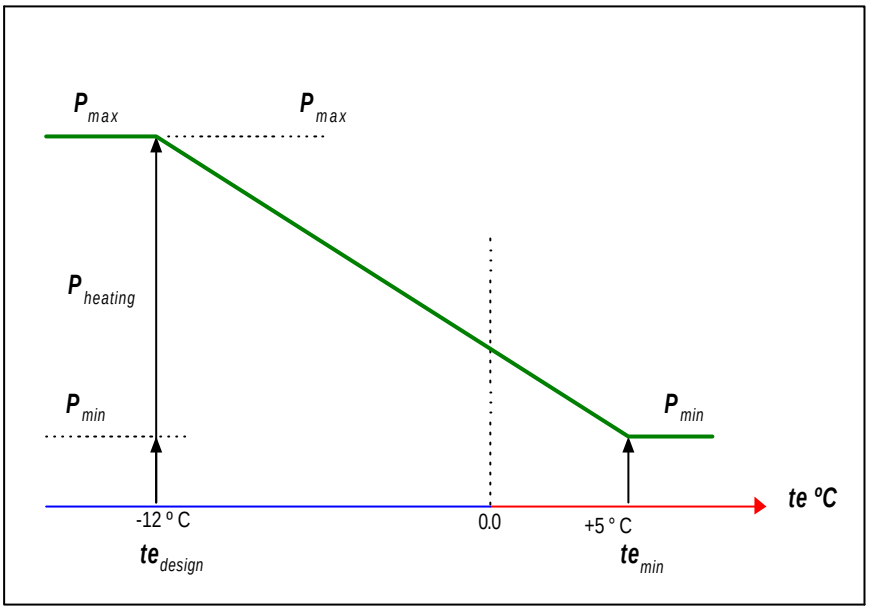

Figure 5. The control curve for available heating power, corresponding to outdoor temperature.

3.2 Results from TSBI3

The results from the TSBI3 simulations show in both cases A and B, that the highest seasonal heating energy requirement for the building with a lightweight construction, and the lowest requirement is for the building with a heavyweight construction, see the values in Table 2 and Figure 6.

Construction type	Lightweight	Massive wood	Heavyweight
A – Triple-glazed	22.1 (100%)	17.8 (81%)	14.7 (67%)
B – Double-glazed	25.2 (100%)	22.3 (88%)	20.1 (80%)

Table 2. Results from TSBI3 calculations: specific energy delivered from the heating system (kWh/m^2, year) (see definition in text) for the three building types. The numbers in parenthesis depict the ratio between the actual buildings specific energy requirement and the largest specific energy requirement.

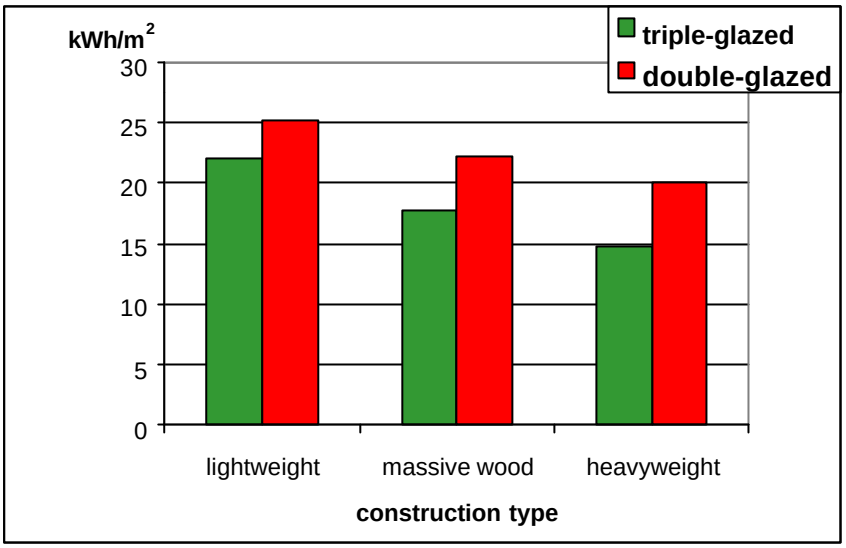

Figure 6. Diagram of specific energy requirement (kWh/m^2, year) (see definition in text) for the building.

Pursuant to the calculation results, even the specific bought energy is highest for the lightweight building, and lowest for the heavyweight building, see the values in Table 3 and Figure 7.

Construction type	Lightweight	Massive wood	Heavyweight
A – Triple-glazed	43.4 (100%)	39.5 (91%)	37.5 (86%)
B – Double-glazed	46.5 (100%)	44.0 (95%)	42.8 (92%)

Table 3. Results from TSBI3 calculations: specific bought energy (electricity and heating system) in kWh/m^2, year (see definition in text) for the three building types. The numbers in parenthesis depict the ratio between the actual buildings specific bought energy and the largest specific bought energy.

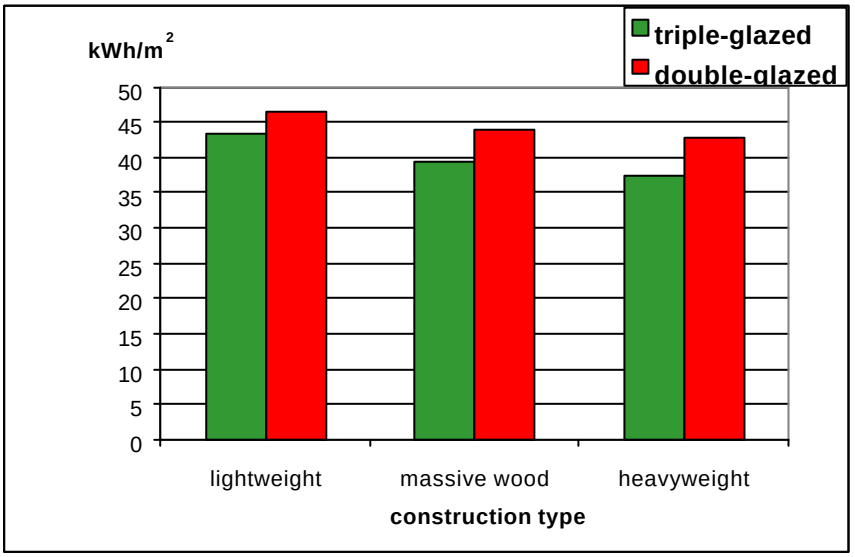

Figure 7. Diagram of specific bought energy (kWh/m^2, year) (see definition in text).

4. Simulations using the BRIS program

4.1 The BRIS-program

The BRIS program is probably one of the oldest programs in use today in the field of environmental engineering. The first working version of the program was developed in 1963 with support from the Swedish Council of Building Research (**BR**own 1964, 1990; **IS**fält 1989). Since then the program has been extended and improved several times and the present version was completed in 1982.

BRIS is based on fundamental physical relationships. The film coefficients and the radiant interchange are temperature dependent in a non-linear fashion and thus dynamically adapted to new temperatures calculated in each time step. This leads to a non-linear system of equations, which are solved by a finite difference method. The control strategy is based on a sequence of restrictions on the possible sources for heating, cooling or heat recovery. The restrictions are relaxed successively within each time step in the building model until a solution is found (Bring 1983).

By combining loads and systems minimum energy strategies can be defined and found by the program. When limiting the installed capacities the building dynamics will be more active in the control process, which has shown to give a surprisingly high potential to reduce peak power problems and energy use. In Sweden, BRIS has for many years been the most widely used program in its field, both for design of HVAC systems (**H**eating **V**entilation and **A**ir **C**onditioning systems) and research purposes.

4.2 The object

In BRIS, it is possible to handle many kinds of objects, from single rooms to whole buildings with coupled rooms. However, as the Fourier equation is solved using finite differences in all walls and slabs, the number of variables grows rapidly with the number of rooms and the results are getting laborious to handle. Therefore, we try to utilise symmetry as far as possible. In this project, where the **influence of building materials on the energy use is the subject**, we found it reasonable to simplify the model to one living room in a mid plane of the building.

Geometry:

Room size 7*10*2.4 m^3.
Three walls are exterior walls:
One 10*2.4 m^2 is facing south with a 5 m^2 window.
The two 7*2.4 m^2 walls are facing west and east respectively, both with a 3.5 m^2 window.
The other 10*2.4 m^2 wall is an interior wall bordered on a similar room (symmetry surface).

All windows are triple-glazed. The window temperature varies due to absorbed solar radiation. On the inside the convective heat transfer is calculated using temperature dependent film coefficients and long wave radiation using the Stefan Boltzmann law. Therefore the U-value will vary and is not used in this kind of simulations. Instead the heat resistance from the inside surface of the window to the ambient is given as input data. For triple-glazed windows the value 0.39 $(W/m^2, K)^{-1}$ has been used. This corresponds to a U-value in the region of 2.0 W/m^2, K (not to be compared with the values above). Three different constructions, all with the same heat resistance are investigated, see above. U-values are valid only during steady-state conditions (that never will occur). During the simulations the conditions are always transient and the U-values are not used.

Heat gains:

Electricity 6.22 kWh/day (lights, refrigerator, cooking, TV)
People 3.0 kWh/day at 20°C room air temperature, linearly reduced to 1.5 at 30 °C.
These gains are average values for apartment buildings in Sweden (Isfält and Johnsson 1986).
The heat gains are unevenly distributed over the twenty-four hour period and the same all days over the season.

Installations and control:

Heating.

One radiator beneath the window in the south facing wall. The same design value has been used in the three alternatives, even though buildings with higher first order time-constants according to Swedish standards require smaller heaters, see below. The radiator set point is 21 °C.

Ventilation.

Airflow rate 0.5 ACH as above. When the room air temperature tends to exceed 24°C cross ventilation up to 5 ACH is allowed.

Infiltration 0.1 ACH as above (constant).

There is a central air handling system in the building with a heat exchanger with maximum temperature effectiveness of 85 % and a reheater.

For our room maximum 150 W is available. Fan power adds 30 W.

Control strategy.

To maintain the room air temperature within the interval 21 – 24 °C the following resources are given. The supply air temperature may vary within 16 – 21 °C. To reach this first the temperature effectiveness of the heat exchanger is changed (0 - 85 %). After that reheating is allowed. As a third step the radiator (set point 21 °C) up to its maximal power may be used. If this, together with the heat gains, is not enough to reach 21 °C room air temperature, the reheating power in the central air handling system is increased up to it's upper limit (150 W). Often, even in wintertime, solar and internal heat gains cover the heat losses and there is no need for heating. In such situations first the heater is turned off. Secondly the supply air heater is turned off and thirdly the heat exchanger efficiency is reduced until the supply air temperature reaches it's lower limit 16°C. If the room air temperature still rises nothing is done until it reaches 24°C when the windows are opened. (This could happen especially at the beginning and end of the heating season).
To avoid numeric instability in complicated situations the simulations are carried through the year with a time step of 0.5 hours.

4.3 Results from BRIS

The energy accounts for the heating season is divided in two parts, heat balance and bought energy for each room. Positive and negative items in the room heat balance should be equal. This has been checked, but the tables are not shown here. Energy required for heating or cooling the ventilation air in central units is external from the room point of view, but of course included in ”bought energy”.

For the heating season, the specific values obtained are shown in Table 4.

Construction type	Lightweight	Massive wood	Heavyweight
Time constant (h)	31	164	325
Specific energy requirement (kWh/m^2)	18.3 (100%)	16.2 (88%)	15.7 (85%)
Specific bought energy (kWh/m^2)	42.1 (100%)	40.0 (95%)	39.5 (94%)

Table 4. Results from BRIS calculations: time constants, specific energy requirement and specific bought energy for the three building types.

The first order time constant, t, is found from a simulation of a slow cooling down period with a constant low outdoor temperature. This gives what we can call a Newtonian time constant. In the beginning of the period heat is taken from the surface layers, and the time constant has a low value. Later heat is coming from the inside of the structure. Therefore this simple model gives a time constant that increases with time, but after one or two days the

indoor temperature follows a simple exponential function. The whole cooling down period can be better described with two time constants, one short and one long. However, even this is a crude approximation compared with the BRIS program where the Fourier equations are solved also with non-linear boundary conditions. Here the time constant is only used to give an idea of how fast the indoor temperature reacts on changes in weather and power supply.

Normally the long time constant is estimated as (heat capacity)/(heat loss factor). As we are working with more detailed tools, the logarithm of the temperature difference in- outdoors during day 2 to 5 is taken and matched to a straight line by the method of least squares. The time constant is the inverse of the coefficient for the independent variable (hour) given by this curve fit.

The lightweight building (low time constant) reacts faster on weather changes and variation in internal heat gains than the more heavy buildings. Even during a short period of cold weather heat must be supplied in the lightweight building, whereas such periods can be passed without heating in the constructions with higher thermal inertia due to heat stored in the structure from previous warmer periods. The room air temperature and effective temperature are therefore often lower in the lightweight building, and this affects even the average values for the whole season. This leads e.g. to somewhat smaller window transmission losses and lower heat emission from people. The lightweight building requires more airing as the temperature rises quicker during periods with excess heat. The only items in bought energy that differs between the alternatives are heat supplied to the radiator and to the ventilating air heater. These are added and the relative values (lightweight building = 100 %) are plotted as function of the Newtonian time constant for the three alternatives in Figure 8. The difference between lightweight and massive wood constructions is larger than between the wood and heavyweight constructions. If the heat gains are higher, like in an office building, this difference is larger.

The fact that a high time constant for the thermal processes in a building decreases the energy requirement for heating makes it possible to choose a higher design winter temperature and this has been accepted in a new Swedish Standard (SS 02 43 10) for design of heating systems.

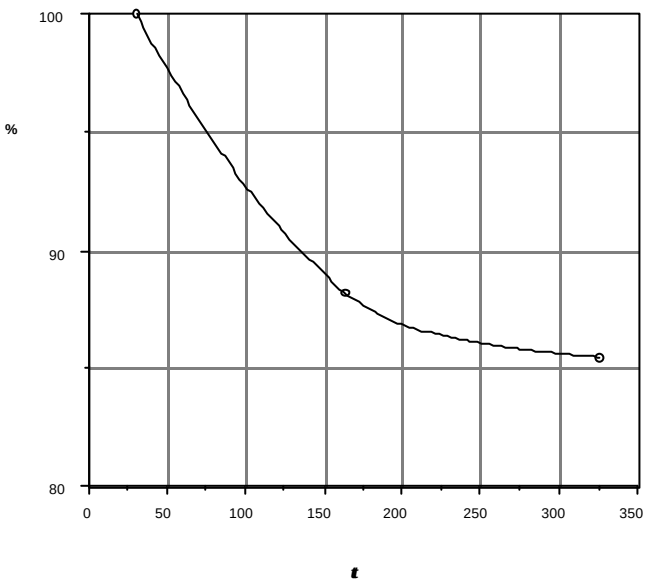

*Figure 8. Influence of the thermal mass (time constant **t**, hours) on the specific energy requirement to the radiator and ventilation air heater.*

5. Simulations using EN 832

A European standard, with the title "Thermal Performance of Buildings - Calculation of energy use for heating - Residential buildings" (EN 832) is "one of a series of standard calculation methods for the design and evaluation of thermal performance of buildings and building components."

5.1 The calculation method

The calculation method is based on a month-wise or seasonal steady state energy balance on the building as a whole or on a particular building zone. The dynamic effect of the building's thermal inertia is introduced in the steady state energy balance in terms of a variable called the utilisation factor. The utilisation factor shows the part of energy gains (solar irradiation and internal energy gains such as heat from electrical appliances and people), when available, can be stored in building constructions to be transmitted into the zone when needed.

A general equation for the energy balance, on a month-wise basis, is as follows

$$Q_{heat} = Q_{loss} - h \cdot Q_{gain} \qquad (2)$$

Where

Q_{heat} is the monthly heat requirement

Q_{loss} is the monthly heat loss

Q_{gain} is the monthly heat gain

h is the monthly utilisation factor, having a value between 0 and 1.

The calculation procedure involves input of the following data or variables:

- Climatic data needed are the monthly mean values for the outdoor air and the global solar radiation onto the buildings exterior surfaces.
- The area, geographical orientation, U-value, effective heat capacity and solar characteristics for each building construction have to be determined. The effective heat capacity is calculated with the assumption that the indoor temperature varies periodically during a day. Also, the effect of thermal bridges in envelope constructions can be accounted for, but has not been treated within this context.
- The rate of ventilation and air leakage has to retain values.
- Internal heat gains are presumed, such as heat from household appliances and people.
- Set-point temperatures in different zones have to be determined. These are monthly or seasonally constant.

The heat loss Q_{loss} is for each month determined from transmission through external constructions, ventilation losses and air leakage. The heat gain Q_{gain} is primarily the sum of heat from household appliances, people and solar irradiation through windows. The utilisation factor h is a function of the building periodic time constant t_p (see below) and ratio Q_{gain}/Q_{loss}. A large periodic time constant results in a large utilisation factor, implying that a larger portion of the heat gains is used to compensate part of heat losses, thus resulting in a smaller heat requirement from the heating system. The time constant, in this paper called the periodic time constant, is defined in the standard as

$$t_p = \frac{\sum C}{\sum H} \qquad (3)$$

The numerator is the sum of thermal capacity C of each construction based on a 24-hour periodic response while the denominator is the sum of heat loss factor H of each construction, ventilation and air leakage. The denominator is fairly the same for the three objects in this study, yet not exactly the same due to differing construction type thickness, whereas the nominator will vary.

5.2 The simulated object

The object studied was the whole building, but it was divided into three separate thermal zones: apartments 1 and 4, apartments 2 and 5, and a zone representing apartments 3 and 6. All other specifications have been mentioned earlier, and the input "building" has been modelled in close correspondence with the input of TSBI3.

5.3 Results from EN 832

The specific energy requirement, and thereby the specific bought energy, increases as the time constant decreases, see Table 5. This tendency agrees well with results from the detailed programs TSBI3 and BRIS, as expected. In order to vary the loss factor of the building, calculations were performed for each building type with double- or triple-glazed windows. The results indicate that the relative influence of the buildings heat capacity increases as the heat loss factor is decreased by means of the triple-glazing, even if the solar irradiation is greater for the double-glazing. Specific bought energy is shown in Table 6. The relative influence of the heat capacity with regard to the specific bought energy is very limited as opposed to the specific energy requirement.

The ratio of the specific energy requirement is in Figure 9 plotted as a function of the periodic time constant. Note that the periodic time constant differs quite radically from the Newtonian time constant used in the results from BRIS. The reason is that the time constant is defined in two different ways.

The periodic time constant is calculated from material parameters and is based on the effective heat capacity calculated from the building's frequency response to a 24-hour periodic. This means that the heat capacity that participates in the thermal exchange between the environment and the construction is limited to the penetration depth for that frequency. The Newtonian time constant is based on the buildings step response to shutting off the heating supply. This step contains a wide range of frequency components; some are higher and the rest are lower than the frequency corresponding to the 24-hour periodic component. Lower frequency components can penetrate deeper into the construction than the 24-hour periodic and will therefore result in larger time constants.

Building type	Lightweight	Massive wood	Heavyweight
A-Periodic time constant Triple-glazed (h)	20.8	43.7	77.4
B-Periodic time constant Double-glazed (h)	18.5	38.8	68.4
A – Triple-glazed	23.6 (100%)	17.7 (75%)	13.9 (59%)
B – Double-glazed	29.3 (100%)	23.2 (80%)	19.2 (67%)

Table 5. Results from EN 832 calculations: specific energy requirement (kWh/m^2) for the three building types. The number in parenthesis depicts the ratio between the actual buildings specific energy requirement and the largest specific energy requirement.

Building type	Lightweight	Massive wood	Heavyweight
A – Triple-glazed	44.5 (100%)	39.1 (88%)	36.5 (82%)
B – Double-glazed	50.3 (100%)	44.6 (89%)	41.8 (83%)

Table 6. Results from EN 832 calculations: specific bought energy (kWh/m2) for the three building types.

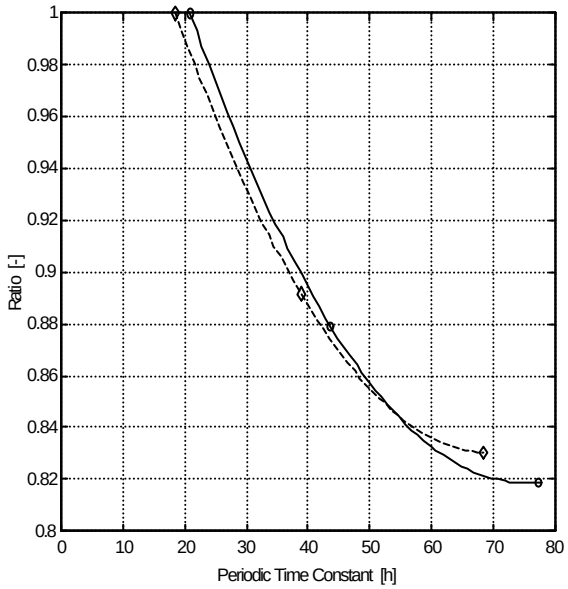

Figure 9. The ratios between total specific energy requirement plotted against the periodic time constant. The dashed curve are results for the building types with double-glazed windows while the filled curve show results for building types with triple-glazed windows.

Since the input data and boundary conditions were the same for the TSBI3 run and that of EN 832, the results can directly be compared, see Table 7. The agreement is best for the massive wood building, whereas the others two give greater deviations. EN 832 gives with this study a greater heating requirement for the lightweight building than TSBI3, but a smaller heating requirement for the heavyweight building. This indicates that the influence of the thermal inertia on the energy requirement is exaggerated in EN 832 as opposed to TSBI3 within the frame of this study. However, the tendency is clear: the building with a higher thermal inertia has a lower specific heating requirement.

Below, a comparison between TSBI3 and EN 832 results in specific bought energy are displayed. Also, the deviations between results from the two calculation methods are shown where results from EN 832 are compared with results from those from TSBI3. For being a simplified method, the norm gives small deviations within the magnitude of 3% with the exception of the lightweight building with double-glazed windows having 8%. A reason for this is that the two programs give differing thermal performances depending on the window type. Table 8 shows the difference in specific bought energy when triple-glazing is replaced by double glazing. The tendencies are actually in conflict.

Building type	Lightweight	Massive wood	Heavyweight
TSBI3 A – Triple-glazed	43.4 (100%)	39.5 (91%)	37.5 (86%)
EN 832 A – Triple-glazed	44.5 (100%)	39.1 (88%)	36.5 (82%)
Deviation – Triple-glazed	2.5%	-1.0%	-2.7%
TSBI3 B – Double-glazed	46.5 (100%)	44.0 (95%)	42.8 (92%)
EN 832 B – Double-glazed	50.3 (100%)	44.6 (89%)	41.8 (83%)
Deviation – Double-glazed	8.2%	1.4%	-2.3%

Table 7. Results from TSBI3 and EN 832 calculations: specific bought energy (kWh/m^2) for the three building types as well as deviations of EN 832 results related TSBI3 results.

Building type	Lightweight	Massive wood	Heavyweight
TSBI3 - Difference	3.1	4.5	5.3
EN 832 – Difference	5.8	5.5	5.3

Table 8. The difference in specific bought energy (kWh/m^2) for a building type with triple-glazing and double-glazing. The tendencies of EN 832 and TSBI3 are in conflict.

6. Discussions and conclusions

The present study indicates that the thermal inertia has an influence on the annual energy requirement for heating of a house located in a country with a northern climate. The effect is rather small for different materials in conventional building constructions that have a large quantity of insulation with a thin surface material layer of a chip or gypsum board. By increasing the massive wood content at the inner surfaces of the construction, the thermal inertia is increased and the specific energy requirement is lower than it is for a lightweight construction. The lowest specific energy requirement is obtained with an extremely heavy concrete construction. However, the highest relative reduction appears between the lightweight construction and the wood construction. The conclusion is that even a small increase of the thermal inertia has a lowering effect on the specific energy requirement, but this effect diminishes with a further increase of the thermal inertia. However, it is to be noted that the influence of the furniture has been neglected in this study. The introduction of furniture would affect the thermal inertia of the lightweight building more than for the heavyweight building leading to a decrease in difference in energy requirement.

In the present investigation the exterior dimensions of the building were kept constant, resulting in different inner dimensions for the different constructions. This was accounted for in the models of TSBI3 and EN 832. These two models gave a specific energy requirement for the heavyweight building that was some 82 - 86 % of the requirement for a lightweight building. The BRIS-program, however, uses constant inner dimensions and a somewhat different model (an apartment) gave a corresponding value of 86 %. The main reason for these differences is that the choice of material influences the thickness of the constructions, thus affecting the total area through which heat is transmitted, as well as the building volume that has to be ventilated. For these reasons the calculated results are presented as the specific energy requirement defined in the text above.

So far the discussion has been focused on varying the heat capacity of the constructions. In one case the heat loss factor has been varied by means of the U-value for windows. As shown in table 7, the energy requirement is decreased when the double-glazing is substituted by triple-glazing. The influence of the heat capacity increases as the heat loss factor of the building decreases. However, it is not within this study evident on the magnitude of this influence since TSBI3 and EN 832 give varying results. The results show that the insulation lowers the

energy requirement not only due to the increase in thermal resistance of constructions, but also due to the increase in thermal inertia.

The advantage with a thermally inertial material in a construction can be increased in non-conventional constructions, which, however, will meet problems with the present national building codes and recommendations. Therefore, it is important to develop and refine the powerful tool computer simulations to demonstrate the potential in choosing a building material with a fairly high thermal inertia e.g. wood.

The recent revolution in hardware price/performance, new developments in computer science like interactive graphical user interfaces, object oriented programming techniques, and advanced numerical methods allow more advanced modelling to become practical also in industry. A new generation of simulation environment, the IDA project (**I**nstitute of Applied Mathematics/**D**ifferential **A**lgebraic Systems), is aiming at bringing these new advances to the hands of the building designers (Sahlin 1996). BRIS has been used to verify IDA and major parts of BRIS are now re-implemented in IDA. A new version, IDA/ICE (**I**ndoor **C**limate and **E**nergy) was recently released.

The next step is to involve the moisture issues in the analysis and that is possible with the next generation of simulation programs (Sahlin et al 1994). Finally, it is important to clearly state that any types of computer simulations must be verified with measurements, both in a laboratory and full-scale buildings, and with practical observations in existing buildings.

This project has been sponsored by BFR, Swedish Council for Building Research and by Trätek, Swedish Institute for Wood Technology Research.

7. References

Abel, E., Isfält, E. and Ljungkrona, I. (1992): Analysis of the dynamic energy balance in an occupied office room using simulations and measurements. TRANS ASHRAE 92 Part 2:363.

Akander, J. (1995): Efficient Modelling of Energy Flow in Building Components. Parts 1 & 2. Licentiate Thesis. Department of Building Sciences, Royal Institute of Technology, Stockholm.

Andersson, L.O., Bernander, K.G., Isfält, E. and Rosenfeld, A.H. (1979): Storage of Heat and Coolth in Hollow Core Concrete Slabs. Swedish Experience and Application to Large, American - Style Buildings. Report LBL-8913. Lawrence Berkeley Laboratory, Berkeley. California.

Barnaby, C., Dean, E., Fuller, F., Nell, D., Shelley, T. and Wexler, T. (1980): Utilizing the thermal mass of structural systems in buildings for energy conservation and power reduction. Lawrence Berkeley Laboratory, Berkeley. California.

Boverket (1997): Vem bor hur och till vilket pris? – Hushållens boendeförhållanden och utgifter. Boverket, Sweden (In Swedish).

Boverket (1998): Boverkets Byggregler (BFS 1993:57 with changes BFS 1998:38). Boverket, Sweden (In Swedish).

Bring, A. (1983): Versatile System Simulation with the BRIS Program. Proceedings of the Fourth Symposium on the Use of Computers for Environmental Engineering related to Buildings. Kenchiku Kaikan, Tokyo, Japan.

Brown, G. (1964): A method of calculating on a computer the thermal and light radiation in a room and also the cooling and heating requirements. National Swedish Institute for Building Research. Reprint No 4:1964.

Brown, G. (1990): The BRIS Simulation Program for Thermal Design of Buildings and their Services. Energy and Buildings *14*: 385 - 400.

Brown, G. and Isfält, E. (1973): Proper use of the heat capacity of buildings to achieve low cooling loads. Contribution to the CIB W 40 Birmingham meeting. (Also published in the IHVE Journal, London).

Brown, G. and Isfält, E. (1983): Use of Building Structure for Reducing Cooling and Heating Requirements. Proceedings of the Fourth Symposium on the Use of Computers for Environmental Engineering related to Buildings. Kenchiku Kaikan, Tokyo, Japan.

Burmeister, H. and Keller, B. (1996): The Climate Surfaces: A Strategic Design Tool for the Early State of Planning. Proc. 4th Symp. Building Physics in the Nordic Countries, Espoo, Finland, Sept 9-10.

Gorman, T.M. (1995): The Thermal Performance of Log Home Walls: WOOD DESIGN FOCUS.

Isfält, E. (1989): The Thermal Balance of Buildings. A basis for comparisons of computer programs for calculations of the room climate and the power and energy requirements for climate control of buildings. A detailed presentation of a number of BRIS simulations with comments. IEA Annex 21 Subtask C.

Isfält, E. and Johnsson, H. (1986): Stockholmsprojektet. Effekt- och energisimuleringar med datorprogrammen BRIS och DEROB. Statens råd för byggnadsforskning. Rapport No R59: 1986.

Johannesson, G. (1981): Active Heat Capacity – Models and parameters for Thermal performance of Buildings. Report TVBH-1003, Lund Technical University, Lund.

Johnsen, K. and Grau, K. (1994): *TSBI3* Computer program for thermal simulation of buildings.:User's Guide vers B.05. Danish Building Research Institute SBI.

EN 832:1998 (1998): Thermal Performance of Buildings- Calculation of Energy use for Heating- Residential Buildings. CEN 1998. Brussels.

Sahlin, P., Bring, A. and Sowell, E.F. (1994): The Neutral Model Format for Building Simulation. Bulletin No. 32, Building Services Engineering, Royal Institute of Technology, Stockholm.

Sahlin, P. (1996): Modelling and Simulation Methods for Modular Continuous Systems in Buildings. Doctoral Dissertation. Bulletin No. 39, Building Services Engineering, Royal Institute of Technology, Stockholm.

Simmonds, P. (1991): The Utilization and Optimization of a Building´s Thermal Inertia in Minimizing the Overall Energy Use. TRANS ASHRAE 92 Part 2:1031.

Standeven, M., Cohen, R., Bordass, B. and Leaman, A. (1998): The best building ever? PROBE Team's verdict on the Elisabeth Fry Building. Building Services Journal April 1998.

Taesler, R. and Isfält, E. (1980): Choice of climatological data for testing of computations of energy requirements in buildings. Inst. för uppvärmnings- och ventilationsteknik, Royal Institute of technology, A4 - serien nr 28, Stockholm.

Winwood, R., Wilkins, R. and Edwards, R. (1994): Modeling the thermal flywheel. Building Services Journal October 1994.

© International Journal of Low Energy and Sustainable Buildings, 1999
Available at http://www.ce.kth.se/bim/leas

PAPER 6

Reducing Ground Loss from a Heated Underfloor Space – A Numerical Steady-state Case Study.

Reducing Ground Loss from a Heated Underfloor Space – A Numerical Steady-state Case Study.

SUBMITTED: April 1999.
REVISED: February 2000.
PUBLISHED: .

Jan Akander, Tekn. Lic.,
Division of Building Technology;
Department of Building Sciences;
Kungl Tekniska Högskolan;
S – 100 44 Stockholm;
akander@ce.kth.se

KEYWORDS*: building heat transfer, ground loss, air tightness, system temperatures, LECA, Termogrund.*

SUMMARY*:*
Termogrund is a suspended floor construction. The underfloor space is equipped with a convective air-heating unit that circulates heated air within the enclosure. The system delivers heat, primarily for thermal comfort, to the living space above via the suspended floor by means of heat conduction. The concept of today can be improved in terms of reducing the system temperatures within the underfloor (heating) space and in terms of decreasing heat loss via the ground. In this paper, suggestions are put forward on how the system of today can be improved and to what extent these modifications influence system temperatures and the total heat balance. Calculations show that system temperatures can be lowered if the thermal conductance of the suspended floor is increased. Additional insulation at the envelope adjacent to and above the ground is a convenient way of reducing heat loss. The calculations were carried out with a steady-state finite difference program for three-dimensional heat conduction and EN ISO 13370 standard procedures. The agreement between the two calculation procedures is quite good for this type of suspended floor. Measurements and simulations show that air infiltration should not be neglected when dealing with heat loss from underfloor spaces.

1. Termogrund – a description

Termogrund is a system that is composed of a suspended floor upon a heated underfloor space. The system is mainly produced with three building materials: EPS (expanded polystyrene) boards, PE-foil (polyethylene) and elements of LECA (light expanded clay aggregates). The few components result in that the system is easily erected during a short time at the building site. Around 100 m^2 of floor can be installed during a day of work. Structures are lifted and positioned by means of a crane. Figure 1 shows the constituents: the PE-foil, two layers of EPS boards, the foundation beams and the suspended floor elements.

In the central regions of the heating space, an electrical heat convector is installed. The fan of the convector continuously circulates the enclosed air through four ducts to the corners of the heating space. Heat is electrically supplied on an on/off basis, but never letting the air temperature rise above the temperature 35 °C. In the living space, a thermostat that is placed on an internal wall controls the heating unit. Termogrund is designed to be a heating system that delivers heat for thermal comfort (warm floors); the surface temperature of the floor should not exceed the indoor temperature by some 2ºC. It's not a heating system that fulfills the buildings total energy requirement during the coldest winter period. A faster complementary heating system has to be accessible at peak loads.

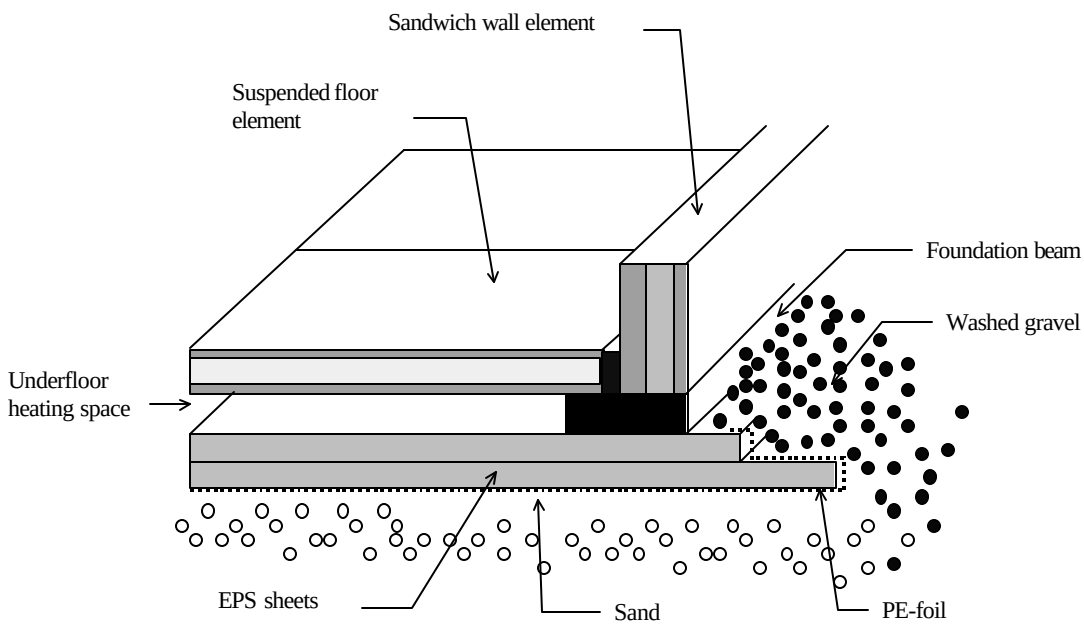

FIG. 1: Sketch of the Termogrund. Seen from above: The suspended floor element, the foundation beam and EPS sheet. A heat convector (not drawn in the figure), situated in the heating space, distributes warm air to the corners of the space by means of ducts.

2. The purpose

The purpose of this paper is to investigate the possibility of lowering the set point temperature and heat loss in the heating space without radically changing neither the whole concept, nor the heat delivered to the living space above. The new system should be composed of the same three building materials and the same type of convective heating unit. The procedures, tools and machines for erecting the system should be the same as for today's system. Dimensions of structure components should be "standardized", as in the present design. Suggested changes should also take into consideration the functionality involved with the changes, such as air-tightness and moisture aspects.

Calculations have been performed using a steady-state three-dimensional (3-D) finite difference heat conduction program. Since 3-D programs require extensive modelling and computational time, an investigation is made to compare results from 3-D calculations with alternative methods. The alternative methods are listed in the EN ISO 13370. These methods comprise a 2-D finite difference calculation procedure and a set of approximate equations. Blomberg (1996) has formulated an effective U-value for this type of heated floor, but this will not be studied in the present paper.

An investigation of how infiltrating air influences the heat balance of the heating space was made. Measurements were performed with the pressurized fan method and with a tracer gas technique. The data should indicate the magnitude of infiltrating air that cross flows through the heating space as opposed to infiltrating air that enters the living space via the heating space.

3. The calculation tools

The calculation tool used is mainly the finite difference program DAVID-32 (Anderlind 1998), which calculates steady state heat conduction in two or three dimensions. The results from this program will be compared with results from EN ISO 13370 on ground loss applied to the Termogrund.

For air infiltration calculations, a computational program was created to track airflow during normal running conditions. The program was validated with measured data. Theory and measurement results are found in Appendix A.

4. Changes in the present design

Due to its simplicity, the present design, as illustrated in figure 2, is fast and easy to erect. In figure 3, the alternative solutions are shown. Three main points can be seen.

1. The suspended floor is of a massive type. The actual thickness is due to mechanical stress reasons and is also a standardized element thickness for moulds used in production. The nominal thermal conductivity of the core material (thickness of 0.150 m) is 0.32 W/(m·K), which gives a relatively low U-value for the floor, 1.338 W/(m^2·K). The U-value of the construction can be increased by means of replacing the lightweight core material with a core of higher density. Then the same amount of heat can be dissipated at a lower temperature difference. A core material with a thermal conductivity corresponding to 0.7 W/(m·K) will give a floor the U-value of 2.030 W/(m^2·K).

2. The second means of modifying the system is by externally applying insulation (EPS) at the vertical edges of the foundation, overlapping the foundation beams and lower parts of the external walls with 200 mm. This will reduce heat loss at the vertical edges. It would also decrease air leakage at the joints, since EPS is a relatively airtight material. Another benefit is that the PE-foil can be folded up to the external wall. This would not only make the heating space more airtight, it would also reduce the risk of having rain or melted snow trickling down between the beams and the foil. Also, by placing the foil between the EPS sheets, the risk of puncturing the foil is reduced. Water that occasionally may be caught by the lower extended EPS sheet can flow down to the drainage system through the joints between adjacent sheets.

3. Another possibility of reducing heat loss to the ground is by increasing the level of insulation on the ground. Such increase should be restricted since there is a risk of having frost in the ground. A criterion that can be recommended is to allow the heat loss to be equivalent to that of well-insulated conventional slab-on–ground constructions. An extra layer of EPS will also increase the air-tightness of the heating space.

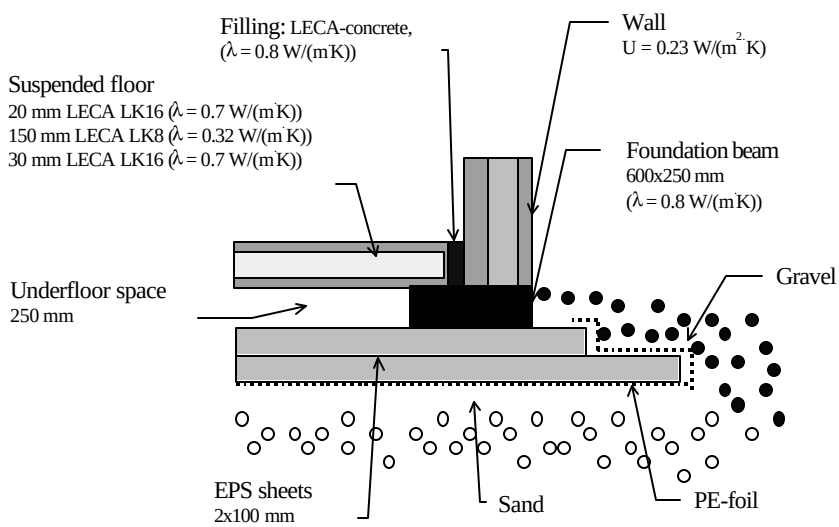

FIG. 2: Drawing of the nominal design. The building components are to a large degree made of Light Expanded Concrete Aggregates (LECA, with material class denoted by LK and a number). The wall is a sandwich element of LECA and EPS, which has the U-value of 0.23 W/(m^2·K).

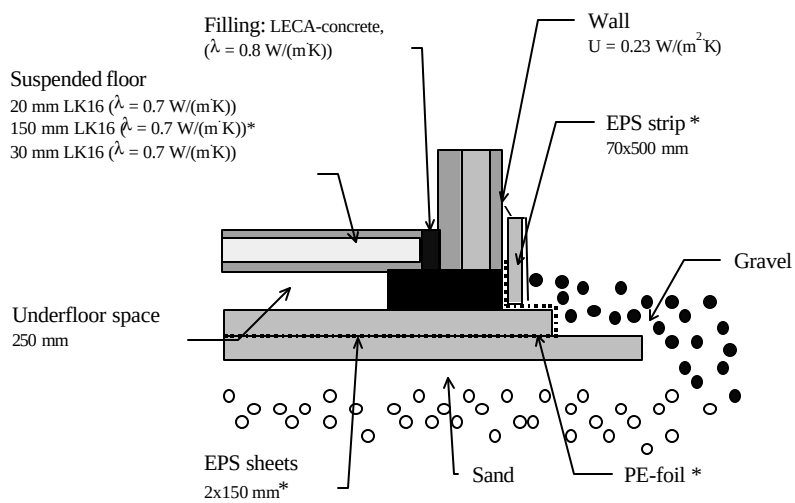

FIG. 3: Drawing of the system with proposed changes. The star (*) marks changes and simulations on ground heat loss will be performed for each case.

5. Simulation with DAVID-32

The finite difference program DAVID-32 is well suited for the task since the optimum design is easily identified in steady-state analysis, even if the ground actually never takes on this state. The system is modelled in accordance with EN ISO 13370 Annex A. The calculated part of the ground is assumed to have adiabatic boundaries with exception of the upper surface that is in contact with the exterior environment and the underfloor space constructions. The depth of the ground is 15 m, whereas the width of the ground is 2.5 times the length of the modelled heated floor, namely from the buildings mid point to the external wall. A number of floor dimensions are used such as to give an internal suspended floor area corresponding to 44 – 100 m^2, which are common figures for single family houses in Sweden.

The indoor and the outdoor temperatures are assumed to be 20 °C and 2 °C, respectively. The latter temperature is the mean outdoor temperature of the heating season in Stockholm. Different values are used for various surface thermal resistances. The value of the internal surface thermal resistance at the floor was set to be 0.10 $m^2 \cdot K/W$, a value which was estimated for a monitored radiant floor (Akander et al 1994). EN ISO 13370 recommends the value 0.11 $m^2 \cdot K/W$. For vertical walls, this value is 0.13 $m^2 \cdot K/W$. The value 0.081 $m^2 \cdot K/W$ is used at the interior surfaces of the heating space. The external surface thermal resistance has a value of 0.04 $m^2 \cdot K/W$. A ground thermal conductivity of 2.3 W/(m·K) is assumed. In order to include thermal bridge effects at the joint between foundation beams and external walls, external walls with the height 1 m having a U-value of 0.23 $W/(m^2 \cdot K)$ was implemented in the model. The sandwich wall thickness is totally 0.3 m.

The air temperature is assumed to be isothermal in the heating space. The thermal influence of supporting beams inside the air space is neglected.

A characteristic length of the floor, *B'* (EN ISO 13370) is used to express the different dimensions of the simulated floors.

$$B' = A/(0.5 \cdot P) \qquad (1)$$

A is the total floor area within *P*, the exposed floor perimeter.

TAB. 1: The thermal conductivity of various materials used in the simulations.

Material	Concrete	EPS	Gravel	Ground soil, sand	Surface layer LECA LK16	Foundation beam LECA	Floor core LECA LK8/LK16
Conductivity W/(m·K)	1.7	0.04	0.75	2.3	0.7	0.8	0.32/0.7

6. Results on ground loss

From the heat balance, DAVID-32 calculates how much heat enters the simulated object, here called Φ_{tot}. Heat supplied by the convector, Φ, is Φ_{tot} reduced by heat that is transmitted through the walls. The computed net rate of heat flow that enters the living space, Φ_u, through the upper floor surface is in the following section shown in the form of heat flux (density of heat flow rate). Heat flux up, q_u, depicts the average heat flow density per square meter of interior floor area A_i, on basis of the temperature in the underfloor space, T_T, and the indoor temperature, T_i, an effective U-value for the suspended floor can be defined, such that

$$U_{ui} = \frac{q_u}{T_T - T_i} = \frac{\Phi_u}{A_i(T_T - T_i)} \tag{2}$$

This U-value includes to a certain extent the effect of the thermal bridge at the joint of the suspended floor, the wall and the foundation beam (here called edges). For a floor with an infinite area where heat loss is negligible at the edges, U_{ui} will be equal to the U-value of the suspended floor.

The ground heat loss, Φ_d, is defined as heat delivered from the convector that is not transmitted through the upper surface of the suspend floor. The effective U-value of the envelope of the heating space, U_d, will have an extra index as to denote if the entity is based on interior (i) or exterior (e) floor dimensions, as such

$$U_{di} = \frac{q_d}{T_T - T_e} = \frac{\Phi_d}{A_i(T_T - T_e)}; \quad U_{de} = \frac{\Phi_d}{A_e(T_T - T_e)} \tag{3}$$

U-values are expressed with three decimals for the sake of numerical studies made in this paper. The downward heat flux q_d is calculated on basis of the internal floor area.

6.1 Case 1: The nominal system

According to the manufacturers of this system, the nominal design assumes an air temperature in the heating space of 35 °C. The heat flow that is transmitted into the living space in this actual case will be the criterion that is to be fulfilled in the altered designs. Results from simulations are shown in table 3. The upward heat flux q_u is for the different floor dimensions somewhat larger than 17 W/m^2 (the heating demand for a modern Swedish dwelling is in average 10 – 20 W/m^2). From this value, an effective U-value for the suspended floor, U_{ui}, can be calculated. This U-value indicates how well heat is conducted into the living space, having a maximum value of 1.338 W/(m^2·K).

TAB. 2: Results for the nominal system.

Temp °C	Interior dimensions	B'	q_u W/m^2	q_d W/m^2	Φ W	U_{ui} W/(m^2·K)	U_{di} W/(m^2·K)	U_{de} W/(m^2·K)
35	5.35x8.25	3.56	17.03	11.49	1259	1.135	0.348	0.292
35	8x8	4.30	17.61	10.22	1781	1.174	0.310	0.268
35	8x10	4.75	17.86	9.65	2201	1.191	0.293	0.257
35	9x9	4.80	17.89	9.59	2226	1.192	0.291	0.255
35	9x10	5.04	18.00	9.33	2460	1.200	0.283	0.250
35	8x12.5	5.19	18.06	9.18	2724	1.204	0.278	0.247
35	10x10	5.30	18.11	9.07	2718	1.207	0.275	0.245

6.2 Case 2: The system with a high-density core

The nominal system has a massive core with the heat conductivity of 0.32 W/(m·K). If this low density LECA is changed to a higher density class, the heat conductivity of the core will be 0.7 W/(m·K). This means that the calculated one dimensional U-value of the suspended floor changes from 1.338 to 2.030 W/(m^2·K). The effective U-value of the suspended floor will increase accordingly. The temperature in the underfloor space was reduced to 30.1ºC as to have the same upward heat flux as in Case 1, the nominal system.

TAB. 3: Results for the system with a high-density core.

Temp °C	Interior dimensions	B'	q_u W/m^2	q_d W/m^2	Φ W	U_{ui} W/(m^2·K)	U_{di} W/(m^2·K)	U_{de} W/(m^2·K)
30.1	5.35x8.25	3.56	16.89	10.20	1196	1.656	0.363	0.304
30.1	8x8	4.30	17.58	9.02	1702	1.740	0.321	0.278
30.1	8x10	4.75	17.87	8.51	2110	1.769	0.303	0.266
30.1	9x9	4.80	17.90	8.45	2135	1.772	0.301	0.264
30.1	9x10	5.04	18.04	8.21	2362	1.786	0.292	0.259
30.1	8x12.5	5.19	18.11	8.08	2619	1.793	0.288	0.255
30.1	10x10	5.30	18.16	7.98	2614	1.798	0.284	0.253

6.3 Case 3: The nominal system with additional edge insulation

It is possible to fasten an additional insulation strip on the exterior side of the foundation beam. This insulation, that overlaps the beam and the lower part of the exterior wall, will primarily reduce heat loss through the beam. For esthetical reasons, the thickness is set to be no greater than 70 mm and 500 mm in height. A temperature of 34.5ºC was found to give the same upward heat dissipation as for the nominal system.

TAB. 4: Results for the system with additional edge insulation.

Temp °C	Interior dimensions	B'	q_u W/m^2	q_d W/m^2	Φ W	U_{ui} W/(m^2·K)	U_{di} W/(m^2·K)	U_{de} W/(m^2·K)
34.5	5.35x8.25	3.56	17.45	8.55	1147	1.203	0.263	0.220
34.5	8x8	4.30	17.83	7.81	1640	1.229	0.240	0.208
34.5	8x10	4.75	17.99	7.46	2036	1.241	0.230	0.202
34.5	9x9	4.80	18.01	7.42	2060	1.242	0.228	0.201
34.5	9x10	5.04	18.08	7.27	2281	1.247	0.224	0.198
34.5	8x12.5	5.19	18.12	7.18	2530	1.250	0.221	0.196
34.5	10x10	5.30	18.15	7.11	2526	1.252	0.219	0.194

6.4 Case 4: The system with a high-density core and additional edge insulation

The substitution of the low-density core with a higher density allowed a temperature of 30 °C in the heating space to maintain an upward heat flux as in the nominal case. In combination with additional edge insulation with a thickness of 70 mm, the temperature can be reduced further. The results from these changes are displayed in table 5.

TAB. 5: Results for the system with a high-density core and additional edge insulation.

Temp °C	Interior dimensions	B'	q_u W/m^2	q_d W/m^2	Φ W	U_{ui} W/(m^2·K)	U_{di} W/(m^2·K)	U_{de} W/(m^2·K)
29.7	5.35x8.25	3.56	17.20	7.33	1083	1.773	0.265	0.222
29.7	8x8	4.30	17.68	6.69	1559	1.822	0.241	0.209
29.7	8x10	4.75	17.89	6.38	1941	1.844	0.230	0.202
29.7	9x9	4.80	17.91	6.35	1964	1.846	0.229	0.201
29.7	9x10	5.04	18.00	6.21	2179	1.856	0.224	0.198
29.7	8x12.5	5.19	18.05	6.14	2418	1.861	0.222	0.197
29.7	10x10	5.30	18.09	6.07	2416	1.865	0.219	0.195

6.5 Case 5: The system with a high-density core, additional edge insulation and extra ground insulation

In this case, all the specified alternatives are implemented in the model. The system has a suspended floor with a high-density core. Additional edge insulation with the thickness of 70 mm is applied as well as an extra ground insulation sheet of 100 mm. Now, the ground insulation has a total thickness of 300 mm.

TAB. 6: Results for the system with a high-density core, additional edge insulation and an extra layer of EPS at the bottom.

Temp °C	Interior dimensions	B'	q_u W/m^2	q_d W/m^2	Φ W	U_{ui} W/(m^2·K)	U_{di} W/(m^2·K)	U_{de} W/(m^2·K)
29.7	5.35x8.25	3.56	17.26	6.04	1028	1.780	0.218	0.183
29.7	8x8	4.30	17.73	5.44	1483	1.828	0.197	0.170
29.7	8x10	4.75	17.93	5.17	1848	1.848	0.187	0.164
29.7	9x9	4.80	17.95	5.15	1871	1.851	0.186	0.163
29.7	9x10	5.04	18.04	5.02	2076	1.860	0.181	0.160
29.7	8x12.5	5.19	18.09	4.96	2304	1.865	0.179	0.159
29.7	10x10	5.30	18.13	4.90	2303	1.869	0.177	0.158

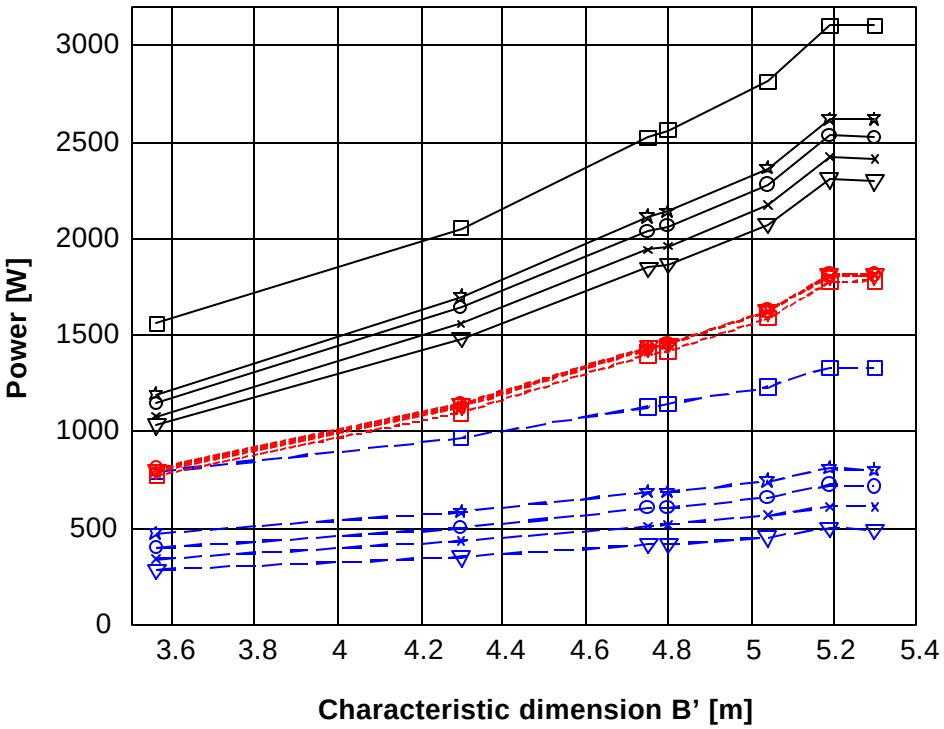

FIG. 4: Power plotted as function of characteristic dimension for the various cases. Filled lines depict power from the convector, dotted lines upward rate of heat flow and the dashed lines show downward rate of heat loss. The symbols represent the following: Case 1 (square), Case 2 (star), Case 3 (ring), Case 4 (cross) and Case 5 (triangle).

6.6 Conclusions on ground loss

The following conclusions may be drawn from the simulations.

- The downward heat flux (average density of heat flow rate) decreases as the floor area increases, for the reason that edge loss becomes a smaller part of the total loss.
- A suspended floor with a small heat resistance allows lower system temperatures to fulfill a given heat demand. The lowered system temperature also results in reduced heat loss.
- Additional edge insulation reduces heat loss from the underfloor space without significantly lowering the system temperature. The lowering of temperature is due to the fact that the edge insulation causes an increased upward heat transfer along the perimeter of the floor in comparison to the nominal type. This has the same effect as reducing the thermal resistance of the floor, but the effect is limited to the areas at the perimeter. The edge insulation may decrease air infiltration.
- Heat transmission through the suspended floor can with acceptable accuracy be considered to be one-dimensional. The agreement is better for large floor areas since heat loss at the perimeter decrease in relation to the total transferred heat.

7. Calculations with EN ISO 13370 procedures

The EN ISO 13370 procedure offers equations that estimate the U-values of various floor/ground constructions and therefore steady-state ground heat loss. The equations can also be used when designing insulation thickness: how much more insulation is needed for a heated ground construction in comparison to a conventional slab-on-ground given that the heat loss should be the same?

The standard does not explicitly have the case suitable for the Termogrund. Instead, the equations for slab-on-ground may be applied. A reason is the small building height of the heating space and another reason is that the system is built at ground level.

Another method is using standard procedures applicable to suspended floors. The equations do not explicitly model heated underfloor spaces. However, heat conductance from the space should be somewhat the same, independent of the temperature in the space. A numerical evaluation is therefore carried out in the following section.

7.1 The slab-on-ground procedure

First, before the EN ISO procedures are introduced, the results of a 3-D model of a slab run in the finite difference program are shown in table 7. The modelled concrete slab, with the thermal conductivity 1.7 W/(m·K), has a reinforced peripheral section, 0.6 m broad and 0.6 m deep. The central slab section has a thickness of 0.15 m. Insulation is evenly distributed having a thickness of 0.2 m. A reason for this thickness is that the Termogrund has the same thickness.

The U-values of table 7 are based on the exterior dimensions of the floor (U_{de}). The calculations were carried out in 2-D (see section 7.3 for details) and in 3-D; deviations between the two methods are negligible. Also shown are the U-values for the nominal Termogrund. These are considerably higher than that of the slab.

TAB. 7: U-value of a slab-on-ground from a 2-D and a 3-D finite difference calculation. U_{de}-values are based on exterior dimensions. The number in parenthesis is the deviation from 3-D calculations.

Interior dimensions	B'	Slab-on-ground 2-D U_{de} W/(m^2·K), (%)	Slab-on-ground 3-D U_{de} W/(m^2·K)	Nominal Termogrund U_{de} W/(m^2·K)
5.35x8.25	3.56	0.205 (2.1)	0.200	0.292
8x8	4.30	0.192 (1.6)	0.189	0.268
8x10	4.75	0.186 (1.4)	0.183	0.257
9x9	4.80	0.185 (1.5)	0.183	0.255
9x10	5.04	0.183 (1.4)	0.180	0.250
8x12.5	5.19	0.181 (1.3)	0.179	0.247
10x10	5.30	0.180 (1.3)	0.177	0.245

The EN ISO procedure is coarsely outlined in equation form below. For a slab-on-ground construction, an equivalent thickness *dt* has to be calculated.

$$dt = w + l\left(R_{si} + R_f + R_{se}\right) \qquad (4)$$

w is the thickness of the wall. Surface thermal resistances R_{si} and R_{se} have the values 0.17 and 0.04 m^2·K, and l is the thermal conductivity of the ground. The parameter R_f is the sum of thermal resistances for layers in the floor construction. In this case, R_f constitutes the thermal resistance of the EPS sheets.

The U-value is determined for the equation of a well-insulated slab ($dt \geq B'$) such that

$$U_o = \frac{\lambda}{0.457 \cdot B' + dt} \tag{5}$$

The sought value U is

$$U = U_o + 2 \cdot \psi / B' \tag{6}$$

of which the last term accounts for the effect of thermal bridges along the perimeter. If the slab is evenly insulated, then the linear thermal transmittance ψ is 0. If the wall insulation does not connect to the floor insulation, then ψ is 0.2 W/(m·K).

TAB. 8: U-values based on ISO slab-on-ground procedures compared to U-values from 3-D computations. U-values are based on exterior dimensions. Numbers in parenthesis depict deviation from 3-D values.

Interior dimensions	B'	Slab-on-ground ISO (ψ = 0.0) U_{de} W/(m^2·K), (%)	Slab-on-ground 3-D U_{de} W/(m^2·K)	Slab-on-ground ISO (ψ = 0.2) U_{de} W/(m^2·K), (%)	Nominal Termogrund U_{de} W/(m^2·K)
5.35x8.25	3.56	0.167 (-16.9)	0.200	0.279 (-4.4)	0.292
8x8	4.30	0.163 (-14.0)	0.189	0.256 (-4.7)	0.268
8x10	4.75	0.160 (-12.7)	0.183	0.245 (-4.8)	0.257
9x9	4.80	0.160 (-12.5)	0.183	0.244 (-4.7)	0.255
9x10	5.04	0.159 (-11.9)	0.180	0.239 (-4.8)	0.250
8x12.5	5.19	0.158 (-11.6)	0.179	0.236 (-4.8)	0.247
10x10	5.30	0.157 (-11.2)	0.177	0.234 (-4.8)	0.245

The U-values calculated with EN ISO procedures are low in comparison with the U-values produced with the slab model of the 3-D program. The EN ISO U-values are for the chosen dimensions some 11% to 17% lower than what should be expected. An explanation for the deviations is that the modelled slab has a reinforced peripheral section, which cannot be accounted for in the standard's procedures.

In the nominal Termogrund case, the foundation beam is not insulated. If the effect of the thermal bridge is included in the U-value of the slab, EN ISO procedures give values ranging between 0.23 – 0.28 W/(m^2·K). These values are in good agreement with the computed U-values, since these are some 5% lower than the 3-D computational U-values for the nominal Termogrund.

7.2 The suspended floor procedure

The equations presented in the EN ISO procedure actually apply to natural ventilated suspended floors. It is also indirectly presumed that the temperature in the underfloor space is less than that of the living space. For this reason, the equations will have to be somewhat manipulated to suite the Termogrund.

The thermal transmittance is given by

$$\frac{1}{U} = \frac{1}{U_f} + \frac{1}{U_g + U_x} \tag{7}$$

where U_g is the thermal transmittance between the underfloor space and the outside, U_x is the equivalent thermal transmittance accounting for heat flow through the walls of the underfloor space and by ventilation, and U_f is the thermal transmittance of suspended part of the floor. The entity U_f is omitted in this application for the reason that the underfloor space is warmer than the indoor temperature.

The latter term of equation 5 is determined by calculating the equivalent thickness d_g, where

$$d_g = w + \lambda\left(R_{si} + R_g + R_{se}\right) \tag{8}$$

so that

$$U_g = \frac{2 \cdot \lambda}{\pi B' + d_g} \ln\left(\frac{\pi B'}{d_g} + 1\right) \tag{9}$$

The term R_g is the thermal resistance of any insulation on the base of the underfloor space.

The thermal transmittance U_x is composed of two terms where

$$U_x = \frac{2 \cdot h \cdot U_w}{B'} + \frac{1450 \cdot \varepsilon \cdot v \cdot f_w}{B'} \tag{10}$$

The latter term is associated with ventilation (cross flow) and will in this context be equal to zero. In the first term, h is the height of the upper surface of the floor above external ground level and U_w is the thermal transmittance of walls above ground level. The height h is in this application set as the height of the foundation beam.

In table 9, the results of equation 7 are listed. Also, 2-D (see section 7.3) and 3-D finite difference program results are shown for the nominal Termogrund. All U-values are based on exterior dimensions and the U-values of the EN ISO and 2-D calculations are compared with the 3-D results.

TAB. 9: U-value of a suspended floor from EN ISO procedures. U-values are based on exterior dimensions. Numbers within parentheses represent deviation from 3-D values.

Interior dimensions	B'	Suspended floor EN ISO U_{de} W/(m^2·K), (%)	Nominal Termogrund 2-D U_{de} W/(m^2·K), (%)	Nominal Termogrund 3-D U_{de} W/(m^2·K)
5.35x8.25	3.56	0.291 (-0.4)	0.305 (4.5)	0.292
8x8	4.30	0.268 (0.1)	0.278 (3.6)	0.268
8x10	4.75	0.258 (0.4)	0.265 (3.1)	0.257
9x9	4.80	0.257 (0.5)	0.263 (3.1)	0.255
9x10	5.04	0.252 (0.7)	0.257 (2.9)	0.250
8x12.5	5.19	0.249 (0.8)	0.254 (2.8)	0.247
10x10	5.30	0.247 (1.0)	0.251 (2.8)	0.245

The results show that the nominal Termogrund is very well modelled with the equations given in the EN ISO standard. If the same application is done to the Termogrund with a high-density core, the magnitude of deviations will be lower than 5%. However, EN ISO U-values will be less than 3-D U-values. The 2-D results are in good agreement with the 3-D results, with deviations below 5%.

7.3 Simulations of the nominal system in 2-D

In Annex A of the EN ISO standard, it is stated that programs modeling two-dimensional heat transfer can be used to simulate three-dimensional ground loss. By using an interior length corresponding to one half of the characteristic dimension *B'*, a U-value for the ground construction can be calculated from the results of the 2-D model. In table 10 below, the results of the 2-D simulations are compared with results of 3-D

models of the nominal system. The U-values are in this table based on the interior dimensions. Table 9 previously showed the results of U-values based on exterior dimensions for the corresponding calculations.

TAB. 10: U-value of a nominal Termogrund calculated with a 2-D finite difference program. U-values are based on interior dimensions (see table 9 for U-values based on external dimensions). The number in parenthesis next to the U_d-value is the relative deviation (%) from the 3-D simulation.

Interior dimensions	B'	q_u W/m^2	q_d W/m^2	U_u W/(m^2·K)	U_{di} W/(m^2·K) 2-D	U_{di} W/(m^2·K) 3-D
5.35x8.25	3.56	17.43	10.09	1.118	0.367 (5.4)	0.348
8x8	4.30	17.43	9.16	1.162	0.323 (4.1)	0.310
8x10	4.75	17.72	8.74	1.181	0.303 (3.6)	0.293
9x9	4.80	17.75	8.69	1.183	0.301 (3.5)	0.291
9x10	5.04	17.87	8.49	1.192	0.292 (3.3)	0.283
8x12.5	5.19	17.94	8.38	1.196	0.287 (3.2)	0.278
10x10	5.30	18.00	8.29	1.200	0.283 (3.1)	0.275

The system can with good accuracy be modelled with a finite difference program that simulates two-dimensional heat transfer only. The U_d-values calculated with such a program are slightly higher than the corresponding U-values produced with the 3-D program. These are therefore on the "safe side" at the design stages.

8. The influence of infiltrating air

There exists an infiltration of air in the Termogrund. This has been measured at different occasions in an experimental building with this type of suspended floor, see Appendix A. These results can be used to give a hint on how the infiltration flows and how this influences the heat balance and heat dissipation of the Termogrund.

The infiltrating air must be heated to the set-point temperature of the underfloor space. This means that the minimum power of the heating unit, as calculated earlier for ground loss, must be increased with the value given by equation 11.

$$\Phi_{\inf} = L_{\inf} \cdot \boldsymbol{r} \cdot c_p \left(T_T - T_e\right) \tag{11}$$

Here, $L_{\inf}$ is the infiltrating airflow, $\boldsymbol{r}$ and c_p is the density and specific heat capacity of air, respectively, T_T is the set-point temperature of the system and T_e is the outdoor temperature.

Some of this infiltrating air may leave the underfloor space through the envelope. This air comprises a heat loss. The rest of the air flows into the living space. This air brings with it heat from the heating space to the living space, thus increasing the amount of heat that is dissipated from the Termogrund to the living space. The airborne heat is

$$\Phi_{up} = L_{up} \cdot \boldsymbol{r} \cdot c_p \left(T_T - T_i\right) \tag{12}$$

Appendix A shows airflow that may arise in the Termogrund. These values are valid for the nominal system only, with interior dimensions of 5.35x8.25 m^2. To set up an example, a computational model was made and validated for the measured cases. The ventilation is set at 0.5 ach/h in the living space. An outdoor temperature of 2 °C and a wind speed of 3.5 m/s are assumed. Computed air infiltration in the heating space corresponds to 3.06 ach/h, which is a flow of 31.6 m^3/h. Heating this air from 2 °C to 35 °C requires 350 W, thus an increase of power demand from 1259 W to 1609 W (see table 2) or by 28 %. However, not all of this airborne heat is lost. On the contrary, around 86 % of the air will rise to the living space. This airflow of 27 m^3/h increases the heat transfer from the underfloor space to the living space by 130 W, or 3.1 W/m^2.

For a system with interior dimensions of 10x10 m^2 (and assuming the same conditions as above), the rate of air change in the heating space would be 1.88 ach/h. This corresponds to a flow of 44 m^3/h. Around 95% of the infiltrated air would reach the living space. These figures give that the increase of power demand is 489 W from initial 2718 W (an increase of 18%). The extra heat transferred to the living space would be 210 W, or 2.1 W/m^2.

9. Conclusions

This study of an underfloor heating system has found means of reducing the system temperature and the heat loss. The most efficient way of reducing the system temperature is by increasing the thermal conductance of the suspended floor. Using materials with high thermal conductivity does this. The lowering of the system temperature leads to a reduction in heat loss.

Insulating the bottom of the system well can minimize heat loss and bring down the power demand. However, this action will not reduce system temperatures. Compared to a conventional slab-on-ground construction with an evenly distributed insulation of 200 mm, the Termogrund would require some 300 mm of insulation to keep the ground loss at the same level. The prime reason for this difference is that the temperature difference over the constructions is not the same.

Additional edge insulation has a small influence on lowering the system temperature. The small decrease in system temperature depends on that the edge insulation weakens the thermal bridge effect at the joint of the suspended floor and the foundation beam. This results in that more heat is transferred to the living space since less is conducted through the joist.

Infiltrating air means that the power demand will increase as opposed to the situation if infiltration was not present. Within this paper, an example shows that the increase can be up to some 30%. However, simulations based on actual air tightness measurement data show that most of the infiltrating air takes some path from the underfloor space and ends up in the living space, increasing heat transfer by some 2 W/m^2 at design temperatures. The actual heat loss due to air infiltration is in this case the cross flow, which is quite small in the heating space for moderate wind speed.

Heat conduction simulations were performed with 2-D and 3-D programs as well as equations given by the EN ISO 13370 standard. The modelling of ground heat loss with 2-D and 3-D computational programs, as recommended in Annex A of the standard, resulted in good agreement between the two methods. On comparing U-values obtained from 2-D and 3-D calculations with U-values from equations given by the standard, an application on a slab-on-ground shows that the EN-ISO procedure considerably underestimates heat loss.

The EN-ISO procedure has a set of equations for suspended floors, but not for the case if heat is supplied to the underfloor space. By modifying the equation, as to only use the U-value for heat flow through the ground and the U-value for heat flow through the walls of the underfloor space, good agreement was found with 2-D and 3-D computational results.

10.References

EN ISO 13370. (1998). *Thermal performance of buildings – Heat transfer via the ground – Calculation methods.* European Committee for Standardization (CEN), Brussels.

Akander J. (1997a). *Air tightness of the LECA-house at Röskär: Using the pressurized fan method – Test 4*. Division of Building Technology, Department of Building Sciences, KTH, Stockholm, Sweden.

Akander J. (1997b). *Measurements of the rate of air change in the LECA-house at Röskär – Test 1*. Division of Building Technology, Department of Building Sciences, KTH, Stockholm, Sweden.

Akander J. (1997c). *Measurements of the rate of air change in the LECA-house at Röskär – Test 2*. Division of Building Technology, Department of Building Sciences, KTH, Stockholm, Sweden.

Akander J. and Jóhannesson G. (1997). The utilisation factor of two Swedish buildings. *Cold Climate HVAC '97, Reykjavik, Iceland*. p. 117-122.

Akander J., Lacour C., Mao G., Johannesson G. (1994). *Ett elbaserat golvvärmesystem - Mätningar och beräkningsmodeller*. Dept. of Building Technology, KTH, Stockholm, Sweden. (In Swedish).

Akander J. and Levin P. (1997). *Air tightness of the LECA-house at Röskär: Using the pressurized fan method – Test 1*. Division of Building Technology, Department of Building Sciences, KTH, Stockholm, Sweden.

Anderlind G. (1998). *Program Description DAVID-32*. http://www.gullfiber.se

Anderlind G. (1999). A new model for calculation the effects of two- and three-dimensional thermal bridges. *Proc. of the 5th Symp.on Building Physics in the Nordic Countries. CTH, Göteborg, Aug. 24-26*, 1999.

Blomberg T. (1996). *Heat Conduction in Two and Three Dimensions - Computer Modelling of Building Physics Applications.* Report TVBH-1008. Department of Building Physics, LTH, Lund, Sweden. p.125-133.

Levin P. (1991). *Building technology and air flow control in housing*. Doctoral Dissertation. Document D16:1991. Swedish Council for Building Research, Stockholm, Sweden.

Nylund, P.O. (1980). *Infiltration and ventilation*. Document D22:1980. Swedish Council for Building Research, Stockholm, Sweden.

Sandin K. (1990). *Värme, luftströmning, fukt. Kompendium i byggnadsfysik*. Avdelningen för byggnadsfysik, LTH, Lund, Sweden. (In Swedish).

Submitted to: Nordic Journal of Building Physics
Available at http://www.ce.kth.se/bphys

APPENDIX 1.

A1. Air tightness.

The air tightness of a building or enclosure is difficult to establish on basis of theory and calculations. It is therefore more convenient to determine the air tightness and air movement by means of measurements complemented with calculations. Measurements have been performed on the Termogrund of a one-story experimental building at Röskär (Akander et al 1997). Data from those measurements can indicate the magnitude of air that infiltrates into the Termogrund. Complemented with a simple numerical model, simulations with input from measured data can show where the infiltrated air moves: up into the living space or through the heating space. In the case of the experimental building, the ventilation system has an exhaust fan that will create a depressurization of the living and also the heating space.

The measurements were performed at two different stages. During the first stage, measurements were done using the pressurized fan method, a tracer gas method and a Venturi tube method. After the measurements of stage one were finished, the building underwent air tightening improvement work. The envelope surrounding the living space was checked, seams between sandwich elements were sealed, as well as penetrations and holes for cables and the ventilation system. Accordingly for the heating space, the foundation beam and PE-foil were externally scrutinized. Visible joints were sealed and the foil was cautiously stretched and covered with gravel. After this work, stage two of measurements was performed.

The volume of the living and the heating spaces are 125.7 and 10.3 m^3, respectively. The height of the living space is on an average 2.8 m (the building has a tilted ceiling) and 0.25 m for the heating space.

A1.1 Measurements during stage 1

The rate of ventilation in the living space was at the time set to 1.0 ach/h. This was confirmed by a tracer gas measurement as well as a Venturi tube measurement on the ventilation system, see table A1 (Akander 1997b). This verifies that the exhaust fan removes all air entering the living space.

TAB. A1: Measurement of the rate of air change during stage 1.

Ach/h	Tracer gas technique	Venturi tube
Heating space - ventilation on	4.4	-
Heating space - ventilation off	1.9	-
Living space - ventilation on	1.0	1.0

Next the air tightness of the building was measured by means of the pressurised fan method. Parts of the measurement procedures are illustrated in figures A1 and A2, whereas some results are shown in table A2 (Akander and Levin 1997).

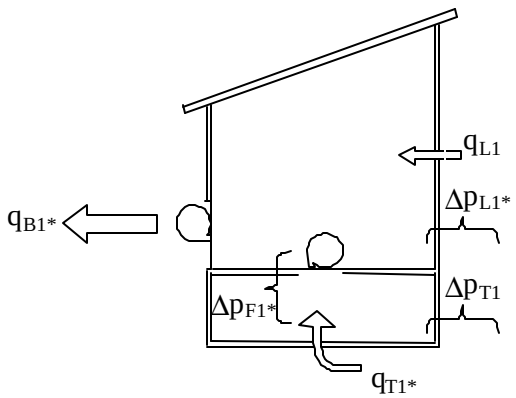

*FIG. A1a: Case1: Two balanced fans giving a pressure difference of zero, $\Delta p_{F1} = 0$. * Measured entity.*

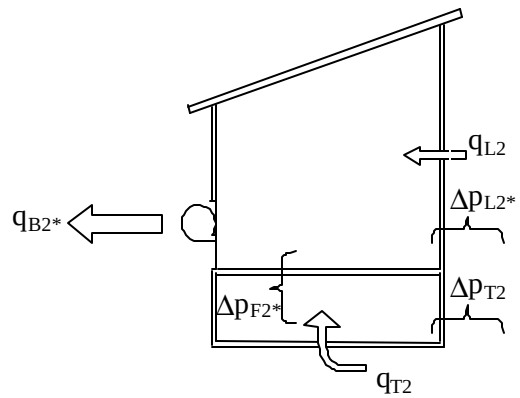

FIG. A1b: Case2: Depressurization of the living zone. This creates a pressure difference over the suspended floor.
** Measured entity.*

TAB. A2: Results from the pressurized fan method measurements during stage 1.

Measurement	Exponential regression	Equation number	R^2
Case1	$q_{T1} = 38.57 \cdot \Delta p_{T1}^{0.62}$	(A1)	0.9949
Case2	$q_{B2} = 25.31 \cdot \Delta p_{L2}^{0.72}$	(A2)	0.9981
	$\Delta p_{T2} = 0.08 \cdot \Delta p_{L2}^{1.32}$	(A3)	0.9969

When the exhaust fan of the ventilation system was turned on, the rate of air change was 1.0 ach/h. This roughly corresponds to an airflow of 126 m^3/h. Insertion of this value into equation A2 gives the pressure in the living space, here -9.3 Pa. This means that the pressure in the heating space is -1.5 Pa, according to equation A2. Insertion of this value into equation A1 gives a flow of 50 m^3/h, which corresponds to 4.9 ach/h in the heating space. This value is larger (11%) than the 4.4 ach/h measured with the tracer gas technique. On the other hand, the inaccuracy of each method is around 10%.

The discrepancy may be due to a number of factors. The largest source of error is probably that test case1 may not have had balanced fans so that the pressure difference over the suspended floor was different from the expected value, zero. Another factor is that the equations from the pressurized fan method are not too reliable at small pressure differences.

The data put in the simulation program (see the section A3) was based on the information in table A2. Simulation results are shown in table A3. The tracer gas tests gave that the rate of air change in the heating space was 4.4 ach/h with the ventilation system on, and 1.7 ach/h with the ventilation system off.

TAB. A3: Results from simulations of stage 1.

Wind velocity [m/s]	Vent sys	1.0	1.5	2.0	3.0
Rate of air change in the underfloor space [ach/h]	On	4.9	5.0	5.1	5.7
Part of infiltrated air exiting for the living space [%]	On	100	100	99.6	98.3
Rate of air change in the underfloor space [ach/h]	Off	1.0	1.3	1.6	2.3
Part of infiltrated air exiting for the living space [%]	Off	96.2	94.6	94.2	92.9

A1.2 Measurements during stage 2

Several of the measurements were repeated after the air tightening improvements (Akander 1997c). The results are displayed in table A4. Note that the Venturi tube measurement was not conducted.

TAB. A4: Measurement of the rate of air change during stage 2.

Ach/h	Before improvements	After improvements
Heating space – ventilation system on	4.4*	1.1
Living space – ventilation system on	0.5	0.395

* The ventilation system was on, corresponding to 1.0 air changes per hour in the living space.

The pressurized fan method was used to determine the air tightness of the building (Akander 1997a). Again, the procedures used at stage 1 were repeated. Relevant results are displayed below, in table A5.

TAB. A5: Results from the pressurized fan method measurements during stage 2.

Measurement	Exponential regression	Equation number	R^2
Case1	$q_{T1} = 22.61 \cdot \Delta p_{T1}^{0.79}$	(A4)	0.9938
Case2	$q_{B2} = 25.05 \cdot \Delta p_{L2}^{0.75}$	(A5)	0.9843
	$\Delta p_{T2} = 0.29 \cdot \Delta p_{L2}^{1.05}$	(A6)	1.0000

The rate of air change in the living space was found to be 0.39 ach/h. This rate corresponds to a flow of 49 m^3/h. Equation A5 indicates that the pressure in the living space is –2.5 Pa. According to equation A6, the pressure in the heating space is -0.7 Pa. The flow is then 17.9 m^3/h, or 1.7 ach/h. Again, the equations over-estimate the infiltration into the underfloor space, here with 59%.

When the system was simulated, results correspond quite well for wind speeds slightly below 2 m/s, which was the average wind speed at the site when tracer gas tests were performed. In the simulations, it is assumed that the airflow corresponding to the measured rate of air change all exits through the exhaust fan. When wind speed picks up towards 3 m/s, cross flow in the living space arises. Cross flow is present in the underfloor space for all wind speeds, but is less in quantity at lower wind speed than at higher.

TAB. A6: Results from simulations of stage 2.

Wind velocity [m/s]	Vent sys	1.0	1.5	2.0	3.0
Rate of air change in the underfloor space [ach/h]	On	1.0	1.2	1.4	2.2*
Part of infiltrated air exiting for the living space [%]	On	96.4	92.1	88.1	85.2

* The living space is now subjected to cross flow (totally 0.44 ach/h)

A1.3 A simple simulation model.

In order to find out how the air flows in the heating and the living space in natural weather conditions, a simple model was set up on basis of the pressurized fan tests. The results from the simulation model can be compared with results from the tracer gas tests as a type of validation.

The three phenomena that give rise to airflow through the building are the stack effect, wind forces and the exhaust fan. Below, a brief description is made on each subject. The calculation methodology is stated in Nylund (1980) and has been applied by Levin (1991).

The stack effect has differences in air density, or temperature, as driving force. Warm indoor air has the tendency of building up pressure under the ceiling, whereas a pressure difference over the envelope of the

lower building regions tends to suck in cold outdoor air. The neutral level at the height h indicates where the pressure difference over the envelope is zero. Infiltration due to the stack effect arises under this height, while air escapes above.

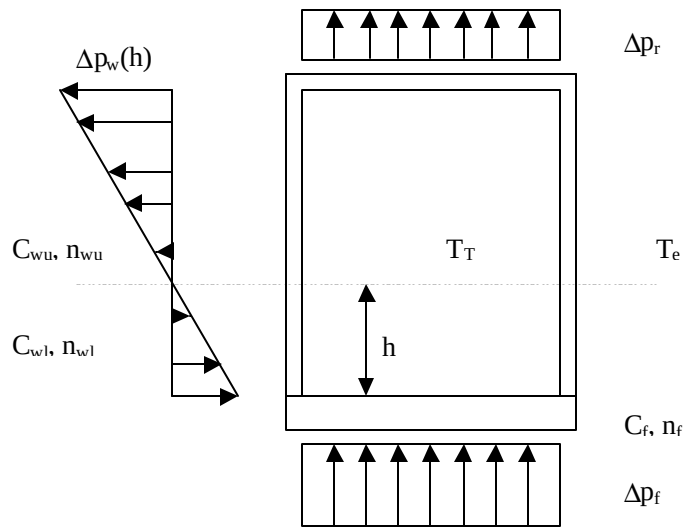

FIG. A2: The neutral level h in the building and the flow coefficient C, the flow exponent n and pressure difference Dp for each construction.

Flow coefficients are computed from the pressurised fan tests, as well as the flow exponents. This has been done with the assumption that air leakage paths are evenly scattered in the envelope of the living space and in the exterior constructions of the heating space. The flow coefficients and exponents are dependent on flow direction.

Both the heating and the living spaces were treated as one enclosure. The driving force that creates the pressure difference is the difference in indoor and the outdoor temperatures, T_i and T_e, and the stack height [redacted] such that

$$\Delta p = \text{[redacted]} \cdot 3462\left(\frac{1}{T_e} - \frac{1}{T_i}\right) \qquad \text{(A7)}$$

The neutral level is determined by means of an airflow balance, where it is assumed that the wind speed is zero and the ventilation system is shut off and sealed. In the case of this simulation, the neutral level has a height of approximately 0.6 m.

Wind creates pressure differences over different parts of the envelope, which are functions of speed and direction as well as geometry and shielding factors. For the measurement object, wind speed and direction were measured close to the building at a height of 2 m. The model uses wind factors as shown in figure A3, the arrows showing flow direction if the internal wind factor is $-0.5 < \mu_i < 0.7$. It is assumed that these wind factors can be applied to the exposed exterior surfaces of the living and the heating space constructions. The wind factor at the ground under the Termogrund is zero. The pressure difference over an envelope construction due to the dynamic effects of wind is

$$\Delta p = (m_e - m_i)\, r \frac{u^2}{2} \qquad \text{(A8)}$$

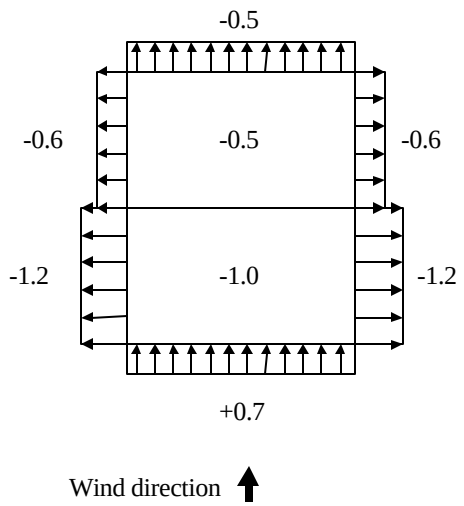

FIG. A3: Wind factors as given by Sandin (1990).

Finally, an airflow balance is made for the living space and the heating space, respectively. The airflow through the exhaust fan is considered in the airflow balance of the living space. The effects of wind and stack forces are taken into consideration by the pressure difference both give rise to. The program works with iterations, where the interior wind factor of the living space and wind factor of the heating space are varied until the flow balance of each space is fulfilled.